

**Design of Switched Reluctance Motors and Development of a
Universal Controller for Switched Reluctance and Permanent
Magnet Brushless DC Motor Drives**

by
Praveen Vijayraghavan

Dissertation submitted to the Faculty of the
Virginia Polytechnic Institute and State University
in partial fulfillment of the requirements for the degree of

DOCTOR OF PHILOSOPHY
IN
ELECTRICAL ENGINEERING

Committee:

Dr. K. Ramu, Chair

Dr. C.E. Nunnally

Dr. H.F. VanLandingham

Dr. P. Kachroo

Dr. R.C. Batra

November 15, 2001

Blacksburg, Virginia

Copyright © 2001, Praveen Vijayraghavan

Keywords: Switched Reluctance Motor, Permanent Magnet Brushless DC Motor, SRM,
PMBDC, Machines

Design of Switched Reluctance Motors and Development of a Universal Controller for Switched Reluctance and Permanent Magnet Brushless DC Motor Drives

by

Praveen Vijayraghavan

(Abstract)

Switched Reluctance Machines (SRMs) are receiving significant attention from industries in the last decade. They are extremely inexpensive, reliable and weigh less than other machines of comparable power outputs. Although the design principles of the machine are available as a concatenation of many different sources, the need for a unified, step-by-step design procedure from first principles of electromagnetics is an absolute requirement. This dissertation discusses a procedure that can be applied by engineers with a basic background in electromagnetics. Subsequent to the design of the machine, existing finite element software can do the analysis of the machine. However, this is a laborious process and the need for an analytical method is preferable to verify the design procedure before the final verification by finite elements. The analytical procedure as well as a procedure to calculate iron losses is also developed in this dissertation. A prototype machine has been developed as an example of the design process and an existing prototype is analyzed to verify the analysis procedure.

The similarities between the SRM and the Permanent Magnet Brushless DC Machine (PMDBC) beg the consideration of the development of a converter that can be used to drive either machine. One such converter has been developed in this dissertation. The design of the drive for both the machines is seen to be very similar. As a consequence, a universal controller that can be used to operate both machines has been developed and implemented with a DSP. Simulations and experimental correlation for both drives have been presented.

Dedication

To my parents,

Dr. Prabha Vijayraghavan and Mr. R. Vijayraghavan

Acknowledgements

I wish to express my gratitude to my advisor, Professor Krishnan Ramu, for his guidance, his support and the confidence he has shown in me over the years. His constant encouragement in my dissertation work and my Graduate Assistant duties has helped me to look forward to the future with enthusiasm and confidence in my abilities.

I would like to thank Professor Romesh Batra, Professor Hugh VanLandingham, Professor Charles Nunnally and Dr. Pushkin Kachroo, for serving on my committee and suggesting some of the directions that I had to follow to make my dissertation possible.

I would like to acknowledge the assistant of my colleague, Dr. Han-Kyung (Andy) Bae, who assisted me in building my hardware and was always available for discussions on my dissertation ideas. I will be indebted to him for all the practical implementation knowledge that he passed on to me.

I would also like to acknowledge my other colleagues, Dr. Byeong-Seok Lee, Mr. Phillip Vallance, Mr. Ajit Bhanot and Mrs. Amanda Martin Staley, for the help that they rendered to me during various stages of my dissertation.

I would like to express my sincere gratitude to my friends Ms. Sridevi Parthasarthy, Ms. Nishita Bakshi and Ms. Mansi Grover, for helping to ensure that I did not have to waste my time cooking and always providing me with dinner during the stretch months of my degree. Their constant encouragement helped me to finish my work successfully.

Finally, I would like to thank my parents, Mr. R. Vijayraghavan and Dr. Prabha Vijayraghavan, and my brother, Mr. Sanjay Vijayraghavan, for their constant support both emotionally and financially, in completing this endeavor. I sincerely appreciate their patience and understanding while waiting for me to complete my degree. Without their overwhelming positive influence on my life, I would not have been able to achieve my goals.

Praveen Vijayraghavan

Blacksburg, VA.

11/15/2001

Table of Contents

1. Introduction	1
2. Design of a Switched Reluctance Motor	5
2.1 Design Procedure for a SRM	5
2.1.1 Machine Specification	5
2.1.2 Frame Size Selection	6
2.1.3 Pole Selection	6
2.1.4 Stator and Rotor Pole Angle Selection	7
2.1.5 Preliminary Design Process	12
2.1.6 Winding Design	20
2.1.7 Calculation of Minimum Inductance	22
2.1.8 Calculation of Average Torque	41
2.2 Design Verification by Finite Element Analysis	44
2.3 Analysis of the SRM	48
2.3.1 Copper Losses	48
2.3.2 Iron Losses	48
2.3.3 Inductance Calculation at Various Rotor Positions	61
2.4 Design of a 5 h.p. SRM	82
2.4.1 Selection of Stator and Rotor Pole Angles	83
2.4.2 Preliminary Design Process	87
2.4.3 Winding Design	90
2.4.4 Calculation of Average Torque	91
2.4.5 Finite Element Verification of the prototype	93
2.4.6 Analysis of the prototype	95
2.5 Analysis of an existing 5 h.p. SRM	98
2.6 Summary	117
3. Switched Reluctance Motor Converters	120
3.1 Eight Switch (Asymmetric Bridge) Converter	120
3.2 Six Switch Converter	121
3.3 Buck Converter	123
3.3.1 Modes of Operation	123

3.3.2 Design of the buck converter	127
3.3.2 Merits and demerits of the proposed converter	128
4. Switched Reluctance Motor Drive Design, Simulations and Experimental Results	130
4.1 Design of the Buck Converter Speed Controlled System	130
4.2 Simulation of a Practical Buck Converter Driven SRM System	138
4.3 Design of a Prototype SRM Buck Converter Drive	146
4.4 Drive System Simulation	152
4.5 Experimental Correlation	155
4.6 Summary	158
5. Permanent Magnet Brushless DC Motor Drive: Converter and Control	159
5.1 Principle of the Half Wave Operation of the PMBDC	159
5.2 Converter Topology	161
5.3 Design of Buck Converter Passive Components	164
5.4 Design of Current and Speed Controllers	166
5.5 PMBDC Drive System Schematic	174
5.6 Design of a Prototype PMBDC Machine Drive	180
5.7 Drive System Simulation	185
5.8 Experimental Results	188
5.9 Merits and Demerits of the Proposed Converter	192
5.9 Conclusions	195
6. Contributions and Future Work	196
Bibliography	199

List Of Figures

Figure 2.1 - Schematic representing the traverse of rotor	9
Figure 2.2 - Ideal inductance vs. rotor position profile	9
Figure 2.3 - Inductance profiles vs. rotor position of two successive phases	10
Figure 2.4 - Diagram of the feasible triangle for a 8/6 machine	11
Figure 2.5 - BH characteristics of DBII Steel	13
Figure 2.6 - 8/6 SRM Schematic	15
Figure 2.7 - Magnetic Circuit of the SRM	18
Figure 2.8 - Simplified Magnetic Circuit of the SRM	19
Figure 2.9 - Identification of 7 flux tubes for analytical calculation of unaligned inductance	22
Figure 2.10 - Tube 1 calculations	23
Figure 2.11 - Reluctance circuit for Tube 1	25
Figure 2.12 - Tube 2 calculations	26
Figure 2.13 - Equivalent reluctance circuit	28
Figure 2.14 - Tube 3 calculations	29
Figure 2.15 - Tube 4 calculations	32
Figure 2.16 - Tube 5 calculations	34
Figure 2.17 - Tube 6 calculations	37
Figure 2.18 - Magnetic Circuit for Tube 6	39
Figure 2.19 - Tube 7 calculations	40
Figure 2.20 - Reluctance Circuit for Tube 7	41
Figure 2.21 - Flux linkage vs. current plot	43
Figure 2.22 - Placement of nodes for 8/6 SRM	46
Figure 2.23 - Finite element subdivision of the 8/6 SRM	46
Figure 2.24 - Equiflux lines of an 8/6 SRM in the unaligned position	47
Figure 2.25 - Equiflux lines of an 8/6 SRM in the aligned position	47
Figure 2.26 - Flux densities over a single revolution of the rotor	52
Figure 2.27 - Sample plot of normalized stator flux vs. time for $\frac{\pi}{3}$ radians	54
Figure 2.28 - Sample plot of normalized rotor flux vs. time for $\frac{\pi}{4}$ radians	55

Figure 2.29 - Sample plot of normalized section 1 yoke flux vs. time for $\frac{\pi}{3}$ radians	57
Figure 2.30 - Sample plot of normalized rotor core flux vs. time for δ radians.	58
Figure 2.31 - Identification of flux tubes in Region I	62
Figure 2.32 - Tube 1 and 2 Calculations	63
Figure 2.33 - Tube 2 and Tube 3 calculations in the overlap region	80
Figure 2.34 - Plot of torque vs. rotor pole angles for varying stator pole angles from 15° to 30°	84
Figure 2.35 - Plot of torque/iron volume vs. rotor pole angles for varying stator pole angles	84
Figure 2.36 - Plot of clearance vs. rotor pole angles for varying stator pole angles	85
Figure 2.37 - Plot of torque vs. rotor pole angles for varying stator pole angles from 15° to 24°	85
Figure 2.38 - Plot of torque/iron volume vs. rotor pole angles	86
Figure 2.39 - Plot of Flux Linkages vs. current for the prototype machine	93
Figure 2.40 - Schematic of the designed prototype	94
Figure 2.41 - Inductance plot of the designed prototype for currents varying from 0A to 16A	94
Figure 2.42 - Finite Element Mesh of the designed prototype	95
Figure 2.43 - Torque plot of the designed prototype for currents varying from 0A to 16A	96
Figure 2.44 - Equiflux lines in the unaligned position of the designed prototype	96
Figure 2.45 - Equiflux lines in the aligned position of the designed prototype	97
Figure 2.46 - Comparison of analytical inductance calculation and FEA results	98
Figure 2.47 - Plot of machine torque	99
Figure 2.48 - Plot of torque vs. position for varying currents obtained by FEA	100
Figure 2.49 - Plot of inductance vs. position for varying currents obtained by FEA	101
Figure 2.50 - Plot of the 4 phase currents vs. rotor position	103
Figure 2.51 - Plot of A phase stator pole flux density vs. rotor position	104
Figure 2.52 - Plot of machine torque	105
Figure 2.53 - Plot of stator normalized flux vs. time for 60° rotation of rotor	105
Figure 2.54 - Plot of rotor normalized flux vs. time for 45° rotation of rotor	106
Figure 2.55 - Plot of section 1 normalized flux vs. time for 60° rotation of rotor	108
Figure 2.56 - Plot of section 2 normalized flux vs. time for 60° rotation of rotor	110
Figure 2.57 - Plot of section 3 normalized flux vs. time for 60° rotation of rotor	111
Figure 2.58 - Plot of section 4 normalized flux vs. time for 60° rotation of rotor	112

Figure 2.59 - Plot of rotor core normalized flux vs. time for 180° rotation of rotor	114
Figure 2.60 - Plot of eddy-current losses with speed varying from 0 to rated speed	115
Figure 2.61 - Plot of hysteresis losses with speed varying from 0 to rated speed	117
Figure 2.62 - Plot of iron losses with speed varying from 0 to rated speed	118
Figure 3.1 - Eight switch converter configuration	121
Figure 3.2 - Operational waveforms for the eight switch converter	122
Figure 3.3 - Six Switch Converter	122
Figure 3.4 - Buck Converter for SRM Drives	124
Figure 3.5 - Operational waveforms for the buck converter	125
Figure 4.1 - Current control loop	133
Figure 4.2 - Speed control loop	134
Figure 4.3 - Equivalent Buck Converter Circuit	135
Figure 4.4 - Current Loop of the buck converter system	138
Figure 4.5 - Closed Loop Buck Converter System	138
Figure 4.6 - Block diagram of the SRM Buck Converter Drive System	139
Figure 4.7 - Current Controller and Converter Schematic	140
Figure 4.8 - Plot of phase a flux linkages vs. rotor position for different currents	143
Figure 4.9 - Plot of torque vs. rotor position for different phase currents	143
Figure 4.10 - Frequency response of the current controlled system	149
Figure 4.11 - Frequency response of the speed controlled system	150
Figure 4.12 - Step response of the speed controlled system	150
Figure 4.13 - Closed loop response of the current controlled buck converter system	151
Figure 4.14 - Closed loop response of the voltage controlled buck converter system	152
Figure 4.15 - Simulation of a speed drive system with a buck converter front end	153
Figure 4.16 - Plots of phase currents and phase voltages	154
Figure 4.17 - Simulation of the speed drive system with a maximum reference of 223 r.p.m.	155
Figure 4.18 - Simulation plots of the switched reluctance motor	156
Figure 4.19 - Experimental plots of the switched reluctance motor	156
Figure 4.20 - Simulation plots of the currents of the switched reluctance motor	157
Figure 4.21 - Phase current plots of the switched reluctance motor drive	157
Figure 5.1 - Voltage, current and air-gap power waveforms of the half-wave converter	160

Figure 5.2 - Voltage, current and air-gap power waveforms of the half-wave converter	161
Figure 5.3 - Converter topology with a buck converter on the front end	162
Figure 5.4 - I Quadrant motoring operation with phase a of the PMBDC drive	163
Figure 5.5 - I Quadrant Motoring Operation: waveforms of the variables	163
Figure 5.6 - IV Quadrant regenerative operation with phase a of the PMBDC drive	164
Figure 5.7 - IV Quadrant Motoring Operation: waveforms of the variables	165
Figure 5.8 - PMBDC and current control loop	166
Figure 5.9 - PMBDC and current control loop – Simplification 1	167
Figure 5.10 - Current control loop	168
Figure 5.11 - Speed control loop	170
Figure 5.12 - Equivalent Buck Converter Circuit	171
Figure 5.13 - Current Loop of the buck converter system	173
Figure 5.14 - Closed Loop Buck Converter System	174
Figure 5.15 - Schematic of the PMBDC Drive System	175
Figure 5.16 - Plot of the back emf functions	177
Figure 5.17 - Frequency response of the current controlled system	183
Figure 5.18 - Frequency response of the speed controlled system	183
Figure 5.19 - Step response of the speed controlled system with no simplifications	184
Figure 5.20 - Closed loop response of the current controlled buck converter system	185
Figure 5.21 - Closed loop response of the voltage controlled buck converter system	186
Figure 5.22 - Simulation of a speed drive	186
Figure 5.23 - Simulation of a four quadrant speed drive	187
Figure 5.24 - Simulation of a prototype speed drive	188
Figure 5.25 - Simulation plot of speed reference and actual speed with absolute values	189
Figure 5.26 - Plot of reference speed and actual speed	189
Figure 5.27 - Simulation plots of speed reference and buck converter output voltage	190
Figure 5.28 - Plot of reference speed and output voltage of the buck converter	190
Figure 5.29 - Gate drive signals from the simulation in Figure 5.24 in the positive direction	191
Figure 5.30 - Plot of the three phase gate drive signals in the positive direction	192
Figure 5.31 - Gate drive signals from the simulation in Figure 5.24 in the negative direction	192
Figure 5.32 - Plot of the three phase gate drive signals in the negative direction	193

Figure 5.33 - Expanded phase current simulation results expanded from Figure 5.24	193
Figure 5.34 - Plot of the reference and actual phase currents	194

List Of Tables

Table 2.1 - In depth examination of 6 possible combinations	87
Table 5.1 - Comparison of the proposed converter and full-wave converter PMBDC drives	105

Chapter 1. Introduction

The concept of switched reluctance motors is extremely old dating back to 1838 when a locomotive was propelled by this motor in Scotland [MIL93]. The stepper motor that includes some of the features of the modern switched reluctance motor was invented and patented in the 1920's in Aberdeen by C.L. Walker. In 1969, S.A. Nasar introduced the basic concepts of the modern day switched reluctance machine [NAS69]. The period of the late 70s was a time of development of concepts of the switched reluctance motor that was helped along with the development of fast switching devices culminating in the work by [BYR76] and [LAW80]. Since then there have been massive developments in the both the design and control of switched reluctance motors. The very nature of the machine demands that the development of the switched reluctance motor drives requires the design of the machine and control to go hand in hand unlike any other machine. While [LAW80] stands out in the development of the concepts of the machine as well as the fundamentals of control, the paper by Krishnan, et. al, [KRI88], stands out in the development of a design procedure from an analytical stand point because it helps equate the design of the machine to the design of other machines in terms of machine dimensions. There are a number of papers that rely heavily into the process of design solely based on finite element analysis but as this work will demonstrate, the design of the machine is rooted in the analytical relationships that govern the machine with finite element analysis being a tool for verification. Finite element analysis of switched reluctance machines had been described in detail first in [ARU85] and subsequently in a number of different papers. The design of the machine as described here is a step by step design process by applying the basic principles of electromagnetics. In this dissertation, the design process is completely described, and illustrated with a design example.

The procedure of design of switched reluctance machine starts with selection of a frame size and progresses to the selection of various dimensions in a methodical manner. With the selection of dimensions, a procedure to calculate the inductance in the aligned and unaligned position is outlined. This was initially done by [COR79] and many methods have been outlined by different authors including [MAT89] and [RAD94]. The problems with this prior material are the lack of transparency between the assumptions that are made and resulting equations. The procedure outlined here allows the designers to use first principles thus making it portable to different configurations of switched reluctance machines. The procedure outlined here has been derived in

detail in [KRI01]. Additionally, there is an attempt to calculate inductance in various intermediate positions of the rotor between the aligned and unaligned portions with varied success. Although, there are some significant errors caused by the assumptions made, the process can still be used as a rough analytical tool till the finite element analysis for the final design can be done.

The completion of a design of a machine necessitates the analysis of the design by various analytical or numerical means or a combination of both. Towards this end, finite element analysis is used to verify the feasibility of the design and a combination of finite element analysis and analytical methods are used to estimate the losses in the machine. The machine like any other machine has losses composed of iron losses, copper losses and friction and windage losses. Friction and windage losses are harder to estimate and guidelines used in other machines can be used for their estimation. Copper losses can be calculated in a straight-forward manner [KRI01]. The iron loss calculation in this machine has its principles rooted in the estimation of iron losses of any machine. The procedure as described here although seemingly complex, is methodical. It was described in [HAY95] and it reduces the problem to one of detail. Although another work has dealt with the estimation of iron losses [MAT92], the procedure outlined in [HAY95] is easier to use in the sense of getting the required data to complete the calculations. This dissertation significantly differs from [HAY95] in the sense that instead of approximations in flux linkage waveforms, a more precise calculation is setup based on finite element analysis and a more precise method of calculating the losses is obtained. In this regard, this dissertation outlines an innovative method of estimating core losses analytically.

Converter development and design for switched reluctance motors in literature has been in existence for almost as long as the development of the modern switched reluctance machine [DAV81]. Since then a number of configurations have been described in literature suitably summarized in [KRI01] and [BAR98]. This reports summarizes two of the more basic configurations while attempting to demonstrate the need for configurations that have lower number of switching devices. A configuration described first by [KRI96], which has been termed as the buck converter configuration is explored further. The reason for choosing this configuration is that it lends itself to four quadrant operation while maintaining independence between the phases of the machine. Another advantage is that this configuration can be easily

used in permanent magnet brushless dc motor drives thereby lending itself to the concept of universal converters.

The design of the converter and drive has been developed in the dissertation. The switched reluctance machine model is highly nonlinear and the process outlined in [JAC96] has been used to aid in design. The resulting steady state results and the simulation of the switched reluctance motor drives with the above converter with the inclusion of nonlinearities will verify the feasibility of the converter and is the logical step to building the drive. The simulation of this buck converter drive does not exist in any literature. The practical implementation of the buck converter drive has never been done before. Towards the implementation, a digital signal processor is used to digitally implement the algorithm used to control the buck converter drive.

As mentioned before, the buck converter can be used in permanent magnet brushless dc motor drives and this is suitably described in this dissertation with simulations. The feature of using the same configuration of the converter for two different machines was described initially in [KRI98]. The design procedure is almost identical for both motor drives. The simulations also verify that the buck converter configuration can be used for permanent magnet brushless dc motor drives. The drive has been implemented experimentally and the results have been included in the dissertation. Hence the goal of developing an universal drive control for both the switched reluctance and brushless dc motors has been achieved.

The major individual contributions of this dissertation are summarized as follows.

- This dissertation covers the design procedure of a 8/6 switched reluctance motor from the first principles. No major assumptions were made in the design procedure. The methodical approach to designing the machine is one of the major contributions of this dissertation.
- The calculation of the unaligned inductance follows the basic principles of electromagnetics. The procedure outlined is easy to follow and is one of the major developments in this dissertation.
- The procedure for calculating inductances for various rotor positions has been developed. The results do show some variation when compared with the finite element analysis but the values at the aligned and unaligned positions show a very small margin of error and these values are used in the calculation of analytical torque developed in the machine.

- A detailed procedure to calculate the eddy-current losses was described. This procedure accounts for the rise time of the current and the variation of inductance with the current while also helping to accurately predict the actual maximum torque developed in the machine.
- The process of finding the hysteresis losses does not rely on approximate flux profiles. Instead accurate flux plots are used to find the hysteresis losses. The calculation and documentation of the iron loss is one of the significant contributions of this dissertation.
- The dissertation describes the design procedure for a SRM drive using the new buck converter configuration. The design procedure was verified with computer simulations and experimental verifications of the drive have been done.
- The design procedure for the buck converter drive for permanent magnet brushless dc machines was done in the dissertation. The design was verified with experimental simulations and experimental results were obtained for the first time for such a drive.
- A universal drive to control two different motor drives has been developed. The dissertation shows the implementation of two different drives using a DSP based controller and a single converter configuration. This is a major contribution of the dissertation.

Chapter 2 describes the design of the switched reluctance motor. A design procedure followed by analytical calculations of inductance in aligned and unaligned positions as well as the analytical estimation of torque is developed. Analytical calculations of inductance at various positions of the rotor have been developed. A procedure to analytically calculate the iron losses (eddy-current and hysteresis) has been developed after the construction of the finite element model. A prototype design with the above procedure has been developed as well as the application of the analysis to an existing prototype has been described.

Chapter 3 describes the buck converter configuration along with its design and various modes of operation. The merits and demerits of the configuration are also clearly outlined.

Chapter 4 outlines the design procedure of the switched reluctance motor drive. Simulation results for an experimental prototype as well as experimental results are described in this chapter.

Chapter 5 describes the application of the buck converter drive to a permanent magnet brushless dc motor drive. The design of the drive, its application to an existing machine, simulation results as well as experimental results are clearly described in this chapter.

Chapter 6 outlines the conclusions and contributions of this dissertation.

Chapter 2. Design Of A Switched Reluctance Motor

The design procedure for Switched Reluctance Motors (SRM) has been explored in detail [ARU85], [SOU87], [KRI88], [MIL93], [RAD94], [TAN97], [RAD99], [RAD00] and [KRI01]. This material attempts to modify the design procedure described in [KRI01] to fit a manufacturer's requirements while helping a machine manufacturer with no background in SRM design to build and test prototypes. [KRI01] develops an output equation similar to the output equation developed for induction machines and d.c. machines. This process requires extensive prior knowledge and experience in designing switched reluctance machines. The procedure outlined in this section requires only basic dimension data for existing induction machines. Once the dimensions are fixed, the calculation of inductances in various positions has to be done. The process was initially developed in [COR79] and refined in other papers like [SOU87], [RAD94] and [TAN97]. The development here follows the procedure outlined in [KRI01] with more flux paths. The accuracy of the analytical estimation is within 2% of measured values. The design procedure developed in this section also outlines the calculation of some variables that help in narrowing the stator and rotor pole angle choices to obtain an optimum output once the frame sizes of the machine are decided. The process of selection of the pole angles has also been summarized in detail with a prototype example. Finally, the estimation of iron losses is done with a process initially outlined in [HAY95]. This dissertation takes the basic principle outlined in [HAY95] and refines it to obtain more realistic estimates of the losses while taking into account the various changes in inductances due to changing currents. The calculations do not depend on the idealized waveforms outlined in [HAY95].

2.1 Design Procedure for a SRM

2.1.1 Machine Specification

The design specifications for the SRM comprise of the required power output P_{hp} in h.p., speed N in rpm, allowable peak phase current i_p in Amps, and available ac supply voltage V_{ac} in volts for the system. Knowing the speed and power output will automatically fix the torque to be developed by the machine as

$$T_{\text{req}} = \frac{P_{\text{hp}} * 745.6}{2\pi \left(\frac{N}{60} \right)} = \frac{P_{\text{kw}}}{2\pi \left(\frac{N}{60} \right)} \text{N.m}, \quad (2.1)$$

where P_{kw} is the power output in watts.

2.1.2 Frame Size Selection

When the design procedure of a SRM is started, a good starting point as regards the physical dimensions of the machine would be a comparison with an equivalent induction motor [IEC71]. A comparison with an equivalent induction motor will fix the frame size of the SRM to be designed. This is advantageous as in many applications a SRM may be used to replace other machines. The IEC standards fixes dimensions for all electrical machines made internationally according to the International Standards Organization (ISO) regulations and for machines made in the United States according to National Electrical Manufacturers Association (NEMA) regulations. During the progression of the design, if the machine size is found to be too large or too small, a different frame size can be used. The preliminary selection of frame size automatically fixes the outer diameter of the stator.

Practically, the outer diameter of the stator is fixed as follows:

$$D_o = (\text{Frame Size} - 3) * 2 \quad (2.2)$$

where the Frame Size is given according to the IEC recommendations [IEC71]. The 3 mm subtraction is used in industry to account for the foot of the machine, which is used for mounting.

2.1.3 Pole Selection

Normally, the designer fixes the number of stator poles N_s and the number of rotor poles N_r and deviates from this fixed value only for very special applications because then converter configurations and feedback devices can be standardized. There are many possible combinations for the number of poles. The advantages and disadvantages have been explored in detail in [MIL93]. This thesis primarily focuses on the popular combination of 8 stator and 6 rotor poles,

also commonly known as the 8/6 machine. This machine has the advantage of lesser torque ripple than the other common combination of 6 stator and 4 rotor poles (6/4 machine) while having the disadvantage of using more switches in the converter, two extra terminals and higher core losses because of higher switching losses.

2.1.4 Stator and Rotor Pole Angle Selection

The stator and rotor pole angle selection form a crucial part of the design process. There are many guidelines to be followed during the selection process. The standard design normally has the stator pole arc angle β_s smaller than the rotor pole angle β_r . The constraints on the values of pole arc angles were described in [LAW80],[MIL93] and is briefly described here. They are as follows:

1. The stator pole arc angle is less than the rotor pole arc angle, i.e., $\beta_s < \beta_r$.
2. The effective torque zone is lesser than the stator pole angle β_s but greater than the stroke angle ϵ . The stroke angle is defined as

$$\epsilon = \frac{2\pi}{\frac{N_s}{2} N_r} \quad (2.3)$$

In an 8/6 machine the stroke angle is $\epsilon = \frac{2\pi}{\frac{8}{2} \cdot 6} = 0.2618 \text{ rads} = 15^\circ$. If $\beta_s < \epsilon$, then there may be

some positions in the machine from where the machine may not start. The inductance profile of the SRM in Figure 2.2 can be examined to understand this phenomenon better.

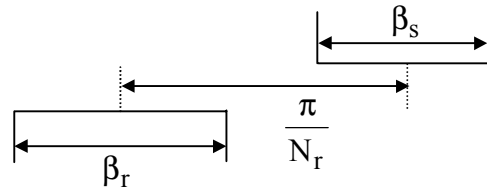
The inductance profile of a phase repeats every $\frac{2\pi}{N_r}$ radians. In the ideal scenario shown in

Figure 2.2, as long as the stator and rotor pole arcs do not overlap, the phase inductance remains at the unaligned value L_u . This region occurs between 0 and θ_1 where 0 is assumed to be the fully unaligned position. From Figure 2.1(a), it can be observed that from the fully unaligned position,

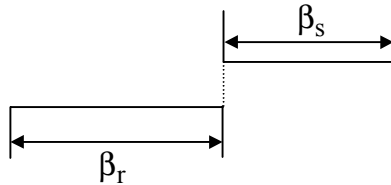
the rotor has to traverse an angle of $\theta_1 = \frac{\pi}{N_r} - \frac{\beta_s}{2} - \frac{\beta_r}{2}$ for the tip of the rotor pole to come

under the tip of the stator pole. From position θ_1 to position θ_2 , the rotor and stator pole overlap to some extent and as the rotor traverses this region, there is a steady rise in inductance value. It

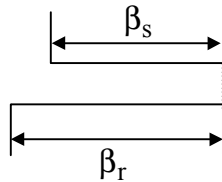
can be seen clearly in Figure 2.1(b), that the angle $\theta_2 - \theta_1 = \beta_s$ and once the rotor reaches position θ_2 , the poles are completely overlapping. The inductance value at position θ_2 is equal to the maximum value L_a . From position θ_2 to θ_3 , there is a complete overlap of the rotor and stator poles as seen in Figure 2.1(c) and the inductance value remains constant at the maximum value of L_a . The angle $\theta_3 - \theta_2 = \beta_r - \beta_s$. From position θ_3 to position θ_4 , the rotor and stator pole overlap to some extent and as the rotor traverses this region, there is a steady decrease in inductance value. It can be seen clearly in Figure 2.1(d), that the angle $\theta_4 - \theta_3 = \beta_s$ and once the rotor reaches position θ_4 , the poles are unaligned. The inductance value at position θ_4 is equal to the minimum value L_u . The rotor then has to traverse an angle of $\theta_5 - \theta_4 = \frac{\pi}{N_r} - \frac{\beta_s}{2} - \frac{\beta_r}{2}$ to reach the fully unaligned position as represented in Figure 2.1(e).



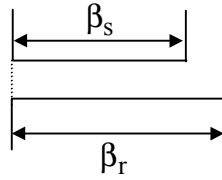
(a) Rotor position from unaligned position 0 to θ_1



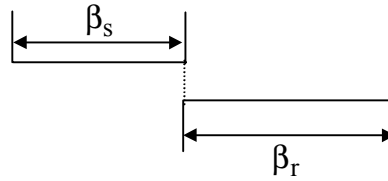
(b) Rotor position from position θ_1 to position θ_2



(c) Rotor position from position θ_2 to position θ_3



(d) Rotor position from position θ_3 to position θ_4



(e) Rotor position from position θ_4 to position θ_5

Figure 2.1. Schematic representing the traverse of rotor

The torque equation for a SRM under linear operating conditions (L is a function of position but not is constant for varying currents as shown in Figure 2.2) is given by

$$T_e = \frac{1}{2} i^2 \frac{dL}{d\theta} \quad (2.4)$$

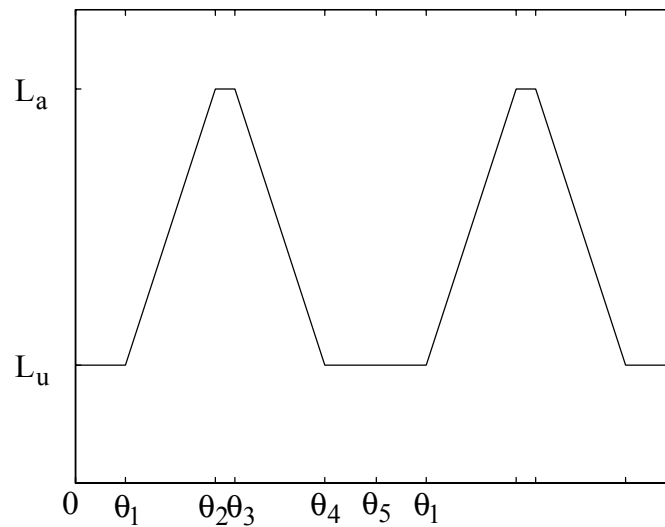


Figure 2.2. Ideal inductance vs. rotor position profile

From the torque equation it can be observed that a positive rate of change of inductance $\frac{dL}{d\theta}$ causes a positive torque to be produced. The examination of two successive phase inductance profiles can give a better insight on the torque generation and starting process.

Figure 2.3 shows the inductance of two successive phases a and b. It is observed that phase b reaches a maximum value of L_{ab} exactly ϵ degrees after phase a reaches its maximum value L_{aa} . Symbolically, $\theta_{1a} = \theta_1 + \epsilon$. It was also observed that $\theta_2 = \theta_1 + \beta_s$. Therefore, $\theta_2 = \theta_{1a} - \epsilon + \beta_s$. Now, if $\beta_s > \epsilon$, then $\theta_2 > \theta_{1a}$, which implies that phase b has a rising inductance before phase a reaches its maximum value and there will be no problems during starting as at all times, one of the phases has a rising inductance profile. If $\beta_s < \epsilon$, then $\theta_2 < \theta_{1a}$, which implies that phase b has a rising inductance only after phase a reaches its maximum value and there will be certain rotor positions when no phase has a rising inductance profile and this could cause problems during starting. Therefore, the requirement that the stator pole arc should be greater than the stroke angle is well justified.

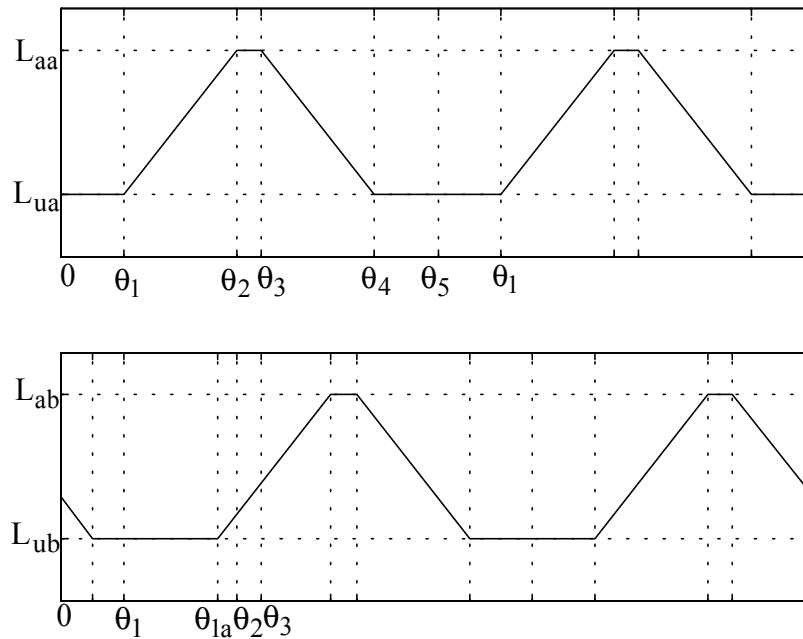


Figure 2.3. Inductance profiles vs. rotor position of two successive phases

3. The angle between the corners of adjacent rotor poles must be greater than the stator pole arc or there will be an overlap between the stator and rotor poles in the unaligned position. This condition is represented as

$$\frac{2\pi}{N_r} - \beta_r > \beta_s \quad (2.5)$$

The implication of this condition not being followed is that the machine will start having a positive inductance profile before reaching the minimum value. This causes the unaligned inductance value to be higher and leads to a lower torque generation. In a 8/6 machine,

$$\frac{2\pi}{6} > \beta_s + \beta_r.$$

The three conditions can be represented in a drawing to describe a feasible triangle. It is required that the machine rotor and stator pole angles lie in this triangle. Figure 2.4 shows the feasible triangle for a 8/6 machine. The region below OE represents condition 1, the region above GH represents condition 2 and the region below DF represents condition 3. For example, if $\beta_s = 20^\circ$, then $20^\circ < \beta_r < 40^\circ$.

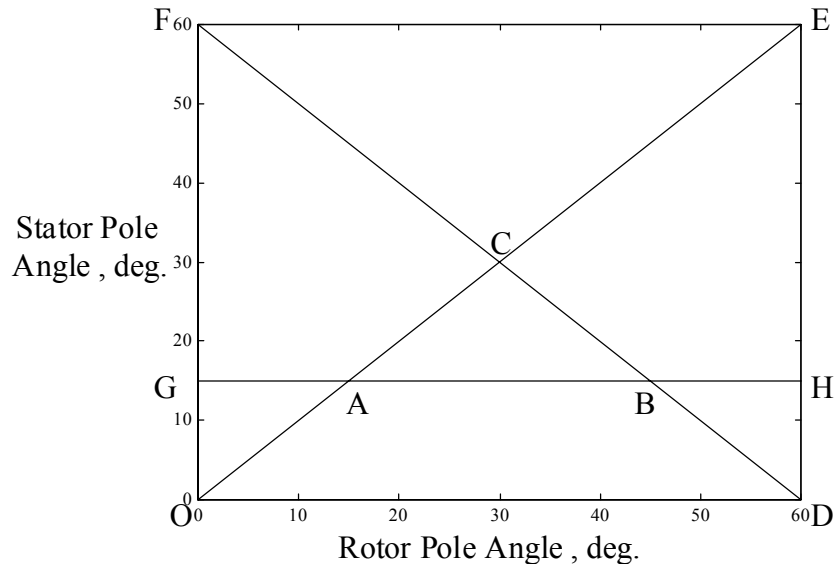


Figure 2.4. Diagram of the feasible triangle for a 8/6 machine

The feasible triangle only gives restrictions on the stator pole and rotor pole angle. It however does not give a way to predict the optimum pole angles. A procedure to obtain the optimum angles is described in [ARU88]. This method involves the calculation of torque for various pole angles and hence obtaining the optimum value of pole angle at the maximum torque angle. The calculation of torque however requires the design of the complete machine and successive iterations have to be performed to obtain the optimum value. The design process is continued with a preliminary selection of stator and rotor pole arcs and various conditions encountered in the design process will bring about changes in these values. The procedure to narrow the choices for the stator and rotor pole angles is described in a subsequent section dealing with the numerical design of a machine.

2.1.5 Preliminary Design Process

Once the outer diameter, pole numbers and preliminary pole arcs are fixed, the preliminary design of the bore diameter D and the stack length L form the next step in the design. The bore diameter is initially assumed to be equal to the frame size. The stack length can be initially chosen to be equal to the distance between the mounting holes in a foot mounted machine. With the selection of preliminary values of D_o , L , D , β_s and β_r , the design process is continued. Only D_o is fixed and can change only with the change of the entire frame size. At this point the shaft diameter D_{sh} can also be selected from the IEC regulations [IEC71] based on the required torque of the machine.

Now, the B-H characteristics of the material, which will be used in the stator and rotor stampings, has to be examined (Figure 2.5). The “knee” point of the characteristics is noted down and it is generally a good design practice to limit the maximum flux density (in Tesla) in any part of the machine to this value. It can be observed that the maximum flux density B_{max} will be at the stator poles and therefore while designing the machine, the stator pole can be assumed to be operating at a flux density equal to the knee value obtained from the B-H characteristics.

Assuming that the stator pole flux density B_s is assumed to be equal to B_{max} the rest of the machine can be designed. Design experience has shown that it is good practice to fix the flux density of the stator yoke B_y at approximately half the value of B_{max} and the rotor core flux density B_{rc} at about 80% of the maximum value. This practice causes a reduction of noise in the machine.

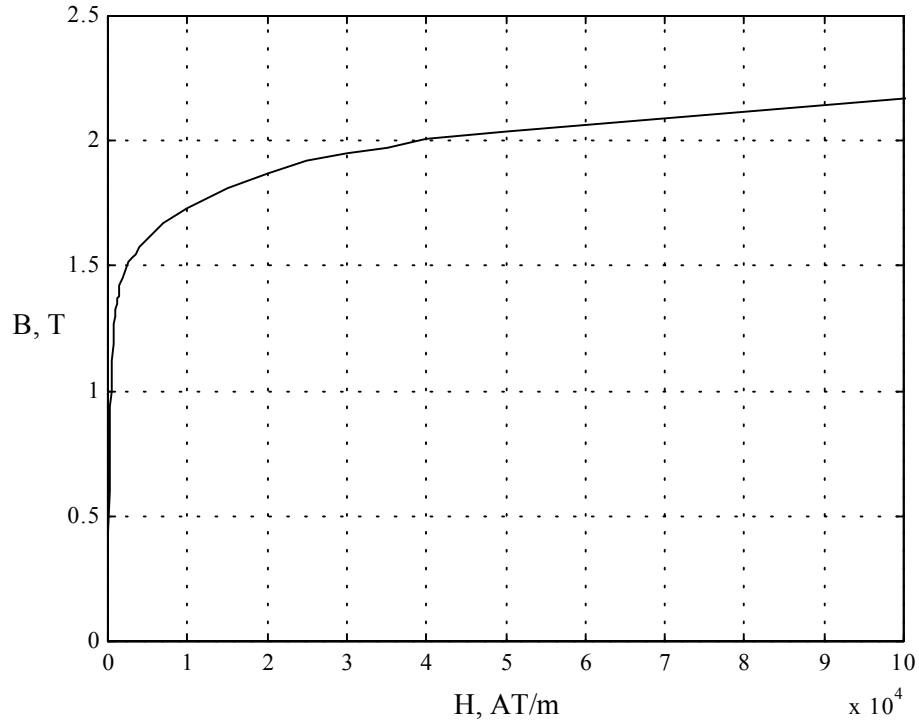


Figure 2.5 BH characteristics of DBII Steel

Neglecting leakage and stacking factor, the stator pole area A_s can be written as,

$$A_s = \frac{D}{2} L \beta_s \quad (2.6)$$

The flux in the stator pole ϕ is given by

$$\phi = B_s A_s \quad (2.7)$$

The flux in the yoke ϕ_y is given by

$$\phi_y = \frac{\phi}{2} = \frac{B_s A_s}{2} \quad (2.8)$$

Assuming that the yoke flux density B_y is half the stator flux density B_s , the yoke flux can be written as,

$$\phi_y = B_y A_y = \frac{B_s}{2} A_y \quad (2.9)$$

Comparing (2.8) and (2.9), the area of the yoke A_y can be set as,

$$A_y = A_s \quad (2.10)$$

The yoke area is the product of back iron thickness C and the stack length. Therefore, the back iron thickness is obtained as,

$$C = \frac{A_y}{L} \quad (2.11)$$

The stator pole height h_s is given by,

$$h_s = \frac{D_o}{2} - C - \frac{D}{2} \quad (2.12)$$

The rotor pole area A_r is given by,

$$A_r = \left(\frac{D}{2} - g \right) L \beta_r \quad (2.13)$$

The rotor pole flux density B_r is given by,

$$B_r = \frac{B_s A_s}{A_r} \quad (2.14)$$

The area of the rotor core A_{rc} is given by,

$$A_{rc} = L \left(\frac{D}{2} - g - h_r - \frac{D_{sh}}{2} \right) \quad (2.15)$$

where g is the length of the air-gap and h_r is the height of the rotor pole. The length of g is kept as small as possible as its effect on torque generation is well documented [KRI95]. The rotor core carries half the flux and is limited to a flux density of approximately 80% of the maximum value. Hence,

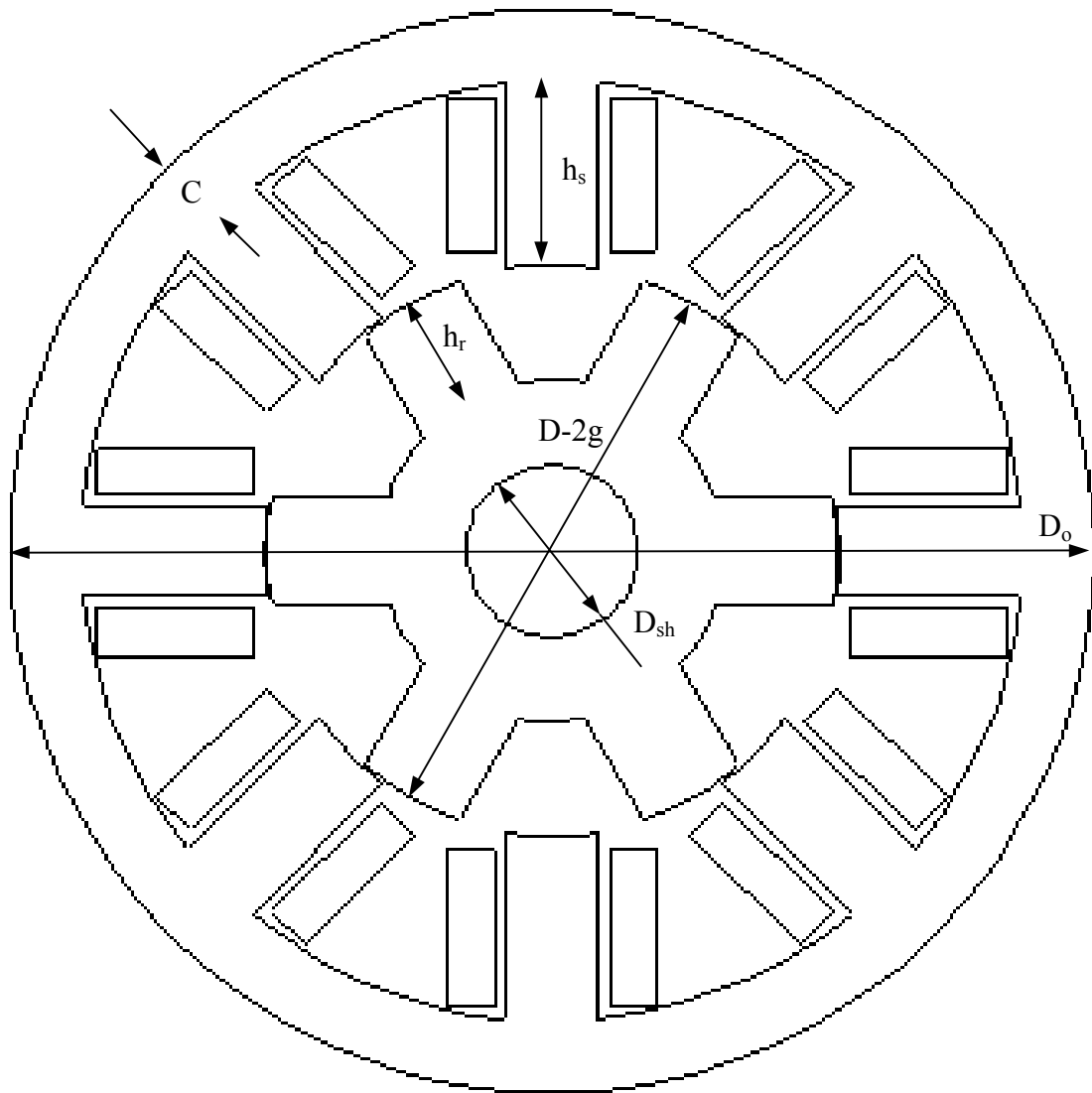


Figure 2.6 8/6 SRM Schematic

$$\phi_{rc} = \frac{\phi}{2} = \frac{B_s A_s}{2} \quad (2.16)$$

Also, the rotor core flux density B_{rc} can be written as,

$$\phi_{rc} = B_{rc} A_{rc} = 0.8 B_s A_{rc} \quad (2.17)$$

Comparing (2.16) and (2.17), the area of the rotor core is calculated as,

$$A_{rc} = \frac{A_s}{1.6} \quad (2.18)$$

The height of the rotor pole h_r is obtained from (2.15) as,

$$h_r = \frac{D}{2} - g - \frac{D_{sh}}{2} - \frac{A_{rc}}{L} \quad (2.19)$$

The average area of A_g is calculated as,

$$A_g = \frac{A_s + A_r}{2} = \frac{L}{2} \left(\beta_s \frac{D}{2} + \beta_r \left(\frac{D}{2} - g \right) \right) \quad (2.20)$$

The reluctance the air gap is given by,

$$\mathfrak{R}_g = \frac{2l_g}{\mu_o A_g} \quad (2.21)$$

The permeance of the air gap is calculated as,

$$P_a = \frac{\mu_o A_{airgap}}{l_{airgap}} \quad (2.22)$$

The mean path lengths of various sections are given as follows:

$$l_s = h_s + \frac{C}{2} \quad (2.23)$$

$$l_g = g \quad (2.24)$$

$$l_r = h_r + \frac{\frac{D}{2} - g - h_r - \frac{D_{sh}}{2}}{2} = \frac{D}{4} - \frac{g}{2} + \frac{h_r}{2} - \frac{D_{sh}}{4} \quad (2.25)$$

$$l_{rc} = \pi \left(\frac{\frac{D}{2} - g - h_r - \frac{D_{sh}}{2}}{2} + \frac{D_{sh}}{2} \right) = \pi \left(\frac{D}{4} - \frac{g}{2} - \frac{h_r}{2} + \frac{D_{sh}}{4} \right) \quad (2.26)$$

The mean length l_y for a circular yoke SRM which is shown in Figure 2.6

$$l_y = \pi \left(\frac{D_o}{2} - \frac{C}{2} \right) \quad (2.27)$$

Using the B-H characteristics for the material used for the laminations, the magnetic field intensity in Ampere-turns per meter for each portion of the machine except the air-gap is obtained. The magnetic field intensities in the stator pole, stator yoke, rotor pole and rotor core are designated as H_s , H_y , H_r and H_{rc} , respectively.

The flux density in the air-gap B_g is given by,

$$B_g = \frac{A_s B_s}{A_g} \quad (2.28)$$

The magnetic field intensity of the air-gap H_g is calculated as,

$$H_g = \frac{B_g}{4\pi * 10^{-7}} \quad (2.29)$$

The magnetic circuit of the SRM is shown in Figure 2.7. The reluctances of the stator pole, yoke, rotor pole, rotor core and air-gap are represented by \mathfrak{R}_s , \mathfrak{R}_y , \mathfrak{R}_r , \mathfrak{R}_{rc} and \mathfrak{R}_g , respectively. The lumped parameter \mathfrak{R}_L in Figure 2.8 is obtained as,

$$\mathfrak{R}_L = 2(\mathfrak{R}_s + \mathfrak{R}_g + \mathfrak{R}_r) + \frac{\mathfrak{R}_{rc}}{2} \quad (2.30)$$

The reluctance \mathfrak{R} in a particular section can be represented as

$$\mathfrak{R} = \frac{H \cdot l}{BA} = \frac{H \cdot l}{\phi} \quad (2.31)$$

where, H is the magnetic field intensity, l is the mean path length in the section, B is the flux density in the section, A is the area of the section and ϕ is the flux in the section. For the magnetic circuit in Figure 2.7, the magnetic circuit equation can be written as,

The magnetic circuit equation of aligned inductance can be written as,

$$\mathfrak{S}_{aligned} = T_{phi} i = \mathfrak{R}_L \phi = 2(H_s l_s + H_r l_r) + \frac{B_g A_g}{\mu_0} + H_{rc} l_{rc} + H_y l_y \quad (2.32)$$

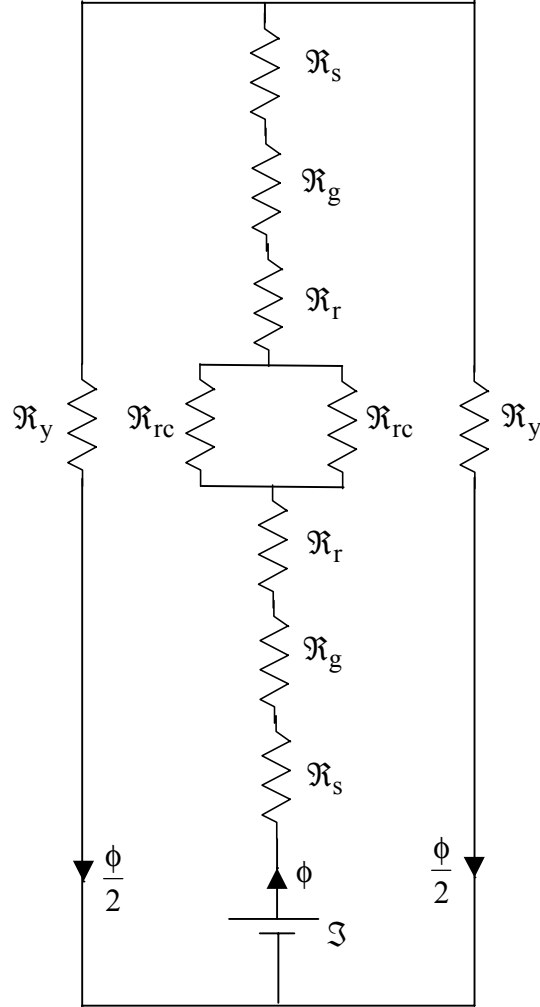


Figure 2.7. Magnetic Circuit of the SRM

Now, the total ampere-turns \mathcal{I} required for the machine operation at full load can be calculated. It is also known that $\mathcal{I} = T_{ph}i$. Since the peak current i_p is assumed initially, the turns per phase T_{ph} can be calculated. The aligned inductance at maximum current is calculated as,

$$L_{aligned} = \frac{T_{ph}\phi}{i} = \frac{\mathcal{I}B_s A_s}{i_p^2} \quad (2.33)$$

The effects of leakage can also be calculated. The leakage tube is shown in Figure 2.19. The area of the leakage tube is assumed as,

$$A_f = \frac{3h_s}{4} L \quad (2.34)$$

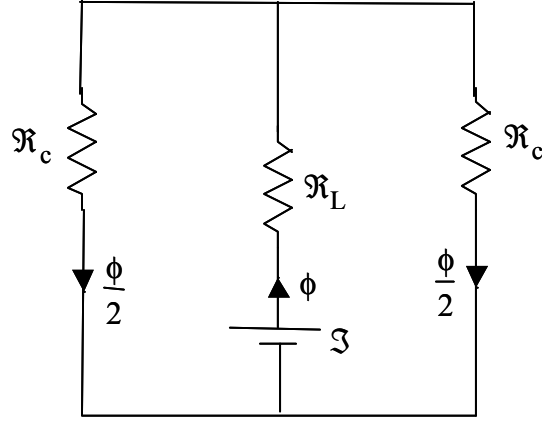


Figure 2.8. Simplified Magnetic Circuit of the SRM

The length is approximately calculated as,

$$l_f = \frac{3h_s \pi}{4 \cdot 2} \quad (2.35)$$

The yoke area is obtained from (2.11) as,

$$A_y = CL. \quad (2.36)$$

The area of the stator pole is given as

$$A_{sf} = \frac{3h_s}{4} L \quad (2.37)$$

The length of the path in the stator is calculated as,

$$l_s = \frac{1}{2} \frac{3h_s}{4} + \frac{C}{2} \quad (2.38)$$

The yoke length is approximately,

$$l_y = \frac{1}{2} \frac{3h_s}{4} \quad (2.39)$$

The reluctance the leakage tube is given by,

$$\mathfrak{R}_f = \frac{l_f}{\mu_o A_f} \quad (2.40)$$

The permeance of the air gap is calculated as,

$$P_f = \frac{1}{\mathfrak{R}_f} \quad (2.41)$$

The magnetic circuit equation of leakage tube can be written as,

$$\mathfrak{S}_f = \frac{1}{2} \frac{3}{4} T_{ph} i = \mathfrak{R}_L \phi = H_s l_s + \frac{B_s A_{sf}}{P_f} + H_y l_y \quad (2.42)$$

The inductance of the leakage tube is then calculated as,

$$L_{af} = \mathfrak{S}_f \frac{B_s \min A_{sf}}{i_p^2} \quad (2.43)$$

The leakage inductance above is calculated for one tube. There are 4 such tubes as can be seen in Figure 2.9. The total aligned inductance is therefore given by,

$$L_a = L_{aligned} + 4L_{af} \quad (2.44)$$

2.1.6 Winding Design

The calculations leading to the selection of the conductor and the winding design are as follows.

Assuming a wedge of h_{wedge} is required to hold the windings in place, the stator pole arc length t_s at the closest point of the winding to the center of the shaft is given by

$$t_s = \left(\frac{D}{2} + h_{wedge} \right) \beta_s \quad (2.45)$$

Accounting for the wedges that hold the windings in place leads to the calculation of a modified stator pole pitch λ_s as,

$$\lambda_s = \frac{\pi D}{N_s} + \frac{\pi(2 * h_{wedge})}{N_s} \quad (2.46)$$

Assuming a maximum value of allowable current density J in the windings, the minimum area of conductor is given as,

$$a_c = \frac{i}{2J} \quad (2.47)$$

Now a standard size conductor is chosen based on the value of a_c calculated above.

The wire diameter d_w including insulation is given by

$$d_w = \sqrt{\frac{4a_c}{\pi}} + 0.1 \text{ mm.} \quad (2.48)$$

The maximum height of the winding h_w which can be accommodated inclusive of the space required to place wedges that hold the windings in place is given by

$$h_w = h_s - h_{\text{wedge}} \quad (2.49)$$

The number of layers that can be accommodated in this available winding height is given by

$$N_v = \frac{h_w f_f}{d_w} \quad (2.50)$$

f_f represents the field factor and is approximately equal to 0.95. The value of N_v is rounded off to the nearest lower integer.

Now the number of horizontal layers required for winding is given by

$$N_h = \frac{T_{ph}}{2N_v} + 1 \quad (2.51)$$

The value of N_h is rounded off to the nearest higher integer.

The width of the winding W_t is given by

$$W_t = \frac{d_w N_h}{f_f} \quad (2.52)$$

The space between 2 stator pole tips at the bore is given by

$$Z = \lambda_s - t_s \quad (2.53)$$

The clearance between the windings at the bore is given by

$$Cl = Z - 2W_t \quad (2.54)$$

This value has to be positive and preferably greater than 3 mm. Naturally, the actual clearance the actual clearance between the windings will be slightly higher than the clearance calculated at

the bore. If the clearance value is acceptable, the designer can proceed with the analysis or else a different size conductor can be chosen and the clearance can be checked again.

2.1.7 Calculation of Minimum Inductance

Although [COR79], [MAT89] and [RAD94] give equations for calculating minimum inductance, the equations cannot be easily verified. The best way to calculate the minimum inductance is to plot the equiflux tubes for a test machine in the unaligned rotor position and calculate the lengths of the equiflux lines in vacuum and then account for the paths in the iron portions. Figure 2.9 shows the equiflux lines in the unaligned position.

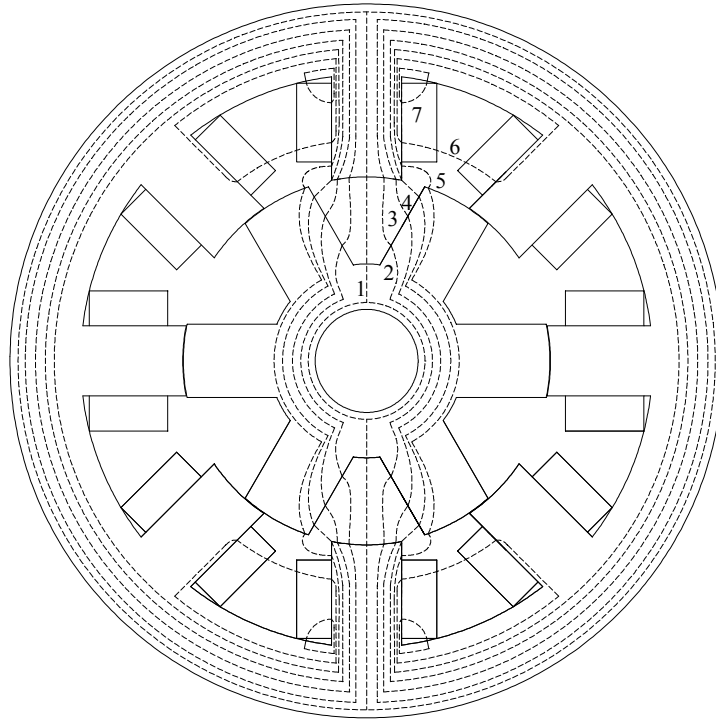


Figure 2.9 Identification of 7 flux tubes for analytical calculation of unaligned inductance

Tube 1: To calculate the length l_1 and area A_1 , consider Figure 2.10. The area of the tube at the stator pole is calculated as,

$$A_{1s} = \frac{\beta_s}{4} \frac{D}{2} L \quad (2.55)$$

The arc subtended by half of the rotor pole is given by,

$$\frac{\beta_r}{2} \left(\frac{D}{2} - g \right) \quad (2.56)$$

The angle θ_2 is given by,

$$\theta_2 = \frac{\frac{\beta_r}{2} \left(\frac{D}{2} - g \right)}{\left(\frac{D}{2} - g - h_r \right)} \quad (2.57)$$

The rotor pole pitch is defined as

$$\theta_{rp} = \frac{2\pi}{N_r} \quad (2.58)$$

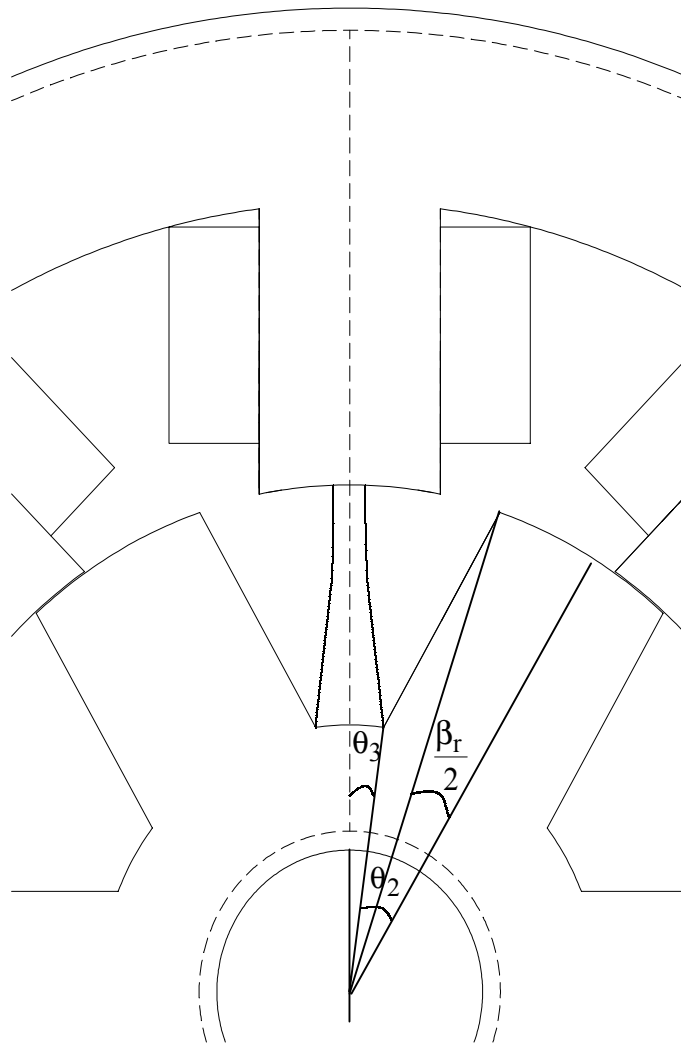


Figure 2.10 Tube 1 calculations

The angle θ_3 is calculated as,

$$\theta_3 = \frac{\theta_{rp}}{2} - \theta_2 \quad (2.59)$$

The area of the tube at the rotor core is calculated,

$$A_{1r} = 2 \left(\frac{D}{2} - g - h_r \right) \theta_3 L \quad (2.60)$$

The average area of the air gap A_1 is calculated as,

$$A_1 = \frac{A_{1s} + A_{1r}}{2} = \frac{1}{2} \frac{\beta_s}{4} \frac{D}{2} L + \left(\frac{D}{2} - g - h_r \right) \theta_3 L \quad (2.61)$$

The length of the air gap is given as,

$$l_1 = \frac{D}{2} - g - h_r \quad (2.62)$$

The length of the path through the stator and yoke are given by (2.23) and (2.27). The area of the rotor core and yoke is given by (2.15) and (2.36) and the length of the path through the rotor core is given by (2.26).

The reluctance of tube 1 in the air gap is given by,

$$\mathfrak{R}_1 = \frac{2l_1}{\mu_0 A_1} \quad (2.63)$$

The permeance of tube 1 is calculated as,

$$P_1 = \frac{1}{\mathfrak{R}_1} \quad (2.64)$$

Using the B-H characteristics for the material used for the laminations, the magnetic field intensity in Ampere-turns per meter for each portion of the machine except the air-gap is obtained. The magnetic field intensities in the stator pole, stator yoke, rotor pole and rotor core are designated as H_s , H_y , H_r and H_{rc} , respectively.

Referring to Figure 2.11, the magnetic circuit equation of tube 1 can be written as,

$$\mathfrak{S}_1 = T_{ph} i = \mathfrak{R}_L \phi + \frac{\mathfrak{R}_c \phi}{2} = 2(H_s l_s) + \frac{B_s A_{1s}}{P_1} + \frac{H_{rc} l_{rc}}{2} + \frac{H_y l_y}{2} \quad (2.65)$$

Since the LHS is known, the RHS can be calculated initially by setting $B_{sp} = B_{max}$. If the RHS is greater than the LHS, the value of the stator flux density can be reduced and the other flux densities can be calculated at this reduced value and the magnetic field intensities can be calculated. This process is repeated till the RHS equals the LHS and the stator flux density is obtained as B_{smin} .

The unaligned inductance of tube 1 is then calculated as,

$$L_{u1} = \mathfrak{S}_1 \frac{B_{smin} A_{1s}}{i_p^2} . \quad (2.66)$$

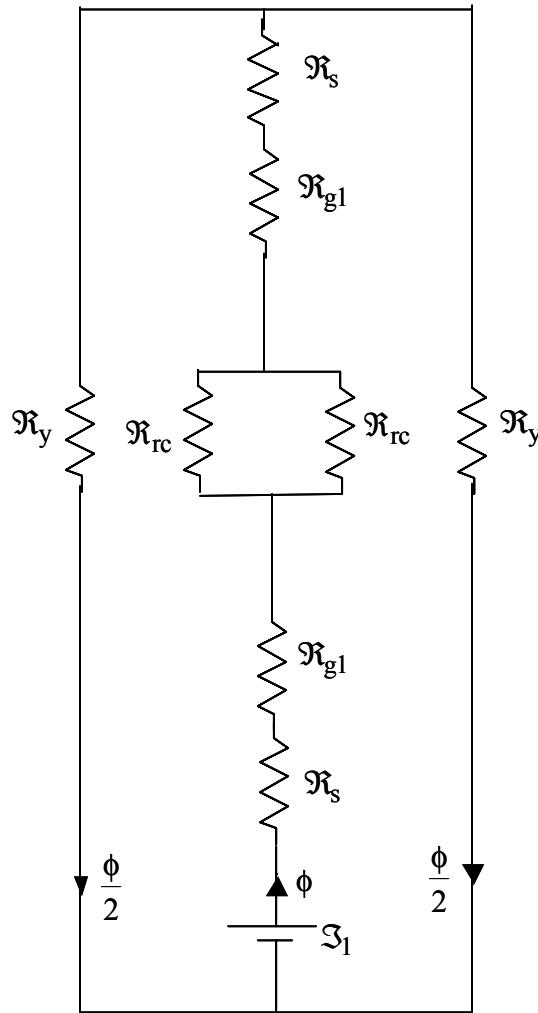


Figure 2.11 Reluctance circuit for Tube 1

Tube 2: To calculate the length l_2 and area A_2 , consider Figure 2.12. The area of the tube at the stator pole is calculated as,

$$A_{2s} = \frac{\beta_s D}{4} \frac{D}{2} L \quad (2.67)$$

The area of the tube at the rotor pole is calculated,

$$A_{2r} = \frac{h_r}{2} L \quad (2.68)$$

The average area of A_2 is calculated as,

$$A_2 = \frac{A_{2s} + A_{2r}}{2} = \frac{L}{2} \left(\frac{\beta_s D}{4} \frac{D}{2} + \frac{h_r}{2} \right) \quad (2.69)$$

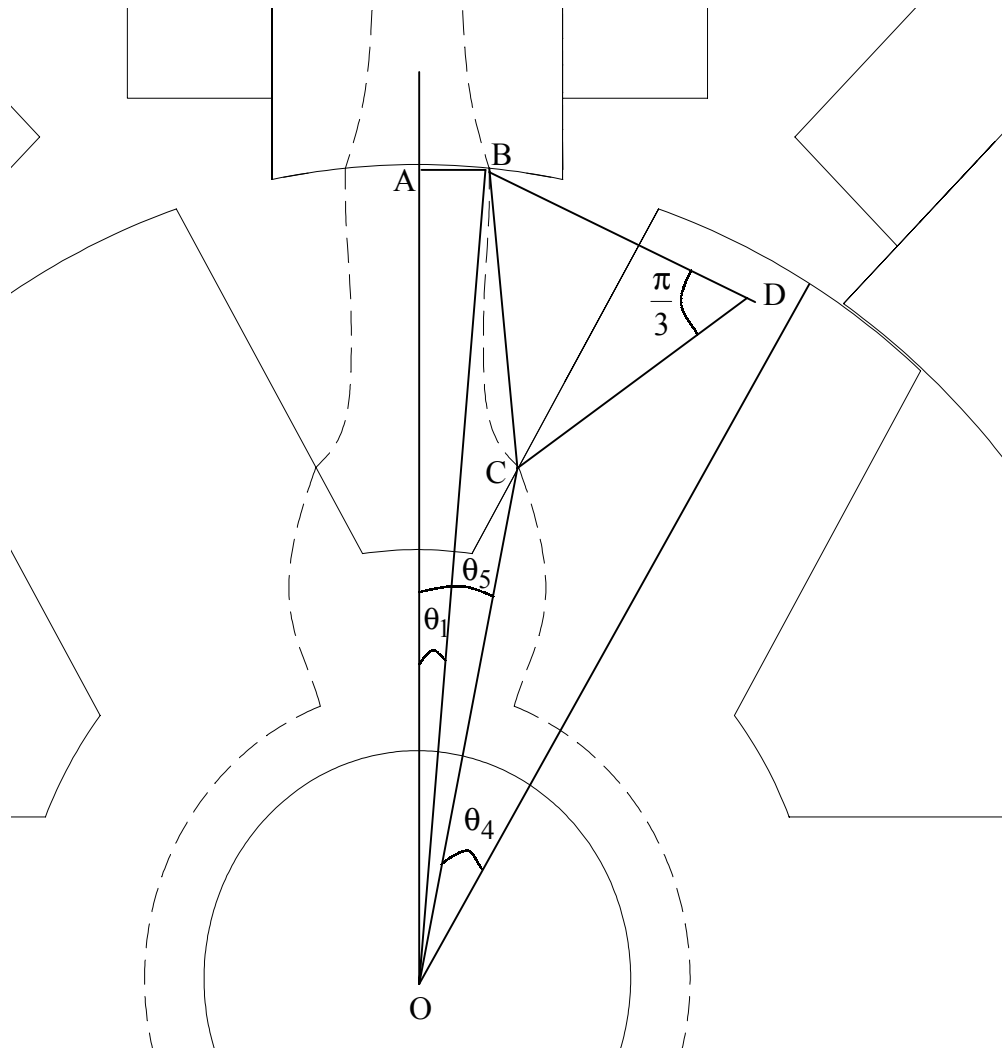


Figure 2.12 Tube 2 Calculations

The angle θ_1 is assumed to be $\frac{\beta_s}{4}$. The length AB is calculated as $x_1 = \frac{D}{2} \sin(\theta_1)$. The length

OA is calculated as $y_1 = \frac{D}{2} \cos(\theta_1)$. Considering that point B has the coordinates as,

$$(x_1, y_1) = \left(\left(\frac{D}{2} \right) \sin \left(\frac{\beta_s}{4} \right), \left(\frac{D}{2} \right) \cos \left(\frac{\beta_s}{4} \right) \right). \quad (2.70)$$

The angle θ_4 is given by,

$$\theta_4 = \frac{\frac{\beta_r}{2} \left(\frac{D}{2} - g \right)}{\left(\frac{D}{2} - g - \frac{3}{4} h_r \right)} \quad (2.71)$$

The angle θ_5 is calculated as,

$$\theta_5 = \frac{\theta_{rp}}{2} - \theta_4 \quad (2.72)$$

The point C is given in coordinate form with respect to point O as,

$$(x_2, y_2) = \left(\left(\frac{D}{2} - g - \frac{3h_r}{4} \right) \sin \theta_5, \left(\frac{D}{2} - g - \frac{3h_r}{4} \right) \cos \theta_5 \right) \quad (2.73)$$

The linear distance between the points B and C, is assumed to be one side of an equilateral triangle and forms the radius of the arc formed by tube 2. From (2.70) and (2.73), this length is given as follows,

$$l_{x2} = \sqrt{(x_2 - x_1)^2 + (y_2 - y_1)^2} \quad (2.74)$$

the length of the tube is given by,

$$l_2 = l_{x2} \frac{\pi}{3}. \quad (2.75)$$

The area of the yoke and rotor core is given by (2.36) and (2.15) respectively. The length of the path through the stator and yoke are given by (2.23) and (2.27). The length of the path through the rotor core is given by,

$$l_{rc} = \frac{2}{3} \pi \left(\frac{\frac{D}{2} - g - h_r - \frac{D_{sh}}{2}}{2} + \frac{D_{sh}}{2} \right) = \frac{2}{3} \pi \left(\frac{D}{4} - \frac{g}{2} - \frac{h_r}{2} + \frac{D_{sh}}{4} \right) \quad (2.76)$$

The length of the path through the rotor,

$$l_r = \frac{h_r}{4} \quad (2.77)$$

The reluctance of tube 2 in the air gap is given by,

$$\mathfrak{R}_2 = \frac{2l_2}{\mu_0 A_2} \quad (2.78)$$

The permeance of tube 2 is calculated as,

$$P_2 = \frac{1}{\mathfrak{R}_2} \quad (2.79)$$

Referring to Figure 2.13, the magnetic circuit equation of tube 2 can be written as,

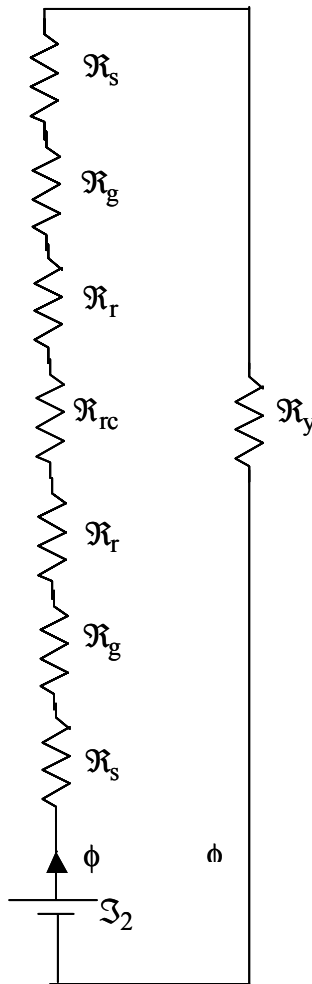


Figure 2.13 Equivalent reluctance circuit

$$\mathfrak{S}_2 = T_{ph} i = \mathfrak{R}_L \phi = 2(H_s l_s + H_r l_r) + \frac{B_s A_{2s}}{P_2} + H_{rc} l_{rc} + H_y l_y \quad (2.80)$$

The unaligned inductance of tube 2 is then calculated as,

$$L_{u2} = \mathfrak{S}_2 \frac{B_s \min A_{2s}}{i_p^2} \quad (2.81)$$

Tube 3: To calculate the length l_3 and area A_3 , consider Figure 2.14. The area of the tube at the stator pole is calculated as,

$$A_{3s} = \frac{3 \beta_s D}{4 \cdot 8 \cdot 2} L \quad (2.82)$$

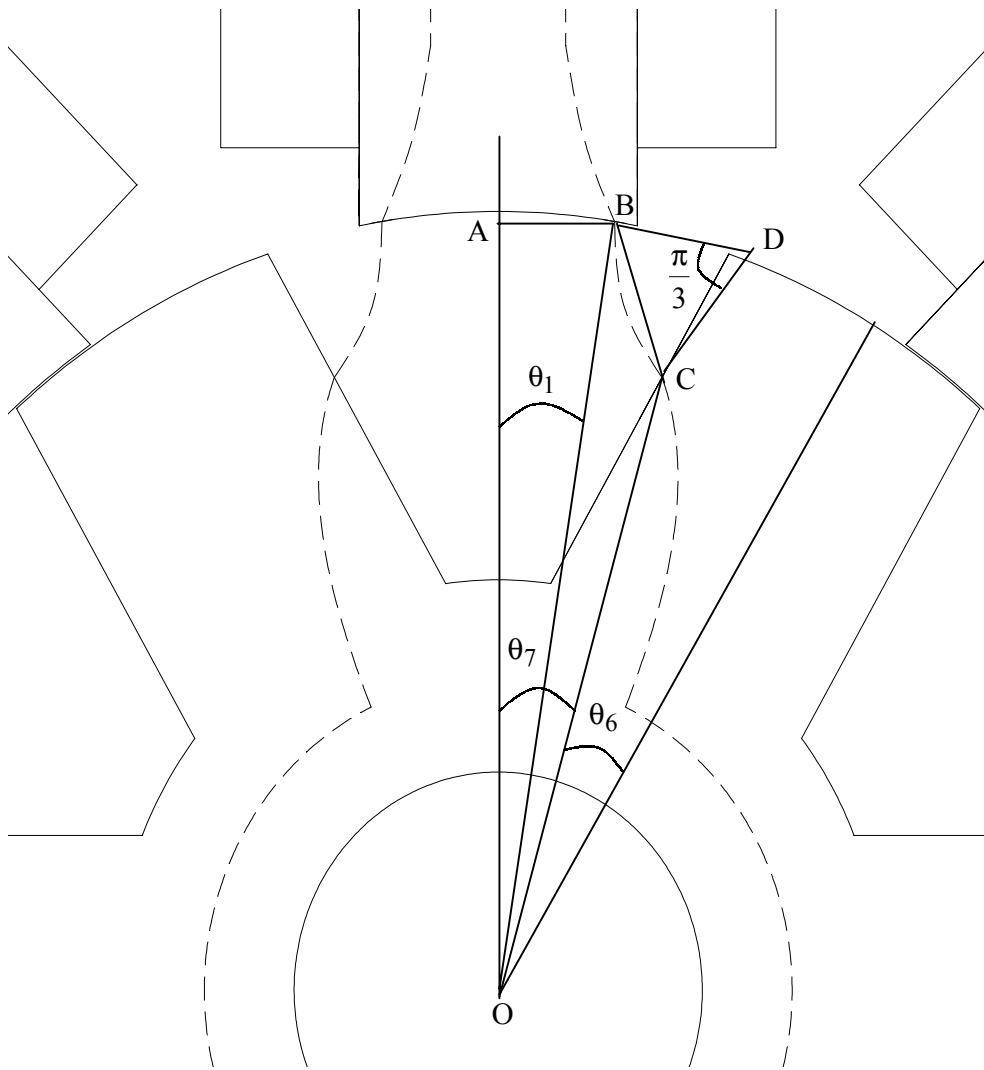


Figure 2.14 Tube 3 Calculations

The area of the tube at the rotor pole is calculated,

$$A_{3r} = \frac{h_r}{4} L \quad (2.83)$$

The average area of A_3 is calculated as,

$$A_3 = \frac{A_{3s} + A_{3r}}{2} = \frac{L}{2} \left(\frac{3\beta_s D}{4} + \frac{h_r}{2} \right) \quad (2.84)$$

The angle θ_1 is assumed to be $\frac{27\beta_s}{64}$. The length AB is calculated as $x_1 = \frac{D}{2} \sin(\theta_1)$. The length

OA is calculated as $y_1 = \frac{D}{2} \cos(\theta_1)$. Considering that, point B has the coordinates as,

$$(x_1, y_1) = \left(\left(\frac{D}{2} \right) \sin \left(\frac{27\beta_s}{64} \right), \left(\frac{D}{2} \right) \cos \left(\frac{27\beta_s}{64} \right) \right) \quad (2.85)$$

The angle θ_6 is given by,

$$\theta_6 = \frac{\frac{\beta_r}{2} \left(\frac{D}{2} - g \right)}{\left(\frac{D}{2} - g - \frac{3}{8} h_r \right)} \quad (2.86)$$

The angle θ_7 is calculated as,

$$\theta_7 = \frac{\theta_{rp}}{2} - \theta_6 \quad (2.87)$$

The point C is given in coordinate form with respect to point O as,

$$(x_2, y_2) = \left(\left(\frac{D}{2} - g - \frac{3h_r}{8} \right) \sin \theta_7, \left(\frac{D}{2} - g - \frac{3h_r}{8} \right) \cos \theta_7 \right) \quad (2.88)$$

The linear distance between the points B and C, is assumed to be one side of an equilateral triangle and forms the radius of the arc formed by tube 3. From (2.85) and (2.88) this length is given as follows,

$$l_{x3} = \sqrt{(x_2 - x_1)^2 + (y_2 - y_1)^2} \quad (2.89)$$

the length of the tube is given by,

$$l_3 = l_{x3} \frac{\pi}{3} \quad (2.90)$$

The area of the yoke and rotor core is given by (2.36) and (2.15) respectively. The length of the path through the stator, yoke and rotor core are given by (2.23), (2.27) and (2.76) respectively. The length of the path in the rotor is calculated as,

$$l_r = \frac{h_r}{2} + \frac{h_r}{8} = \frac{5h_r}{8}. \quad (2.91)$$

The reluctance of tube 3 in the air gap is given by,

$$\mathfrak{R}_3 = \frac{2l_3}{\mu_0 A_3} \quad (2.92)$$

The permeance of tube 3 is calculated as,

$$P_3 = \frac{1}{\mathfrak{R}_3} \quad (2.93)$$

Referring to Figure 2.13, the magnetic circuit equation of tube 3 can be written as,

$$\mathfrak{S}_3 = T_{ph} i = \mathfrak{R}_L \phi = 2(H_s l_s + H_r l_r) + \frac{B_s A_{3s}}{P_3} + H_{rc} l_{rc} + H_y l_y \quad (2.94)$$

The unaligned inductance of tube 3 is then calculated as,

$$L_{u3} = \mathfrak{S}_3 \frac{B_s \min A_{3s}}{i_p^2}. \quad (2.95)$$

Tube 4: To calculate the length l_4 and area A_4 , consider Figure 2.14. The area of the tube at the stator pole is calculated as,

$$A_{4s} = \frac{1}{4} \frac{\beta_s}{8} \frac{D}{2} L + \frac{1}{4} \frac{h_s}{4} L \quad (2.96)$$

The area of the tube at the rotor pole is calculated,

$$A_{4r} = \frac{h_r}{4} L \quad (2.97)$$

The average area of A_4 is calculated as,

$$A_4 = \frac{A_{4s} + A_{4r}}{2} = \frac{L}{2} \left(\frac{1}{4} \frac{\beta_s}{8} \frac{D}{2} + \frac{1}{4} \frac{h_s}{4} + \frac{h_r}{4} \right) \quad (2.98)$$

Tube 4 can be assumed to be a straight line between points B and C. The angle θ_1 is assumed to be,

$$\theta_1 = \frac{\beta_s}{2}. \tag{2.99}$$

The length AB is calculated as $x_1 = \frac{D}{2} \sin(\theta_1)$. The length OA is calculated as $y_1 = \frac{D}{2} \cos(\theta_1)$.

Considering that point B has the coordinates as,

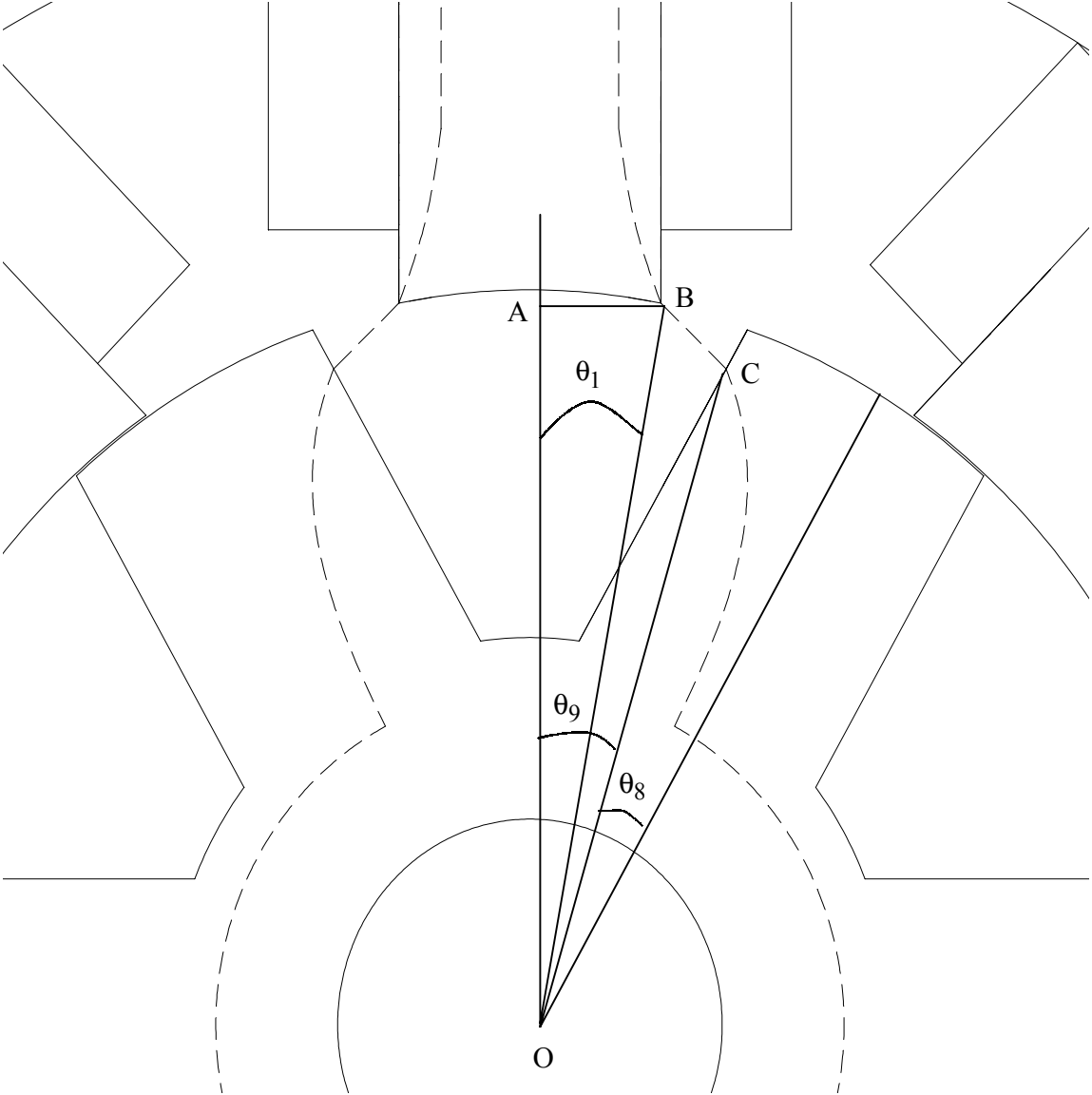


Figure 2.15 Tube 4 Calculations

$$(x_1, y_1) = \left(\left(\frac{D}{2} \right) \sin \left(\frac{\beta_s}{2} \right), \left(\frac{D}{2} \right) \cos \left(\frac{\beta_s}{2} \right) \right). \quad (2.100)$$

The angle θ_8 is given by,

$$\theta_8 = \frac{\frac{\beta_r}{2} \left(\frac{D}{2} - g \right)}{\left(\frac{D}{2} - g - \frac{1}{8} h_r \right)} \quad (2.101)$$

The angle θ_9 is calculated as,

$$\theta_9 = \frac{\theta_{rp}}{2} - \theta_8 \quad (2.102)$$

The point C is given in coordinate form with respect to point O as,

$$(x_2, y_2) = \left(\left(\frac{D}{2} - g - \frac{h_r}{8} \right) \sin \theta_5, \left(\frac{D}{2} - g - \frac{h_r}{8} \right) \cos \theta_5 \right) \quad (2.103)$$

From (2.100) and (2.103), the linear distance between the points B and C, is given as follows,

$$l_4 = \sqrt{(x_2 - x_1)^2 + (y_2 - y_1)^2} \quad (2.104)$$

The area of the yoke and rotor core is given by (2.36) and (2.15) respectively. The length of the path through the stator, yoke and rotor core are given by (2.23), (2.27) and (2.76) respectively.

The length of the path in the rotor is calculated as,

$$l_r = \frac{3h_r}{4} + \frac{h_r}{8} = \frac{7h_r}{8}. \quad (2.105)$$

The reluctance of tube 4 in the air gap is given by,

$$\mathfrak{R}_4 = \frac{2l_4}{\mu_o A_4} \quad (2.106)$$

The permeance of tube 4 is calculated as,

$$P_4 = \frac{1}{\mathfrak{R}_4} \quad (2.107)$$

Referring to Figure 2.13, the magnetic circuit equation of tube 4 can be written as,

$$\mathfrak{S}_4 = T_{ph}i = \mathfrak{R}_L \phi = 2(H_s l_s + H_r l_r) + \frac{B_s A_{4s}}{P_4} + H_{rc} l_{rc} + H_y l_y \tag{2.108}$$

The unaligned inductance of tube 4 is then calculated as,

$$L_{u4} = \mathfrak{S}_4 \frac{B_s \min A_{4s}}{i_p^2} . \tag{2.109}$$

Tube 5: To calculate the length l_5 and area A_5 , consider Figure 2.16. The area of the tube at the stator pole is calculated as,

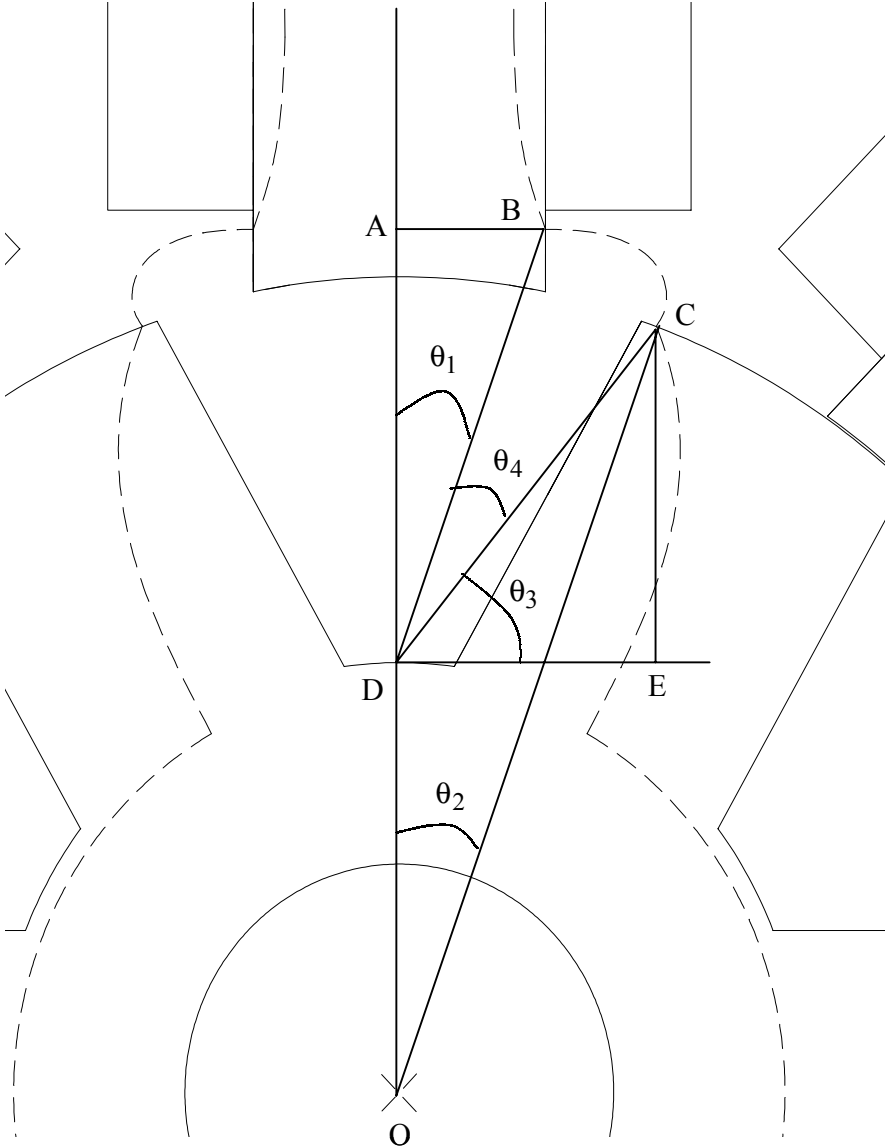


Figure 2.16 Tube 5 Calculations

$$A_{5s} = \frac{3}{4} \frac{h_s}{4} L \quad (2.110)$$

The area of the tube at the rotor pole is calculated,

$$A_{5r} = \frac{\beta_r}{8} L \left(\frac{D}{2} - g \right) \quad (2.111)$$

The average area of A_5 is calculated as,

$$A_5 = \frac{A_{5s} + A_{5r}}{2} = \frac{L}{2} \left(\frac{3}{4} \frac{h_s}{4} + \frac{\beta_r}{8} \left(\frac{D}{2} - g \right) \right) \quad (2.112)$$

Tube 5 can be assumed to be an arc centered at the point D. The length AO is assumed to be,

$$y_1 = \frac{D}{2} \cos \left(\frac{\beta_s}{2} \right) + \frac{5h_s}{32}. \quad (2.113)$$

The length AB is equal to

$$x_1 = \frac{D}{2} \sin \left(\frac{\beta_s}{2} \right). \quad (2.114)$$

The angle θ_1 can be calculated from (2.113) and (2.114) as,

$$\theta_1 = \tan^{-1} \left(\frac{x_1}{y_1 - \left(\frac{D}{2} - g - h_r \right)} \right). \quad (2.115)$$

The angle θ_2 is assumed to be,

$$\theta_2 = \frac{\pi}{N_r} - \frac{7\beta_r}{16}. \quad (2.116)$$

The length CE is given by,

$$y_2 = \left(\frac{D}{2} - g \right) \cos(\theta_2) - \left(\frac{D}{2} - g - h_r \right). \quad (2.117)$$

The length DE is given by,

$$x_2 = \left(\frac{D}{2} - g \right) \sin(\theta_2). \quad (2.118)$$

The angle θ_3 can be calculated from (2.117) and (2.118) as,

$$\theta_3 = \tan^{-1} \left(\frac{y_2}{x_2} \right). \quad (2.119)$$

The angle θ_4 is obtained from (2.115) and (2.119) as

$$\theta_4 = \frac{\pi}{2} - \theta_1 - \theta_3. \quad (2.120)$$

The length DB is given by

$$r_1 = \frac{x_1}{\sin(\theta_1)}. \quad (2.121)$$

The length CD is given from (2.117) and (2.118) as

$$r_2 = \sqrt{x_2^2 + y_2^2}. \quad (2.122)$$

The length of the flux path is approximately given from (2.120) – (2.122) as,

$$l_5 = \frac{r_1 + r_2}{2} \theta_4. \quad (2.123)$$

The area of the yoke and rotor core is given by (2.36) and (2.15) respectively. The lengths of the path through the yoke and rotor core are given by (2.27) and (2.76) respectively. The length of the path in the rotor is calculated as,

$$l_r = h_r. \quad (2.124)$$

The length of the path in the stator is calculated as,

$$l_s = h_s + \frac{C}{2} - \frac{3}{8} \frac{h_s}{4} \quad (2.125)$$

The reluctance of tube 5 in the air gap is given by,

$$\mathfrak{R}_5 = \frac{2l_5}{\mu_0 A_5} \quad (2.126)$$

The permeance of tube 5 is calculated as,

$$P_5 = \frac{1}{\mathfrak{R}_5} \quad (2.127)$$

Referring to Figure 2.13, the magnetic circuit equation of tube 5 can be written as,

$$\mathfrak{S}_5 = T_{ph} i = \mathfrak{R}_L \phi = 2(H_s l_s + H_r l_r) + \frac{B_s A_{5s}}{P_5} + H_{rc} l_{rc} + H_y l_y \quad (2.128)$$

The unaligned inductance of tube 5 is then calculated as,

$$L_{u5} = \mathfrak{S}_5 \frac{B_s \min A_{5s}}{i_p^2}. \quad (2.129)$$

Tube 6: To calculate the length l_6 and area A_6 , consider Figure 2.17. The area of the tube is calculated as,

$$A_6 = \frac{h_s}{4} L \quad (2.130)$$

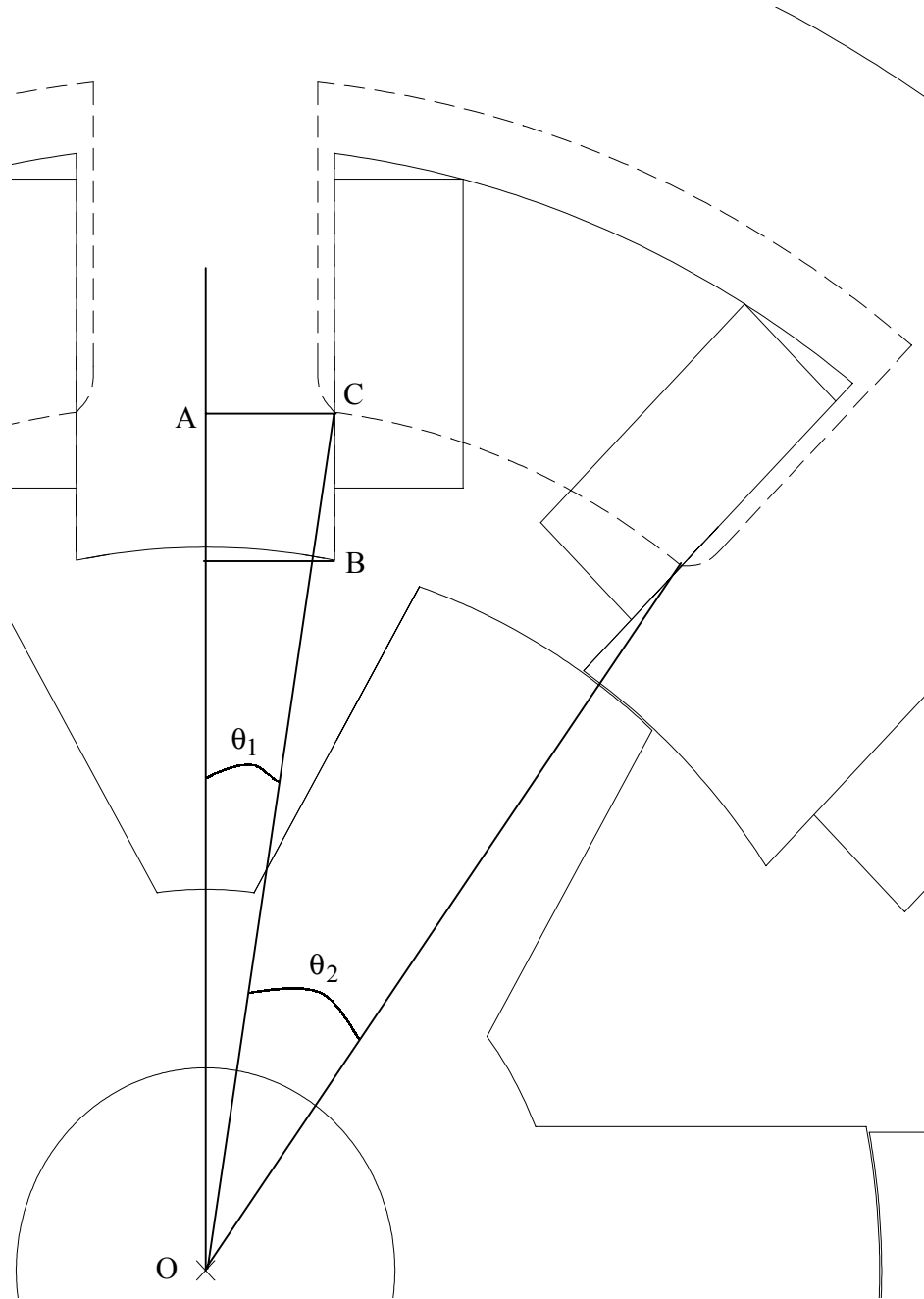


Figure 2.17 Tube 6 Calculations

Tube 6 can be assumed to be an arc centered at the center of the shaft. The length AO is assumed to be,

$$y_1 = \frac{D}{2} \cos\left(\frac{\beta_s}{2}\right) + \frac{3h_s}{8}. \quad (2.131)$$

The length AB is defined in (2.114). From (2.114) and (2.131). the angle θ_1 can be calculated as,

$$\theta_1 = \tan^{-1}\left(\frac{x_1}{y_1}\right). \quad (2.132)$$

The angle θ_2 is assumed to be,

$$\theta_2 = \frac{2\pi}{N_s} - 2\theta_1. \quad (2.133)$$

The length CO is given from (2.114) and (2.132) by

$$r_1 = \frac{x_1}{\sin(\theta_1)}. \quad (2.134)$$

The length of the tube is given from (2.133) and (2.134) by,

$$l_6 = r_1 \theta_2. \quad (2.135)$$

The yoke area is given by (2.36). The stator pole area is equal to the air gap area. Therefore,

$$A_{6s} = A_6 = \frac{h_s}{4} L \quad (2.136)$$

The length of the path in the stator is calculated as,

$$l_s = \frac{h_s}{2} + \frac{1}{2} \frac{h_s}{4} + \frac{C}{2} \quad (2.137)$$

The yoke length is given by,

$$l_y = \frac{\pi}{4} \left(\frac{D_o}{2} - \frac{C}{2} \right) \quad (2.138)$$

The reluctance of tube 6 in the air gap is given by,

$$\mathfrak{R}_6 = \frac{l_6}{\mu_o A_6} \quad (2.139)$$

The permeance of tube 6 is calculated as,

$$P_6 = \frac{1}{\mathfrak{R}_6} \quad (2.140)$$

Referring to Figure 2.18, the magnetic circuit equation of tube 6 can be written as,

$$\mathfrak{S}_6 = \frac{1}{2} \frac{3T_{\text{phi}}}{4} = \mathfrak{R}_L \phi = 2(H_s l_s) + \frac{B_s A_6}{P_6} + H_y l_y \quad (2.141)$$

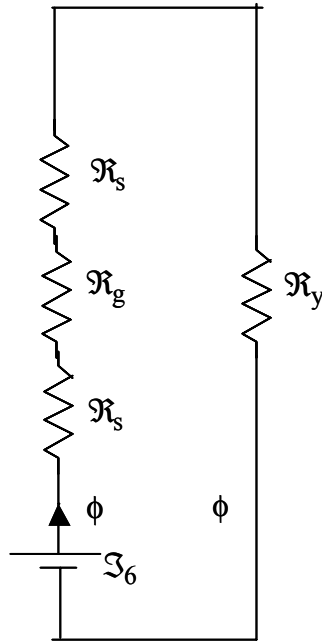


Figure 2.18 Magnetic Circuit for Tube 6

The unaligned inductance of tube 6 is then calculated as,

$$L_{u6} = \mathfrak{S}_6 \frac{B_{s \text{ min}} A_6}{i_p^2} \quad (2.142)$$

Tube 7: To calculate the length l_7 and area A_7 , consider Figure 2.19. The area of the tube is calculated as,

$$A_7 = \frac{h_s}{2} L \quad (2.143)$$

Tube 7 is assumed to be an arc centered about point B. The length is approximately calculated as,

$$l_7 = \frac{h_s}{4} \frac{\pi}{2} \quad (2.144)$$

The stator area is equal to the air gap area. Therefore,

$$A_{7s} = \frac{h_s}{2} L \quad (2.145)$$

The yoke area is given by (2.36). The length of the path in the stator is calculated as,

$$l_s = \frac{1}{2} \frac{h_s}{2} + \frac{C}{2} \quad (2.146)$$

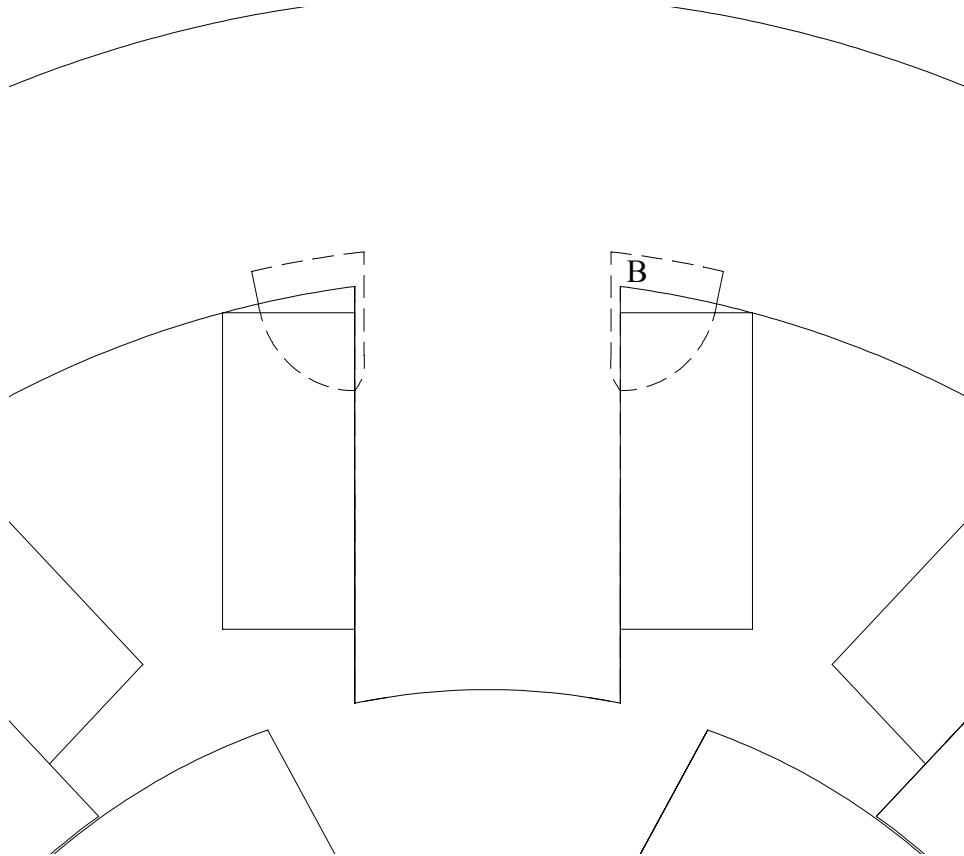


Figure 2.19 Tube 7 Calculations

The yoke length is approximately,

$$l_y = \frac{1}{2} \frac{h_s}{2} \quad (2.147)$$

The reluctance of tube 7 in the air gap is given by,

$$\mathfrak{R}_7 = \frac{l_7}{\mu_0 A_7} \quad (2.148)$$

The permeance of tube 7 is calculated as,

$$P_7 = \frac{1}{\mathfrak{R}_7} \quad (2.149)$$

Referring to Figure 2.20, the magnetic circuit equation of tube 7 can be written as,

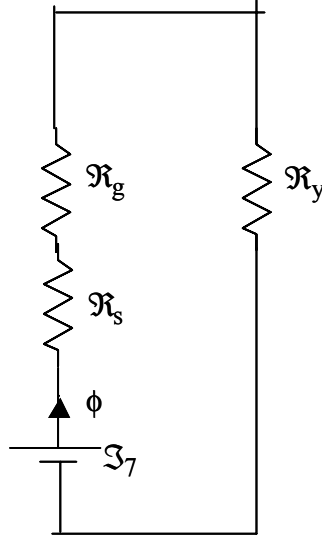


Figure 2.20 Reluctance Circuit for Tube 7

$$\mathfrak{S}_7 = \frac{1}{2} \frac{T_{ph} i}{2} = \mathfrak{R}_L \phi = H_s l_s + \frac{B_s A_7}{P_7} + H_y l_y \quad (2.150)$$

The unaligned inductance of tube 7 is then calculated as,

$$L_{u7} = \mathfrak{S}_7 \frac{B_s \min A_s}{i_p^2} . \quad (2.151)$$

The total unaligned inductance is given by,

$$L_u = L_{u1} + 2(L_{u2} + L_{u3} + L_{u4} + L_{u5}) + 4(L_{u6} + L_{u7}) \quad (2.152)$$

2.1.8 Calculation of Average Torque

In the SRM, a linear relationship is not present between the current in the machine and the torque developed. Therefore, to calculate the average torque developed by the machine at peak current, a more complex system has been evolved [KRI95]. First, the peak current i_p can be split into n

equal parts, which is decided by the designer. Of course, if the number of parts is higher, the result will be more accurate but the time of computation will be much higher.

Let $\delta i = \frac{i_p}{n}$. At the first point of calculation, n_1 , current $i_1 = \delta i$.

Then $\mathfrak{S}_1 = T_{ph} i_1$. Now assuming initially that $B_{s1}=B_s$, the flux densities, the AT/m and the ampere-turns for all the sections are calculated and the total AT is obtained. If this value is greater than \mathfrak{S}_1 , then the value of B_{s1} is reduced and the calculations are done again. If it is higher, then the value of B_{s1} can be increased and the calculations can be redone. This particular exercise is repeated till the error between the calculated value of ampere-turns and \mathfrak{S}_1 is negligible. When this value is obtained the corresponding flux at this point

$$\phi_1 = B_{s1} * A_s ,$$

is calculated. The aligned inductance value for this particular current is calculated as

$$L_{a1} = \frac{T_{ph} \phi_1}{i_1}$$

The flux linkage at this point is also obtained as $\lambda_{a1} = L_{a1} * i_1$.

The above procedure is repeated after each interval of δi , i.e., $i_2 = i_1 + \delta i$ and so on till we reach i_p . The value of $L_a^S = L_a$ at current i_p indicates the aligned saturated inductance at peak current or rated current. The flux linkage at this point is also obtained. The aligned flux linkages can then be plotted against various currents as shown in Figure 2.21.

The unaligned inductance does not change with varying current and so the unaligned flux linkages can be obtained at the various currents above as $\lambda_{u1} = L_u * i_1$ and so on till the rated current and is plotted in Figure 2.21.

The aligned work done $W_{aligned}$ is given by the area 0AC0 and the unaligned work done $W_{unaligned}$ is given by the area 0AB0. The total work done W is given by

$$W = W_{aligned} - W_{unaligned} = \text{Area } 0BC0 \quad (2.153)$$

The aligned work $W_{aligned}$ work is given by

$$W_{aligned} = \delta i (\lambda_1 + \lambda_2 + \dots + \lambda_{n-1}) + \frac{\lambda_n \delta i}{2} \quad (2.154)$$

The unaligned work $W_{\text{unaligned}}$ is given by

$$W_{\text{unaligned}} = \frac{1}{2} i_p \lambda_u = \frac{1}{2} i_p^2 L_u \quad (2.155)$$

The average torque is given by

$$T_{\text{av}} = \frac{W N_s N_r}{4\pi} \text{N.m.} \quad (2.156)$$

If the average torque calculated above is less than the required torque then some machine parameters have to be redesigned. The current can also be increased provided the designer is satisfied that the machine does not go into saturation. This iteration is done till the designer is satisfied with the average developed torque value.

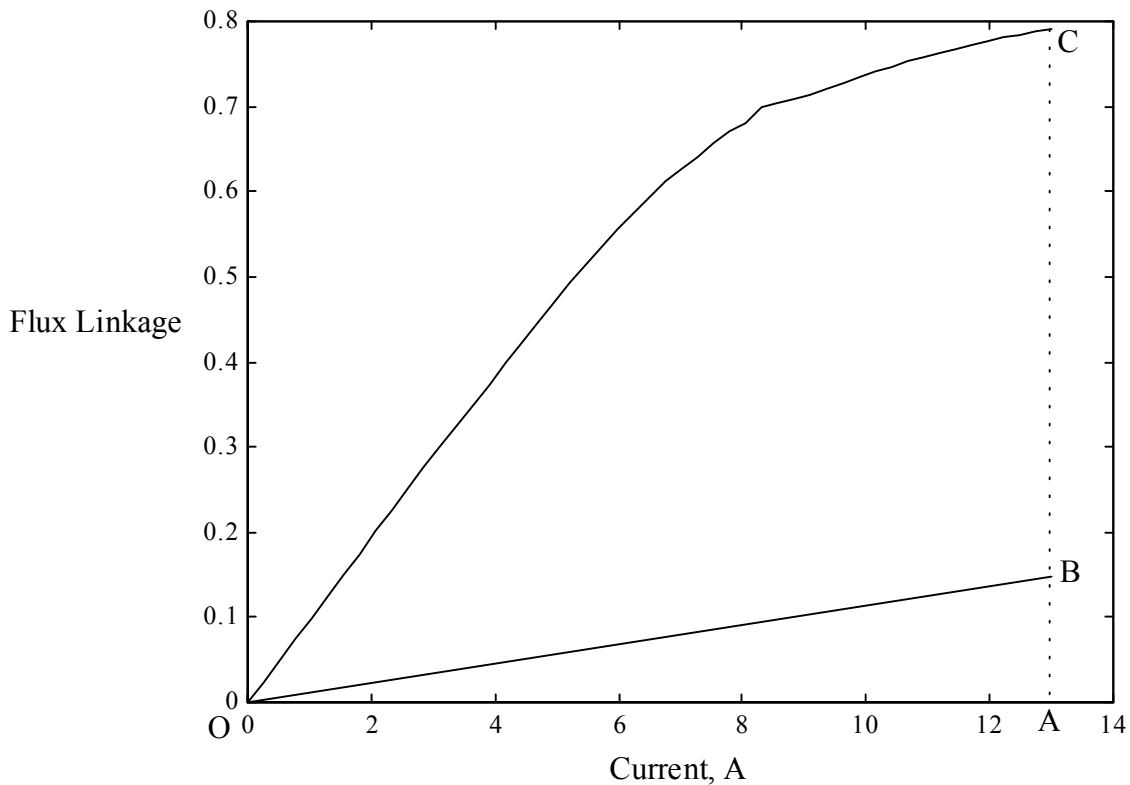


Figure 2.21 Flux linkage vs. current plot

2.2 Design Verification by Finite Element Analysis

Finite Element Analysis (FEA) is used to predict the torque produced at various currents and rotor positions as well as calculate the phase inductances. The equations governing description of the problem is described in [LIN86]. The following assumptions are made in determining the magnetic field distribution inside the motor:

- a. The outer periphery of the stator stamping can be treated as a zero magnetic vector potential line as the magnetic field outside the stator stamping is negligible.
- b. Magnetic materials of the stator and rotor stampings are isotropic and the magnetization curve is single valued (hysteresis effects are neglected).
- c. Magnetic vector potential A and current density J have only z-directed components.
- d. Magnetic field distribution inside the motor is constant along the axial direction of the motor.
- e. End effects are neglected.

The magnetic flux density \mathbf{B} in a magnetic material can be given as,

$$\mathbf{B} = \mu \mathbf{H} = \frac{\mathbf{H}}{\gamma} \quad (2.157)$$

where \mathbf{H} is the magnetic field density, μ is permeability of the magnetic material and γ is the reluctivity of the magnetic material. From Ampere's law [KRA93],

$$\text{curl } \mathbf{B} = \mu \mathbf{J} \quad (2.158)$$

Defining the magnetic vector potential A as,

$$\mathbf{B} = \text{curl } \mathbf{A} \quad (2.159)$$

$$\text{curl} (\text{curl } \mathbf{A}) = \mu \mathbf{J} \quad (2.160)$$

Setting $\nabla \cdot \mathbf{A} = 0$, and from the vector identity for the curl of the curl of the vector,

$$\nabla(\nabla \cdot \mathbf{A}) - \nabla^2 \mathbf{A} = \mu \mathbf{J} \quad (2.161)$$

This implies that,

$$\nabla^2 \mathbf{A} = -\mu \mathbf{J} \quad (2.162)$$

Using the assumption (c), the above expression can be written as,

$$\frac{\delta}{\delta x} \frac{\delta \mathbf{A}}{\delta x} + \frac{\delta}{\delta y} \frac{\delta \mathbf{A}}{\delta y} = -\mu \mathbf{J} \quad (2.163)$$

The solution of (2.163) yields the magnetic vector potential \mathbf{A} inside the motor using appropriate boundary conditions. The stator outer surface is a flux line of zero magnetic vector potential and the homogeneous Dirichlet boundary condition ($\mathbf{A} = 0$) defines the nodes along this flux line. The nonlinearity of the magnetization curve of the iron and the complex geometry of the stator and rotor do not permit an analytical solution for the magnetic vector potential and hence numerical methods are chosen. The solution is obtained using an interpolation technique by minimizing the nonlinear energy functional,

$$F = \int_R \left[\int_0^B \mathbf{H} \cdot d\mathbf{B} - \int_0^A \mathbf{J} \cdot d\mathbf{A} \right] dR \quad (2.164)$$

where R is the problem region of integration.

The entire problem region R is subdivided into triangular finite elements. The elements are defined such that the sides of the triangles coincide with the boundary of each material. The software used in this work FLUX2D implements this by allowing the placement of nodes on each of the boundaries. A sample placement of nodes and the finite element mesh of a 8/6 SRM is shown in Figure 2.22 and Figure 2.23.

It can be noticed in Figure 2.23 that there is a higher concentration of elements near the air-gap. The equiflux lines obtained by FEA in the unaligned position are shown in Figure 2.24. The equiflux lines obtained by FEA in the aligned position are shown in Figure 2.25. From the finite element analysis, the torque and inductance values for different currents and for the rotor position varying from 0° to 30° is shown in the prototype design that follows in a subsequent section.

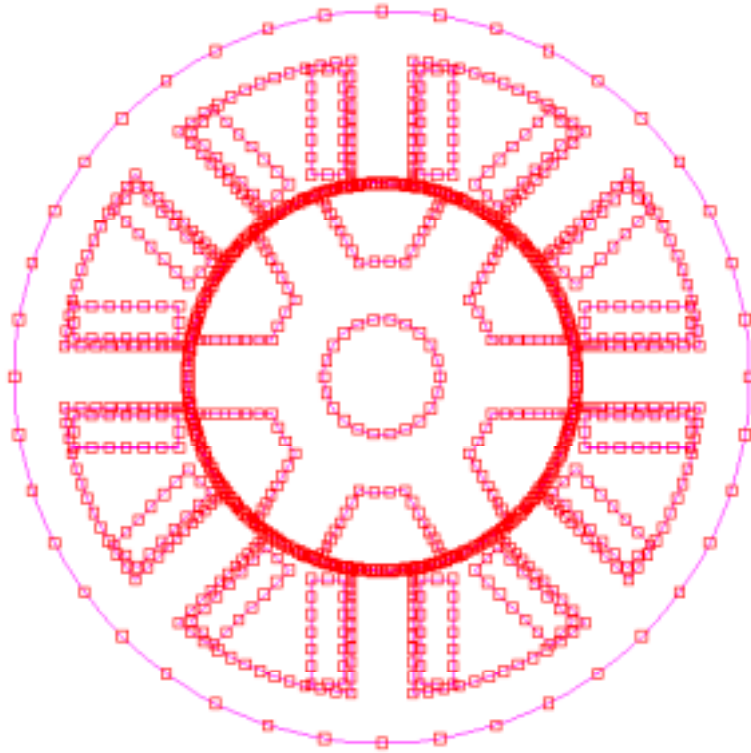


Figure 2.22 Placement of nodes for 8/6 SRM

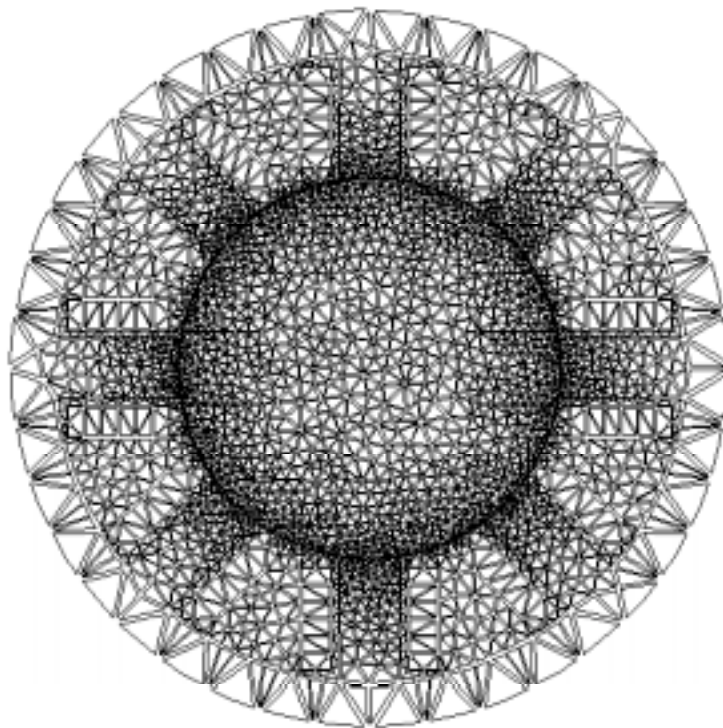


Figure 2.23 Finite element subdivision of the 8/6 SRM

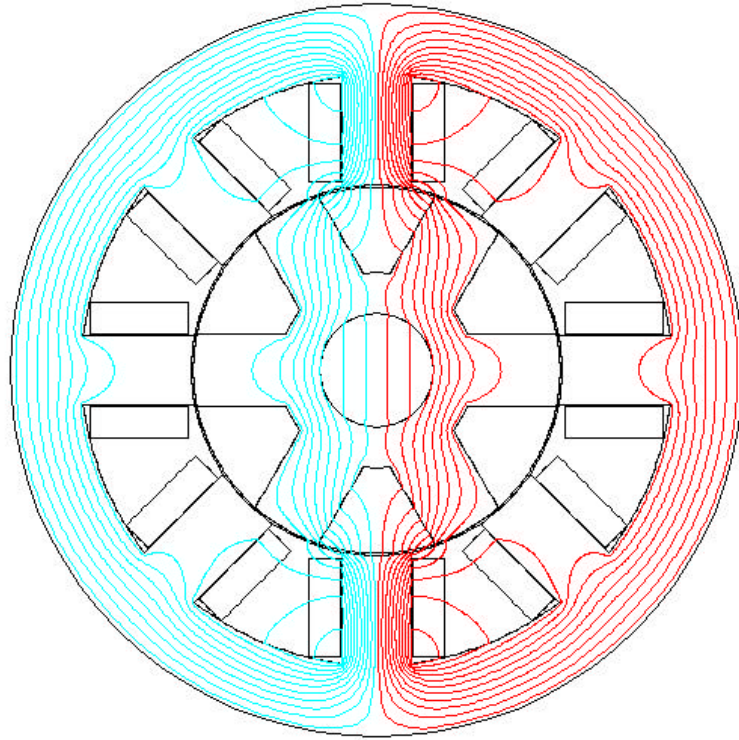


Figure 2.24 Equiflux lines of an 8/6 SRM in the unaligned position

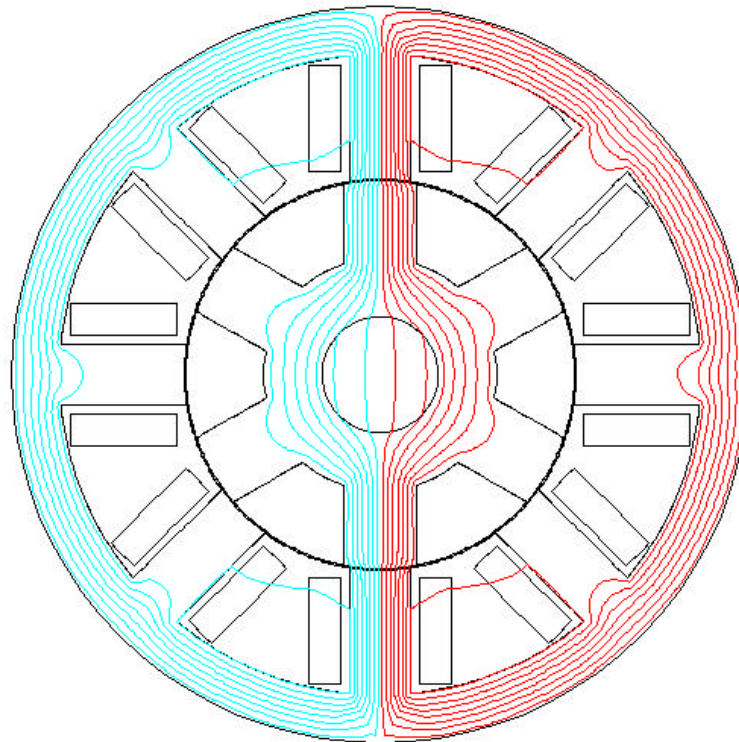


Figure 2.25 Equiflux lines of an 8/6 SRM in the aligned position

2.3 Analysis of the SRM

The analysis of the SRM involves the calculation of losses and thermal study of the designed machine. The inductance of the machine as the rotor moves from the unaligned position to the aligned position is calculated analytically. The thermal study will be covered in the final dissertation. The losses can be split into two sections, copper losses and iron losses.

2.3.1 Copper Losses

The first step in calculating the copper losses involves the calculation of the resistance of each phase winding of the SRM. The mean length of a winding turn is given as,

$$l_m = \left(2L + 4W_t + 2D \sin\left(\frac{\beta_s}{2}\right) \right) * 10^{-3} \text{ m.} \quad (2.165)$$

The resistance of a single phase is calculated as,

$$R_s = \frac{0.0177 * l_m T_{ph}}{a_c} \Omega. \quad (2.166)$$

The copper losses at rated current is given by

$$P_{cu} = i_p^2 R_s \text{ W.} \quad (2.167)$$

2.3.2 Iron Losses

Iron losses or core losses can be split into two major portions, hysteresis and eddy-current losses. In most machines, the core losses can be calculated using the Steinmetz equation. However, the nonsinusoidal flux waveforms of the switched reluctance motor require a different method of calculating core losses. The two major works in this field are by Materu, et al., [MAT92] and Hayashi, et al., [HAY95]. The first work studied core losses using harmonic analysis of the flux density at different parts of the magnetic circuit that has the advantage that the losses contributed by each harmonic can be obtained by look-up process from core loss data. However there is no separation of hysteresis and eddy-current losses and assumes that the core-loss data is valid in the presence of arbitrary combinations of harmonics. The second work describes a method to clearly separate the hysteresis and eddy-current losses. Although the work claims that the

equations developed can be simplified to obtain working formulas, the subsequent write-up will show that working formulas are possible only if approximations are acceptable. It can also be clearly seen that finite element analysis has to be completed before core losses can be calculated. In fact, additional finite element calculations may be required before obtaining the results.

Eddy-Current Losses

The first step in calculating the eddy-current losses is to obtain the plot of flux vs. time at rated speed. Although, theoretically this is an extremely simple concept, the procedure to obtain this is elaborate.

During the beginning of commutation, the voltage equation of the phase being commutated can be written as,

$$-V_{dc} = R_s i + \frac{d}{dt}(L_d i) \quad (2.168)$$

where $-V_{dc}$ is the negative dc link voltage applied to the phase being commutated, R_s is the stator resistance, i is the current being carried by the phase at the time of commutation and L_d is the difference in the aligned and unaligned inductance, i.e., $L_d = L_a - L_u$. Assuming L_d is constant and taking the Laplace transform of (2.168),

$$\begin{aligned} -\frac{V_{dc}(s)}{s} &= R_s I(s) + L_d (sI(s) - I(0)) \\ \Rightarrow \left(s + \frac{R_s}{L_d} \right) I(s) &= -\frac{V_{dc}(s)}{sL_d} + I(0) \\ \Rightarrow I(s) &= -\frac{\frac{V_{dc}(s)}{L_d}}{s \left(s + \frac{R_s}{L_d} \right)} + \frac{I(0)}{\left(s + \frac{R_s}{L_d} \right)} \end{aligned} \quad (2.169)$$

Assuming that the current at the beginning of commutation is equal to the rated current i_p , the equation of the current can be obtained as,

$$i(t) = -\frac{V_{dc}}{R_s} + \frac{V_{dc}}{R_s} e^{-\frac{tR_s}{L_d}} + i_p e^{-\frac{tR_s}{L_d}} \quad (2.170)$$

The time required to commutate the current is obtained by setting the LHS of equation (2.170) to 0 and calculating the fall time t_f . Therefore,

$$\begin{aligned}
0 &= -\frac{V_{dc}}{R_s} + \frac{V_{dc}}{R_s} e^{-\frac{t_f R_s}{L_d}} + i_p e^{-\frac{t_f R_s}{L_d}} \Rightarrow \frac{V_{dc}}{R_s} = \left(\frac{V_{dc}}{R_s} + i_p \right) e^{-\frac{t_f R_s}{L_d}} \\
\Rightarrow e^{\frac{t_f R_s}{L_d}} &= \frac{\left(\frac{V_{dc}}{R_s} + i_p \right)}{\frac{V_{dc}}{R_s}} \Rightarrow e^{\frac{t_f R_s}{L_d}} = 1 + \frac{i_p R_s}{V_{dc}} \Rightarrow \frac{t_f R_s}{L_d} = \ln \left[1 + \frac{i_p R_s}{V_{dc}} \right] \\
\Rightarrow t_f &= \frac{L_d}{R_s} \ln \left[1 + \frac{i_p R_s}{V_{dc}} \right]
\end{aligned} \tag{2.171}$$

At a rated speed of N r.p.m., the number of radians traversed in this time is given by,

$$\theta_f = \frac{2\pi N}{60} t_f. \tag{2.172}$$

In a 8/6 machine full alignment occurs at an angle of $\frac{\pi}{6}$ and commutation can be assumed to

start at an angle $\theta_c = \frac{\pi}{6} + \frac{\beta_r - \beta_s}{2} - \theta_f$. Assuming that the machine phase is on for the entire

stroke period ϵ , ($\frac{\pi}{12}$ for 8/6 machine), the excitation of the phase is assumed to start at an angle

of $\theta_r = \frac{\pi}{6} + \frac{\beta_r - \beta_s}{2} - \theta_f - \frac{\pi}{12}$. The calculation of the commutation angle θ_f assumes that the

machine is not saturated and the value of L_d is constant for the duration of the fall in current.

This is normally not true and it can be seen in the subsequent numerical example that as the current in the phase falls, inductance would rise thereby increasing the commutation angle. The

numerical example demonstrates the choice of firing angle θ_r and commutation angle θ_c . Now

with the choice of firing angle and commutation angle, it is necessary to calculate the current values during the excitation period and the commutation period.

During the calculation of the currents the assumption that the current is held at the rated value once it rises to that value is made thereby not taking into account the effects of pulse width

modulation. From the plot of position vs. inductance for various currents (Figure 2.41), the

minimum inductance at position θ_r is obtained as L_{θ_r} . Assuming that full dc link voltage V_{dc} is applied, and the machine is running at rated speed, the rotor pole traverses each degree in

$t_s = \frac{\pi}{2\pi N} = \frac{1}{6N}$ sec. The equation of the current at position $\theta_r + 1^\circ$ is calculated as,

$$i_{(\theta_r+1)} = \frac{V_{dc}}{R_s} \left(1 - e^{-\frac{R_s}{L_{\theta_r}} t_s} \right). \quad (2.173)$$

The equation of the current at position $\theta_r + 2^\circ$ is calculated as,

$$i_{(\theta_r+2)} = \frac{V_{dc}}{R_s} \left(1 - e^{-\frac{R_s}{L_{(\theta_r+1)}} t_s} \right) + i_{(\theta_r+1)} e^{-\frac{R_s}{L_{(\theta_r+1)}} t_s} \quad (2.174)$$

The inductance value $L_{(\theta_r+1)}$ is obtained from the plot of position vs. inductance for various currents at precisely the angle $(\theta_r + 1^\circ)$ at a current of $i_{(\theta_r+1)}$. The current at position $(\theta_r + 2^\circ)$ can be obtained in a similar manner. If this value is greater than the rated current i_p , the current is assumed to i_p . If not the procedure is repeated till the rated current is reached or exceeded. Once the rated current is reached, the current is assumed to be constant till position θ_c . At this position, full negative dc link voltage is applied and the current at position $(\theta_c + 1^\circ)$ is calculated as,

$$i_{(\theta_c+1)} = -\frac{V_{dc}}{R_s} \left(1 - e^{-\frac{R_s}{L_{(\theta_c)}} t_s} \right) + i_p e^{-\frac{R_s}{L_{(\theta_c)}} t_s}. \quad (2.175)$$

The current at position $(\theta_c + 2^\circ)$ is calculated as,

$$i_{(\theta_c+2)} = -\frac{V_{dc}}{R_s} \left(1 - e^{-\frac{R_s}{L_{(\theta_c+1)}} t_s} \right) + i_{(\theta_c+1)} e^{-\frac{R_s}{L_{(\theta_c+1)}} t_s}. \quad (2.176)$$

The procedure is repeated till the current value becomes 0, which implies that the phase is fully commutated. It should be remembered that the inductance for each current and position has to be calculated.

Now that the current value at each rotor position is obtained, finite element analysis is used to calculate the flux density in the stator pole for each current value and rotor position keeping in mind that the excitation of adjoining phases has to be simulated as well. This is a time intensive procedure and need not be done during the preliminary design of the machine. The resultant flux densities can be plotted over a full revolution of the rotor as can be seen in Figure 2.26.

B_{sp} represents the flux density of a single stator pole over the entire revolution. The diametrically opposite pole would have a similar waveform except that the polarity would be reversed. The other poles would have the similar waveforms but would be offset by the stroke angle, in this case, 15° .

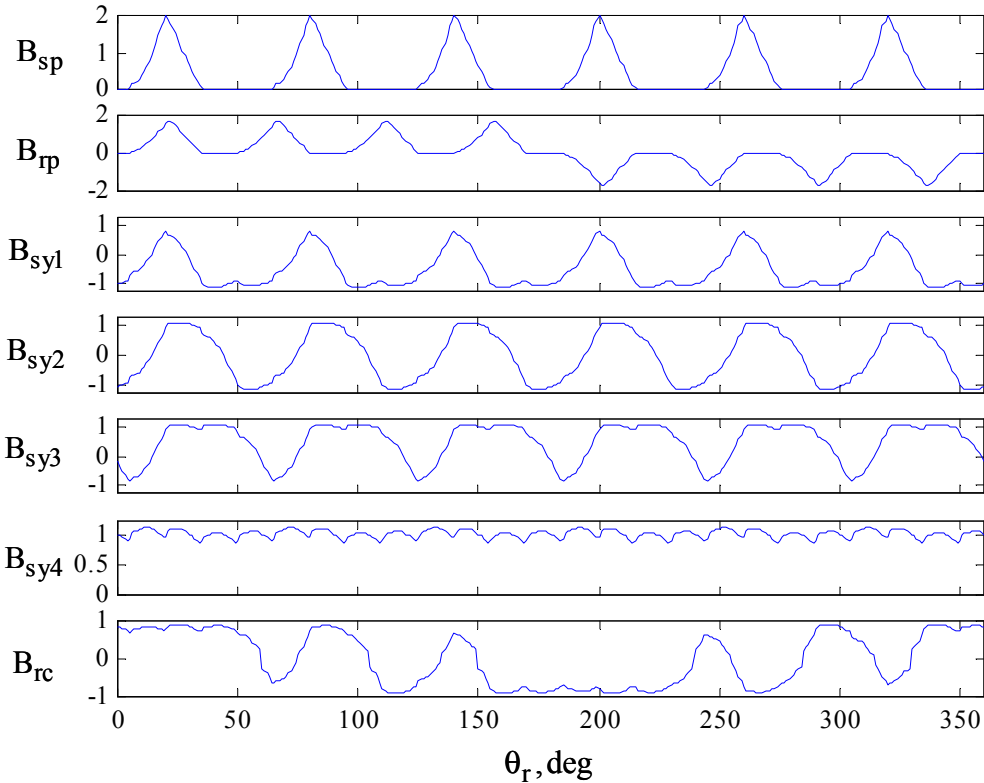


Figure 2.26 Flux densities over a single revolution of the rotor

B_{rp} represents the flux density of a single rotor pole over the entire revolution. The diametrically opposite pole would have a similar waveform except that the polarity would be reversed. The other poles would have the similar waveforms but would be offset by the stroke angle.

The flux densities of the stator yoke vary from section to section based which phase is being activated. The flux densities for four different sections are plotted for a full rotation. The corresponding diametrically opposite sections have the reverse polarities.

Finally, the flux density experienced by one of six sections of the rotor core over a revolution is plotted. The other sections have the identical waveforms but are offset by 60° .

It can be clearly seen that the stator flux density repeats every $\frac{\pi}{3}$ radians. The normalized stator flux vs. time can be plotted for a rotation of the rotor by $\frac{\pi}{3}$ radians. After this period, the waveform would repeat. The flux at each rotor position can be obtained by using the equation $\phi = B_s A_s$ where A_s is the stator pole area. A normalized sample flux waveform is shown in Figure 2.27.

It can be observed that the normalized stator flux has a rising portion and a falling portion. Both the rising and falling portions can be fairly approximated by 2 fourth order polynomials of t and the flux waveforms for the stator can be written mathematically as,

$$g_s(t) = \begin{cases} a_{s1}t^4 + a_{s2}t^3 + a_{s3}t^2 + a_{s4}t + a_{s5} & \text{for } 0 \leq t \leq T_{rs} \\ b_{s1}t^4 + b_{s2}t^3 + b_{s3}t^2 + b_{s4}t + b_{s5} & \text{for } T_{rs} \leq t \leq T_{fs} \\ 0 & \text{for } T_{fs} \leq t < T_s \end{cases} \quad (2.177)$$

where $T_s = 60t_s$, t_s is the time taken by the rotor pole to traverse a single degree, T_{rs} is the time taken for the flux to rise to the maximum value and T_{fs} is the time when the flux falls to zero.

A sample normalized rotor flux vs. time is plotted over $\frac{\pi}{4}$ radians in Figure 2.28. After that time, the waveform would repeat as shown in Figure 2.26. It can be observed that the normalized rotor

flux has a rising portion and a falling portion. Both the rising and falling portions can be fairly approximated by 2 fourth order polynomials of t and the flux waveforms for the rotor can be written mathematically as,

$$g_r(t) = \begin{cases} a_{r1}t^4 + a_{r2}t^3 + a_{r3}t^2 + a_{r4}t + a_{r5} & \text{for } 0 \leq t \leq T_{rr} \\ b_{r1}t^4 + b_{r2}t^3 + b_{r3}t^2 + b_{r4}t + b_{r5} & \text{for } T_{rr} \leq t \leq T_{fr} \\ 0 & \text{for } T_{fr} \leq t < T_r \end{cases} \quad (2.178)$$

where $T_r = 45t_s$, T_{rr} is the time taken for the flux to rise to the maximum value and T_{fr} is the time when the flux falls to zero.

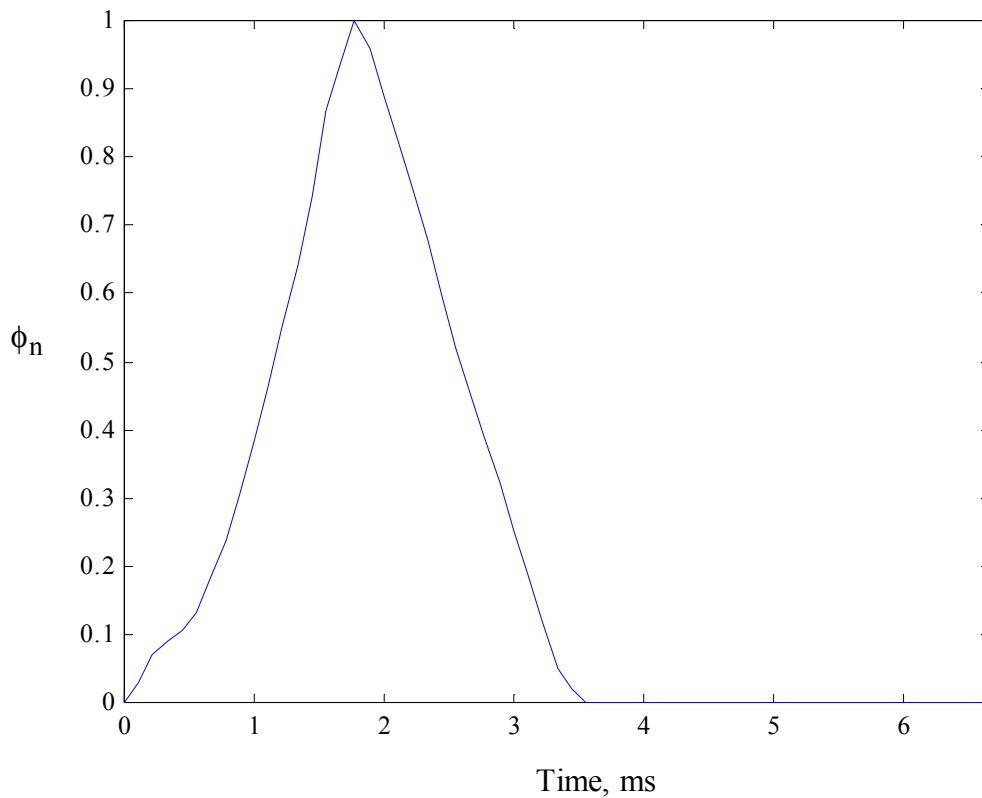


Figure 2.27 Sample plot of normalized stator flux vs. time for $\frac{\pi}{3}$ radians.

Eddy-current losses per unit weight are normally given by,

$$P_e = C_e f^2 B_m^2 \quad (2.179)$$

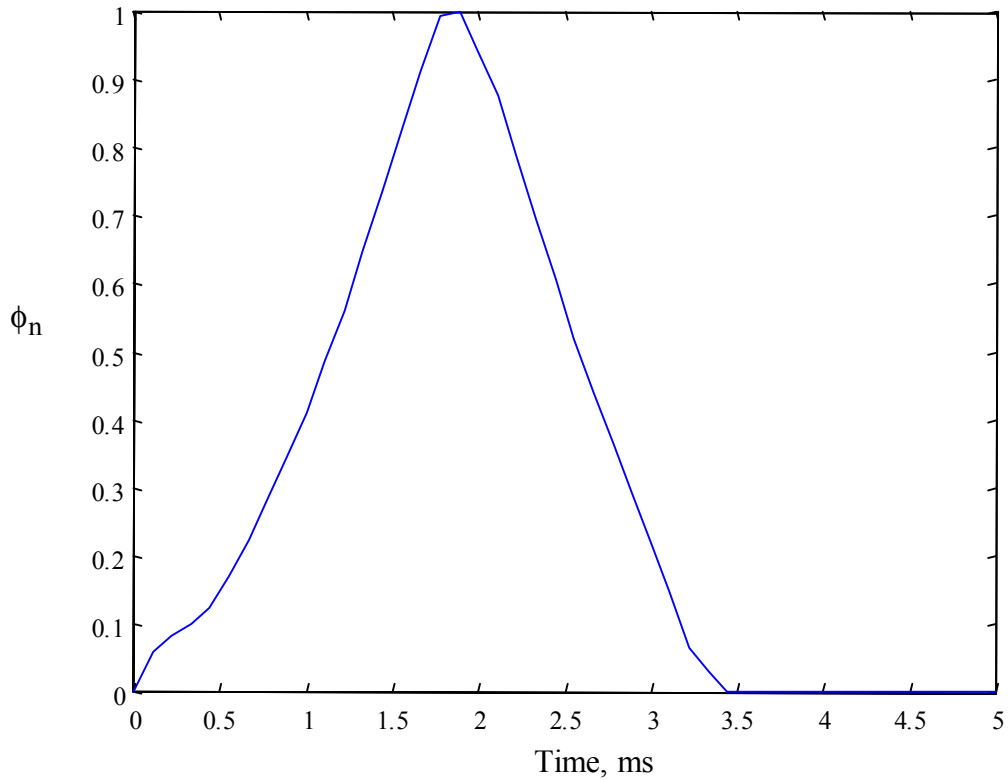


Figure 2.28 Sample plot of normalized rotor flux vs. time for $\frac{\pi}{4}$ radians.

where C_e is the coefficient of eddy-current losses, f is the sinusoidal frequency and B_m is the maximum flux density. The value is calculated as [SAW84],

$$C_e = \frac{\pi^2 t^2}{6\rho\rho_1} \quad (2.180)$$

where t is the thickness of the lamination and ρ is the specific resistivity of the lamination material and ρ_1 is the specific density of the lamination material. Considering that the average of

$\left(\frac{dB}{dt}\right)^2 = 2\pi^2 f^2 B_m^2$ for the sinusoidal flux variation, $B = B_m \sin(2\pi ft)$, eddy current term can be written as [HAY95],

$$P_e = C_e f^2 \frac{\left(\frac{dB}{dt}\right)^2}{2\pi^2 f^2} = \frac{C_e}{2\pi^2} \left(\frac{dB}{dt}\right)^2 = C_{el} \left(\frac{dB}{dt}\right)^2. \quad (2.181)$$

Since the number of strokes per revolution is given by $\frac{N_s N_r}{2}$, two poles are energized at each stroke and there is no overlap between flux pulses, the eddy-current losses for the stator poles P_{spe} and rotor poles P_{rpe} are given as,

$$P_{spe} = \frac{2\pi N}{60} \frac{1}{2\pi} N_s N_r W_{sp} C_{el} (B_{spm})^2 \int_{t=0}^{T_s} \left[\frac{d}{dt} g_s(t) \right]^2 dt \quad (2.182)$$

and,

$$P_{rpe} = \frac{2\pi N}{60} \frac{1}{2\pi} N_s N_r W_{rp} C_{el} (B_{rpm})^2 \int_{t=0}^{T_r} \left[\frac{d}{dt} g_r(t) \right]^2 dt. \quad (2.183)$$

W_{sp} and W_{rp} are the weights of the stator pole and rotor pole, respectively, and are calculated as,

$$W_{sp} = \frac{D}{2} \beta_s h_s L \rho_1 \quad (2.184)$$

and,

$$W_{rp} = h_r L \left(\frac{D}{2} - g \right) \beta_r \rho_1 \quad (2.185)$$

A sample normalized stator flux for section 1 vs. time is plotted over $\frac{\pi}{3}$ radians in Figure 2.29.

After that time, the waveform would repeat as shown in Figure 2.26. It can be observed that the normalized flux has four distinct portions. The flux waveforms for the section can be written mathematically as,

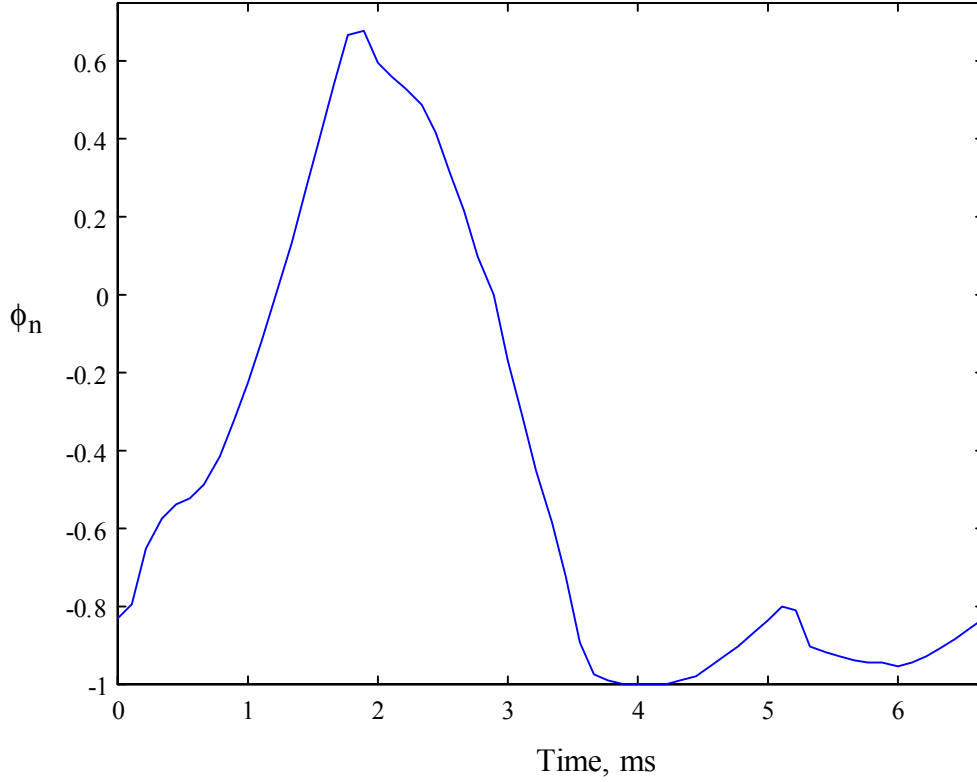


Figure 2.29 Sample plot of normalized section 1 yoke flux vs. time for $\frac{\pi}{3}$ radians.

$$\mathbf{g}_{\text{sy}1}(t) = \begin{cases} a_{\text{sy}11}t^4 + a_{\text{sy}12}t^3 + a_{\text{sy}13}t^2 + a_{\text{sy}14}t + a_{\text{sy}15} & \text{for } 0 \leq t \leq T_{\text{sy}1} \\ b_{\text{sy}11}t^4 + b_{\text{sy}12}t^3 + b_{\text{sy}13}t^2 + b_{\text{sy}14}t + b_{\text{sy}15} & \text{for } T_{\text{sy}1} \leq t \leq T_{\text{sy}2} \\ c_{\text{sy}11}t^2 + c_{\text{sy}12}t + c_{\text{sy}13} & \text{for } T_{\text{sy}2} \leq t < T_{\text{sy}3} \\ d_{\text{sy}11}t^2 + d_{\text{sy}12}t + d_{\text{sy}13} & \text{for } T_{\text{sy}3} \leq t < T_{\text{sy}} \end{cases} \quad (2.186)$$

where $T_{\text{sy}} = 60t_s$. The weight of the stator yoke is calculated as,

$$W_{\text{sy}1} = \frac{D_o - C}{2} \frac{2\pi}{N_s} CL\rho_1. \quad (2.187)$$

The equation for calculating the eddy-current loss in the stator yoke section is given by,

$$P_{\text{sy}1e} = \frac{N}{60} 2N_r W_{\text{sy}1} C_{el} (B_{\text{sy}m1})^2 \left\{ \int_{t=0}^{T_{\text{sy}}} \left[\frac{d}{dt} \mathbf{g}_{\text{sy}1}(t) \right]^2 dt \right\} \quad (2.188)$$

Similarly the losses in the other sections of the yoke can be calculated. The total eddy current loss in the stator yoke is given as,

$$P_{sye} = P_{syle} + P_{sy2e} + P_{sy3e} + P_{sy4e} \quad (2.189)$$

A sample normalized rotor core flux for vs. time is plotted over π radians in Figure 2.30. It can be observed that the normalized flux has six distinct portions portion. The flux waveforms for the section can be written mathematically as,

$$g_{rc}(t) = \begin{cases} a_{rc1}t^4 + a_{rc2}t^3 + a_{rc3}t^2 + a_{rc4}t + a_{rc5} & \text{for } 0 \leq t \leq T_{rc1} \\ b_{rc1}t^6 + b_{rc2}t^5 + b_{rc3}t^4 + b_{rc4}t^3 + b_{rc5}t^2 + b_{rc6}t + b_{rc7} & \text{for } T_{rc1} \leq t \leq T_{rc2} \\ c_{rc1}t^6 + c_{rc2}t^5 + c_{rc3}t^4 + c_{rc4}t^3 + c_{rc5}t^2 + c_{rc6}t + c_{rc7} & \text{for } T_{rc2} \leq t < T_{rc3} \\ d_{rc1}t^4 + d_{rc2}t^3 + d_{rc3}t^2 + d_{rc4}t + d_{rc5} & \text{for } T_{rc3} \leq t < T_{rc4} \\ e_{rc1}t^4 + e_{rc2}t^3 + e_{rc3}t^2 + e_{rc4}t + e_{rc5} & \text{for } T_{rc4} \leq t < T_{rc5} \\ f_{rc1}t^4 + f_{rc2}t^3 + f_{rc3}t^2 + f_{rc4}t + f_{rc5} & \text{for } T_{rc5} \leq t < T_{rc} \end{cases} \quad (2.190)$$

where $T_{rc} = 180t_s$. The weight of the rotor core is calculated as,

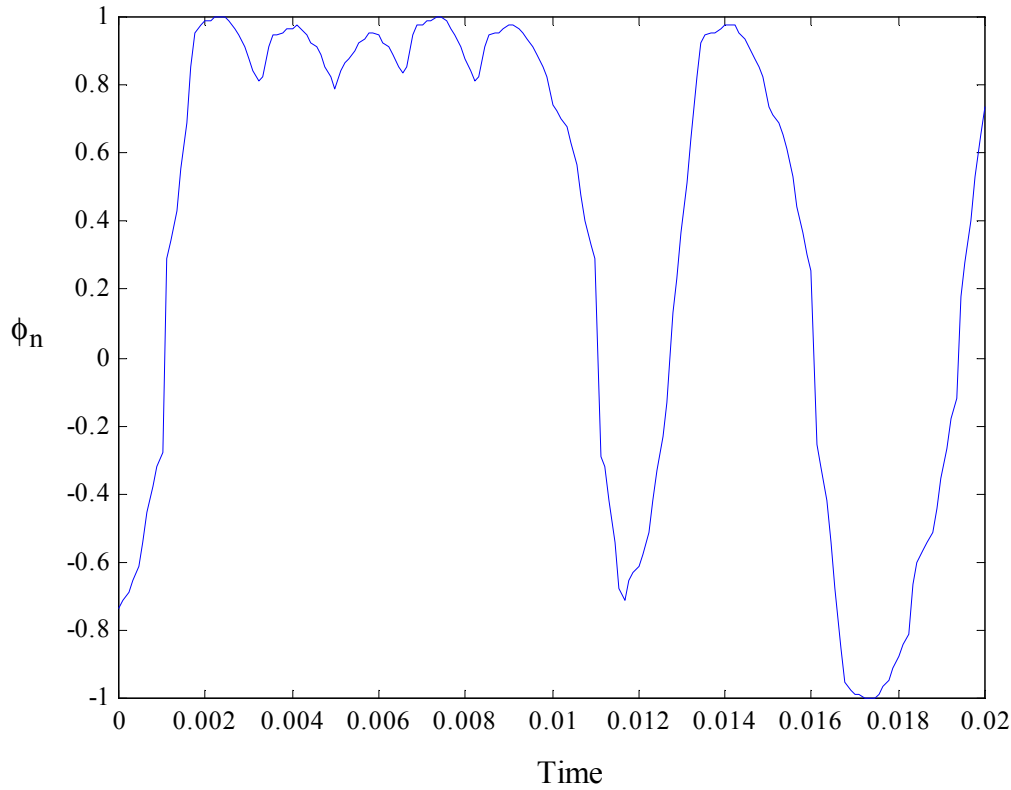


Figure 2.30 Sample plot of normalized rotor core flux vs. time for π radians.

$$W_{rc} = A_{ry} \frac{\pi}{3} \frac{1}{2} \frac{D - 2g - 2h_r + D_{sh}}{2} \rho_1. \quad (2.191)$$

The equation for calculating the eddy-current loss in the rotor core section is given by,

$$P_{rce} = \frac{N}{60} 2N_r W_{rc} C_{el} (B_{rcm})^2 \left\{ \int_{t=0}^{T_{rc}} \left[\frac{d}{dt} g_{rc}(t) \right]^2 dt \right\} \quad (2.192)$$

The total eddy-current losses of the machine at rated speed and power output is given as,

$$P_e = P_{spe} + P_{rpe} + P_{sye} + P_{rce} \quad (2.193)$$

Hysteresis Losses

The hysteresis losses can be calculated from the process described in [HAY95]. The classical equation describing the hysteresis losses was given by Steinmetz as,

$$P_h = C_h f B_m^{1.6} \quad (2.194)$$

where C_h is the hysteresis coefficient, f is the frequency and B_m is the maximum flux density.

In [HAY95], the hysteresis loss is calculated as,

$$P_h = C_h f B_m^{a+bB_m} \quad (2.195)$$

[RIC36] describes the hysteresis loss to follow the equation,

$$P_h = f \left(a B_m + b B_m^2 \right) \quad (2.196)$$

In all of the cases, the hysteresis loss can be re-written as,

$$P_h = f \cdot E_h(-B_m, B_m) \quad (2.197)$$

where $E_h(-B_m, B_m)$ represents the hysteresis loss energy for a full loop. The hysteresis loss energy for a variation of the flux density between 0 and B_m can be written empirically as,

$$E_h(0, B_m) = 0.4 E_h(-B_m, B_m) \quad (2.198)$$

The loss energy for variation between a value B_0 and B_m can be written as,

$$E_h(B_0, B_m) = \frac{B_m - B_0}{B_m} E_h(0, B_m) \quad (2.199)$$

In the calculation of the hysteresis loss energy, the following points must be clearly noted.

- a. The value of the hysteresis loss energy varies with the frequency. For instance, in the stator pole, the flux density for a 8/6 machine operating at N r.p.m. changes between 0 and B_{spm} at $\frac{N}{60}N_r$ times per second. Hence, the loss energy calculated from curves at a fixed frequency cannot be directly applied at primary switching frequency of the stator pole when the machine is running at rated speed.
- b. The primary switching frequency varies in different portions of the machine. Hence there is no way to separate the losses produced by different portions of the machine by attempting a single frequency calculation at standstill.
- c. The most reliable way to measure the core losses would be to run the machine at rated speed and subtract the copper losses and account for friction and windage as described in [MAT92]. The further separation of hysteresis and eddy-current losses can be done only by analytically calculating the eddy-current losses and designating the rest of the losses to be the hysteresis losses.

The flux in the stator poles are unipolar and can be calculated as,

$$P_{sph} = \frac{\omega_m}{2\pi} N_r N_s W_{sp} E_h(0, B_{spm}) \quad (2.200)$$

The other portions of the machine are not straightforward as there are flux reversals. The equations to calculate the losses are described in [HAY95].

Designating winding polarities as p_1, p_2, p_3 and p_4 (p_i is 1 when the direction of the flux of the i^{th} pole is from inside to outside and -1 for the opposite direction), the following parameters can be calculated [HAY95]:

$$K_{sy} = 2 \left(N_{ph} + \frac{N_{ph} - 2}{2} \left\{ \left| p_{N_{ph}} + p_1 \right| + \sum_{i=1}^{N_{ph}-1} |p_i - p_{i+1}| \right\} \right) \quad (2.201)$$

$$K_{rp} = \frac{N_r}{N_{wkpp}} \left\{ \left| p_{N_{ph}} + p_1 \right| + \sum_{i=1}^{N_{ph}-1} |p_i - p_{i+1}| \right\} \quad (2.202)$$

$$K_{rc} = \frac{N_r}{N_{wkpp}} \left\{ 2N_{ph} + \left(\frac{N_r}{2N_{wkpp}} - 2 \right) \cdot \left(\left| p_{N_{ph}} + p_1 \right| + \sum_{i=1}^{N_{ph}-1} |p_i - p_{i+1}| \right) \right\} \quad (2.203)$$

where N_{wkpp} is the number of working pole pairs.

The hysteresis losses in the stator yoke can be calculated as,

$$P_{\text{syh}} = \frac{\omega_m}{2\pi} N_r N_s N_{\text{ph}} W_{\text{sy}} \left\{ \frac{h_{\text{syh}}}{2} E_h(-B_{\text{sym}}, B_{\text{sym}}) + (1 - h_{\text{syh}}) E_h(B_{\text{sy0}}, B_{\text{sym}}) \right\} \quad (2.204)$$

where,

$$h_{\text{syh}} = \frac{K_{\text{sy}}}{2N_{\text{ph}}^2} \quad (2.205)$$

The hysteresis losses in the rotor pole can be calculated as,

$$P_{\text{rph}} = \frac{\omega_m}{2\pi} N_r N_s W_{\text{rp}} \left\{ \frac{h_{\text{rph}}}{2} E_h(-B_{\text{rpm}}, B_{\text{rpm}}) + (1 - h_{\text{rph}}) E_h(0, B_{\text{rpm}}) \right\} \quad (2.206)$$

where,

$$h_{\text{rph}} = \frac{N_{\text{wkpp}} K_{\text{rp}}}{2N_{\text{ph}} N_r} \quad (2.207)$$

The hysteresis losses in the rotor core can be calculated as,

$$P_{\text{rch}} = \frac{\omega_m}{2\pi} N_r^2 N_{\text{ph}} W_{\text{rc}} \left\{ \frac{h_{\text{rch}}}{2} E_h(-B_{\text{rcm}}, B_{\text{rcm}}) + (1 - h_{\text{rch}}) E_h(B_{\text{rc0}}, B_{\text{rcm}}) \right\} \quad (2.208)$$

where,

$$h_{\text{rch}} = \frac{N_{\text{wkpp}}^2 K_{\text{rc}}}{N_{\text{ph}} N_r^2} \quad (2.209)$$

The total hysteresis losses are given by,

$$P_h = P_{\text{sph}} + P_{\text{syh}} + P_{\text{rph}} + P_{\text{rch}} \quad (2.210)$$

2.3.3 Inductance Calculation at Various Rotor Positions

The inductance can be calculated for various rotor positions as follows. There are primarily to regions to be considered while calculating the inductance at different positions. The regions can be identified as the portion when the rotor and stator poles are not overlapping and the portion where the stator and rotor poles are overlapping. Assuming that $\theta = 0^\circ$ is the completely

unaligned position and $\theta = 30^\circ$ is the completely aligned position the inductances can be calculated as follows.

Region I: $0 \leq \theta \leq \frac{\pi}{N_r} - \left(\frac{\beta_s + \beta_r}{2} \right)$

The flux tubes are identified as shown in Figure 2.31.

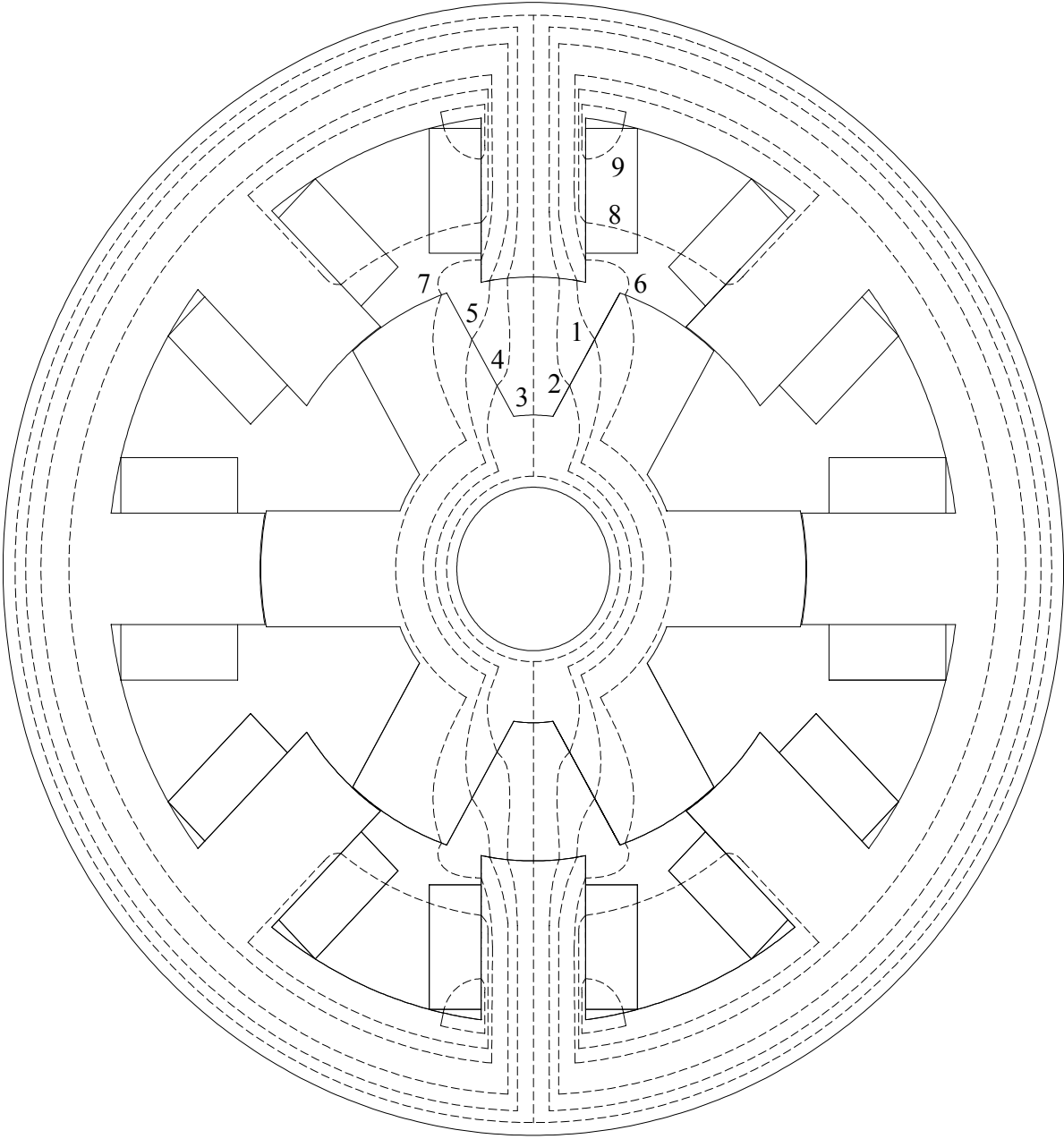


Figure 2.31 Identification of flux tubes in Region I

Tube 1: Considering Figure 2.32, the center of the shaft has the xy coordinates of (0,0), and the stator pole is divided into five equal angles of $\frac{\beta_s}{5}$. The angle θ_1 is assumed to be $\frac{2\beta_s}{5}$. The length AB is calculated as $x_1 = \frac{D}{2} \sin(\theta_1)$. The length OA is calculated as $y_1 = \frac{D}{2} \cos(\theta_1)$. Considering that point B has the coordinates as,

$$(x_1, y_1) = \left(\left(\frac{D}{2} \right) \sin \left(\frac{2\beta_s}{5} \right), \left(\frac{D}{2} \right) \cos \left(\frac{2\beta_s}{5} \right) \right). \quad (2.211)$$

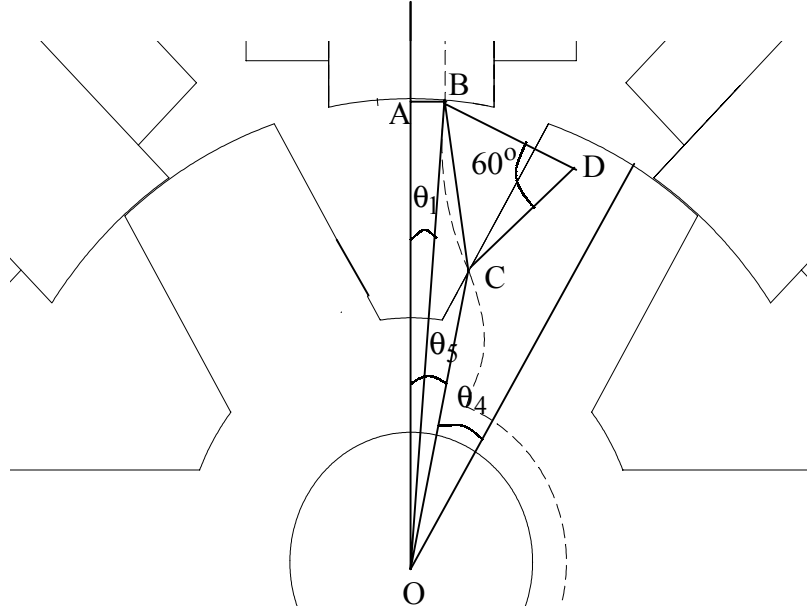


Figure 2.32 Tube 1 and 2 Calculations

Considering that the rotor is moving towards the stator, the length of the tube in the air gap is constantly changing as is the area.

The angle θ_5 is calculated as,

$$\theta_5 = \frac{\theta_{rp}}{2} - \frac{\beta_r}{2} - \theta \quad (2.212)$$

The coordinates of point C is given as,

$$(x_2, y_2) = \left(\left(\frac{D}{2} - g - h_{elu} \right) \sin \theta_5, \left(\frac{D}{2} - g - h_{elu} \right) \cos \theta_5 \right) \quad (2.213)$$

where,

$$h_{e1u} = \frac{h_r}{6} \left(1 - \frac{\theta}{2 \left(\frac{\theta_{rp}}{2} - \frac{\beta_s + \beta_r}{2} \right)} \right) \quad (2.214)$$

The linear distance between the points B and C, is assumed to be one side of an equilateral triangle and forms the radius of the arc formed by tube 1. If this length is given from (2.211) and (2.213) as follows,

$$l_{x1} = \sqrt{(x_2 - x_1)^2 + (y_2 - y_1)^2} \quad (2.215)$$

the length of the tube is given by,

$$l_1 = l_{x1} \frac{\pi}{3}. \quad (2.216)$$

The rotor area varies from $L \frac{h_r}{3}$ when $\theta = 0^\circ$ to $L \frac{h_r}{6}$ when $\theta = \left(\frac{\theta_{rp}}{2} - \frac{\beta_s + \beta_r}{2} \right)$. Therefore,

$$A_{1r} = L \frac{h_r}{3} \left(1 - \frac{\theta}{2 \left(\frac{\theta_{rp}}{2} - \frac{\beta_s + \beta_r}{2} \right)} \right) \quad (2.217)$$

The area of the tube is calculated as,

$$A_1 = \frac{1}{2} (A_{1s} + A_{1r}) \quad (2.218)$$

where the area of the stator pole is given by,

$$A_{1s} = \frac{D \beta_s}{2 \cdot 5} L \quad (2.219)$$

The length of the path through the rotor is given as,

$$l_r = h_r - h_{e1u} \quad (2.220)$$

The length of the path through the stator, yoke and rotor core is given by (2.23), (2.27) and (2.76), respectively. The area of the yoke and rotor core is given by (2.36) and (2.15).

The reluctance of the air gap of path 1 in the upper portion is given as,

$$\mathfrak{R}_1 = \frac{l_1}{\mu_o A_1} \quad (2.221)$$

The above calculations are valid for the tube passing in the upper portion of the stator. In the lower portion, the pole is moving away from the excited portion. This is similar to the effects experienced by tube 5 in the upper portion. Therefore, path 5 calculations are performed next.

Tube 5: Considering Fig. 16, the point B₅ has the coordinates as,

$$(x_1, y_1) = \left(-\left(\frac{D}{2}\right) \sin\left(\frac{2\beta_s}{5}\right), \left(\frac{D}{2}\right) \cos\left(\frac{2\beta_s}{5}\right) \right). \quad (2.222)$$

The angle θ_5 is calculated as,

$$\theta_5 = \frac{\theta_{rp}}{2} - \frac{\beta_r}{2} + \theta \quad (2.223)$$

The coordinates of point C is given as,

$$(x_2, y_2) = \left(\left(\frac{D}{2} - g - h_{e5u}\right) \sin \theta_5, \left(\frac{D}{2} - g - h_{e5u}\right) \cos \theta_5 \right) \quad (2.224)$$

where,

$$h_{e5u} = \frac{h_r}{6} \left(1 + \frac{\theta}{2 \left(\frac{\theta_{rp}}{2} - \frac{\beta_s + \beta_r}{2} \right)} \right) \quad (2.225)$$

The linear distance between the points B and C, is assumed to be one side of an equilateral triangle and forms the radius of the arc formed by tube 5. If this length is given as follows,

$$l_{x5} = \sqrt{(x_2 - x_1)^2 + (y_2 - y_1)^2} \quad (2.226)$$

the length of the tube is given by,

$$l_5 = l_{x5} \frac{\pi}{3}. \quad (2.227)$$

The rotor area varies from $L \frac{h_r}{3}$ when $\theta = 0^\circ$ to $L \frac{h_r}{2}$ when $\theta = \left(\frac{\theta_{rp}}{2} - \frac{\beta_s + \beta_r}{2} \right)$. Therefore,

$$A_{5r} = L \frac{h_r}{3} \left(1 + \frac{\theta}{2 \left(\frac{\theta_{rp}}{2} - \frac{\beta_s + \beta_r}{2} \right)} \right) \quad (2.228)$$

The area of the tube is calculated as,

$$A_5 = \frac{1}{2} (A_{5s} + A_{5r}) \quad (2.229)$$

where the area of the stator pole remains the same as path 1 and is given by,

$$A_{5s} = L \frac{\beta_s D}{5 \cdot 2} \quad (2.230)$$

The length of the path through the rotor is given as,

$$l_r = h_r - h_{e5u} \quad (2.231)$$

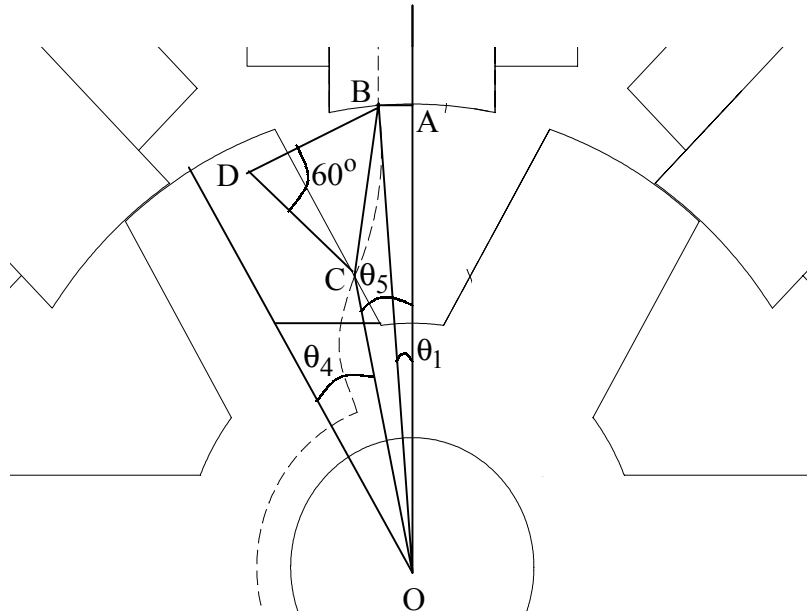


Fig. 16 Tube 4 and 5 Calculations

The length of the path through the stator, yoke and rotor core is given by (2.23), (2.27) and (2.76), respectively. The area of the yoke and rotor core is given by (2.36) and (2.15).

The reluctance of the air gap of path 5 in the upper portion is given as,

$$\mathfrak{R}_5 = \frac{l_5}{\mu_0 A_5} \quad (2.232)$$

The combined reluctance for path 1 is given by,

$$\mathfrak{R}_{1,5} = \mathfrak{R}_1 + \mathfrak{R}_5 \quad (2.233)$$

The permeance of tube 1 is calculated as,

$$P_1 = \frac{1}{\mathfrak{R}_{1,5}} \quad (2.234)$$

Using the B-H characteristics for the material used for the laminations, the magnetic field intensity in Ampere-turns per meter for each portion of the machine except the air-gap is obtained. The magnetic field intensities in the stator pole, stator yoke, rotor pole and rotor core are designated as H_s , H_y , H_r and H_{rc} , respectively.

The magnetic circuit equation of tube 1 can be written as,

$$\mathfrak{S}_1 = T_{ph}i = 2(H_s l_s + H_r l_r) + \frac{B_s A_{ls}}{P_1} + H_{rc} l_{rc} + H_y l_y \quad (2.235)$$

Since the LHS is known, the RHS can be calculated initially by setting $B_s = B_{max}$. If the RHS is greater than the LHS, the value of the stator flux density can be reduced and the other flux densities can be calculated at this reduced value and the magnetic field intensities can be calculated. This process is repeated till the RHS equals the LHS and the stator flux density is obtained as B_{smin} .

The inductance of tube 1 is then calculated as,

$$L_{u1} = \mathfrak{S}_1 \frac{B_{smin} A_{ls}}{i_p^2} \quad (2.236)$$

Obviously, path 5 has the exact same inductance and the procedure need not be repeated.

Therefore,

$$L_{u5} = L_{u1} \quad (2.237)$$

Tube 2: Considering Figure 2.32, since tube 2 has a similar shape as tube 1, the center of the shaft has the xy coordinates of (0,0). The angle θ_1 is assumed to be $\frac{\beta_s}{5}$. The length AB is

calculated as $x_1 = \frac{D}{2} \sin(\theta_1)$. The length OA is calculated as $y_1 = \frac{D}{2} \cos(\theta_1)$. Considering that point B has the coordinates as,

$$(x_1, y_1) = \left(\left(\frac{D}{2} \right) \sin \left(\frac{\beta_s}{5} \right), \left(\frac{D}{2} \right) \cos \left(\frac{\beta_s}{5} \right) \right). \quad (2.238)$$

The angle θ_5 is calculated as,

$$\theta_5 = \frac{\theta_{rp}}{2} - \frac{\beta_r}{2} - \theta \quad (2.239)$$

The coordinates of point C is given as,

$$(x_2, y_2) = \left(\left(\frac{D}{2} - g - h_{e2u} \right) \sin \theta_5, \left(\frac{D}{2} - g - h_{e2u} \right) \cos \theta_5 \right) \quad (2.240)$$

where,

$$h_{e2u} = \frac{h_r}{2} \left(1 - \frac{\theta}{2 \left(\frac{\theta_{rp}}{2} - \frac{\beta_s + \beta_r}{2} \right)} \right) \quad (2.241)$$

The linear distance between the points B and C, is assumed to be one side of an equilateral triangle and forms the radius of the arc formed by tube 2. If this length is given from (2.238) and (2.240) as follows,

$$l_{x2} = \sqrt{(x_2 - x_1)^2 + (y_2 - y_1)^2} \quad (2.242)$$

the length of the tube is given by,

$$l_2 = l_{x2} \frac{\pi}{3}. \quad (2.243)$$

The rotor area can be calculated as,

$$A_{2r} = h_r L - A_{1r} \quad (2.244)$$

where A_{1r} is the rotor area for that particular position calculated for path 1 in (2.217).

The area of the tube is calculated as,

$$A_2 = \frac{1}{2} \left(L \frac{\beta_s}{5} \frac{D}{2} + A_{2r} \right) \quad (2.245)$$

The length of the path through the rotor is given as,

$$l_r = h_r - h_{e2u} \quad (2.246)$$

The length of the path through the stator, yoke and rotor core is given by (2.23), (2.27) and (2.76), respectively. The area of the stator pole, yoke and rotor core is given by (2.218), (2.36) and (2.15), respectively. The reluctance of the air gap of path 2 in the upper portion is given as,

$$\mathfrak{R}_2 = \frac{l_2}{\mu_0 A_2} \quad (2.247)$$

The above calculations are valid for the tube passing in the upper portion of the stator. In the lower portion, the pole is moving away from the excited portion. This is similar to the effects experienced by tube 4 in the upper portion. Therefore, path 4 calculations are performed next.

Tube 4: Considering that point B has the coordinates as,

$$(x_1, y_1) = \left(-\left(\frac{D}{2}\right) \sin\left(\frac{\beta_s}{5}\right), \left(\frac{D}{2}\right) \cos\left(\frac{\beta_s}{5}\right) \right). \quad (2.248)$$

The angle θ_5 is calculated as,

$$\theta_5 = \frac{\theta_{rp}}{2} - \frac{\beta_r}{2} + \theta \quad (2.249)$$

The coordinates of point C is given as,

$$(x_2, y_2) = \left(\left(\frac{D}{2} - g - h_{e4u}\right) \sin \theta_5, \left(\frac{D}{2} - g - h_{e4u}\right) \cos \theta_5 \right) \quad (2.250)$$

where,

$$h_{e4u} = \frac{h_r}{2} \left(1 + \frac{\theta}{2 \left(\frac{\theta_{rp}}{2} - \frac{\beta_s + \beta_r}{2} \right)} \right) \quad (2.251)$$

The linear distance between the points B and C, is assumed to be one side of an equilateral triangle and forms the radius of the arc formed by tube 4. If this length is given from (2.248) and (2.250) as follows,

$$l_{x4} = \sqrt{(x_2 - x_1)^2 + (y_2 - y_1)^2} \quad (2.252)$$

the length of the tube is given by,

$$l_4 = l_{x4} \frac{\pi}{3}. \quad (2.253)$$

The rotor area can be calculated as,

$$A_{4r} = h_r L - A_{5r} \quad (2.254)$$

where A_{5r} is the rotor area for that particular position obtained from (2.228).

The area of the tube is calculated as,

$$A_4 = \frac{1}{2} \left(L \frac{\beta_s D}{5} + A_{4r} \right) \quad (2.255)$$

The length of the path through the rotor is given as,

$$l_r = h_r - h_{e4u} \quad (2.256)$$

The reluctance of the air gap of path 4 in the upper portion is given as,

$$\mathfrak{R}_4 = \frac{l_4}{\mu_o A_4} \quad (2.257)$$

The combined reluctance for path 2 is given by,

$$\mathfrak{R}_{2,4} = \mathfrak{R}_2 + \mathfrak{R}_4 \quad (2.258)$$

The permeance of tube 2 is calculated as,

$$P_2 = \frac{1}{\mathfrak{R}_{2,4}} \quad (2.259)$$

The magnetic circuit equation of tube 2 can be written as,

$$\mathfrak{S}_2 = T_{ph} i = 2(H_s l_s + H_r l_r) + \frac{B_s A_{2s}}{P_2} + H_{rc} l_{rc} + H_y l_y \quad (2.260)$$

The inductance of tube 2 is then calculated as,

$$L_{u2} = \mathfrak{S}_2 \frac{B_s \min A_{2s}}{i_p^2}. \quad (2.261)$$

Obviously, path 4 has the exact same inductance and the procedure need not be repeated.

Therefore,

$$L_{u4} = L_{u2} \cdot \quad (2.262)$$

Tube 3: Considering Figure 2.10, the area of the tube at the stator pole is calculated as,

$$A_{3s} = \frac{\beta_s}{5} \frac{D}{2} L \quad (2.263)$$

The angle θ_2 is given by,

$$\theta_2 = \frac{\frac{\beta_r}{2} \left(\frac{D}{2} - g \right)}{\left(\frac{D}{2} - g - h_r \right)} \quad (2.264)$$

The angle θ_3 is calculated as,

$$\theta_3 = \frac{\theta_{rp}}{2} - \theta_2 \quad (2.265)$$

The area of the tube at the rotor core is calculated,

$$A_{3rc} = 2 \left(\frac{D}{2} - g - h_r \right) \theta_3 L \quad (2.266)$$

The average area of A_3 is calculated as,

$$A_3 = \frac{A_{3s} + A_{3rc}}{2} = \frac{1}{2} \frac{\beta_s}{5} \frac{D}{2} L + \left(\frac{D}{2} - g - h_r \right) \theta_3 L \quad (2.267)$$

The length of the air gap is given as,

$$l_3 = \frac{D}{2} - g - h_r \quad (2.268)$$

The area of the stator pole is given as

$$A_{3s} = \frac{\beta_s}{5} \frac{D}{2} L \quad (2.269)$$

The length of the path through the stator, yoke and rotor core is given by (2.23), (2.27) and (2.26), respectively. The area of the yoke is given by (2.36).

As the rotor moves, although the shape of the tube changes, the length and the area of the path is assumed to be same without too much error in the calculations.

The reluctance of the air gap of path 3 is given as,

$$\mathfrak{R}_3 = \frac{2l_3}{\mu_0 A_3} \quad (2.270)$$

The permeance of tube 3 is calculated as,

$$P_3 = \frac{1}{\mathfrak{R}_3} \quad (2.271)$$

The magnetic circuit equation of tube 3 can be written as,

$$\mathfrak{S}_3 = T_{ph} i = 2(H_s l_s) + \frac{B_s A_{3s}}{P_3} + \frac{H_{rc} l_{rc}}{2} + \frac{H_y l_y}{2} \quad (2.272)$$

The unaligned inductance of tube 3 is then calculated as,

$$L_{u3} = \mathfrak{S}_3 \frac{B_s \min A_{3s}}{i_p^2}. \quad (2.273)$$

Tube 6: To calculate the length l_6 and area A_6 , consider Figure 2.16. The area of the tube at the stator pole is calculated as,

$$A_{6s} = \frac{h_s}{4} L \quad (2.274)$$

The area of the tube at the rotor pole is calculated,

$$A_{6r} = \frac{\beta_r}{4} L \left(\frac{D}{2} - g \right) \quad (2.275)$$

The average area of A_6 is calculated as,

$$A_6 = \frac{A_{6s} + A_{6r}}{2} \quad (2.276)$$

Tube 6 can be assumed to be an arc centered at the point D. The length AO is assumed to be,

$$y_1 = \frac{D}{2} \cos\left(\frac{\beta_s}{2}\right) + \frac{h_s}{8}. \quad (2.277)$$

The length AB is obtained in (2.114). The angle θ_1 can be calculated from (2.114) and (2.277) as,

$$\theta_1 = \tan^{-1} \left(\frac{x_1}{y_1 - \left(\frac{D}{2} - g - h_r \right)} \right). \quad (2.278)$$

The angle θ_2 is assumed to be

$$\theta_2 = \frac{\pi}{N_r} - \frac{3\beta_r}{8} - \theta. \quad (2.279)$$

The length CE is given by

$$y_2 = \left(\frac{D}{2} - g \right) \cos(\theta_2) - \left(\frac{D}{2} - g - h_r \right). \quad (2.280)$$

The length DE is given by

$$x_2 = \left(\frac{D}{2} - g \right) \sin(\theta_2). \quad (2.281)$$

The angle θ_3 can be calculated as

$$\theta_3 = \tan^{-1} \left(\frac{y_2}{x_2} \right). \quad (2.282)$$

The angle θ_4 is obtained from (2.278) and (2.282) as,

$$\theta_4 = \frac{\pi}{2} - \theta_1 - \theta_3. \quad (2.283)$$

The length DB is given from (2.114) and (2.278) as,

$$r_1 = \frac{x_1}{\sin(\theta_1)}. \quad (2.284)$$

The length CD is given from (2.280) and (2.281) as,

$$r_2 = \sqrt{x_2^2 + y_2^2}. \quad (2.285)$$

The length of the flux path is approximately given from (2.283)-(2.285) as,

$$l_6 = \frac{r_1 + r_2}{2} \theta_4. \quad (2.286)$$

The area of the yoke and rotor core is given by (2.36) and (2.15), respectively. The length of the path in the rotor is given by (2.124). The length of the path in the stator is calculated as,

$$l_s = h_s + \frac{C}{2} - \frac{1}{2} \frac{h_s}{4} \quad (2.287)$$

The reluctance of the air gap of path 6 in the upper portion is given as,

$$\mathfrak{R}_6 = \frac{l_6}{\mu_0 A_6} \quad (2.288)$$

The above calculations are valid for the tube passing in the upper portion of the stator. In the lower portion, the pole is moving away from the excited portion. This is similar to the effects experienced by tube 7 in the upper portion. Therefore, path 7 calculations are performed next.

Tube 7: To calculate the length l_7 and area A_7 , consider Figure 2.16. The area of the tube at the stator pole is calculated as,

$$A_{7s} = \frac{h_s}{4} L \quad (2.289)$$

The area of the tube at the rotor pole is calculated,

$$A_{7r} = \frac{\beta_r}{4} L \left(\frac{D}{2} - g \right) \quad (2.290)$$

The average area of A_7 is calculated as,

$$A_7 = \frac{A_{7s} + A_{7r}}{2} \quad (2.291)$$

Tube 7 can be assumed to be an arc centered at the point D. The length AO is given (2.277) and the length AB is given by (2.114). The angle θ_1 can be calculated by (2.278). The angle θ_2 is assumed to be

$$\theta_2 = \frac{\pi}{N_r} - \frac{3\beta_r}{8} + \theta. \quad (2.292)$$

The length CE is given by,

$$y_2 = \left(\frac{D}{2} - g \right) \cos(\theta_2) - \left(\frac{D}{2} - g - h_r \right). \quad (2.293)$$

The length DE is given by,

$$x_2 = \left(\frac{D}{2} - g \right) \sin(\theta_2). \quad (2.294)$$

The angle θ_3 can be calculated as,

$$\theta_3 = \tan^{-1} \left(\frac{y_2}{x_2} \right). \quad (2.295)$$

The angle θ_4 is obtained from (2.278) and (2.295) as,

$$\theta_4 = \frac{\pi}{2} - \theta_1 - \theta_3. \quad (2.296)$$

The length DB is given by (2.284). The length CD is given from (2.293) and (2.294) as,

$$r_2 = \sqrt{x_2^2 + y_2^2}. \quad (2.297)$$

The length of the flux path is approximately given from (2.284), (2.296) and (2.297) by,

$$l_7 = \frac{r_1 + r_2}{2} \theta_4. \quad (2.298)$$

The length of the path in the rotor is calculated from (2.124). The length of the path in the stator is calculated from (2.287). The reluctance of the air gap of path 7 in the upper portion is given as,

$$\mathfrak{R}_7 = \frac{l_7}{\mu_0 A_7} \quad (2.299)$$

The combined reluctance for path 6 is given by,

$$\mathfrak{R}_{6,7} = \mathfrak{R}_6 + \mathfrak{R}_7 \quad (2.300)$$

The permeance of tube 6 is calculated as,

$$P_6 = \frac{1}{\mathfrak{R}_{6,7}} \quad (2.301)$$

The magnetic circuit equation of tube 6 can be written as,

$$\mathfrak{S}_6 = T_{ph} i = \mathfrak{R}_L \phi = 2(H_s l_s + H_r l_r) + \frac{B_s A_{6s}}{P_6} + H_{rc} l_{rc} + H_y l_y \quad (2.302)$$

The unaligned inductance of tube 6 is then calculated as,

$$L_{u6} = \mathfrak{S}_6 \frac{B_s \min A_{6s}}{i_p^2}. \quad (2.303)$$

Obviously, path 7 has the exact same inductance and the procedure need not be repeated.

Therefore,

$$L_{u7} = L_{u6}. \quad (2.304)$$

Tube 8: To calculate the length l_8 and area A_8 , consider Figure 2.17. The area of the tube is calculated as,

$$A_8 = \frac{h_s}{2} L \quad (2.305)$$

Tube 8 can be assumed to be an arc centered at the center of the shaft.

The length AO is assumed to be,

$$y_1 = \frac{D}{2} \cos\left(\frac{\beta_s}{2}\right) + \frac{h_s}{2}. \quad (2.306)$$

The length AB is given by (2.114). The angle θ_1 can be calculated from (2.114) and (2.306) as,

$$\theta_1 = \tan^{-1}\left(\frac{x_1}{y_1}\right). \quad (2.307)$$

The angle θ_2 is assumed to be,

$$\theta_2 = \frac{2\pi}{N_s} - 2\theta_1. \quad (2.308)$$

The length CO is given from (2.114) and (2.307) as,

$$r_1 = \frac{x_1}{\sin(\theta_1)}. \quad (2.309)$$

The length of the tube is given from (2.308) and (2.309) as,

$$l_8 = r_1 \theta_2. \quad (2.310)$$

The area of the stator core is given by,

$$A_s = \frac{h_s}{2} L \quad (2.311)$$

The length of the path through the stator,

$$l_s = \frac{h_s}{2} + \frac{C}{2} \quad (2.312)$$

The area of the yoke is given by (2.36). The length of the path through the yoke is given by (2.138). The magnetic circuit equation of tube 8 can be written as,

$$\mathfrak{S}_8 = \frac{1}{2} \frac{3T_{ph} i}{4} = \mathfrak{R}_L \phi = 2(H_s l_s) + \frac{B_s A_8}{P_8} + H_y l_y \quad (2.313)$$

The unaligned inductance of tube 8 is then calculated as,

$$L_{u8} = \mathfrak{S}_8 \frac{B_s \min A_8}{i_p^2}. \quad (2.314)$$

Tube 9: To calculate the length l_9 and area A_9 , consider Figure 2.19. The area of the tube is calculated as,

$$A_9 = \frac{h_s}{4} L \quad (2.315)$$

Tube 9 is assumed to be an arc centered about point B. The length is approximately calculated as,

$$l_9 = \frac{h_s}{8} \frac{\pi}{2} \quad (2.316)$$

The stator and yoke area remain same as above. The length of the path in the stator is calculated as,

$$l_s = \frac{1}{2} \frac{h_s}{4} + \frac{C}{2} \quad (2.317)$$

The yoke length is approximately,

$$l_y = l_s \quad (2.318)$$

The magnetic circuit equation of tube 9 can be written as,

$$\mathfrak{S}_9 = \frac{1}{2} \frac{T_{ph} i}{2} = \mathfrak{R}_L \phi = H_s l_s + \frac{B_s A_9}{P_9} + H_y l_y \quad (2.319)$$

The unaligned inductance of tube 9 is then calculated as,

$$L_{u9} = \mathfrak{S}_9 \frac{B_s \min A_9}{i_p^2}. \quad (2.320)$$

The total inductance at a position θ in region I is given by,

$$L_{u\theta} = (L_{u1} + L_{u2} + L_{u3} + L_{u4} + L_{u5} + L_{u6} + L_{u7}) + 4(L_{u8} + L_{u9}) \quad (2.321)$$

Region II: $\frac{\pi}{N_r} - \left(\frac{\beta_s + \beta_s}{2} \right) < \theta < \frac{\pi}{N_r} - \left(\frac{-\beta_s + \beta_r}{2} \right)$

The flux tubes are identified as follows:

Tube 1: This tube is considered to be a tube that encompasses the overlap region. Therefore the area of the tube is given by,

$$A_1 = L \frac{D}{2} \left(\theta - \frac{\pi}{N_r} + \left(\frac{\beta_s + \beta_r}{2} \right) \right) \quad (2.322)$$

The length of the air gap is given by,

$$l_1 = g \quad (2.323)$$

The area of the stator core is given by,

$$A_{1s} = A_1 \quad (2.324)$$

The length of the path through the stator, yoke, rotor and rotor core is given by (2.23), (2.27), (2.124) and (2.26), respectively. The area of the yoke and rotor core is given by (2.36) and (2.15).

The area of the rotor core is given by,

$$A_{1r} = A_1 \quad (2.325)$$

The reluctance of tube 1 is calculated as,

$$\mathfrak{R}_1 = \frac{2l_1}{\mu_0 A_1} \quad (2.326)$$

The permeance of tube 1 is,

$$P_1 = \frac{1}{\mathfrak{R}_1} \quad (2.327)$$

The magnetic circuit equation of tube 1 can be written as,

$$\mathfrak{S}_1 = T_{ph} i = 2(H_s l_s + H_r l_r) + \frac{B_s A_1}{P_1} + \frac{H_{rc} l_{rc}}{2} + \frac{H_y l_y}{2} \quad (2.328)$$

The inductance of tube 1 is then calculated as,

$$L_{a1} = \mathfrak{S}_1 \frac{B_{s \min} A_1}{i_p^2} \quad (2.329)$$

Tube 2: To calculate the length l_2 and area A_2 , consider Figure 2.33. The area of the tube at the rotor pole is calculated and is assumed to be equal to the tube area,

$$A_2 = L \frac{D}{2} \left(\beta_r - \theta + \frac{\pi}{N_r} - \left(\frac{\beta_s + \beta_r}{2} \right) \right) \quad (2.330)$$

Tube 2 can be assumed to be an arc centered at the point D. The angle θ_2 is assumed to be,

$$\theta_2 = \frac{\left(\beta_r - \theta + \frac{\pi}{N_r} - \left(\frac{\beta_s + \beta_r}{2} \right) \right)}{2} + \frac{\beta_s}{2}. \quad (2.331)$$

The length CE is given by,

$$y_2 = \left(\frac{D}{2} - g \right) \cos(\theta_2) - \left(\frac{D}{2} - g - h_r \right). \quad (2.332)$$

The length DE is given by,

$$x_2 = \left(\frac{D}{2} - g \right) \sin(\theta_2). \quad (2.333)$$

The angle θ_3 can be calculated from (2.332) and (2.333) as,

$$\theta_3 = \tan^{-1} \left(\frac{y_2}{x_2} \right). \quad (2.334)$$

The length CD is given from (2.332) and (2.333) as,

$$r_2 = \sqrt{x_2^2 + y_2^2}. \quad (2.335)$$

The angle θ_1 is assumed as,

$$\theta_1 = \frac{\beta_s}{2}. \quad (2.336)$$

The angle θ_4 is obtained from (2.334) and (2.336) as,

$$\theta_4 = \frac{\pi}{2} - \theta_1 - \theta_3. \quad (2.337)$$

The length of the flux path is approximately given from (2.335) and (2.337) by,

$$l_2 = r_2 \theta_4. \quad (2.338)$$

The reluctance of tube 2 is calculated as,

$$\mathfrak{R}_2 = \frac{2l_2}{\mu_0 A_2} \quad (2.339)$$

The permeance of tube 2 is,

$$P_2 = \frac{1}{\mathfrak{R}_2} \quad (2.340)$$

The yoke and rotor core area are given by (2.36) and (2.15). The stator pole area and the rotor pole area are given by,

$$A_{2s} = A_{2r} = A_2 \quad (2.341)$$

The length of the path in the rotor is calculated from (2.124). The length of the path in the stator is calculated approximately as,

$$l_s = h_s + \frac{C}{2} - \left(\frac{D}{2} - g \right) (\theta_2) \quad (2.342)$$

The magnetic circuit equation of tube 2 can be written as,

$$\mathfrak{S}_2 = T_{ph} i = \mathfrak{R}_L \phi = 2(H_s l_s + H_r l_r) + \frac{B_s A_2}{P_2} + \frac{H_{rc} l_{rc}}{2} + \frac{H_y l_y}{2} \quad (2.343)$$

The inductance of tube 2 is then calculated as,

$$L_{a2} = \mathfrak{S}_2 \frac{B_s \min A_2}{i_p^2}. \quad (2.344)$$

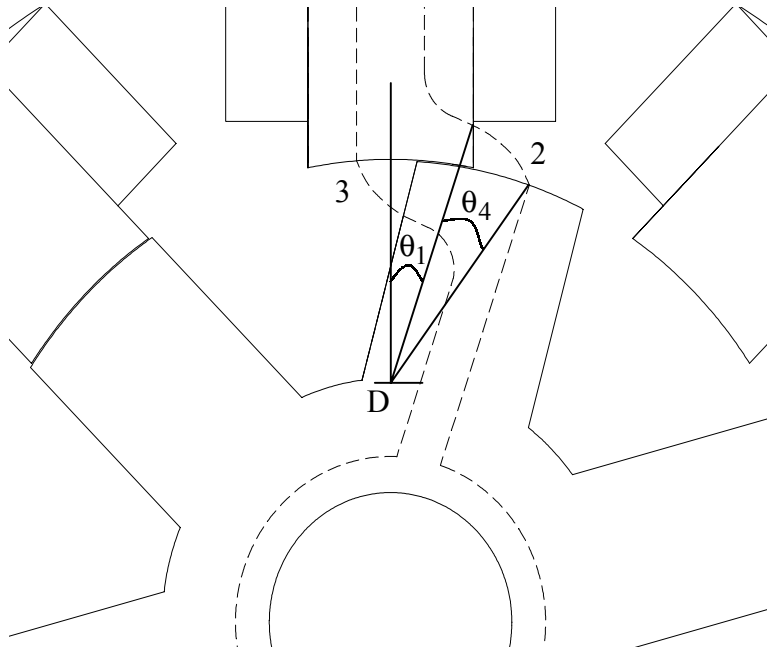


Figure 2.33 Tube 2 and Tube 3 calculations in the overlap region

Tube 3: To calculate the length l_3 and area A_3 , consider Figure 2.33. The area of the tube at the rotor pole is calculated and is assumed to be equal to the tube area,

$$A_3 = L \frac{D}{2} \left(\beta_s - \theta + \frac{\pi}{N_r} - \left(\frac{\beta_s + \beta_r}{2} \right) \right) \quad (2.345)$$

Tube 3 can be assumed to be an arc similar to the arc in tube 1 of region 1.

The coordinate of the corner of the rotor pole is given by

$$(x_1, y_1) = \left(\left(\frac{D}{2} - g \right) \sin \left(\frac{\pi}{N_r} - \theta - \frac{\beta_r}{2} \right), \left(\frac{D}{2} - g \right) \cos \left(\frac{\pi}{N_r} - \theta - \frac{\beta_r}{2} \right) \right) \quad (2.346)$$

The varying point on the stator pole has the coordinates as,

$$(x_2, y_2) = \left(-\frac{D}{2} \sin \left(\frac{\theta - \left(\frac{\pi}{N_r} - \frac{\beta_s + \beta_r}{2} \right)}{2} \right), \frac{D}{2} \cos \left(\frac{\theta - \left(\frac{\pi}{N_r} - \frac{\beta_s + \beta_r}{2} \right)}{2} \right) \right) \quad (2.347)$$

The arc length can be considered to be,

$$l_{x3} = \sqrt{(x_2 - x_1)^2 + (y_2 - y_1)^2} \quad (2.348)$$

the length of the tube is approximately given by,

$$l_3 = l_{x3} \frac{\pi}{2}. \quad (2.349)$$

The area of the stator pole and rotor pole are given as,

$$A_{3s} = A_{3r} = A_3 \quad (2.350)$$

The yoke and rotor core areas, and the length of the path through the stator, yoke and rotor core are given by (2.36), (2.15), (2.23), (2.27) and (2.26), respectively.

The length of the path through the rotor,

$$l_r = h_r - l_{x3} \quad (2.351)$$

The reluctance of tube 3 is calculated as,

$$\mathfrak{R}_3 = \frac{2l_3}{\mu_0 A_3} \quad (2.352)$$

The permeance of tube 3 is,

$$P_3 = \frac{1}{\mathfrak{R}_3} \quad (2.353)$$

The magnetic circuit equation of tube 3 can be written as,

$$\mathfrak{S}_3 = T_{ph}i = 2(H_s l_s + H_r l_r) + \frac{B_s A_3}{P_3} + \frac{H_{rc} l_{rc}}{2} + \frac{H_y l_y}{2} \quad (2.354)$$

The unaligned inductance of tube 3 is then calculated as,

$$L_{a3} = \mathfrak{S}_3 \frac{B_{s \min} A_3}{i_p^2} . \quad (2.355)$$

The tubes 4 and 5 are assumed to be similar to tubes 8 and 9 from region I.

The total inductance at a position θ in region II is given by,

$$L_{a\theta} = (L_{a1} + L_{a2} + L_{a3}) + 4(L_{u4} + L_{u5}) \quad (2.356)$$

Region III: $\frac{\pi}{N_r} - \left(\frac{-\beta_s + \beta_r}{2} \right) \leq \theta < \frac{\pi}{N_r}$

Region III can be assumed to be the region where the rotor and stator are completely overlapping. The calculation of the inductance in this position is described by the aligned inductance calculations given by (2.44).

2.4 Design of a 5 h.p. SRM

A prototype 5 h.p. 8/6 machine is designed in this section. A complete analysis along with extensive selection criteria for the various parameters is performed to obtain a viable design of the machine. The prototype has the following specifications:

Power Output $P_{hp} = 5$ h.p.

Speed $N = 1500$ r.p.m.

Peak Current $i_p = 12$ A

Input AC voltage $V_{ac} = 480$ V

The torque to be developed by the machine is

$$T_{req} = \frac{P_{hp} * 746}{2\pi \left(\frac{N}{60} \right)} = \frac{5 * 746}{2\pi \left(\frac{1500}{60} \right)} = 23.7459 \text{ N-m.}$$

The machine will be designed with an IEC frame size of 100. The outer diameter of the stator is fixed as follows:

$$D_o = (\text{Frame Size} - 3) * 2 = (100 - 3) * 2 = 194 \text{ mm.}$$

The maximum possible stack length for frame 100 is initially restricted to 200 mm. This can be reduced if the design requires it but not increased. Therefore, $L = 200 \text{ mm}$.

IEC recommendations also require that if the greatest continuous torque is greater than 18 N-m and less than 31.5 N-m, the minimum shaft diameter required is 28 mm. Hence, $D_{sh} = 28 \text{ mm}$.

For a machine of this frame size, a practical air-gap length can be assumed to be $g = 0.5 \text{ mm}$. In some of the more advanced manufacturing facilities, this value can be reduced to approximately 0.3 mm.

An initial bore diameter D which is equal to the frame size is selected. Hence, initially $D = 100 \text{ mm}$. In the later stages of the design, this value will be optimized.

2.4.1 Selection of Stator and Rotor Pole Angles

For the 8/6 machine, the feasible triangle is shown in Figure 2.4. The procedure to calculate the average torque when the selection of D_o , D_{sh} , L , D , g , β_s and β_r is complete is described in sections 2.1.5-2.1.8. Since the values of β_s and β_r are still unknown, initially designs will be made for all possible integer combinations of the pole angles and then various criteria will be used to eliminate a number of the combinations. Although this process may seem to be long and complicated as there are possibly 256 integer combinations, this exercise may be worth the effort since it would give some guidelines on reducing the possible combinations. Figure 2.34 shows the plot of developed torque vs. rotor pole angles for various stator pole angles. Figure 2.35 shows the plot of developed torque per unit iron volume vs. rotor pole angles for various stator pole angles. Eliminating the combinations when $\beta_s = \beta_r$ reduces the number of viable combinations to 240. Noticing that there is a massive drop in torque/unit iron volume when $\beta_r - \beta_s > 5^\circ$, all combinations beyond that value are eliminated. This reduces the number of feasible combinations to 71. For the remaining combinations, a plot of the available clearance space between the tips of windings in adjacent poles is plotted as shown in Figure 2.36. The winding design was done to uniformly have a maximum current density of 6 A/mm^2 . Obviously this value cannot be less than zero and preferably the clearance should be greater than 5 mm.

This allows the elimination of some more combinations reducing the number of possible combinations to 45.

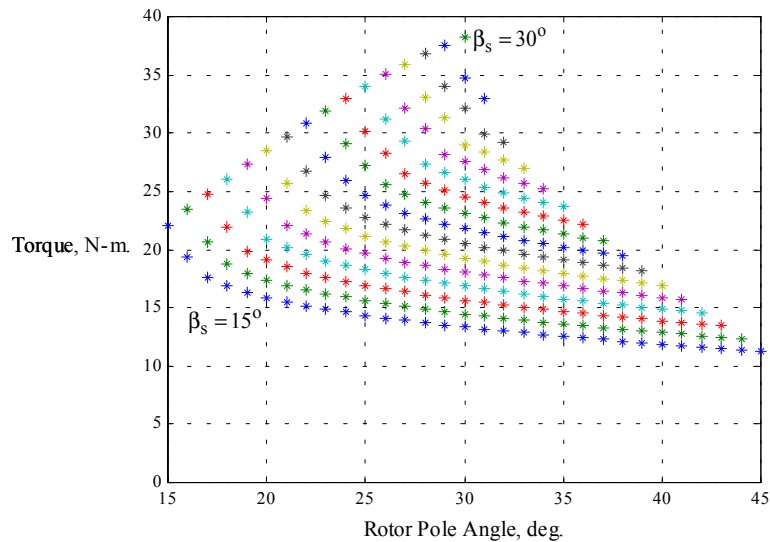


Figure 2.34 Plot of torque vs. rotor pole angles for varying stator pole angles from 15° to 30°

Assuming that some errors may be present in the calculation of the minimum inductance, all combinations which produce an average torque lower than 23.75 N-m is eliminated. Examining Figure 2.37, this reduces the number of possible combinations to 13.

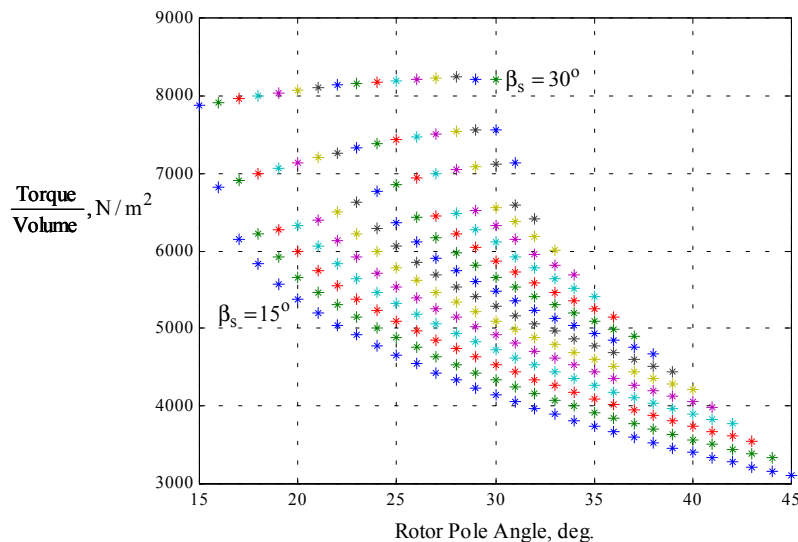


Figure 2.35 Plot of torque/iron volume vs. rotor pole angles for varying stator pole angles from 15° to 30°

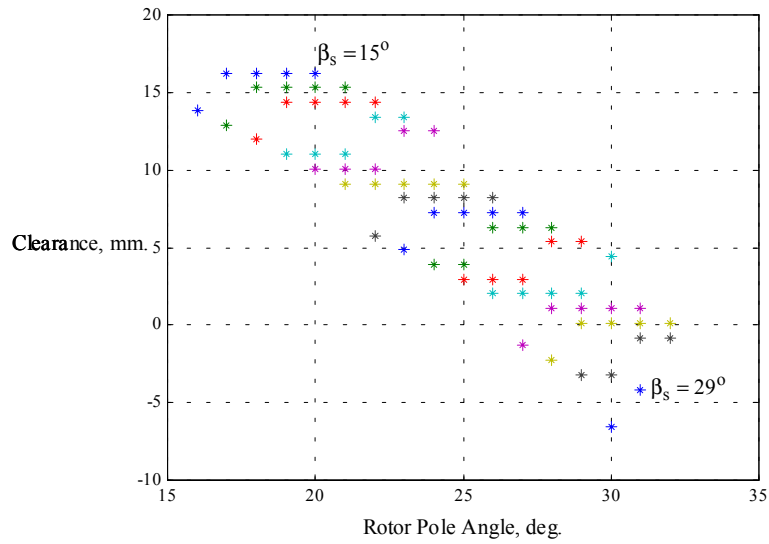


Figure 2.36 Plot of clearance vs. rotor pole angles for varying stator pole angles from 15° to 29°

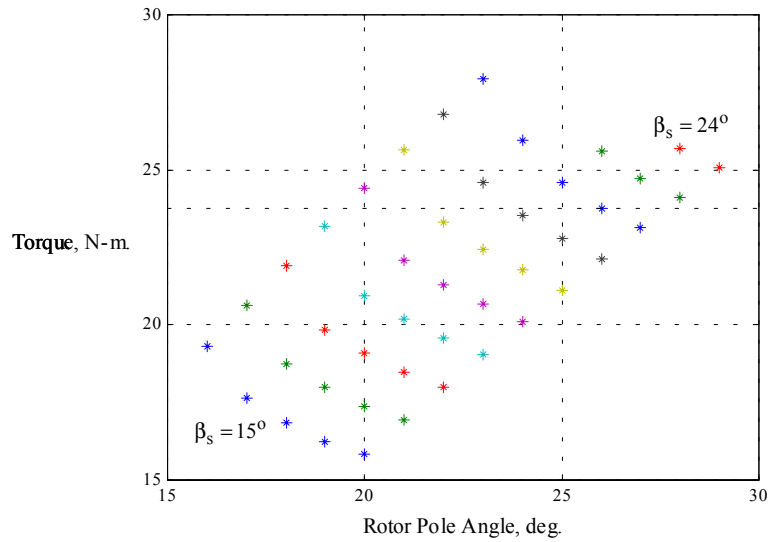


Figure 2.37 Plot of torque vs. rotor pole angles for varying stator pole angles from 15° to 24°

A re-examination of the torque/iron volume for the remaining combinations (Figure 2.38) clearly demonstrates that there are 6 possible combinations for this prototype. Since the 6 combinations produce different output torques, the stack lengths are reduced so as to obtain the desired output torque. The 6 combinations are examined more closely in Table 2.1. It can be seen that the possibilities narrow down to the combination 3, 4 and 6. Since combination 6 has a lower

torque/iron volume ratio, combination 4 is selected for this prototype. This combination has a stator pole arc of 22° and a rotor pole arc of 23° .

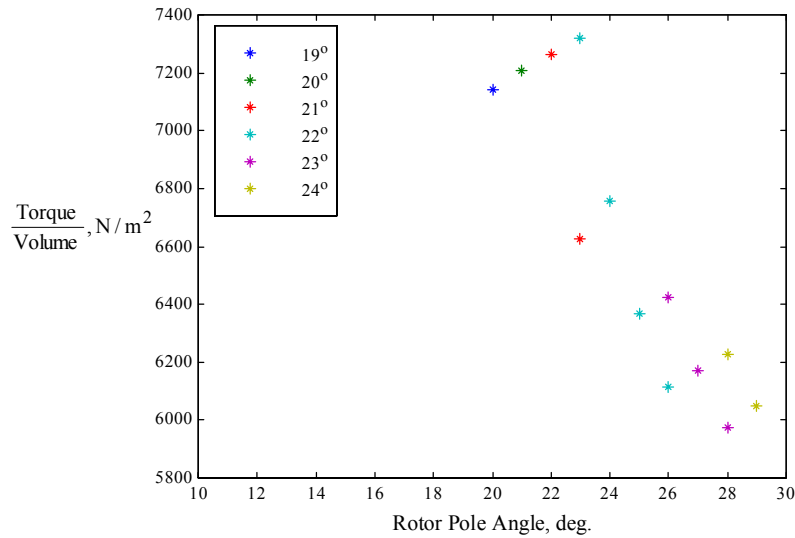


Figure 2.38 Plot of torque/iron volume vs. rotor pole angles

Summary of selection process for stator and rotor pole angles:

1. Limit initial possible combinations of rotor pole angles to 2° greater than the stator pole angle. This cuts down the initial set of combinations to 30.
2. Check the clearance between windings for these combinations and eliminate combinations that have very low or negative clearances. The actual minimum value varies with frame size. Adequate clearance also reduces mutual inductance between windings.
3. Check the torque produced for the remaining combinations and eliminate combinations that have an average torque less than the required rated torque.
4. Check the average torque per unit iron volume and select the combinations that produce the highest values.
5. Normalize torque output by varying stack lengths and examine the remaining combinations in depth.

Table 2.1 In depth examination of 6 possible combinations

	1	2	3	4	5	6
Stator pole angle, deg	19	20	21	22	21	22
Rotor pole angle, deg	20	21	22	23	23	24
Output torque, N.m	23.1457	23.7459	23.7459	23.7459	23.2835	23.7459
Clearance, mm.	7.8438	6.9014	3.1821	2.2396	5.9589	5.0164
Copper loss, W	177.954	175.579	171.95	166.01	168.25	164.77
Stack length, mm.	200	196.08	187.87	179.53	200	193.75
Iron volume, m ³	0.00342	0.003486	0.003464	0.003425	0.003712	0.003719
Torque/iron volume, N/m ²	6767.52	6811.06	6854.46	6933.03	6271.93	6384.46

2.4.2 Preliminary Design Process

Once the outer diameter, pole numbers, stack length and preliminary pole arcs are fixed, the bore diameter D is initially assumed to be equal to the frame size. And the stack length is set as $L = 180$ mm. Now, the B-H characteristics of the material, which will be used in the stator and rotor stampings, is examined. From Figure 2.5 the “knee” point of the characteristics is noted down as $B_{\max} = 1.65$ T.

Assuming that the stator pole flux density B_s is assumed to be equal to B_{\max} the rest of the machine can be designed. Neglecting leakage and stacking factor, the stator pole area A_s can be written as,

$$A_s = \frac{D}{2} L \beta_s = \frac{100}{2} 180 \frac{22 \cdot \pi}{180} 10^{-6} = 3.456 * 10^{-3} \text{ m}^2.$$

The flux in the stator pole ϕ is given by

$$\phi = B_s A_s = 1.65 * 3.264 * 10^{-3} = 5.702 \text{ mWb.}$$

The flux in the yoke ϕ_y is given by

$$\phi_y = \frac{\phi}{2} = \frac{B_s A_s}{2} = \frac{5.702 * 10^{-3}}{2} = 2.8512 \text{ mWb.}$$

The area of the yoke A_y can be set as,

$$A_y = A_s = 3.456 * 10^{-3} \text{ m}^2.$$

The back iron thickness C is obtained as,

$$C = \frac{A_y}{L} = \frac{3.456 * 10^{-3}}{180 * 10^{-3}} = 19.2 \text{ mm.}$$

The stator pole height h_s is given by,

$$h_s = \frac{D_o}{2} - C - \frac{D}{2} = \frac{194}{2} - 19.2 - \frac{100}{2} = 27.8 \text{ mm.}$$

The rotor pole area A_r is given by,

$$A_r = \left(\frac{D}{2} - g \right) L \beta_r = \left(\frac{100}{2} - 0.5 \right) 180 \frac{23 \cdot \pi}{180} 10^{-6} = 0.00358 \text{ m}^2.$$

The rotor pole flux density B_r is given by,

$$B_r = \frac{B_s A_s}{A_r} = \frac{1.65 * 0.003456}{0.00358} = 1.593 \text{ T.}$$

The area of the rotor core A_{rc} is given by,

$$A_{rc} = \frac{A_s}{1.6} = \frac{0.003456}{1.6} = 0.00216 \text{ m}^2.$$

The height of the rotor pole h_r is calculated as,

$$h_r = \frac{D}{2} - g - \frac{D_{sh}}{2} - \frac{A_{rc}}{L} = \left(\frac{100}{2} - 0.5 - \frac{28}{2} \right) * 10^{-3} - \frac{0.00216}{180 * 10^{-3}} = 23.5 \text{ mm.}$$

Neglecting leakage and fringing, the air-gap area can be approximately written as,

$$A_g = \left(\frac{D}{2} - \frac{g}{2} \right) \left(\frac{\beta_r + \beta_s}{2} \right) L = \left(\frac{100}{2} - \frac{0.5}{2} \right) \left(\frac{22 + 23}{2} \right) \frac{\pi}{180} 180 * 10^{-6} = 0.003517 \text{ m}^2.$$

The flux density in the air-gap B_g is given by,

$$B_g = \frac{A_s B_s}{A_g} = \frac{0.003456 * 1.65}{0.003517} = 1.6214 \text{ T.}$$

The magnetic field intensity of the air-gap H_g is calculated as,

$$H_g = \frac{B_g}{4\pi * 10^{-7}} = \frac{1.6214}{4\pi * 10^{-7}} = 1290255 \text{ AT/m.}$$

The magnetic field intensities in the stator pole, stator yoke, rotor pole and rotor core are designated as H_s , H_y , H_r and H_{rc} , respectively. They are obtained from the BH characteristics shown in Figure 2.5 as,

$$H_s = 6179.17 \text{ AT/m}$$

$$H_y = 238.54 \text{ AT/m}$$

$$H_r = 4445.4 \text{ AT/m}$$

$$H_{rc} = 960.34 \text{ AT/m}$$

The mean path lengths of various sections are given as follows:

$$l_s = h_s + \frac{C}{2} = 27.8 + \frac{19.2}{2} = 37.4 \text{ mm.}$$

$$l_g = g = 0.5 \text{ mm.}$$

$$l_r = \frac{D}{4} - \frac{g}{2} + \frac{h_r}{2} - \frac{D_{sh}}{4} = \frac{100}{4} - \frac{0.5}{2} + \frac{23.5}{2} - \frac{28}{4} = 29.5 \text{ mm.}$$

$$l_{rc} = \pi \left(\frac{D}{4} - \frac{g}{2} - \frac{h_r}{2} + \frac{D_{sh}}{4} \right) = \pi \left(\frac{100}{4} - \frac{0.5}{2} - \frac{23.5}{2} + \frac{28}{4} \right) = 62.83 \text{ mm.}$$

The mean length l_y for a circular yoke SRM is calculated as,

$$l_y = \pi \left(\frac{D_o}{2} - \frac{C}{2} \right) = \pi \left(\frac{194}{2} - \frac{19.2}{2} \right) = 274.58 \text{ mm.}$$

Now, the total ampere-turns \mathfrak{S} required for the machine operation at full load can be calculated.

The magnetic circuit equation is written as,

$$\begin{aligned} \mathfrak{S} = T_{ph} i &= 2(H_s l_s + H_g l_g + H_r l_r) + \frac{H_{rc} l_{rc}}{2} + \frac{H_y l_y}{2} = \\ &2(6179.17 * 0.0374 + 1290394 * 0.0005 + 4445.4 * 0.0295) + \frac{960.34 * 0.0628}{2} + \frac{238.54 * 0.2746}{2} = \\ &2077.7. \end{aligned}$$

Since initially the peak current was assumed to be $i_p = 12 \text{ A}$, the turns per phase is calculated as,

$$T_{ph} = \frac{\mathfrak{S}}{i_p} = \frac{2077.7}{12} = 173.14 \approx 172.$$

The rated current is calculated as,

$$i_p = \frac{\mathfrak{S}}{T_{ph}} = \frac{2077.7}{172} = 12.08 \text{ A.}$$

The aligned saturated inductance at maximum current neglecting leakage is calculated as,

$$L_{aligned} = \frac{T_{ph}\phi}{i_p} = \frac{\mathfrak{S}B_s A_s}{i_p^2} = \frac{2077.7 * 1.65 * 0.003456}{12.08^2} = 81.19 \text{ mH.}$$

2.4.3 Winding Design

Assuming a wedge thickness $h_{wedge} = 4 \text{ mm.}$, The stator pole arc length t_s is given by

$$t_s = \left(\frac{D}{2} + h_{wedge} \right) \beta_s = \left(\frac{100}{2} + 4 \right) \frac{22\pi}{180} = 20.73 \text{ mm.}$$

The stator pole pitch λ_s is given by

$$\lambda_s = \frac{\pi(D + 2h_{wedge})}{N_s} = \frac{(100 + 2 * 4)\pi}{8} = 42.41 \text{ mm.}$$

Assuming a maximum value of allowable current density $J = 6 \text{ A/mm}^2$ in the windings, the minimum area of conductor is given as,

$$a_c = \frac{i}{2J} = \frac{12.08}{2 * 6} = 1.007 \text{ mm}^2$$

Now a standard size conductor of area 1.167 mm^2 is chosen. The wire diameter d_w including insulation is given by

$$d_w = \sqrt{\frac{4a_c}{\pi}} + 0.1 = \sqrt{\frac{4 * 1.167}{\pi}} + 0.1 = 1.319 \text{ mm.}$$

The maximum height of the winding h_w which can be accommodated inclusive of the space required to place wedges that hold the windings in place is given by

$$h_w = h_s - h_{wedge} = 27.8 - 4 = 23.8 \text{ mm.}$$

The number of layers that can be accommodated in this available winding height is given by

$$N_{tlayer} = \frac{h_w f_f}{d_w} = \frac{23.8 * 0.95}{1.319} = 17.14 \approx 17.$$

f_f represents the field factor and is approximately equal to 0.95. Now the number of horizontal layers required for winding is given by

$$N_{layer} = \frac{T_{ph}}{2N_{tlayer}} + 1 = \frac{172}{2 * 17} + 1 = 6.058 \approx 7.$$

The width of the winding W_t is given by

$$W_t = \frac{d_w N_{\text{layer}}}{f_f} = \frac{1.319 \cdot 7}{0.95} = 9.719 \text{ mm.}$$

The space between 2 stator pole tips at the base of the windings is given by

$$Z = \lambda_s - t_s = 42.41 - 20.73 = 21.68 \text{ mm.}$$

The clearance between the windings at the bore is given by

$$Cl = Z - 2W_t = 21.68 - 2 \cdot 9.719 = 2.24 \text{ mm.}$$

Since this clearance is too small, the bore diameter can be changed from 100 mm to 98 mm in subsequent iterations. Since it has been shown before [KRI95] that the output torque, $T_{\text{av}} \propto D^2 L$, the stack length is raised from 180 mm to 200 mm.

Recalculating the parameters as shown above, it can be shown, $A_s = 3.763 \cdot 10^{-3} \text{ m}^2$, $\phi = 6.208 \text{ mWb}$, $\phi_y = 3.104 \text{ mWb}$, $C = 18.8 \text{ mm}$, $h_s = 29.2 \text{ mm}$, $A_r = 0.00389 \text{ m}^2$, $B_r = 1.595 \text{ T}$, $A_{rc} = 0.00235 \text{ m}^2$, $h_r = 22.74 \text{ mm}$, $A_g = 0.003829 \text{ m}^2$, $B_g = 1.6216 \text{ T}$, $H_g = 1290433 \text{ AT/m}$, $H_s = 6179.17 \text{ AT/m}$, $H_y = 238.54 \text{ AT/m}$, $H_r = 4453.5 \text{ AT/m}$, $H_{rc} = 960.34 \text{ AT/m}$, $l_s = 38.59 \text{ mm}$, $l_g = 0.5 \text{ mm}$, $l_r = 28.62 \text{ mm}$, $l_{rc} = 62.45 \text{ mm}$, $l_y = 275.18 \text{ mm}$, $\mathfrak{S} = 2085.12$, $T_{\text{ph}} = 172$, $i_p = 12.12 \text{ A}$ and $L_{\text{aligned}} = 79.3 \text{ mH}$. For the calculation of the clearance, it can be shown that, $t_s = 20.35 \text{ mm}$, $\lambda_s = 41.626 \text{ mm}$, $a_c = 1.167 \text{ mm}^2$, $d_w = 1.319 \text{ mm}$, $h_w = 25.2 \text{ mm}$, $N_{\text{tlayer}} = 18$, $N_{\text{layer}} = 6$, $W_t = 8.33 \text{ mm}$, $Z = 21.28 \text{ mm}$, and the clearance between the windings is calculated as $Cl = 4.62 \text{ mm}$.

Using the equations described in section (2.1.7), the unaligned inductance can be calculated as, $L_u = 16.08 \text{ mH}$. The aligned inductance including leakage is calculated as $L_a = 87.9 \text{ mH}$.

2.4.4 Calculation of Average Torque

In the SRM, a linear relationship is not present between the current in the machine and the torque developed. First, the peak current $i_p = 12.12 \text{ A}$ can be split into $n = 30$ equal parts.

Let $\delta i = \frac{i_p}{n} = \frac{12.12}{30} = 0.404 \text{ A}$. At the first point of calculation, $n_1 = 1$, current $i_1 = \delta i = 0.404 \text{ A}$.

Then $\mathfrak{S}_1 = T_{ph} i_1 = 172 \cdot 0.404 = 69.488$. Now assuming initially that $B_{s1} = B_s$, the flux densities, the AT/m and the ampere-turns for all the sections are calculated and the total AT is obtained. If this value is greater than \mathfrak{S}_1 , then the value of B_{s1} is reduced and the calculations are done again. If it is higher, then the value of B_{s1} can be increased and the calculations can be redone. This particular exercise is repeated till the error between the calculated value of ampere-turns and \mathfrak{S}_1 is negligible. When this value is obtained the corresponding flux at this point

$$\phi_1 = B_{s1} \cdot A_s = 0.08113 \cdot 0.00376 = 0.3058 \text{ mWb,}$$

is calculated. The aligned inductance value for this particular current is calculated as

$$L_{a1} = \frac{T_{ph} \phi_1}{i_1} = \frac{172 \cdot 0.3058 \cdot 10^{-3}}{0.404} = 0.1302 \text{ H.}$$

The flux linkage at this point is also obtained as $\lambda_{a1} = L_{a1} \cdot i_1 = 0.1302 \cdot 0.404 = 0.0526$.

The above procedure is repeated after each interval of δi , i.e., $i_2 = i_1 + \delta i$ and so on till we reach i_p . The value of $L_a^s = L_a = 81.976 \text{ mH}$ at current $i_p = 12.12 \text{ A}$ indicates the aligned saturated inductance at peak current or rated current. The flux linkage at this point is also obtained. The aligned flux linkages can then be plotted against various currents as shown in Figure 2.39.

The unaligned inductance does not change with varying current and so the unaligned flux linkages can be obtained at the various currents above as $\lambda_{u1} = L_u \cdot i_1 = 0.0231 \cdot 0.404 = 0.00934$ and so on till the rated current and is plotted in Figure 2.39.

The aligned work done $W_{aligned}$ is given by the area 0AC0 and the unaligned work done $W_{unaligned}$ is given by the area 0AB0. The total work done W is given by

$$W = W_{aligned} - W_{unaligned} = \text{Area 0BC0}$$

The aligned work $W_{aligned}$ work is given by

$$\begin{aligned} W_{aligned} &= \delta i (\lambda_1 + \lambda_2 + \dots + \lambda_{n-1}) + \frac{\lambda_n \delta i}{2} \\ &= 0.404 (0.0526 + 0.1051 + \dots + 1.0482) + \frac{1.0572 \cdot 0.404}{2} = 8.3938. \end{aligned}$$

The unaligned work $W_{unaligned}$ is given by

$$W_{unaligned} = \frac{1}{2} i_p \lambda_u = \frac{1}{2} i_p^2 L_u = \frac{1}{2} 12.12^2 \cdot 0.0231 = 1.6996.$$

The average torque is given by

$$T_{av} = \frac{WN_s N_r}{4\pi} = \frac{(8.3938 - 1.6996) \cdot 8 \cdot 6}{4\pi} = 25.6846 \text{ N} - \text{m}.$$

Since the average torque calculated above is slightly more than the required torque, no more redesign is required.

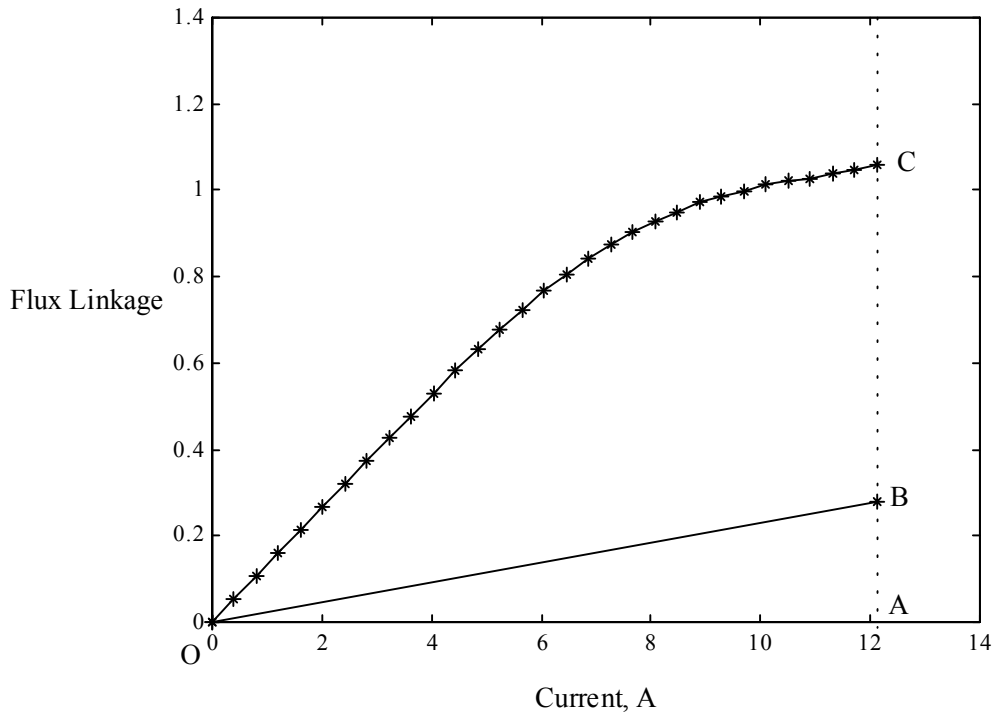


Figure 2.39. Plot of Flux Linkages vs. current for the prototype machine

2.4.5 Finite Element Verification of the Prototype

The finite element model is constructed for the given prototype and is shown in Figure 2.40. The finite element mesh is constructed with about 15665 nodes and 7812 surface elements and is shown in Figure 2.42. The finite element model is constructed with a moving air-gap that allows the calculation of the parameters for the movement of the rotor by 30° for a given current in each simulation. This allows simulations to be conducted for each current rather than each current and each position thereby speeding the entire verification procedure. The plot of inductance vs. position for different currents from 0A to 16A is shown in Figure 2.41 and the plot of torque vs. position for different currents from 0A to 16A is shown in Figure 2.43. It can be clearly seen that the rated torque is developed at a value close to 13 A and not 12 A as designed. This error

probably occurs due to the miscalculation of the inductance value. This exact value of inductance and torque can be confirmed only with practical experiments on a real prototype since the end effects are ignored both in the analytical and finite element processes in this design methodology.



Figure 2.40 Schematic of the designed prototype

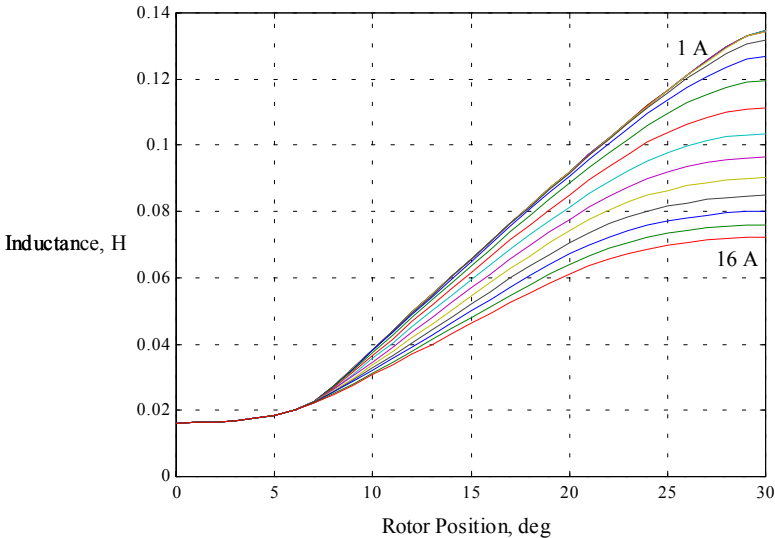


Figure 2.41 Inductance plot of the designed prototype for currents varying from 0A to 16A

2.4.6 Analysis of the Prototype

From the finite element analysis, it can be seen that a current of $i_p = 13$ A is required to produce the rated torque. The rest of the analysis is carried out at this peak current value instead of the designed peak current of 12.12 A. The main analysis parameters that are to be calculated are the stator phase resistance, copper losses, eddy-current losses, hysteresis losses and temperature rise of the machine and the losses associated with temperature rise. As mentioned before, the hysteresis loss calculation and the temperature related effects will be described in the final dissertation.

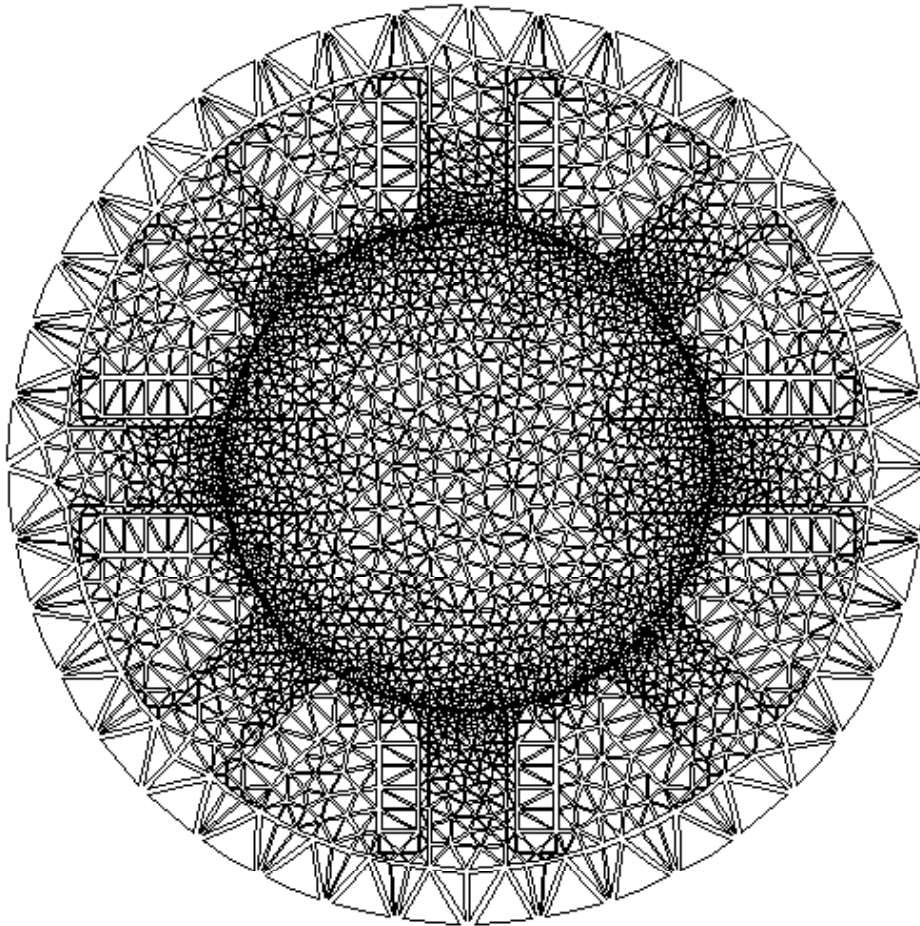


Figure 2.42 Finite Element Mesh of the designed prototype

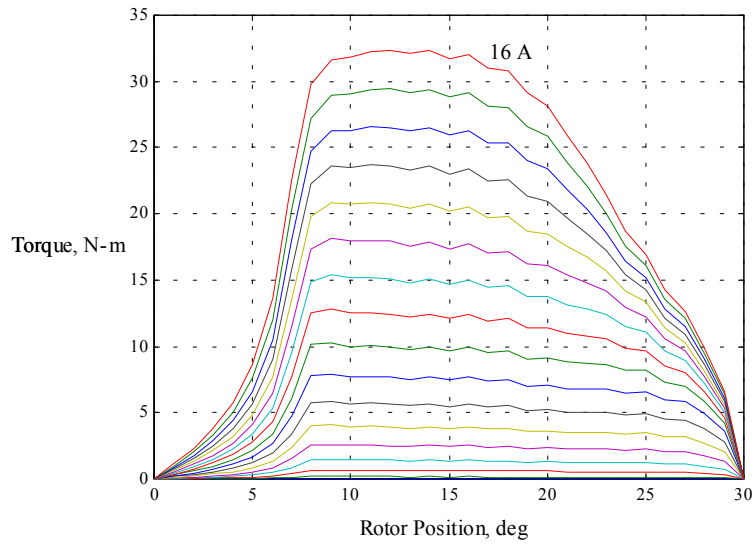


Figure 2.43 Torque plot of the designed prototype for currents varying from 0A to 16A

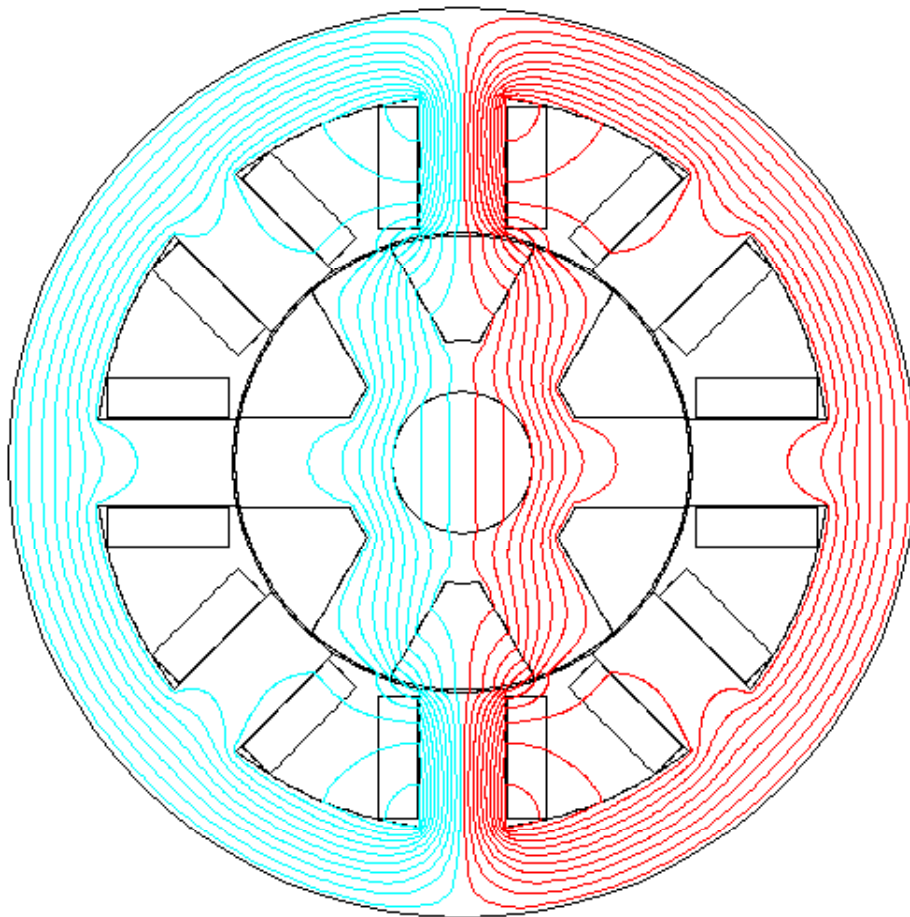


Figure 2.44 Equiflux lines in the unaligned position of the designed prototype

Copper Losses

The first step in calculating the copper losses involves the calculation of the resistance of each phase winding of the SRM. The mean length of a winding turn is given as,

$$l_m = \left(2L + 4W_t + 2D \sin\left(\frac{\beta_s}{2}\right) \right) * 10^{-3} = \left(2 \cdot 200 + 4 \cdot 8.33 + 2 \cdot 98 \sin\left(\frac{22\pi}{2 \cdot 180}\right) \right) * 10^{-3} = 0.471 \text{ m.}$$

The resistance of a single phase is calculated as,

$$R_s = \frac{0.0177 * l_m T_{ph}}{a_c} = \frac{0.0177 * 0.471 * 172}{1.167} = 1.229 \Omega.$$

The copper losses at rated current is given by

$$P_{cu} = i_p^2 R_s = 13^2 * 1.229 = 207.65 \text{ W.}$$

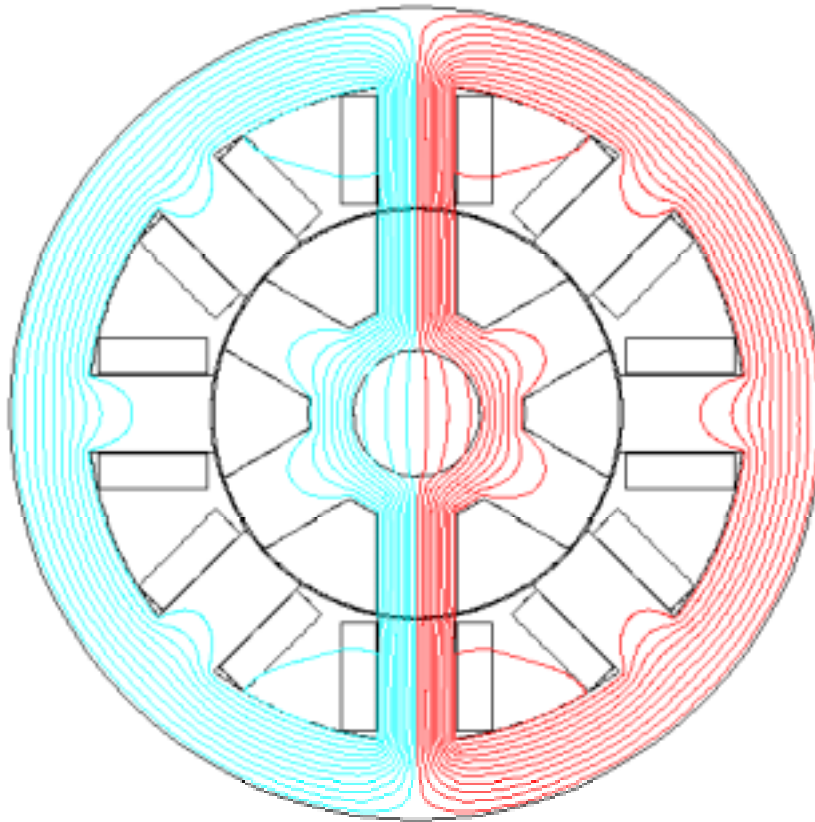


Figure 2.45 Equiflux lines in the aligned position of the designed prototype

Inductance Calculations: The inductance of a phase is calculated analytically using the procedure described in section 2.3.3. A very good correlation is seen in Figure 2.46 between the results especially at the unaligned and aligned position.

	Analytical Results	FEA Results
Unaligned Inductance	15.9 mH	16.18 mH
Aligned Inductance	83.8 mH	84.92 mH

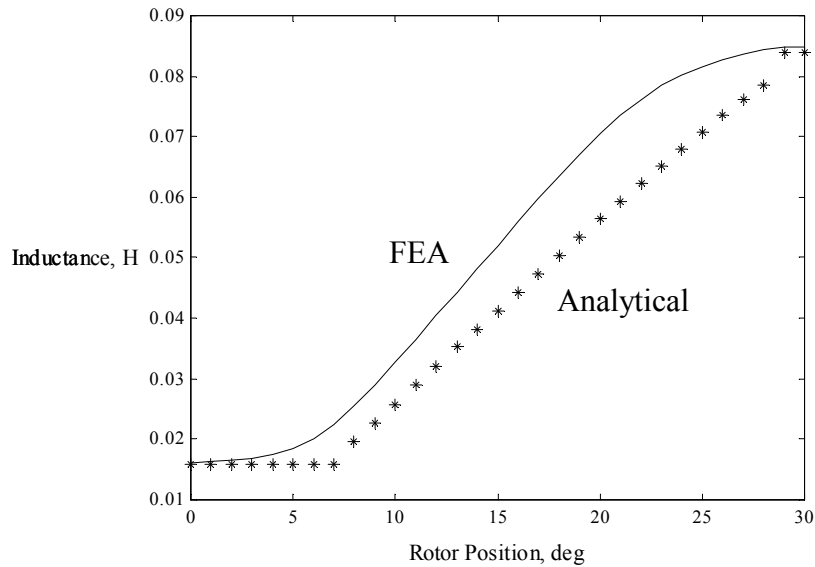


Figure 2.46 Comparison of analytical inductance calculation and FEA results at rated current.

The data of torque vs. rotor position when phase A is obtained to see if the mean torque developed is equal to the rated torque. The plot is shown in Figure 2.47 and the average torque developed is calculated as 23.82 N-m, which is slightly higher than the required rated torque.

2.5 Analysis of an existing 5 h.p. SRM

A 5 h.p. SRM which is currently present is analyzed and is compared to the design described in the previous section. The SRM has the following parameters.

Power Output $P_{hp} = 5$ h.p.

Speed $N = 1500$ r.p.m.

Peak Current $i_p = 13$ A

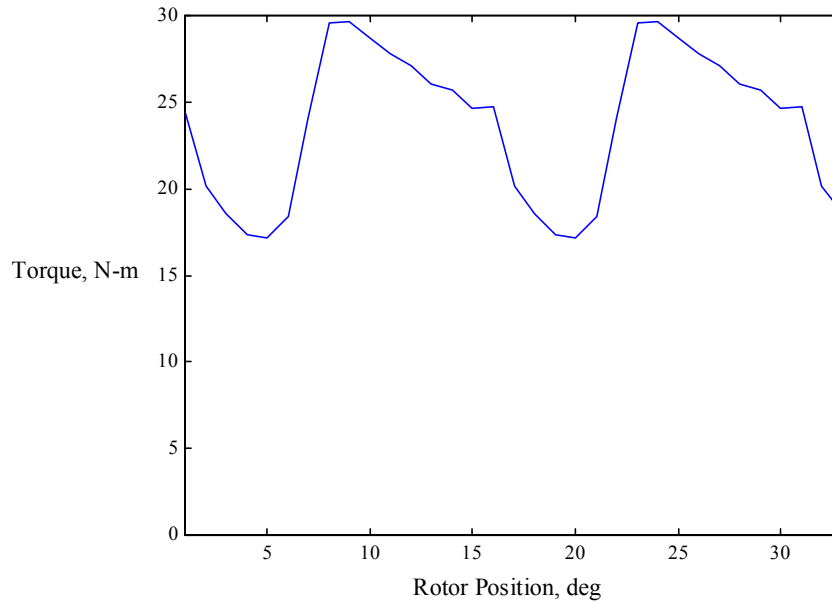


Figure 2.47 Plot of machine torque (the torque developed when current is falling in one phase while rising in another phase is accounted for)

Input AC voltage $V_{ac} = 480 \text{ V}$

The torque to be developed by the machine is

$$T_{req} = \frac{P_{hp} * 746}{2\pi \left(\frac{N}{60} \right)} = \frac{5 * 746}{2\pi \left(\frac{1500}{60} \right)} = 23.7459 \text{ N-m.}$$

$D_o = 190 \text{ mm}$, $L = 200 \text{ mm}$, $D_{sh} = 28 \text{ mm}$, $g = 0.5 \text{ mm}$, $D = 100.6 \text{ mm}$, $h_s = 32.7 \text{ mm}$, $h_r = 19.8 \text{ mm}$, $T_{ph} = 154$, and $a_c = 1.588 \text{ mm}^2$.

The analytically calculated parameters are as follows:

$$J = 3.6812 \text{ A/mm}^2$$

$$L_u = 11.35 \text{ mH}$$

$$L_a = 65.03 \text{ mH}$$

$$T_{av} = 21.1 \text{ N.m}$$

It can be clearly seen that the average torque developed is only about 88% of the required maximum torque. It will be seen in further analysis whether this analytical prediction is confirmed by finite element analysis.

Figure 2.48 shows that at the rated current the rated torque of 23.79 N-m is obtained but it is crucial to check the maximum average torque obtained by restricting the maximum flux density in the stator pole to the knee point. This is one of the results obtained while calculating the eddy-current losses.

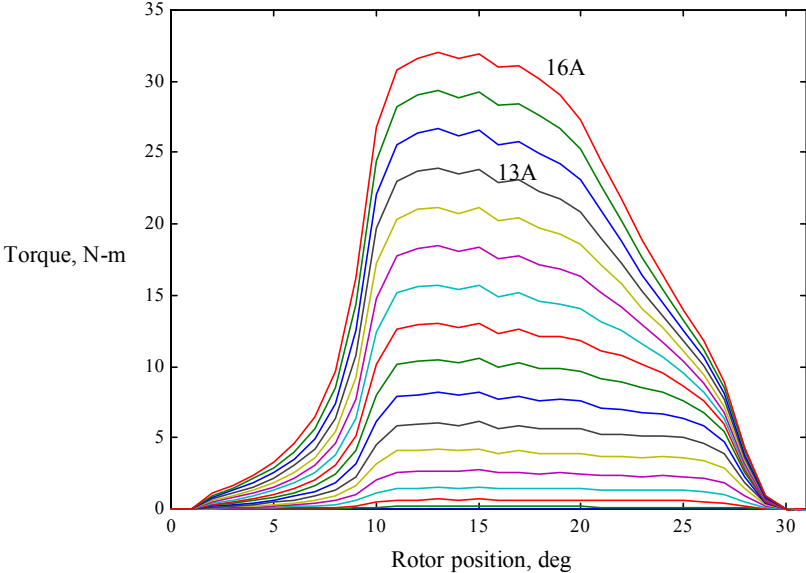


Figure 2.48 Plot of torque vs. rotor position for varying currents from 0A to 16A obtained by finite element analysis

Figure 2.49 shows the plot of inductance vs. rotor position for phase current varying from 0A to 16A. This set of curves is used for the procedure described in Section 2.3.2.

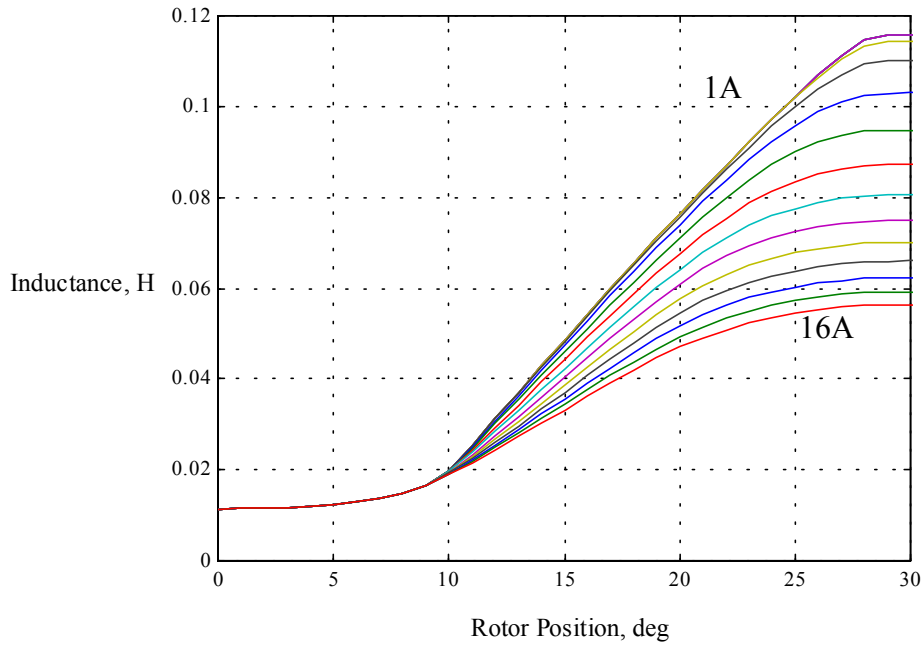


Figure 2.49 Plot of inductance vs. rotor position for varying currents from 0A to 16A obtained by finite element analysis

Eddy-Current Losses

The fall time is calculated as,

$$t_f = \frac{L}{R_s} \ln \left[1 + \frac{i_p R_s}{V_{dc}} \right] = \frac{0.06503 - 0.01135}{0.8} \ln \left[1 + \frac{13 \cdot 0.8}{1.35 \cdot 480} \right] = 0.001068 \text{ s.}$$

At a rated speed of 1500 r.p.m., the number of radians traversed in this time is given by,

$$\theta_f = \frac{2\pi N}{60} t_f = \frac{2\pi \cdot 1500}{60} \cdot 0.001068 = 0.1678 \text{ rads} = 9.615^\circ.$$

In a 8/6 machine full alignment occurs at an angle of $\frac{\pi}{6}$ and commutation can be assumed to

start at an angle $\theta_c = \frac{\pi}{6} + \frac{\beta_r - \beta_s}{2} - \theta_f = 30 + \frac{22 - 18}{2} - 9.615 = 22.38^\circ$. To account for the rise

in inductance as the current value drops, let us assume that the commutation starts at an angle of

$\theta_c = 19^\circ = 0.3316 \text{ rads}$. Assuming that the machine phase is on for the entire stroke period ϵ , ($\frac{\pi}{12}$

for 8/6 machine), the excitation of the phase is assumed to start at an angle of

$$\theta_r = \theta_c - \frac{\pi}{12} = 0.3316 - \frac{\pi}{12} = 0.0698 \text{ rads} = 4^\circ.$$

From the plot of position vs. inductance for various currents (Figure 2.49), the minimum inductance at position $\theta_r = 4^\circ$ is obtained as $L_{\theta_r} = 0.012 \text{ H}$. Assuming that full dc link voltage

$V_{dc} = 1.35 \cdot 480 = 648 \text{ V}$ is applied, and the machine is running at rated speed of 1500 r.p.m., the

rotor pole traverses each degree in $t_s = \frac{1}{6N} = \frac{1}{6 \cdot 1500} = 0.000111 \text{ sec}$. The equation of the

current at position $\theta_r + 1^\circ = 5^\circ$ is calculated as,

$$i_{(5)} = \frac{648}{0.8} \left(1 - e^{-\frac{0.8}{0.012} \cdot 0.000111} \right) = 5.9778 \text{ A}.$$

The equation of the current at position $\theta_r + 2^\circ = 6^\circ$ is calculated as,

$$i_{(6)} = \frac{648}{0.8} \left(1 - e^{-\frac{0.8}{0.0124} \cdot 0.000111} \right) + 5.9778 e^{-\frac{0.8}{0.0124} \cdot 0.000111} = 11.72 \text{ A}.$$

The inductance value $L_{(\theta_r + 1)} = 0.0124 \text{ H}$ is obtained from the plot of position vs. inductance for various currents at precisely the angle $(\theta_r + 1^\circ) = 5^\circ$ at a current of $i_{(\theta_r + 1)} = 5.9778 \text{ A}$. The current at position $(\theta_r + 2^\circ) = 6^\circ$ equals $i_{(6)} = 11.72 \text{ A}$. The current at position $(\theta_r + 3^\circ) = 7^\circ$ exceeds rated current of $i_p = 13 \text{ A}$ and hence is assumed to be fixed at 13 A till position $\theta_c = 19^\circ$. At this position, full negative dc link voltage is applied and the current at position $(\theta_c + 1^\circ) = 20^\circ$ is calculated as,

$$i_{(20)} = -\frac{648}{0.8} \left(1 - e^{-\frac{0.8}{0.0513} \cdot 0.000111} \right) + 13 e^{-\frac{0.8}{0.0513} \cdot 0.000111} = 11.5753 \text{ A}.$$

The current at position $(\theta_c + 2^\circ) = 21^\circ$ is calculated as,

$$i_{(21)} = -\frac{648}{0.8} \left(1 - e^{-\frac{0.8}{0.0594} \cdot 0.000111} \right) + 11.5753 e^{-\frac{0.8}{0.0594} \cdot 0.000111} = 10.3468 \text{ A}.$$

The procedure is repeated till the current value becomes 0, which implies that the phase is fully commutated. It should be remembered that the inductance for each current and position has to be

calculated. It can be noticed that the current is fully commutated at angle of 34° . Although this clearly is in the region of the negative slope of the inductance profile and produces some negative torque, the value is small. If required an effort can be made to further advance the angle but is not really necessary as only the losses are calculated and the procedure is not really used for any control strategy and the error caused will be minimal. Figure 2.50 shows the plot of the 4 phase currents vs. the rotor position.

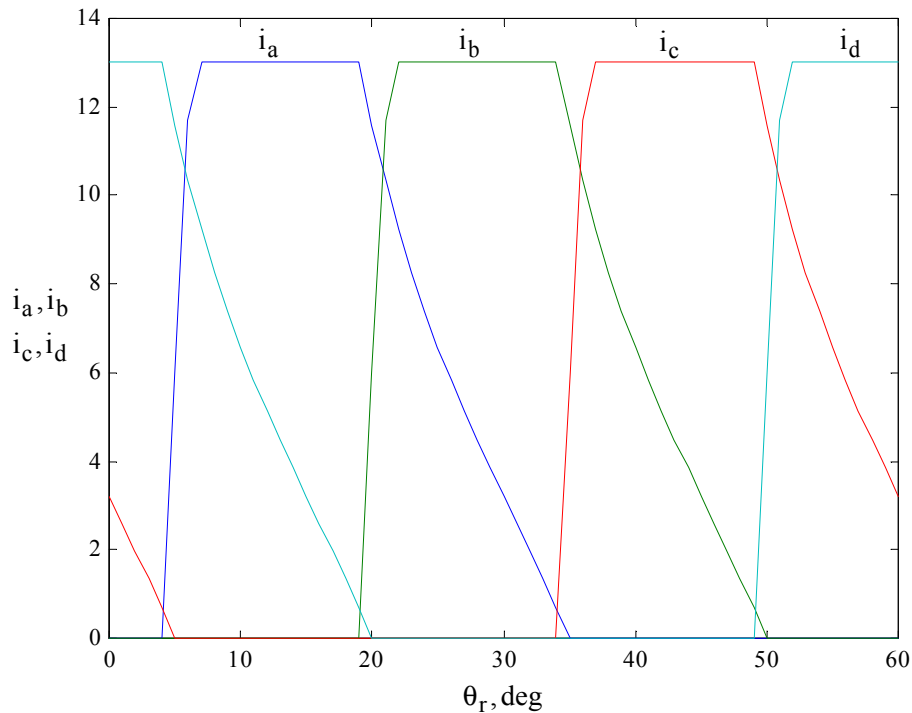


Figure 2.50 Plot of the 4 phase currents vs. rotor position

Now that the current value at each rotor position is obtained, finite element analysis is used to calculate the flux density in the stator pole for each current value and rotor position keeping in mind that the excitation of adjoining phases have to be simulated as well. The resultant stator pole flux density vs. position is plotted in Figure 2.51. It is also advisable to obtain the data of torque vs. rotor position to check if the mean torque developed is equal to the rated torque. The plot is shown in Figure 2.52 and the average torque developed is calculated as 20.19 N-m, which is lower than the rated torque. The flux at each rotor position can be obtained by using the equation $\phi = B_s A_s$ where A_s is the stator pole area. The normalized stator pole flux waveform with respect to time is shown in Figure 2.53. The relative rotor position is shifted to 0° just for convenience of representation.

The normalized rotor pole flux waveform with respect to time is shown in Figure 2.54. The plot is shown for a rotation of 45°. Both the rising and falling portions are approximated by 2 fourth order differential equations and the flux waveforms for the stator and rotor can be written mathematically as,

$$g_s(t) = \begin{cases} -2.709 * 10^{11} t^4 + 0.89 * 10^9 t^3 - 6.064 * 10^5 t^2 + 366.88t - 6.41 * 10^{-4}, & \text{for } 0 \leq t \leq 0.0018 \\ 1.661 * 10^{10} t^4 - 5.886 * 10^7 t^3 - 1.977 * 10^5 t^2 + 384.57t + 1.114, & \text{for } 0.0018 \leq t \leq 0.0036 \\ 0, & \text{for } 0.0036 \leq t < 0.006667 \end{cases}$$

$$g_r(t) = \begin{cases} -2.09 * 10^{11} t^4 + 6.74 * 10^8 t^3 - 4.42 * 10^5 t^2 + 375.08t + 0.0075 & \text{for } 0 \leq t \leq 0.0019 \\ -3.99 * 10^{10} t^4 + 6.08 * 10^8 t^3 - 3.04 * 10^6 t^2 + 5.52 * 10^3 t - 2.16 & \text{for } 0.0019 \leq t \leq 0.0034 \\ 0 & \text{for } 0.0034 \leq t < 0.005 \end{cases}$$

Eddy-current losses are normally given by the Steinmetz equation,

$$P_e = C_e f^2 B_m^2$$

where C_e is the coefficient of eddy-current losses, f is the sinusoidal frequency and B_m is the maximum flux density. The value of C_e is calculated as [SAW84],

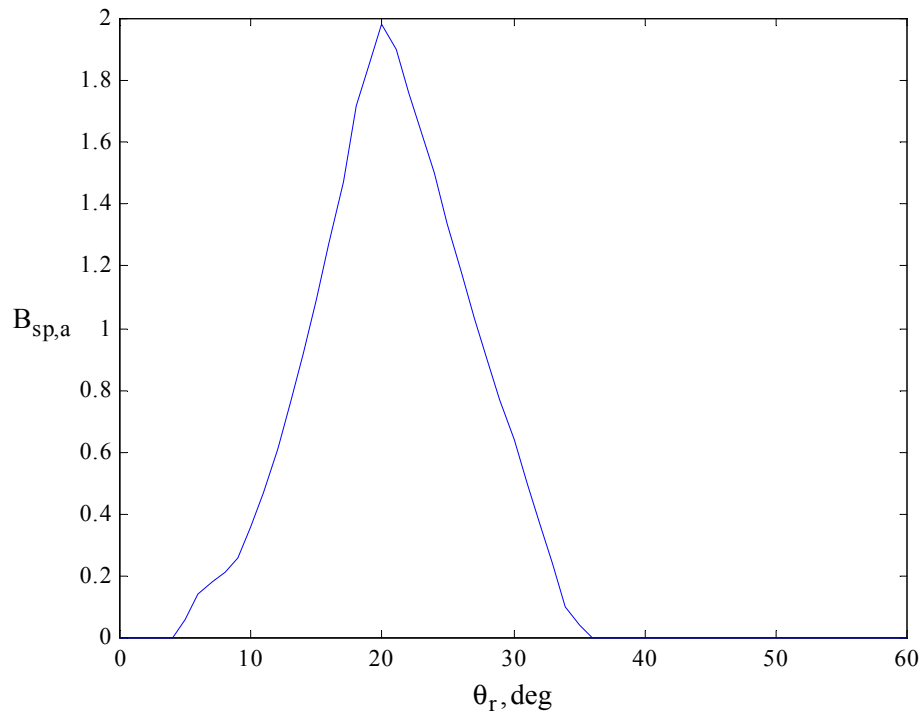


Figure 2.51 Plot of A phase stator pole flux density vs. rotor position

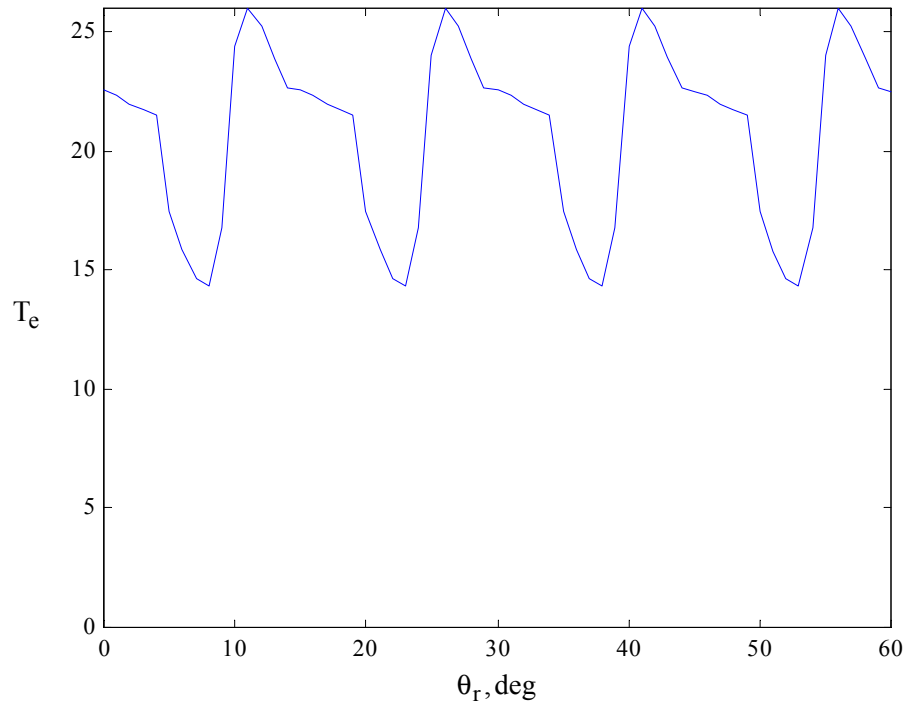


Figure 2.52 Plot of machine torque

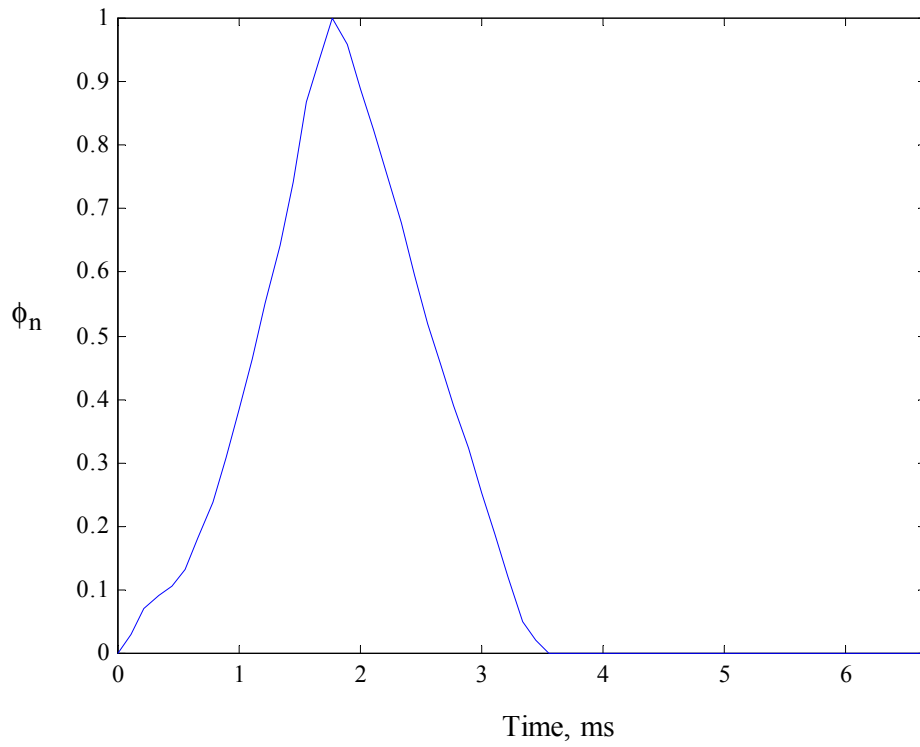


Figure 2.53 Plot of stator normalized flux vs. time for 60° rotation of rotor

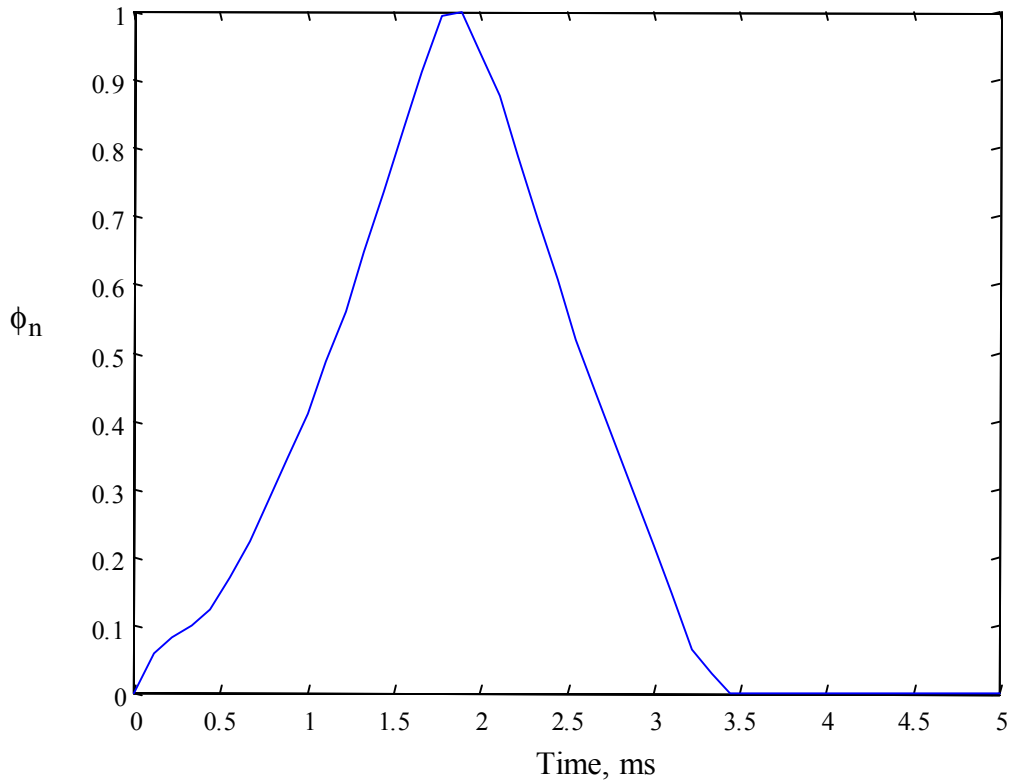


Figure 2.54 Plot of rotor normalized flux vs. time for 45° rotation of rotor

$$C_e = \frac{\pi^2 t^2}{6\rho\rho_1} = \frac{\pi^2 (0.5 * 10^{-3})^2}{6(0.6 * 10^{-6})7850} = 8.731 * 10^{-5}.$$

where the thickness of the lamination t is 0.5 mm, the specific resistivity of the lamination material ρ is $0.6 * 10^{-6} \Omega\text{m}$ and the specific weight of the material is 7850 kg/m^3 . The value C_{e1} is calculated as,

$$C_{e1} = \frac{C_e}{2\pi^2} = \frac{8.731 * 10^{-5}}{2\pi^2} = 4.42 * 10^{-6}.$$

The weight of the stator pole is given by,

$$W_{sp} = \frac{D}{2} \beta_s h_s L \rho_1 = \frac{100.6}{2} * 0.314 * 32.7 * 200 * 10^{-9} * 7850 = 0.8113 \text{ kg}.$$

Seeing that $B_{spm} = 1.98\text{T}$, and noting that $T_{rs} = 0.0018 \text{ s}$ and $T_{fs} = 0.0036 \text{ s}$, the integral

$$\int_{t=0}^{T_s} \left[\frac{d}{dt} g_s(t) \right]^2 dt \text{ is evaluated as,}$$

$$\begin{aligned}
& \int_{t=0}^{T_s} \left[\frac{d}{dt} g_s(t) \right]^2 dt = \int_{t=0}^{T_{rs}} \left[\frac{d}{dt} g_s(t) \right]^2 dt + \int_{t=T_{rs}}^{T_{fs}} \left[\frac{d}{dt} g_s(t) \right]^2 dt \\
& = \int_{t=0}^{T_{rs}} \left[4a_1 t^3 + 3a_2 t^2 + 2a_3 t + a_4 \right]^2 dt + \int_{t=T_{rs}}^{T_{fs}} \left[4b_1 t^3 + 3b_2 t^2 + 2b_3 t + b_4 \right]^2 dt \\
& = \int_{t=0}^{T_{rs}} \left[16a_1^2 t^6 + 24a_1 a_2 t^5 + (16a_1 a_3 + 9a_2^2) t^4 + (8a_1 a_4 + 12a_2 a_3) t^3 + (6a_2 a_4 + 4a_3^2) t^2 \right. \\
& \quad \left. + 4a_3 a_4 t + a_4^2 \right] dt \\
& + \int_{t=T_{rs}}^{T_{fs}} \left[16b_1^2 t^6 + 24b_1 b_2 t^5 + (16b_1 b_3 + 9b_2^2) t^4 + (8b_1 b_4 + 12b_2 b_3) t^3 \right. \\
& \quad \left. + (6b_2 b_4 + 4b_3^2) t^2 + 4b_3 b_4 t + b_4^2 \right] dt \\
& = \left[\frac{16a_1^2}{7} t^7 + 4a_1 a_2 t^6 + \frac{(16a_1 a_3 + 9a_2^2)}{5} t^5 + (2a_1 a_4 + 3a_2 a_3) t^4 + \left(2a_2 a_4 + \frac{4a_3^2}{3} \right) t^3 \right. \\
& \quad \left. + 2a_3 a_4 t^2 + a_4^2 t \right]_{t=0}^{T_{rs}} + \\
& \left[\frac{16b_1^2}{7} t^7 + 4b_1 b_2 t^6 + \frac{(16b_1 b_3 + 9b_2^2)}{5} t^5 + (2b_1 b_4 + 3b_2 b_3) t^4 + \left(2b_2 b_4 + \frac{4b_3^2}{3} \right) t^3 \right. \\
& \quad \left. + 2b_3 b_4 t^2 + b_4^2 t \right]_{t=T_{rs}}^{T_{fs}} \\
& = \frac{16a_1^2}{7} T_{rs}^7 + 4a_1 a_2 T_{rs}^6 + \frac{(16a_1 a_3 + 9a_2^2)}{5} T_{rs}^5 + (2a_1 a_4 + 3a_2 a_3) T_{rs}^4 \\
& + \left(2a_2 a_4 + \frac{4a_3^2}{3} \right) T_{rs}^3 + 2a_3 a_4 T_{rs}^2 + a_4^2 T_{rs} + \frac{16b_1^2}{7} (T_{fs}^7 - T_{rs}^7) + 4b_1 b_2 (T_{fs}^6 - T_{rs}^6) \\
& + \frac{(16b_1 b_3 + 9b_2^2)}{5} (T_{fs}^5 - T_{rs}^5) + (2b_1 b_4 + 3b_2 b_3) (T_{fs}^4 - T_{rs}^4) \\
& + \left(2b_2 b_4 + \frac{4b_3^2}{3} \right) (T_{fs}^3 - T_{rs}^3) + 2b_3 b_4 (T_{fs}^2 - T_{rs}^2) + b_4^2 (T_{fs} - T_{rs}) \\
& = 1.2802 * 10^3
\end{aligned}$$

The eddy-current loss for the stator poles P_{spe} is given as,

$$\begin{aligned}
P_{spe} &= \frac{2\pi N}{60} \frac{1}{2\pi} N_s N_r W_{sp} C_{el} (B_{spm})^2 \int_{t=0}^{T_s} \left[\frac{d}{dt} g_s(t) \right]^2 dt = \\
& \frac{1500}{60} 8 \cdot 6 \cdot 0.8113 \cdot 4.42 * 10^{-6} \cdot (1.98)^2 \cdot 1.2802 * 10^3 = 21.613 \text{ W.}
\end{aligned}$$

It can be seen that that the maximum rotor flux density is $B_{rpm} = 1.71 \text{ T}$. The rotor pole weight is given as,

$$W_{rp} = h_r L \left(\frac{D}{2} - g \right) B_r \rho_1 = 19.8 * 200 * \left(\frac{100.6}{2} - 0.5 \right) 0.384 * 7850 = 0.5944 \text{ kg.}$$

The eddy-current loss for the rotor poles P_{rpe} is given as,

$$P_{rpe} = \frac{2\pi N}{60} \frac{1}{2\pi} N_s N_r W_{rp} C_{el} (B_{rpm})^2 \int_{t=0}^{T_r} \left[\frac{d}{dt} g_r(t) \right]^2 dt =$$

$$\frac{1500}{60} 8 \cdot 6 \cdot 0.5944 \cdot 4.42 * 10^{-6} \cdot (1.71)^2 \cdot 1.2925 * 10^3 = 11.924 \text{ W.}$$

The normalized stator flux for section 1 vs. time is plotted over $\frac{\pi}{3}$ radians in Figure 2.55. After that time, the waveform would repeat as shown in Figure 2.26. It can be observed that the normalized flux has four distinct portions. The flux waveforms for the section can be written mathematically as,

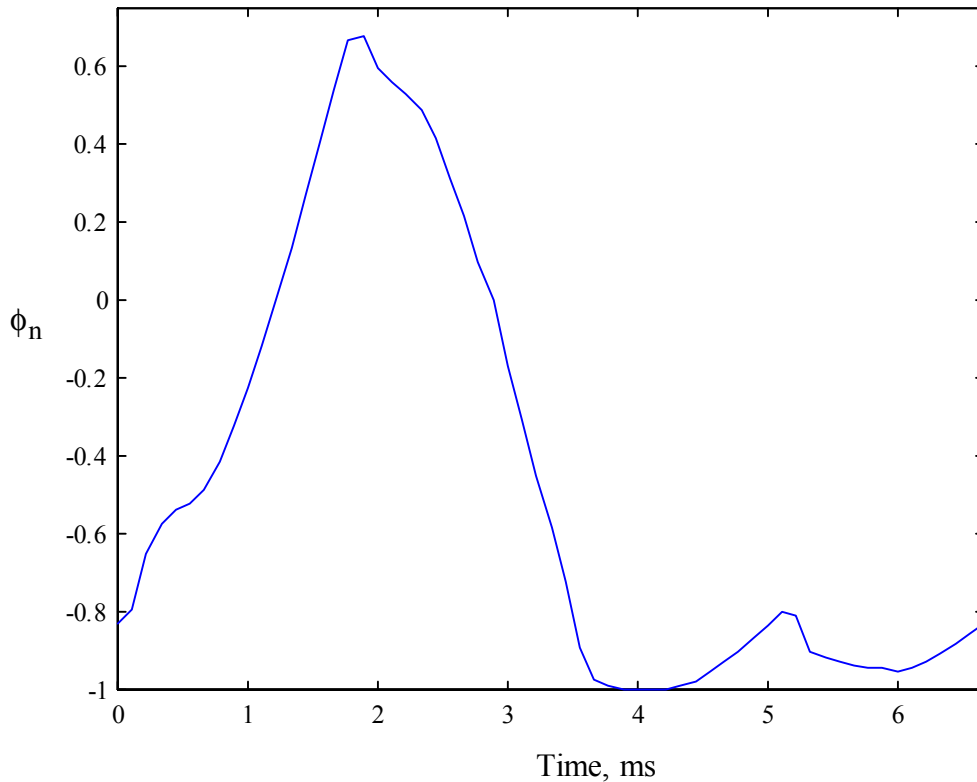


Figure 2.55 Plot of section 1 normalized flux vs. time for 60° rotation of rotor

$$\begin{aligned}
& -5.53 * 10^{11} t^4 + 2.06 * 10^9 t^3 - 2.16 * 10^6 t^2 + 1.27 * 10^3 t && \text{for } 0 \leq t \leq 0.0019 \\
& -0.8545 \\
g_{sy1}(t) = & 3.56 * 10^{11} t^4 - 3.74 * 10^9 t^3 + 1.4 * 10^7 t^2 - 2.32 * 10^4 t && \text{for } 0.0019 \leq t \leq 0.0039 \\
& + 14.94 \\
& 1.79 * 10^5 t^2 - 1.44 * 10^3 t + 1.909 && \text{for } 0.0039 \leq t < 0.0051 \\
& 2.36 * 10^5 t^2 - 2.79 * 10^3 t + 7.301 && \text{for } 0.0051 \leq t < 0.00667
\end{aligned}$$

The weight of the stator yoke is calculated as,

$$W_{sy1} = \frac{D_o - C}{2} \frac{2\pi}{N_s} CL\rho_1 = \frac{190 - 12.5}{2} \frac{2\pi}{8} 12.5 * 200 * 10^{-9} * 7850 = 1.3169.$$

The equation for calculating the eddy-current loss in the stator yoke section is given by,

$$\begin{aligned}
P_{sy1e} &= \frac{N}{60} 2N_r W_{sy1} C_{el} (B_{sym1})^2 \left\{ \int_{t=0}^{T_{sy}} \left[\frac{d}{dt} g_{sy1}(t) \right]^2 dt \right\} \\
&= \frac{1500}{60} 2 \cdot 6 \cdot 1.3169 \cdot 4.42 * 10^{-6} (1.11)^2 \left\{ 3.2996 * 10^3 \right\} = 7.104W.
\end{aligned}$$

The normalized stator flux for section 2 vs. time is plotted over $\frac{\pi}{3}$ radians in Figure 2.56. After that time, the waveform would repeat as shown in Figure 2.26. It can be observed that the normalized flux has three distinct portions. The flux waveforms for the section can be written mathematically as,

$$\begin{aligned}
& -3.52 * 10^{11} t^4 + 1.41 * 10^9 t^3 - 1.47 * 10^6 t^2 + 1.01 * 10^3 t && \text{for } 0 \leq t \leq 0.0022 \\
& -0.8456 \\
g_{sy2}(t) = & 4.53 * 10^9 t^4 - 7.66 * 10^7 t^3 + 2.02 * 10^5 t^2 + 162.03t && \text{for } 0.0022 \leq t \leq 0.0053 \\
& + 0.3257 \\
& 1.97 * 10^5 t^2 - 2.25 * 10^3 t + 5.4384 && \text{for } 0.0053 \leq t < 0.00667
\end{aligned}$$

The weight of the stator yoke is calculated as,

$$W_{sy2} = W_{sy1} = 1.3169 \text{ kg.}$$

The equation for calculating the eddy-current loss in the stator yoke section is given by,

$$\begin{aligned}
P_{sy2e} &= \frac{N}{60} 2N_r W_{sy2} C_{el} (B_{sym2})^2 \left\{ \int_{t=0}^{T_{sy}} \left[\frac{d}{dt} g_{sy2}(t) \right]^2 dt \right\} \\
&= \frac{1500}{60} 2 \cdot 6 \cdot 1.3169 \cdot 4.42 * 10^{-6} (1.11)^2 \left\{ 3.765 * 10^3 \right\} = 8.107W.
\end{aligned}$$

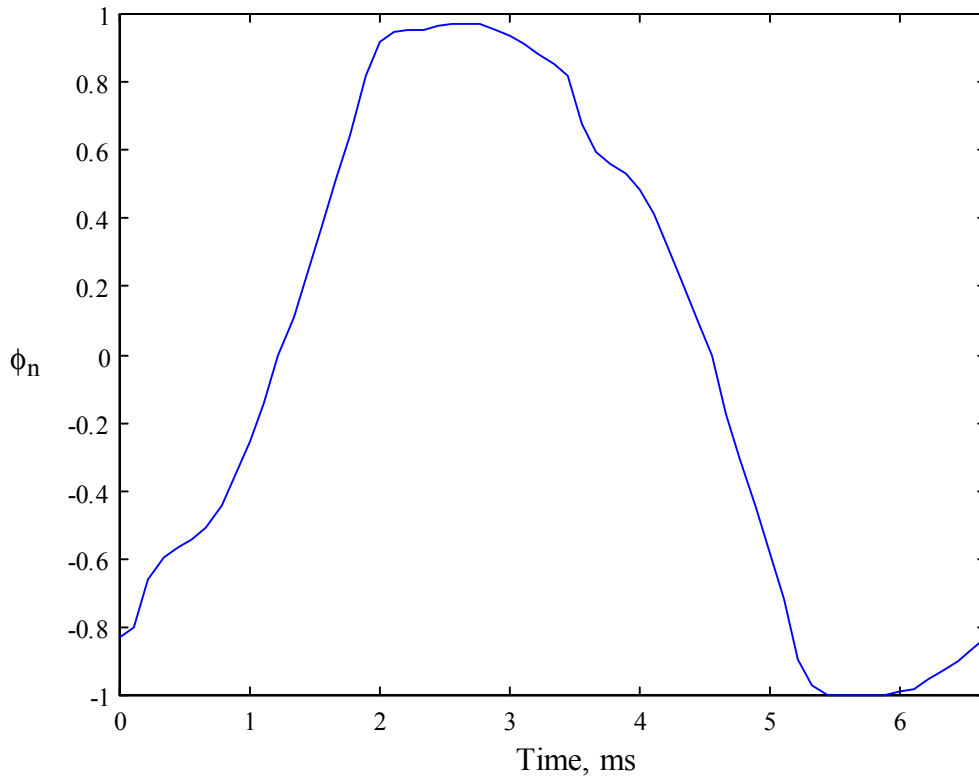


Figure 2.56 Plot of section 2 normalized flux vs. time for 60° rotation of rotor

The normalized stator flux for section 3 vs. time is plotted over $\frac{\pi}{3}$ radians in Figure 2.57. After that time, the waveform would repeat as shown in Figure 2.26. It can be observed that the normalized flux has four distinct portions. The flux waveforms for the section can be written mathematically as,

$$\begin{aligned}
 & -2.52 * 10^{11} t^4 + 6.33 * 10^8 t^3 + 4.03 * 10^4 t^2 + 267.75t && \text{for } 0 \leq t \leq 0.0021 \\
 & -0.7523 \\
 \xi_{sy3}(t) = & -2.15 * 10^5 t^2 + 1.01 * 10^3 t - 0.2073 && \text{for } 0.0021 \leq t \leq 0.0032 \\
 & -2.52 * 10^5 t^2 + 2.04 * 10^3 t - 3.1342 && \text{for } 0.0039 \leq t < 0.0049 \\
 & 7.06 * 10^{11} t^4 - 1.62 * 10^{10} t^3 + 1.39 * 10^8 t^2 - 5.26 * 10^5 t && \text{for } 0.0049 \leq t < 0.00667 \\
 & + 746.61
 \end{aligned}$$

The weight of the stator yoke is calculated as,

$$W_{sy3} = W_{syt} = 1.3169 \text{ kg.}$$

The equation for calculating the eddy-current loss in the stator yoke section is given by,

$$P_{sy3e} = \frac{N}{60} 2N_r W_{sy3} C_{el} (B_{sym3})^2 \left\{ \int_{t=0}^{T_{sy}} \left[\frac{d}{dt} g_{sy3}(t) \right]^2 dt \right\}$$

$$= \frac{1500}{60} 2 \cdot 6 \cdot 1.3169 \cdot 4.42 \cdot 10^{-6} (1.08)^2 \left\{ 3.6245 \cdot 10^3 \right\} = 7.3879W.$$

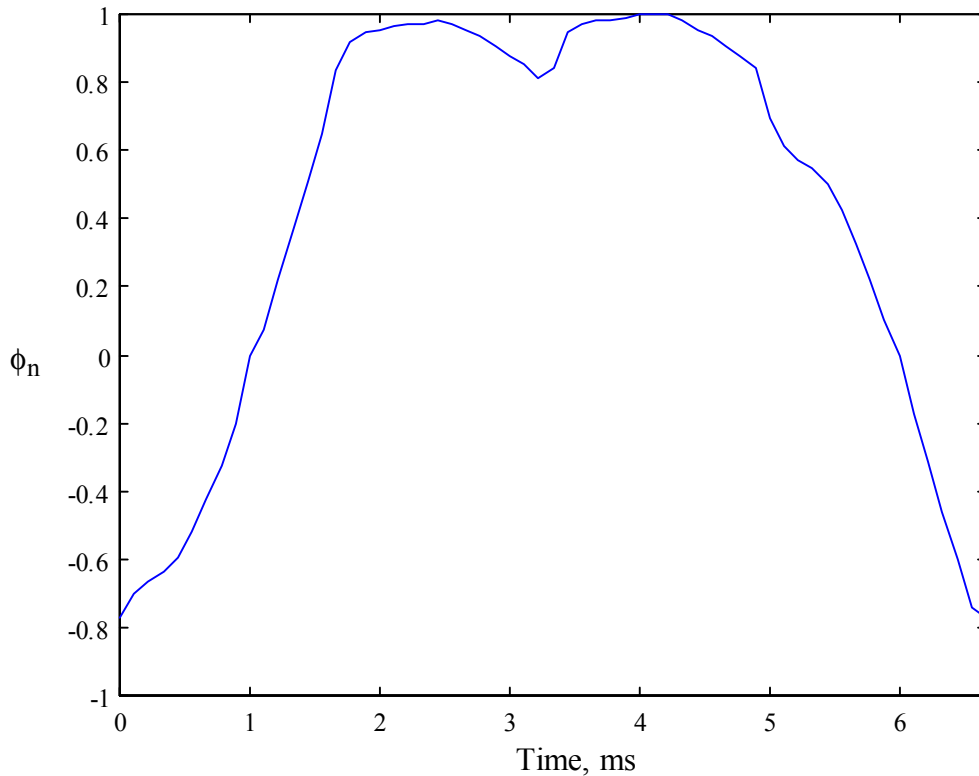


Figure 2.57 Plot of section 3 normalized flux vs. time for 60° rotation of rotor

The normalized stator flux for section 4 vs. time is plotted over $\frac{\pi}{3}$ radians in Figure 2.58. After that time, the waveform would repeat as shown in Figure 2.26. It can be observed that the normalized flux has four distinct portions. The flux waveforms for the section can be written mathematically as,

$$g_{sy4}(t) = \begin{cases} -5.61 \cdot 10^{10} t^4 + 2.45 \cdot 10^8 t^3 - 5.9 \cdot 10^5 t^2 + 603.83t + 0.7912 & \text{for } 0 \leq t \leq 0.0017 \\ -7 \cdot 10^9 t^4 + 1.51 \cdot 10^8 t^3 - 1.09 \cdot 10^6 t^2 + 2.96 \cdot 10^3 t - 1.696 & \text{for } 0.0017 \leq t \leq 0.0033 \\ -1.35 \cdot 10^{10} t^4 + 2.71 \cdot 10^8 t^3 - 2.19 \cdot 10^6 t^2 + 8.05 \cdot 10^3 t - 10.0586 & \text{for } 0.0033 \leq t < 0.005 \\ -8.12 \cdot 10^{10} t^4 + 1.99 \cdot 10^9 t^3 - 1.84 \cdot 10^7 t^2 - 7.6 \cdot 10^4 t - 117.4328 & \text{for } 0.005 \leq t < 0.00667 \end{cases}$$

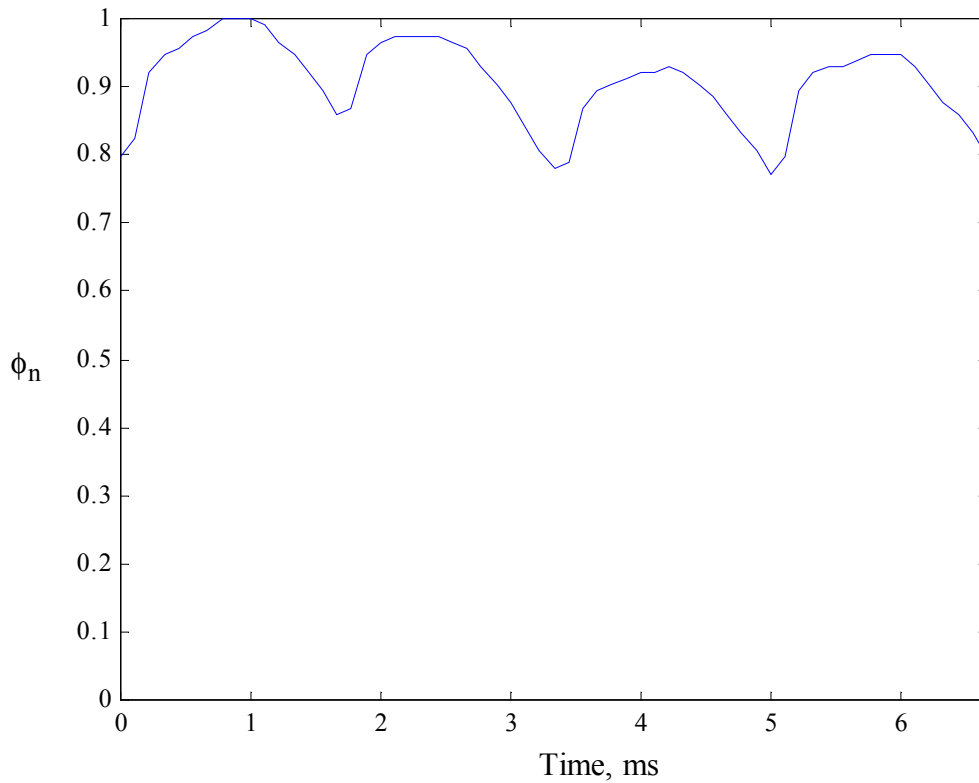


Figure 2.58 Plot of section 4 normalized flux vs. time for 60° rotation of rotor

The weight of the stator yoke is calculated as,

$$W_{sy4} = W_{sy1} = 1.3169 \text{ kg.}$$

The equation for calculating the eddy-current loss in the stator yoke section is given by,

$$P_{sy4e} = \frac{N}{60} 2N_r W_{sy4} C_{el} (B_{sym4})^2 \left\{ \int_{t=0}^{T_{sy}} \left[\frac{d}{dt} g_{sy4}(t) \right]^2 dt \right\}$$

$$= \frac{1500}{60} 2 \cdot 6 \cdot 1.3169 \cdot 4.42 \cdot 10^{-6} (1.14)^2 \{382.09\} = 0.8678 \text{ W.}$$

The total eddy-current losses in the stator yoke is given by,

$$P_{sye} = P_{syle} + P_{sy3e} + P_{sy3e} + P_{sy4e} = 7.104 + 8.107 + 7.3879 + 0.8678 = 23.4665 \text{ W.}$$

A sample normalized rotor core flux for vs. time is plotted over π radians in Figure 2.59. It can be observed that the normalized flux has six distinct portions. The flux waveforms for the section can be written mathematically as,

$$g_{rc}(t) = \begin{cases} -4.48 \cdot 10^{11} t^4 + 1.19 \cdot 10^9 t^3 - 2.42 \cdot 10^5 t^2 + 140.39t - 0.7244 & \text{for } 0 \leq t \leq 0.0019 \\ -1.95 \cdot 10^{16} t^6 + 4.72 \cdot 10^{14} t^5 - 4.63 \cdot 10^{12} t^4 + 2.35 \cdot 10^{10} t^3 - 6.47 \cdot 10^7 t^2 + 9.17 \cdot 10^4 t - 51.2043 & \text{for } 0.0019 \leq t \leq 0.006 \\ 1.77 \cdot 10^{16} t^6 - 8.76 \cdot 10^{14} t^5 + 1.79 \cdot 10^{13} t^4 - 1.93 \cdot 10^{11} t^3 + 1.17 \cdot 10^9 t^2 - 3.72 \cdot 10^6 t + 4.92 \cdot 10^3 & \text{for } 0.006 \leq t < 0.0101 \\ -2 \cdot 10^{11} t^4 + 9.54 \cdot 10^9 t^3 - 1.69 \cdot 10^8 t^2 + 1.33 \cdot 10^6 t - 3.87 \cdot 10^3 & \text{for } 0.0101 \leq t < 0.0136 \\ 2.7 \cdot 10^{10} t^4 - 1.69 \cdot 10^9 t^3 + 3.91 \cdot 10^7 t^2 - 4.01 \cdot 10^5 t + 1.527 \cdot 10^3 & \text{for } 0.0136 \leq t < 0.0168 \\ 7.92 \cdot 10^9 t^4 - 5.64 \cdot 10^8 t^3 + 1.52 \cdot 10^7 t^2 - 1.85 \cdot 10^5 t + 852.574 & \text{for } 0.0168 \leq t < 0.02 \end{cases}$$

The weight of the rotor core is calculated as,

$$W_{rc} = A_{ry} \frac{\pi}{3} \frac{1}{2} \frac{D - 2g - 2h_r + D_{sh}}{2} \rho_1$$

$$= 0.0032 \frac{\pi}{3} \frac{1}{2} \frac{100.6 - 2 \cdot 0.5 - 2 \cdot 19.8 + 28}{2} \cdot 10^{-3} \cdot 7850 = 0.5787 \text{ kg.}$$

The equation for calculating the eddy-current loss in the rotor core section is given by,

$$P_{rce} = \frac{N}{60} 2N_r W_{rc} C_{el} (B_{rcm})^2 \left\{ \int_{t=0}^{T_{rc}} \left[\frac{d}{dt} g_{rc}(t) \right]^2 dt \right\}$$

$$= \frac{1500}{60} 2 \cdot 6 \cdot 0.5787 \cdot 4.42 \cdot 10^{-6} (0.9)^2 \{9.697 \cdot 10^3\} = 9.6779 \text{ W}$$

The total eddy-current losses of the machine at rated speed and power output is given as,

$$P_e = P_{spe} + P_{rpe} + P_{sye} + P_{rce} = 21.6125 + 11.9241 + 23.4665 + 9.6779 = 66.681 \text{ W.}$$

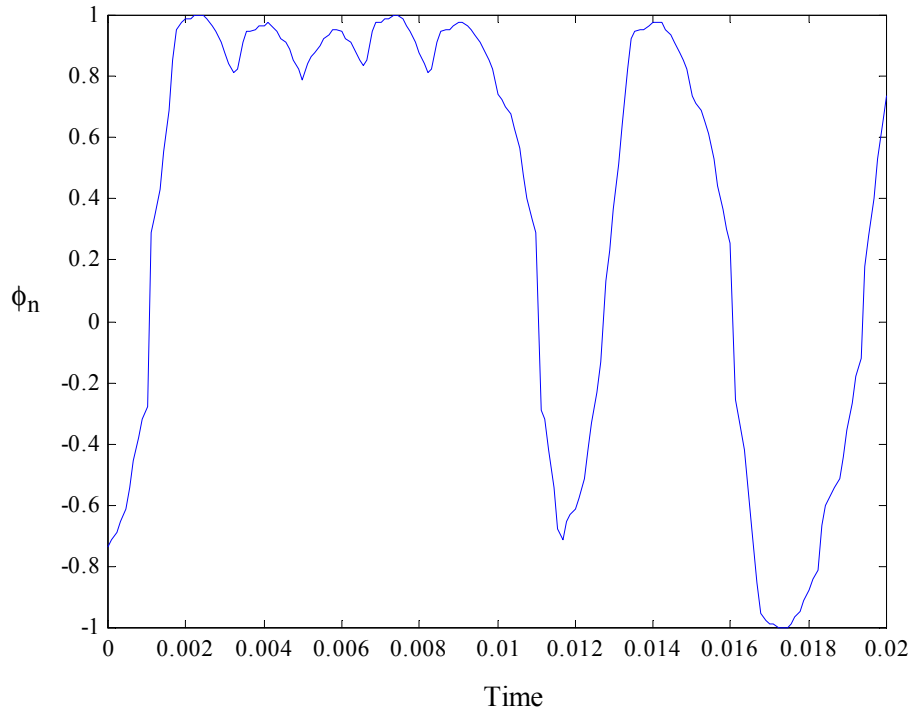


Figure 2.59 Plot of rotor core normalized flux vs. time for 180° rotation of rotor

The eddy-current losses can also be plotted for various speeds as shown in Figure 2.60. The losses are seen to rise exponentially with rise in speed.

Hysteresis Losses

The hysteresis losses can be calculated from the process described in [HAY95]. The flux in the stator poles are unipolar and can be calculated as,

$$P_{sph} = \frac{\omega_m}{2\pi} N_r N_s W_{sp} E_h(0, B_{spm}) = \frac{1500}{60} 6 \cdot 8 \cdot 0.8113 \cdot 0.02275 = 22.1477 \text{ W}$$

Assuming that $N_{wkpp} = 2$, and designating winding polarities as $p_1 = 1$, $p_2 = 1$, $p_3 = 1$ and $p_4 = 1$, the following parameters can be calculated [HAY95]:

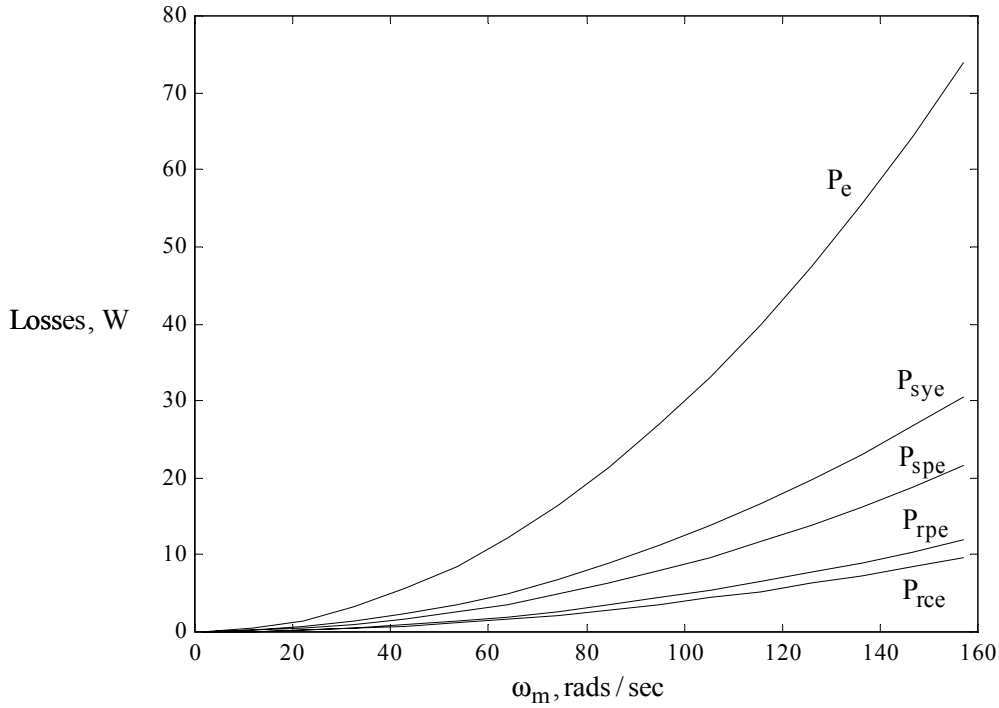


Figure 2.60 Plot of eddy-current losses with speed varying from 0 to rated speed for the rated load torque output

$$K_{sy} = 2 \left(N_{ph} + \frac{N_{ph} - 2}{2} \left\{ |p_{N_{ph}} + p_1| + \sum_{i=1}^{N_{ph}-1} |p_i - p_{i+1}| \right\} \right)$$

$$= 2 \left(4 + \frac{4-2}{2} \left\{ |p_4 + p_1| + \sum_{i=1}^3 |p_i - p_{i+1}| \right\} \right) = 2 \left(4 + \frac{4-2}{2} \{2\} \right) = 12$$

$$K_{rp} = \frac{N_r}{N_{wkpp}} \left\{ |p_{N_{ph}} + p_1| + \sum_{i=1}^{N_{ph}-1} |p_i - p_{i+1}| \right\} = \frac{6}{2} \left\{ |p_4 + p_1| + \sum_{i=1}^3 |p_i - p_{i+1}| \right\} = \frac{6}{2} \{2\} = 6$$

$$K_{rc} = \frac{N_r}{N_{wkpp}} \left\{ 2N_{ph} + \left(\frac{N_r}{2N_{wkpp}} - 2 \right) \cdot \left(|p_{N_{ph}} + p_1| + \sum_{i=1}^{N_{ph}-1} |p_i - p_{i+1}| \right) \right\}$$

$$= \frac{6}{2} \left\{ 2 \cdot 4 + \left(\frac{6}{2 \cdot 4} - 2 \right) \cdot \left(|p_4 + p_1| + \sum_{i=1}^3 |p_i - p_{i+1}| \right) \right\} = \frac{6}{2} \left\{ 2 \cdot 4 + \left(\frac{6}{2 \cdot 4} - 2 \right) \cdot 2 \right\} = 16.5$$

Calculating the value of h_{syh} as,

$$h_{\text{syh}} = \frac{K_{\text{sy}}}{2N_{\text{ph}}^2} = \frac{12}{2 \cdot 4^2} = 0.375$$

the hysteresis losses in the stator yoke can be calculated as,

$$\begin{aligned} P_{\text{syh}} &= \frac{\omega_m}{2\pi} N_r N_s N_{\text{ph}} W_{\text{sy}} \left\{ \frac{h_{\text{syh}}}{2} E_h(-B_{\text{sym}}, B_{\text{sym}}) + (1 - h_{\text{syh}}) E_h(B_{\text{sy}0}, B_{\text{sym}}) \right\} \\ &= \frac{1500}{60} 6 \cdot 8 \cdot 4 \cdot (1.3169) \left\{ \frac{0.375}{2} 0.0104 + (1 - 0.375) 9.4877 \cdot 10^{-4} \right\} \\ &= 16.0748 \text{ W} \end{aligned}$$

Calculating the value of h_{rph} as,

$$h_{\text{rph}} = \frac{N_{\text{wkpp}} K_{\text{rp}}}{2N_{\text{ph}} N_r} = \frac{2 \cdot 6}{2 \cdot 4 \cdot 6} = 0.25$$

the hysteresis losses in the rotor pole can be calculated as,

$$\begin{aligned} P_{\text{rph}} &= \frac{\omega_m}{2\pi} N_r N_s W_{\text{rp}} \left\{ \frac{h_{\text{rph}}}{2} E_h(-B_{\text{rpm}}, B_{\text{rpm}}) + (1 - h_{\text{rph}}) E_h(0, B_{\text{rpm}}) \right\} \\ &= \frac{1500}{60} 6 \cdot 8 \cdot 0.5944 \left\{ \frac{0.25}{2} 0.04036 + (1 - 0.25) 0.016144 \right\} \\ &= 12.2353 \text{ W} \end{aligned}$$

Calculating the value of h_{rch} as,

$$h_{\text{rch}} = \frac{N_{\text{wkpp}}^2 K_{\text{rc}}}{N_{\text{ph}} N_r^2} = \frac{2^2 16.5}{4 \cdot 6^2} = 0.4583$$

the hysteresis losses in the rotor core can be calculated as,

$$\begin{aligned} P_{\text{rch}} &= \frac{\omega_m}{2\pi} N_r^2 N_{\text{ph}} W_{\text{rc}} \left\{ \frac{h_{\text{rch}}}{2} E_h(-B_{\text{rcm}}, B_{\text{rcm}}) + (1 - h_{\text{rch}}) E_h(B_{\text{rc}0}, B_{\text{rcm}}) \right\} \\ &= \frac{1500}{60} 6^2 4 \cdot 0.5787 \left\{ \frac{0.4583}{2} 0.0092 + (1 - 0.4583) 0.0032 \right\} \\ &= 6.8884 \text{ W} \end{aligned}$$

The total hysteresis losses are given by,

$$P_h = P_{\text{sph}} + P_{\text{syh}} + P_{\text{rph}} + P_{\text{rch}} = 22.1477 + 16.0748 + 12.2353 + 6.8884 = 57.3462 \text{ W}$$

The hysteresis losses can be plotted for various speeds for the same rated load torque as shown in Figure 2.61. The losses are seen to increase linearly with the increase in speed.

The overall iron losses can also be plotted with respect to the speed. It can be seen that the hysteresis losses vary linearly and the eddy-current losses vary exponentially which is very similar to other machines. The combined iron losses is plotted in Figure 2.62.

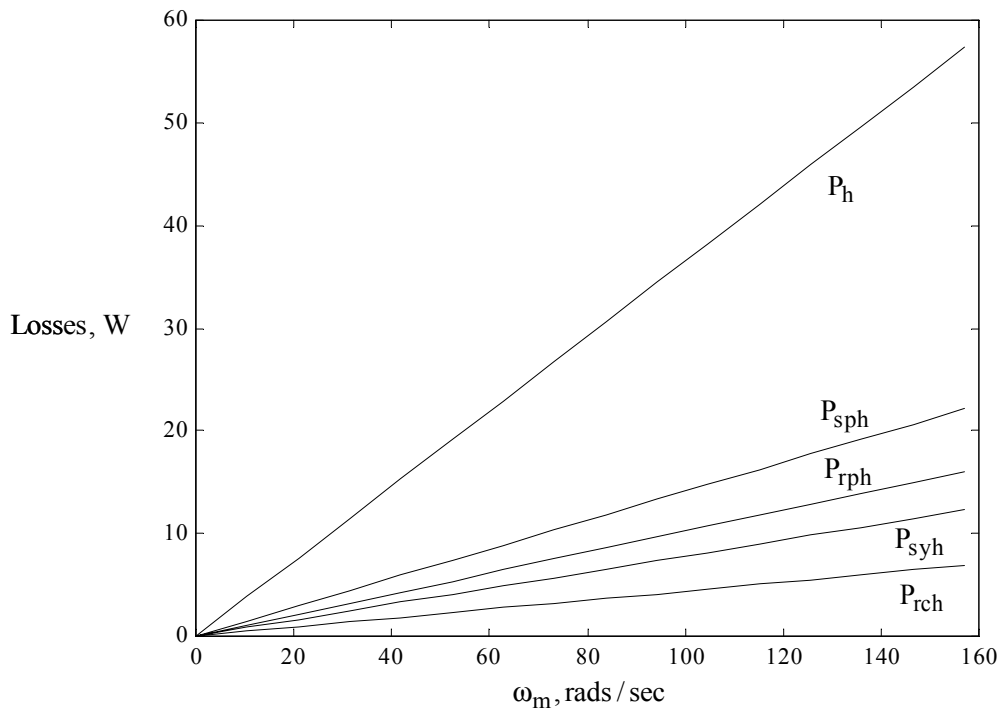


Figure 2.61 Plot of hysteresis losses with speed varying from 0 to rated speed for the rated load torque output

2.6 Summary

This chapter covers the design procedure of a 8/6 switched reluctance motor from the first principles. No major assumptions are made in the design although a few assumptions are made in the analysis section of the design procedure. It differs from some of the sources cited in the procedure of designing the machine, which is simplified for a person with basic knowledge to achieve. The procedure is intuitive and it may be argued that there is no major contribution. But an intensive literature search did not reveal the procedure followed although it may be claimed

that other sources may follow the same procedure but did not document them. Certain references such as [KRI01] do have a design procedure outlined but this does require a lot of background knowledge to implement. The procedure outlined in [KRI01] also depends on some variable parameters, which requires intense design experience in SRM.

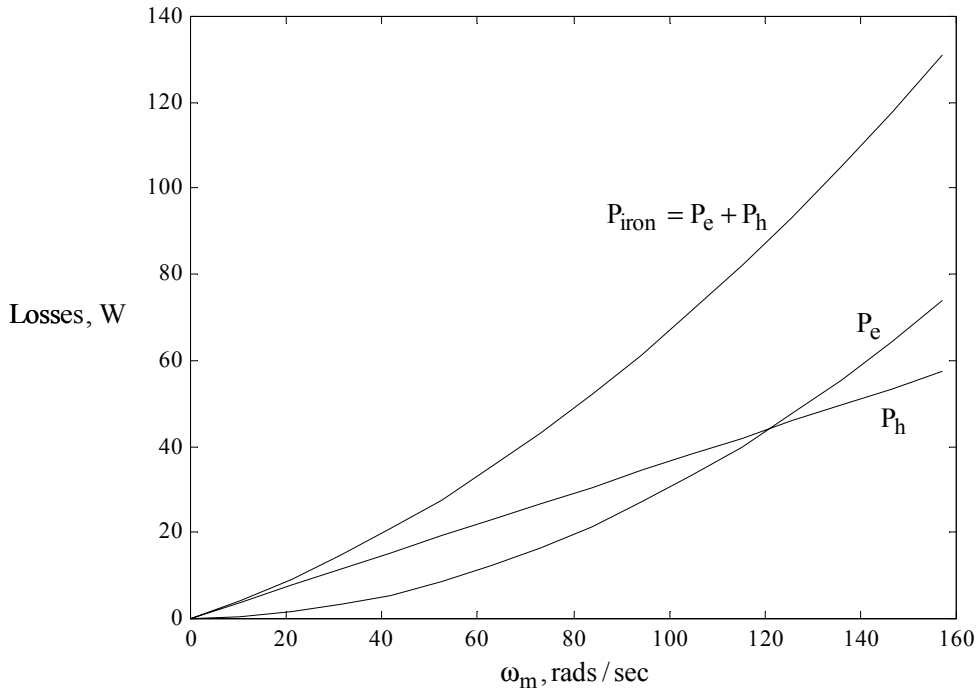


Figure 2.62 Plot of iron losses with speed varying from 0 to rated speed for the rated load torque output

The calculation of the unaligned inductance in the above chapter follows the basic principles of electromagnetics and does not rely on any previous sources whose documentation is hard to verify. The procedure outlined in this material is easy to follow and while it has approximately the same error as in other methods when compared to the finite element analysis, the value tends to be higher than the finite element analysis value which is a positive as far as machine design is concerned since the analytical output torque would be calculated to be lower than the finite element value or the actual measured value in the machine. This would lead to a slight over-design of the machine that would be perfectly acceptable rather than designing a machine that would not produce the required output torque.

The procedure for calculating inductances for various rotor positions has been developed in this material. The selection of the various flux tubes and their areas are intuitive with many approximations. The results do show some variation when compared with the finite element analysis. Better accuracy can probably be achieved by defining more regions of variations but is not required. The values at the aligned and unaligned positions show a very small margin of error and these values are used in the calculation of analytical torque developed in the machine. The outlining of the procedure is in a manner to allow users to develop their own procedure with minor modifications.

The calculation of eddy-current losses was done by following the procedure outlined in [HAY95]. The material covered here gives a more detailed procedure to obtain the eddy-current losses than the reference and also accounts for the rise time of the current and the variation of inductance with the current. The by-product of this analysis outlined here is that it can be accurately used to predict the actual maximum torque developed in the machine and this is an invaluable result, as other methods tend to approximate the possible output torque. Even in earlier sections in this report, during initial parameter calculation, there is a tendency to approximate and the initial finite element result demonstrates the possible torque output for a particular current and position. But only during the eddy-current analysis is it fully confirmed whether the machine can produce the required output.

The process of finding the hysteresis losses is directly adapted from [HAY95]. The results of the analysis may be flawed due to the lack of accurate data for the material. The procedure is however clearly demonstrated and can be used without problems with accurate information. The calculation and documentation of the iron losses is one of the significant contributions of this dissertation.

Chapter 3. Switched Reluctance Motor Converters

Switched reluctance motors operate on the principle of unipolar current, i.e., the current flows only in one direction in the windings regardless of whether positive or negative torque is required. This principle requires only one switch to be in series with a phase winding. The turning on or off of this switch regulates the flow of current in the phase. Two of the more popular converters are discussed in this section along with a new converter to be implemented as part of this dissertation. Various different topologies of converters have been described in [KRI01].

Section 3.1 describes the operation of the popular $2m$ -switch converter that uses 2 switches per phase. This converter while being popular has the disadvantage of requiring $(m+1)$ gate drive power supplies (where m is the number of phases). Section 3.2 describes the configuration of a $1.5m$ -switch converter. This converter can be used for machines that have even number of phases. Section 3.3 describes a converter developed in [KRI96]. This converter uses $(m+1)$ switches and has a buck converter in the front-end to reduce the voltage applied to the phases of the machine. The various modes of operation, design of the front-end converter and the various advantages and the disadvantages of this converter are also described. This converter is implemented in this dissertation and its operation has been verified for the first time in this dissertation.

3.1 Eight Switch (Asymmetric Bridge) Converter

Figure 3.1 shows the configuration of an eight switch converter. To turn on a particular phase, say phase a, switches T_{aH} and T_{aL} are turned on. Neglecting the drop across the devices, a voltage of V_{dc} is applied across the phase winding. If the current in the winding exceeds the reference current, either T_{aH} or T_{aL} is turned off. This means the voltage across the phase winding is zero and the current that is flowing in the winding is free-wheeling through D_{aL} or D_{aH} respectively. When the current in the winding is to be commutated, both the phase switches are turned off and voltage equal to $-V_{dc}$ is applied to the winding as long as current flows in the winding. Then zero voltage is applied to the winding till it has to be turned on once again.

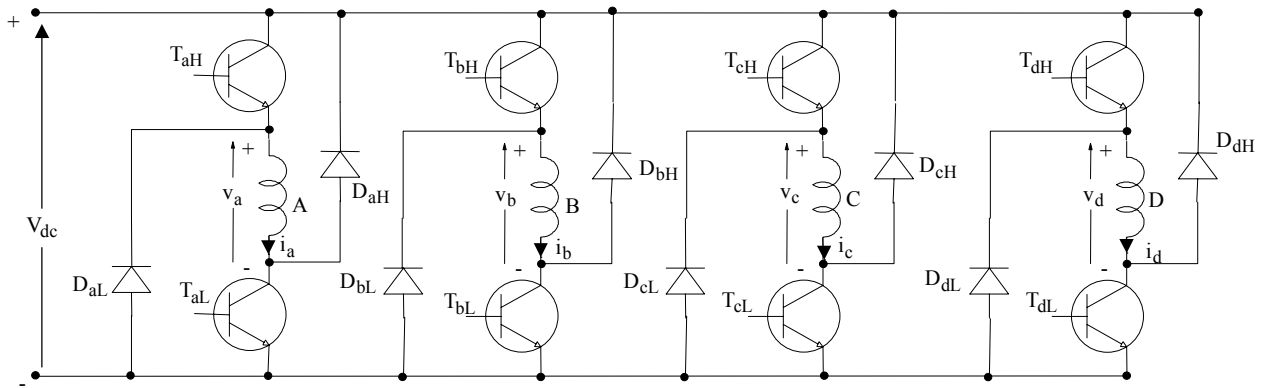


Figure 3.1 Eight Switch Converter Configuration

Figure 3.2 shows the operational waveforms of the asymmetrical bridge converter. During the current control phase the top switch is kept on as long as the phase is to be on and the bottom switch is turned on and off.

Advantages: 1. Complete freedom to apply voltages $+V_{dc}$, 0 or $-V_{dc}$ to the phase.

2. Two or even three phases can be turned on regardless of the currents in other phases thereby allowing for negative torque to be instantly generated for changing the direction of rotation.

3. If one switch is damaged, the drive can still function at reduced power levels with just three phases.

Disadvantages: 1. 8 switches and 8 diodes are required for the converter.

2. 8 switches under normal circumstances would require 5 gate drive power supplies and 8 gate drive circuits.

3. Size of the drive as well as cost increases.

3.2 Six Switch Converter

The six switch converter has four phase switches and a common upper switch for phases a and c and a common upper switch for phases b and d. If phase a is to be operated, switches T_{acH} and T_{aL} and diodes D_{aH} and D_{acL} form a circuit similar to the eight switch converter. The operational modes are identical to that of the eight switch converter.

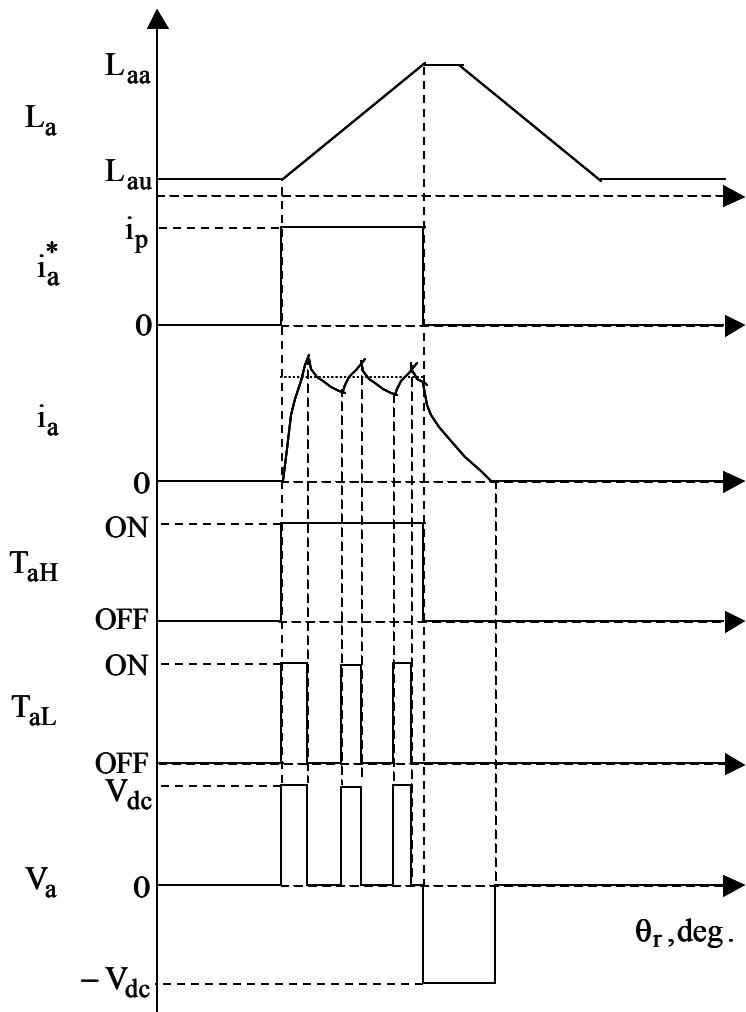


Figure 3.2 Operational waveforms for the eight switch converter

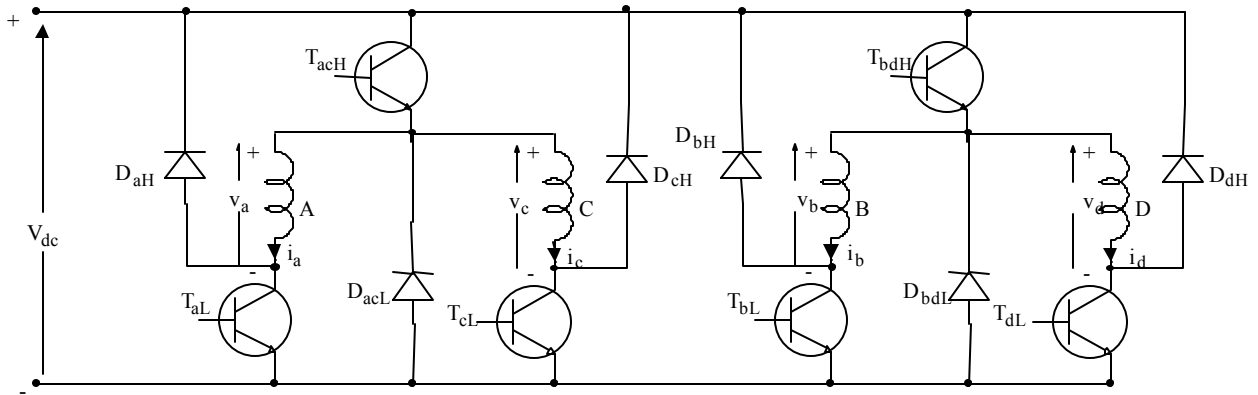


Figure 3.3 Six switch converter

- Advantages:
1. 2 lesser diodes and switches when compared to the eight switch converter.
 2. Only 3 power supplies are required for the gate drive circuits.
 3. Complete freedom to apply voltages $+V_{dc}$, 0 or $-V_{dc}$ to the phase.

Disadvantages:

1. Phases a and c or phases b and d cannot be turned on simultaneously. When changing direction of the machine, the reference speed should be set to zero till all machine currents are zero and only then negative speed can be commanded. In this respect, the freedom of operation is more limited than the eight switch converter.

3.3 Buck Converter

Converter configurations that use more than one switch per phase and less than two switches per phase have been under investigation for SRM drives. The previous section using six-switches is one such configuration. The converter described in this section was developed in [KRI96]. This configuration has the advantage of the two-switch per phase converter of having independent control of energization and four quadrant operation. The converter is shown in Figure 3.4. The switch T, diode D, inductor L and capacitor C form a buck converter power stage. This stage varies the input dc voltage to the machine windings. When phase switch T_1 is turned on, voltage V_i is applied to phase a. To regulate the current in the phase winding, switch T_1 is turned off and the current freewheels through the diode D_1 , source voltage V_{dc} and the capacitor C if main switch T is off. This applies a negative voltage of $V_i - V_{dc}$ to the phase winding. Energy stored in the capacitor C will be sufficient to turn on an incoming phase. This way complete independence is maintained during the operation of the machine. The operational waveforms of the buck converter are shown in Figure 3.5.

3.3.1 Modes of Operation

The modes of operation of the converter considering only one phase, say a, are as follows.

Mode 1: T on, D off, $i_L > 0$, T_1 off, D_1 off, $i_a = 0$.

During this mode, phase a is not in operation but some other phase is energized.

Mode 2: T off, D on, $i_L > 0$, T_1 off, D_1 off, $i_a = 0$.

During this mode, phase a is not in operation but some other phase is energized and the main switch is being regulated to supply energy to a different phase.

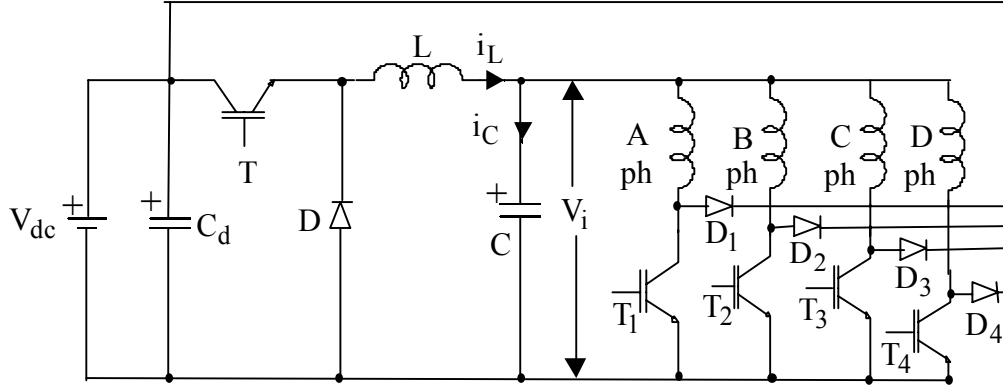


Figure 3.4 Buck Converter for SRM Drives

Mode 3: T off, D off, $i_L = 0$, T_1 off, D_1 off, $i_a = 0$.

During this mode, no phase is energized and the machine is not under operation.

Mode 4: T on, D off, $i_L > 0$, T_1 on, D_1 off, $i_a > 0$.

During this mode, phase a is energized. The buck converter equations are as follows:

$$\frac{di_L}{dt} = \frac{V_{dc} - V_i}{L} \quad (3.1)$$

$$\frac{dV_i}{dt} = \frac{i_C}{C} = \frac{i_L - (i_a + i_b + i_c + i_d)}{C} \quad (3.2)$$

It can be seen that all four currents are considered in equation 3.2. If all the other phase currents have been commutated, then only phase a current exists. Considering only phase a operation, the machine equation is written as,

$$\frac{d\lambda_a}{dt} = V_i - R_s i_a \quad (3.3)$$

The value of current i_a can be obtained from a two dimensional table linking flux linkage λ_a and rotor position which is described in detail in the subsequent chapter.

Mode 5: T on, D off, $i_L > 0$, T_1 off, D_1 on, $i_a > 0$.

During this mode, phase a current is being regulated or commutated. The buck converter equations are as follows:

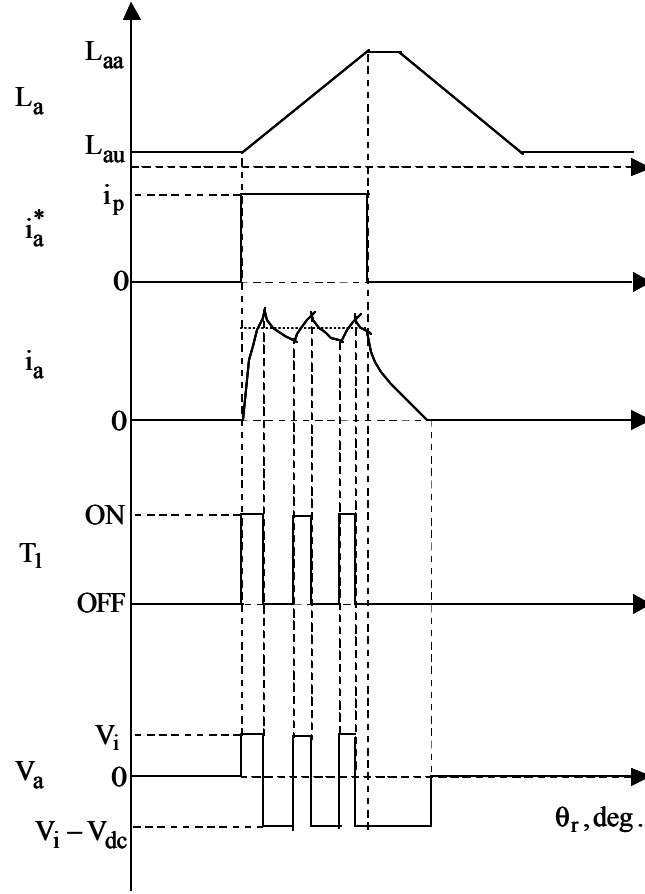


Figure 3.5 Operational waveforms for the buck converter

$$\frac{di_L}{dt} = \frac{V_{dc} - V_i}{L} \quad (3.4)$$

$$\frac{dV_i}{dt} = \frac{i_C}{C} = \frac{i_L - (i_a + i_b + i_c + i_d)}{C} \quad (3.5)$$

Considering only phase a operation, negative voltage is applied to the machine and the machine equation is written as,

$$\frac{d\lambda_a}{dt} = V_i - V_{dc} - R_s i_a \quad (3.6)$$

Mode 6: T off, D on, $i_L > 0$, T_1 off, D_1 on, $i_a > 0$.

During this mode, phase a current is being regulated or commutated and the main switch current is being regulated. The buck converter equations are as follows:

$$\frac{di_L}{dt} = \frac{-V_i}{L} \quad (3.7)$$

$$\frac{dV_i}{dt} = \frac{i_C}{C} = \frac{i_L - (i_a + i_b + i_c + i_d)}{C} \quad (3.8)$$

Considering only phase a operation, negative voltage is applied to the machine and the machine equation is written as,

$$\frac{d\lambda_a}{dt} = V_i - V_{dc} - R_s i_a \quad (3.9)$$

Mode 7: T off, D on, $i_L > 0$, T_1 on, D_1 off, $i_a > 0$.

During this mode, phase a is energized and the main switch current is being regulated. The buck converter equations are as follows:

$$\frac{di_L}{dt} = \frac{-V_i}{L} \quad (3.10)$$

$$\frac{dV_i}{dt} = \frac{i_C}{C} = \frac{i_L - (i_a + i_b + i_c + i_d)}{C} \quad (3.11)$$

Considering only phase a operation, positive voltage is applied to the machine and the machine equation is written as,

$$\frac{d\lambda_a}{dt} = V_i - R_s i_a \quad (3.12)$$

Mode 8: T off, D off, $i_L = 0$, T_1 on, D_1 off, $i_a > 0$.

This mode never occurs under normal circumstances but may occur when the machine is turned off. The equations can be written as follows:

$$\frac{di_L}{dt} = 0 \quad (3.13)$$

$$\frac{dV_i}{dt} = \frac{-(i_a + i_b + i_c + i_d)}{C} \quad (3.14)$$

Considering only phase a operation, positive voltage is applied to the machine and the machine equation is written as,

$$\frac{d\lambda_a}{dt} = V_i - R_s i_a \quad (3.15)$$

Mode 9: T off, D off, $i_L = 0$, T_1 off, D_1 on, $i_a > 0$.

This mode never occurs under normal circumstances but may occur when the machine is turned off and the phase currents are discharging. The equations can be written as follows:

$$\frac{di_L}{dt} = 0 \quad (3.16)$$

$$\frac{dV_i}{dt} = \frac{-(i_a + i_b + i_c + i_d)}{C} \quad (3.17)$$

Considering only phase a operation, negative voltage is applied to the machine and the machine equation is written as,

$$\frac{d\lambda_a}{dt} = V_i - V_{dc} - R_s i_a \quad (3.18)$$

If other phase are operating at the same instant that phase a is operating, their machine equations will come into the picture but is not described here since essentially they operate independently.

3.3.2 Design of the Buck Converter

The design of L and C in the buck converter is done by the procedure outlined in [KRI96]. The inductor rating is based on the ripple current rating that allows minimum energy storage to enable faster charging of the capacitor C. If the maximum allowed ripple current per phase is I_p , and if only two phase are operating at a given instant, the maximum capacitor ripple is,

$$\Delta i_{C,\max} = \frac{V_{dc}}{L f_c} = 2I_p \quad (3.19)$$

The inductor L can be calculated as,

$$L = \frac{V_{dc}}{2f_c I_p}, H \quad (3.20)$$

The capacitor C is designed so that the energy stored can be depleted in n cycles of PWM and transferred to the machine windings. Therefore,

$$\frac{1}{2} C V_i^2 = n \frac{2 V_i I_p}{f_c} \Rightarrow C = 2n \frac{2 I_p}{f_c V_i} \quad (3.21)$$

The minimum value of capacitance is obtained when $V_i = V_{dc}$. Therefore,

$$C = 2n \frac{2 I_p}{f_c V_{dc}} \quad (3.22)$$

n is a design variable which determines how many times the phase switch is operated after it is turned on and before the phase current is commutated. For example, if a machine is operating at 1500 r.p.m. and it is determined that each phase is on for 15° (8/6 machine), the time for traversing 15° is given by,

$$t = \frac{15}{\frac{1500}{60} \cdot 360} = 1.666 \text{ ms.}$$

If the main switch is turned on and off twice, i.e., $n = 2$, the frequency of the phase switch PWM carrier would be $f = \frac{n}{t} = \frac{2}{1.666 \cdot 10^{-3}} = 1200 \text{ Hz}$. The value of n is decided based on application.

Higher values of n are required for high performance applications.

3.3.3 Merits and Demerits of the Proposed Converter

The merits of the converter are as follows:

1. Only 5 switches and diodes are required for full four quadrant operation.
2. Independent operation of the machine phases is achieved. This is critical since there may be some instants when three phases have currents at the same time and unlike the six-switch converter there are no conflicts. Thereby the freedom of the eight switch converter is achieved with 5 switches.
3. Having smaller values of n implies fewer switchings of the machine phase and hence lower switch losses.

4. Only 2 logic power supplies are required unlike the eight switch converter which requires 5 and the six switch converter which requires 3.
5. The proposed topology can be used for PMBDC drives as described in a subsequent chapter and hence lends itself to the development of a universal drive.

The demerits of the converter are as follows:

1. Full negative dc link voltage cannot be applied to the phases and hence commutation times are longer. This would lead to advancing the firing of the phases and may result in lower average torque output. Hence the machine may not be used to its full capacity based on the design of the machine. A cooperative relationship with a machine manufacturer may be required to design machines with this converter in mind.
2. The buck converter is normally rated at the same power ratings of the machine and hence may become impractical for high power machines.
3. Losses in the system may be higher due to an extra power stage. The efficiency of the system may perhaps be improved by having lower values of n .

Chapter 4. Switched Reluctance Motor Drive Design, Simulations And Experimental Results

This chapter covers the key simulations and experimental results of a switched reluctance motor drive system. The buck converter described in Chapter 3 is simulated with a four phase switched reluctance motor. Although the basic converter was described in [KRI96] and subsequently in [BAR98], no simulation results were presented. The design of the drive following a basic procedure outlined in [JAC96] is completed and simulations are conducted for the drive. Experimental results of the drive are also presented in this chapter. There has been no implementation of this drive in literature.

Section 4.1 describes the design of the buck converter based speed controlled switched reluctance motor drive system. Section 4.2 elaborates on the various components that are used to setup the simulation of the system. The design of the drive for a prototype machine is described in section 4.3 while the simulation results are presented in section 4.4. Experimental results for the prototype system are described in section 4.5. Results are summarized in section 4.6.

4.1 Design of the Buck Converter Speed Controlled System

The buck converter system described in detail in Chapter 3 is designed in this section. The current and speed controllers are designed by the procedure outlined in [JAC96]. The design of the controllers can be primarily considered when a single phase is conducting at a time although there will be some portions when two phases are conducting at a time. It may not be necessary to design for the periods of multi-phase conduction.

Assuming that phase a is under consideration, the voltage equation with this converter is written as,

$$\begin{aligned}
 V_i &= R_s i_a + \frac{d}{dt}(L_a i_a) = R_s i_a + L_a \frac{di_a}{dt} + i_a \frac{dL_a}{dt} \\
 &= R_s i_a + L_a \frac{di_a}{dt} + i_a \frac{dL_a}{d\theta} \frac{d\theta}{dt} = R_s i_a + L_a \frac{di_a}{dt} + i_a \omega_m \frac{dL_a}{d\theta}
 \end{aligned} \tag{4.1}$$

Assuming that the rate of change of inductance is constant and defining,

$$g_L = \frac{dL_a}{d\theta} \quad (4.2)$$

(4.1) can be rewritten as,

$$V_i = i_a (R_s + \omega_m g_L) + L_a \frac{di_a}{dt} \quad (4.3)$$

The electromagnetic torque can be calculated as,

$$T_e = \frac{1}{2} g_L i_a^2 \quad (4.4)$$

Assuming that the load is proportional to the speed, at rated speed and rated load torque,

$$B_\ell = \frac{T_{e, \text{rated}}}{\omega_m} \quad (4.5)$$

The total inertia of the machine can be calculated as,

$$B_t = B + B_\ell \quad (4.6)$$

The speed equation can be written as,

$$T_e = J \frac{d\omega_m}{dt} + B_t \omega_m \Rightarrow \frac{1}{2} g_L i_a^2 = J \frac{d\omega_m}{dt} + B_t \omega_m \quad (4.7)$$

Equations (4.3) and (4.7) represent the machine equations. Since (4.7) is nonlinear, the equation can be linearized and the small signal equations can be used for analysis. Therefore,

$$V_{i0} + \delta V_i = (i_{a0} + \delta i_a) (R_s + (\omega_{m0} + \delta \omega_m) g_L) + L_a \frac{d(i_{a0} + \delta i_a)}{dt} \quad (4.8)$$

$$\frac{1}{2} g_L (i_{a0} + \delta i_a)^2 = J \frac{d(\omega_{m0} + \delta \omega_m)}{dt} + B_t (\omega_{m0} + \delta \omega_m) \quad (4.9)$$

The small signal equations are given by,

$$\delta V_i = \delta i_a (R_s + \omega_{m0} g_L) + L_a \frac{d(\delta i_a)}{dt} + i_{a0} g_L (\delta \omega_m) \quad (4.10)$$

$$i_{a0} g_L \delta i_a = J \frac{d(\delta \omega_m)}{dt} + B_t (\delta \omega_m) \quad (4.11)$$

In terms of state space equations, the above equations can be written as,

$$\begin{bmatrix} \frac{d(\delta i_a)}{dt} \\ \frac{d(\delta \omega_m)}{dt} \end{bmatrix} = \begin{bmatrix} -\frac{(R_s + \omega_{mo} g_L)}{L_a} & -\frac{i_{ao} g_L}{L_a} \\ \frac{i_{ao} g_L}{J} & -\frac{B_t}{J} \end{bmatrix} \begin{bmatrix} (\delta i_a) \\ (\delta \omega_m) \end{bmatrix} + \begin{bmatrix} \frac{1}{L_a} \\ 0 \end{bmatrix} (\delta V_i) \quad (4.12)$$

To calculate the current loop transfer function and its response, it is necessary to calculate the transfer function,

$$\frac{\delta i_a(s)}{\delta V_i(s)} = \frac{(B_t + sJ)}{s^2 L_a J + s(L_a B_t + R_s J + \omega_{mo} g_L J) + R_s B_t + \omega_{mo} g_L B_t + g_L^2 i_{ao}^2} \quad (4.13)$$

Defining the mechanical time constant of the machine and the electrical time constant of the machine respectively as,

$$T_m = \frac{J}{B_t}, \quad (4.14)$$

$$\tau = \frac{L_a}{R_s}, \quad (4.15)$$

$$\frac{\delta i_a(s)}{\delta V_i(s)} = \frac{B_t (1 + sT_m)}{L_a J \left(s^2 + s \left(\frac{1}{T_m} + \frac{1}{\tau} + \frac{\omega_{mo} g_L}{L_a} \right) + \frac{1}{T_m \tau} + \frac{\omega_{mo} g_L}{T_m L_a} + \frac{g_L^2 i_{ao}^2}{L_a J} \right)} \quad (4.16)$$

Setting $b = \frac{1}{T_m} + \frac{1}{\tau} + \frac{\omega_{mo} g_L}{L_a}$ and $c = \frac{1}{T_m \tau} + \frac{\omega_{mo} g_L}{T_m L_a} + \frac{g_L^2 i_{ao}^2}{L_a J}$, T_1 and T_2 are calculated as,

$$-T_1 = \frac{-b - \sqrt{b^2 - 4c}}{2} \quad (4.17)$$

$$-T_2 = \frac{-b + \sqrt{b^2 - 4c}}{2} \quad (4.18)$$

Therefore, (4.13) is rewritten as,

$$\frac{\delta i_a(s)}{\delta V_i(s)} = \frac{(1 + sT_m)}{L_a T_m (s + T_1)(s + T_2)} \quad (4.19)$$

The current control loop is shown in Figure 4.1. The transfer function of the pulse width modulator is obtained as,

$$G_r(s) = \frac{d(s)}{V_i(s)} = \frac{K_r}{1 + sT_r} \quad (4.20)$$

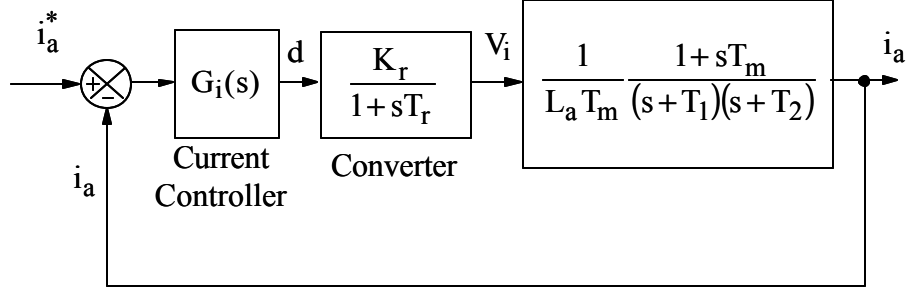


Figure 4.1 Current control loop.

where the gain K_r is given by $K_r = \frac{V_i}{V_{\text{ramp, max}} - V_{\text{ramp, min}}}$ and the delay T_r is given by

$$T_r = \frac{1}{2f_c}.$$

The current controller is of the proportional type. It is represented as,

$$G_i(s) = K_i \quad (4.21)$$

The closed loop transfer function of the current loop system is given by,

$$G_{ic}(s) = \frac{K_i \frac{K_r}{1 + sT_r} \frac{(1 + sT_m)}{L_a T_m (s + T_1)(s + T_2)}}{1 + K_i \frac{K_r}{1 + sT_r} \frac{(1 + sT_m)}{L_a T_m (s + T_1)(s + T_2)}} \quad (4.22)$$

The following approximations are made in the vicinity of the crossover frequency as,

$$1 + sT_r \cong 1 \quad (4.23)$$

$$1 + sT_m \cong sT_m \quad (4.24)$$

The current loop system is simplified as,

$$\begin{aligned} G_{ic}(s) &= \frac{K_i K_r \frac{s}{L_a (s + T_1)(s + T_2)}}{1 + K_i K_r \frac{s}{L_a (s + T_1)(s + T_2)}} = \frac{\frac{sK_i K_r}{L_a (s + T_1)(s + T_2)}}{\frac{L_a (s + T_1)(s + T_2) + sK_i K_r}{L_a (s + T_1)(s + T_2)}} \\ &= \frac{sK_i K_r}{L_a (s + T_1)(s + T_2) + sK_i K_r} = \frac{\frac{sK_i K_r}{L_a}}{s^2 + s \left((T_1 + T_2) + \frac{K_i K_r}{L_a} \right) + T_1 T_2} \end{aligned} \quad (4.25)$$

If the value of K_i can be designed to have a bandwidth of about 1/20 times the switching frequency.

The speed control system is shown in Figure 4.2. From (4.11), the speed to phase current transfer function is given by,

$$\frac{\delta\omega_m(s)}{\delta i_a(s)} = \frac{i_{ao}g_L}{sJ + B_t} = \frac{i_{ao}g_L}{sT_m + 1} = \frac{K_b}{sT_m + 1} \quad (4.26)$$

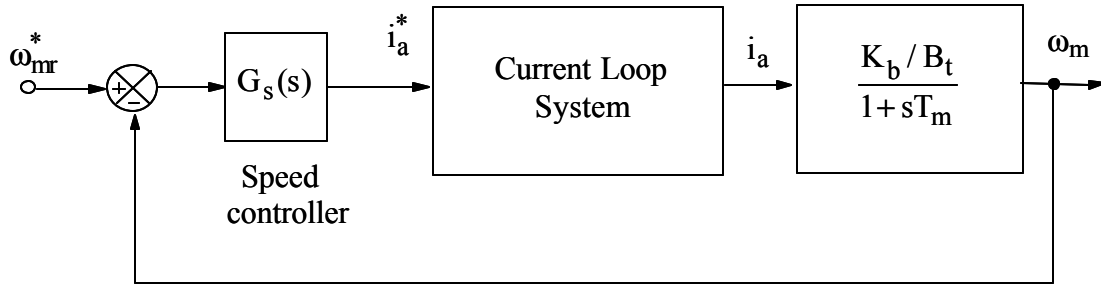


Figure 4.2 Speed control loop

The speed controller is of the proportional type. It is represented as,

$$G_s(s) = K_s \quad (4.27)$$

The transfer function of the overall system is given by,

$$\frac{\omega_m}{\omega_m^*} = \frac{K_s \frac{sK_i K_r}{L_a} \frac{K_b}{B_t}}{s^2 + s \left((T_1 + T_2) + \frac{K_i K_r}{L_a} \right) + T_1 T_2} \frac{1}{1 + sT_m} \quad (4.28)$$

$$1 + K_s \frac{sK_i K_r}{L_a} \frac{K_b}{B_t} \frac{1}{s^2 + s \left((T_1 + T_2) + \frac{K_i K_r}{L_a} \right) + T_1 T_2} \frac{1}{1 + sT_m}$$

Using the assumption in (4.24),

$$\frac{\omega_m}{\omega_m^*} = \frac{\frac{\frac{sK_i K_r K_b K_s}{L_a B_t} \frac{1}{sT_m}}{s^2 + s\left((T_1 + T_2) + \frac{K_i K_r}{L_a}\right) + T_1 T_2}}{\left(s^2 + s\left((T_1 + T_2) + \frac{K_i K_r}{L_a}\right) + T_1 T_2\right) sT_m + \frac{sK_i K_r K_s}{L_a} \frac{K_b}{B_t}} \quad (4.29)$$

$$\Rightarrow \frac{\omega_m}{\omega_m^*} = \frac{\frac{sK_i K_r K_b K_s}{L_a B_t}}{\left(s^2 + s\left((T_1 + T_2) + \frac{K_i K_r}{L_a}\right) + T_1 T_2\right) sT_m + \frac{sK_i K_r K_s}{L_a} \frac{K_b}{B_t}}$$

The value for K_s can be designed such that the speed loop bandwidth is about 10% of the current loop bandwidth. It should be remembered that the output of the speed controller is normally the torque and the torque constant should be accounted for in the process of obtaining the current command.

Unlike the traditional inverter used in SRM drives, a buck converter is used in this configuration and hence the transfer function will be different. From equation (4.3) the required input voltage to the machine V_i can be calculated from the actual speed of the machine. The buck converter circuit can be assumed to be a system that delivers the required input voltage to the machine windings and can be considered as an independent system. The converter can be modeled as follows. The equivalent circuit of the buck converter is shown in Figure 4.3.

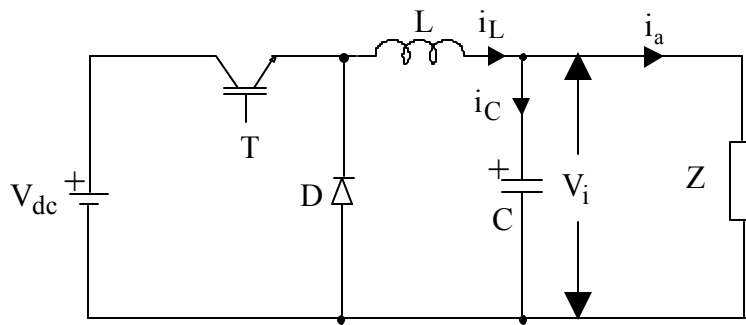


Figure 4.3 Equivalent Buck Converter Circuit

Although the machine normally operates at the rated current, it may be wise to design for a maximum current since the current controllers are designed with the maximum value in mind. If the maximum allowed current in the machine is restricted to $i_{a,max}$, the equivalent load Z can be calculated in steady state as,

$$Z = \frac{R_s i_{a,max} + K_b \omega_m^* + C_L}{i_{a,max}} \quad (4.30)$$

where the back emf constant is defined as,

$$K_b = i_{a0} g_L \quad (4.31)$$

The value C_L represents the product of rate of change of current and self inductance and is assumed to be a constant.

When the main switch T is on, the state equations can be written as,

$$\begin{bmatrix} \frac{di_L}{dt} \\ \frac{dV_i}{dt} \end{bmatrix} = \begin{bmatrix} 0 & -\frac{1}{L} \\ \frac{1}{C} & -\frac{1}{ZC} \end{bmatrix} \begin{bmatrix} i_L \\ V_i \end{bmatrix} + \begin{bmatrix} \frac{1}{L} \\ 0 \end{bmatrix} V_{dc} = A_1 x + B_1 u \quad (4.32)$$

$$V_i = \begin{bmatrix} 0 & 1 \end{bmatrix} \begin{bmatrix} i_L \\ V_i \end{bmatrix} = C_1 x$$

When the main switch T is off, the state equations can be written as,

$$\begin{bmatrix} \frac{di_L}{dt} \\ \frac{dV_i}{dt} \end{bmatrix} = \begin{bmatrix} 0 & -\frac{1}{L} \\ \frac{1}{C} & -\frac{1}{ZC} \end{bmatrix} \begin{bmatrix} i_L \\ V_i \end{bmatrix} + \begin{bmatrix} 0 \\ 0 \end{bmatrix} V_{dc} = A_2 x + B_2 u \quad (4.33)$$

$$V_i = \begin{bmatrix} 0 & 1 \end{bmatrix} \begin{bmatrix} i_L \\ V_i \end{bmatrix} = C_2 x$$

If $d(s)$ is the transfer function of the input duty cycle, the converter transfer function can be obtained as [MOH89],

$$\frac{V_i(s)}{d(s)} = C[s\mathbf{I} - \mathbf{A}]^{-1} \cdot [[(A_1 - A_2)x(s) + (B_1 - B_2)V_{dc}(s)] + (C_1 - C_2)x(s)] \quad (4.34)$$

where $\mathbf{C} = d C_1 + (1 - d) C_2 = C_2$ and $\mathbf{A} = d A_1 + (1 - d) A_2 = A_2$.

Therefore the transfer function is calculated as,

$$\begin{aligned}
G_b(s) &= \frac{V_i(s)}{d(s)} = [0 \quad 1] \left[\begin{array}{c|c} \begin{bmatrix} s & 0 \\ 0 & s \end{bmatrix} & \begin{bmatrix} 0 & -\frac{1}{L} \\ \frac{1}{C} & -\frac{1}{ZC} \end{bmatrix} \\ \hline & \end{array} \right]^{-1} \cdot \begin{bmatrix} V_{dc} \\ L \\ 0 \end{bmatrix} \\
&= [0 \quad 1] \begin{bmatrix} \frac{(sZC+1)L}{s^2LZC+sL+Z} & -\frac{ZC}{s^2LZC+sL+Z} \\ \frac{ZL}{s^2LZC+sL+Z} & \frac{sZCL}{s^2LZC+sL+Z} \end{bmatrix} \cdot \begin{bmatrix} V_{dc} \\ L \\ 0 \end{bmatrix} \\
&= \begin{bmatrix} \frac{ZL}{s^2LZC+sL+Z} & \frac{sZCL}{s^2LZC+sL+Z} \end{bmatrix} \begin{bmatrix} V_{dc} \\ L \\ 0 \end{bmatrix} \\
&= \frac{Z}{(s^2LZC+sL+Z)} V_{dc} = \frac{1}{\left(s^2LC + s\frac{L}{Z} + 1\right)} V_{dc}
\end{aligned} \tag{4.35}$$

The transfer function of the inductor current to the duty cycle can be obtained as,

$$\begin{aligned}
G_{bi}(s) &= \frac{i_L(s)}{d(s)} = [1 \quad 0] \left[\begin{array}{c|c} \begin{bmatrix} s & 0 \\ 0 & s \end{bmatrix} & \begin{bmatrix} 0 & -\frac{1}{L} \\ \frac{1}{C} & -\frac{1}{ZC} \end{bmatrix} \\ \hline & \end{array} \right]^{-1} \cdot \begin{bmatrix} V_{dc} \\ L \\ 0 \end{bmatrix} \\
&= [1 \quad 0] \begin{bmatrix} \frac{(sZC+1)L}{s^2LZC+sL+Z} & -\frac{ZC}{s^2LZC+sL+Z} \\ \frac{ZL}{s^2LZC+sL+Z} & \frac{sZCL}{s^2LZC+sL+Z} \end{bmatrix} \cdot \begin{bmatrix} V_{dc} \\ L \\ 0 \end{bmatrix} \\
&= \begin{bmatrix} \frac{(sZC+1)L}{s^2LZC+sL+Z} & -\frac{ZC}{s^2LZC+sL+Z} \end{bmatrix} \begin{bmatrix} V_{dc} \\ L \\ 0 \end{bmatrix} = \frac{(sZC+1)}{s^2LZC+sL+Z} V_{dc}
\end{aligned} \tag{4.36}$$

The transfer function of the pulse width modulator is obtained as,

$$G_{rb}(s) = \frac{d(s)}{V_i^*(s)} = \frac{K_{rb}}{1 + sT_{rb}} \tag{4.37}$$

where the gain K_{rb} is given by $K_{rb} = \frac{1}{V_{ramp,max} - V_{ramp,min}}$ and the delay T_{rb} is given by

$$T_{rb} = \frac{1}{2f_{cb}}.$$

The current control system of the buck converter uses a proportional control and the current control loop is shown in Figure 4.4. The proportional gain of the current controller is designed such that the response is extremely fast.

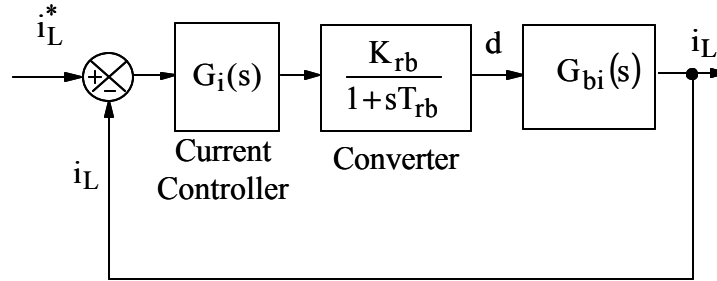


Figure 4.4 Current Loop of the buck converter system

The transfer function of the output voltage to the inductor current can be derived from (4.35) and (4.36) as,

$$\frac{V_i(s)}{i_L(s)} = \frac{V_i(s)}{d(s)} \frac{d(s)}{i_L(s)} = \frac{Z}{sZC + 1} \quad (4.38)$$

The closed loop buck converter system is shown in Figure 4.5. The voltage controller is designed to be of a proportional type. The gain of the controller is set such that the output response has a minimal overshoot as well as fast response.

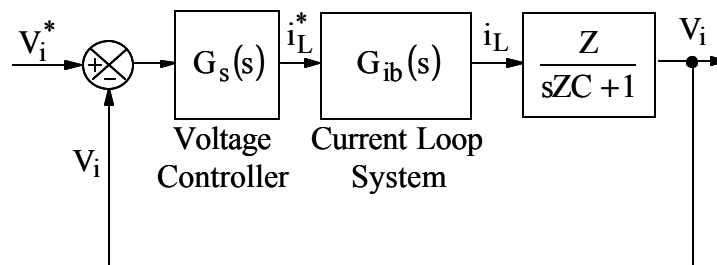


Figure 4.5 Closed Loop Buck Converter System

4.2 Simulation of a Practical Buck Converter Driven SRM System

The buck converter is described in Chapter 3. The drive system is shown in Figure 4.6. One of the key points to be noted in this set of simulations is that it is assumed that,

$$\frac{d\theta}{dt} = \omega_r \Rightarrow \theta = \int \omega_r dt, \quad (4.39)$$

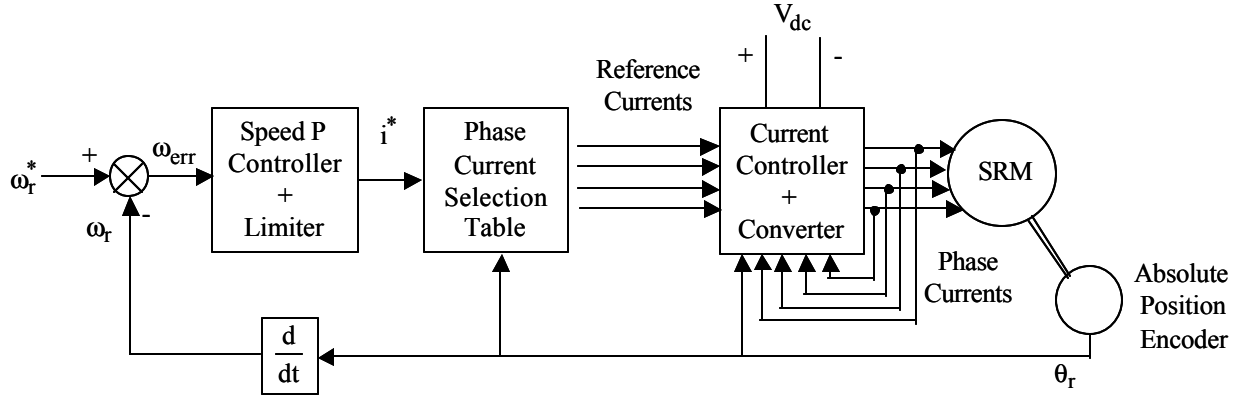


Figure 4.6 Block diagram of the SRM Buck Converter Drive System

The reference speed ω_r^* is compared to the actual speed of the machine, ω_r , to obtain the speed error, ω_{err} . Therefore,

$$\omega_{err} = \omega_r^* - \omega_r. \quad (4.40)$$

The speed error is passed through a PI controller whose output is the reference current i^* . Normally, the output of the PI controller is the torque reference T_e^* . But in the experimental system, accurate position system was hard to obtain and hence the current is directly controlled instead of using a torque to current conversion table. Therefore,

$$i^* = K_{ps} \omega_{err} \quad (4.41)$$

where K_{ps} is the proportional gain. The reference current is limited to the allowable maximum current. Since the reference current can be positive or negative, consequently, the reference current can also be positive or negative. Since the converter itself uses only unipolar current and the current polarity is normally used only to decide which phase has to be excited, the main reference current i_L^* can be written as,

$$i_L^* = |i^*| \quad (4.42)$$

As seen from Figure 4.7, the reference current is compared with the active phase currents to obtain the current error as,

$$i_{x,err} = i_L^* - i_x, x = a, b, c, d \text{ based on active phase} \quad (4.43)$$

Based on the rotor position and the quadrant of operation, the equations to obtain phase a current is described below. The logic can be extended to the other phases. It should be noted that during the operation of each phase, the current in the phase has to be regulated. Although, the reduced input voltage will have the effect of limiting the current in the phase, nevertheless the presence of the capacitor C may lead to extremely high phase currents if not regulated properly.

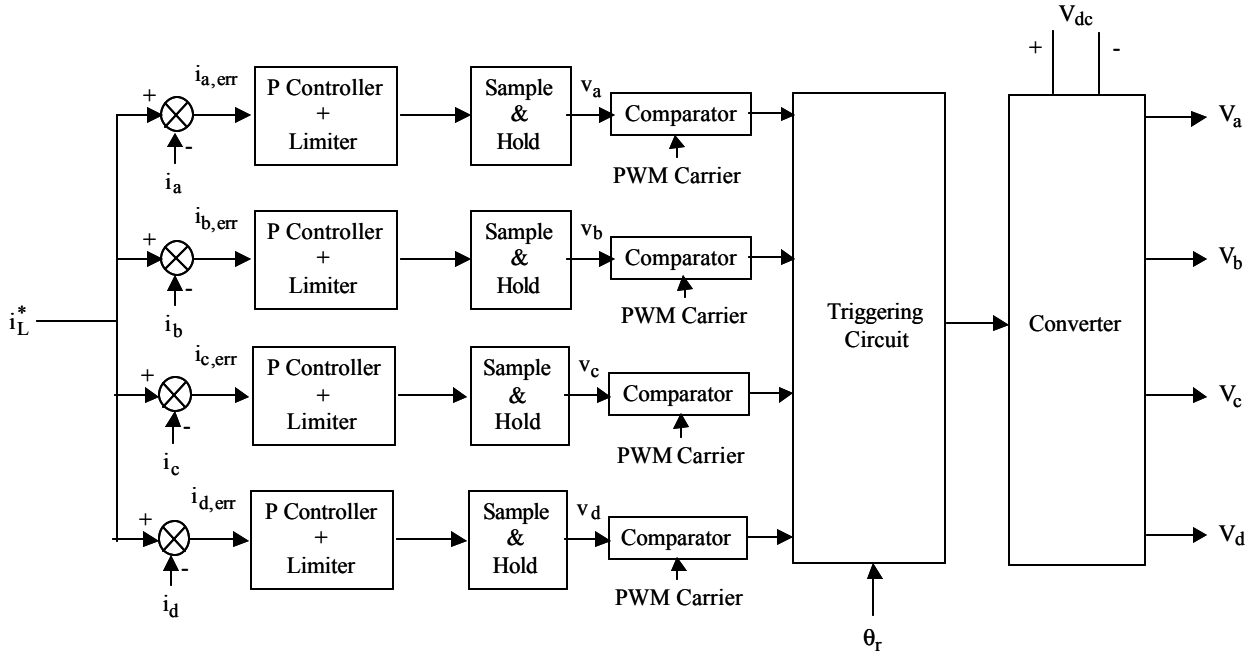


Figure 4.7 Current Controller and Converter Schematic

The current error is passed through a P controller with a gain of K_i . The output of the P controllers and limiters are passed through a sample and hold circuit operating at the same frequency as the PWM carrier frequency to prevent multiple switchings in a single cycle of the PWM carrier. The output of the sample and hold circuits, v_k , for $k = a, b, c, d$, represent the actual control voltages used for comparison with the PWM carrier frequency. The PWM carrier voltage is operating at a frequency of f_c with a minimum value of 0V and a maximum value of 2V. The control voltage is given as,

$$v_k = K_i (i_L^* - i_k), \quad k = a, b, c, d \quad (4.44)$$

Obviously the control voltages are limited to maximum and minimum values of the ramp voltage $V_{\text{switch_ramp}}$. For phase a, if the operation is in the I quadrant, i.e., $i^* \geq 0$ and $\omega_m \geq 0$, and it is the active phase as a result of its rotor position, $(13^\circ - \text{advance angle}) \leq \theta_r \leq (28^\circ - \text{delay angle})$,

$$\begin{aligned} \text{If } v_k \geq V_{\text{switch_ramp}}, V_a &= V_i \\ \text{If } v_k < V_{\text{switch_ramp}}, V_a &= V_i - V_{\text{dc}} \end{aligned} \quad (4.45)$$

If the rotor position is $(28^\circ - \text{delay angle}) < \theta_r$ or $\theta_r < (13^\circ - \text{advance angle})$, and $i_a > 0$, the phase switch is completely turned off and the applied voltage is $V_a = V_i - V_{\text{dc}}$ as long as the current is flowing in the windings and when the phase current reaches zero, the applied voltage is assumed to be $V_a = 0$.

The triggering circuit decides the voltage that has to be applied to each phase. If the command current $i^* \geq 0$, then the following logic is applied in the triggering circuit for phase a.

$$\begin{aligned} \text{For } (13^\circ - \text{advance angle}) \leq \theta_r \leq (28^\circ - \text{delay angle}), \text{ if } v_a \geq V_{\text{switch_ramp}}, V_a &= V_i \\ \text{For } (13^\circ - \text{advance angle}) \leq \theta_r \leq (28^\circ - \text{delay angle}), \text{ if } v_a < V_{\text{switch_ramp}}, V_a &= V_i - V_{\text{dc}} \\ \text{For } (28^\circ - \text{delay angle}) < \theta_r \text{ or } \theta_r < (13^\circ - \text{advance angle}), \text{ if } i_a > 0, V_a &= V_i - V_{\text{dc}} \\ \text{For } (28^\circ - \text{delay angle}) < \theta_r \text{ or } \theta_r < (13^\circ - \text{advance angle}), \text{ if } i_a = 0, V_a &= 0 \end{aligned} \quad (4.46)$$

where, θ_r is the rotor position, V_a is the voltage applied to a phase and V_{dc} is the dc link voltage.

The firing angles 13° and 28° are obtained from Chapter 2. Also it must be noted that when $\theta_r = 60^\circ$, the value is reset to 0° . The logic can also be decided for phases b, c and d, as follows:

$$\begin{aligned} \text{For } (28^\circ - \text{advance angle}) \leq \theta_r \leq (43^\circ - \text{delay angle}), \text{ if } v_b \geq V_{\text{switch_ramp}}, V_b &= V_i \\ \text{For } (28^\circ - \text{advance angle}) \leq \theta_r \leq (43^\circ - \text{delay angle}), \text{ if } v_b < V_{\text{switch_ramp}}, V_b &= V_i - V_{\text{dc}} \\ \text{For } (43^\circ - \text{delay angle}) < \theta_r \text{ or } \theta_r < (28^\circ - \text{advance angle}), \text{ if } i_b > 0, V_b &= V_i - V_{\text{dc}} \\ \text{For } (43^\circ - \text{delay angle}) < \theta_r \text{ or } \theta_r < (28^\circ - \text{advance angle}), \text{ if } i_b = 0, V_b &= 0 \end{aligned} \quad (4.47)$$

$$\begin{aligned} \text{For } (43^\circ - \text{advance angle}) \leq \theta_r \leq (58^\circ - \text{delay angle}), \text{ if } v_c \geq V_{\text{switch_ramp}}, V_c &= V_i \\ \text{For } (43^\circ - \text{advance angle}) \leq \theta_r \leq (58^\circ - \text{delay angle}), \text{ if } v_c < V_{\text{switch_ramp}}, V_c &= V_i - V_{\text{dc}} \\ \text{For } (58^\circ - \text{delay angle}) < \theta_r \text{ or } \theta_r < (43^\circ - \text{advance angle}), \text{ if } i_c > 0, V_c &= V_i - V_{\text{dc}} \\ \text{For } (58^\circ - \text{delay angle}) < \theta_r \text{ or } \theta_r < (43^\circ - \text{advance angle}), \text{ if } i_c = 0, V_c &= 0 \end{aligned} \quad (4.48)$$

$$\begin{aligned}
&\text{For } (58^\circ - \text{advance angle}) \leq \theta_r \leq (13^\circ - \text{delay angle}), \text{ if } v_d \geq V_{\text{switch_ramp}}, V_d = V_i \\
&\text{For } (58^\circ - \text{advance angle}) \leq \theta_r \leq (13^\circ - \text{delay angle}), \text{ if } v_d < V_{\text{switch_ramp}}, V_d = V_i - V_{\text{dc}} \\
&\text{For } (13^\circ - \text{delay angle}) < \theta_r \text{ or } \theta_r < (58^\circ - \text{advance angle}), \text{ if } i_d > 0, V_d = V_i - V_{\text{dc}} \\
&\text{For } (13^\circ - \text{delay angle}) < \theta_r \text{ or } \theta_r < (58^\circ - \text{advance angle}), \text{ if } i_d = 0, V_d = 0
\end{aligned} \tag{4.49}$$

If the command torque $i^* < 0, T_e^* < 0$, then the following logic is applied in the triggering circuit for phase a.

$$\begin{aligned}
&\text{For } (32^\circ + \text{delay angle}) \leq \theta_r \leq (47^\circ + \text{advance angle}), \text{ if } v_a \geq V_{\text{switch_ramp}}, V_a = V_i \\
&\text{For } (32^\circ + \text{delay angle}) \leq \theta_r \leq (47^\circ + \text{advance angle}), \text{ if } v_a < V_{\text{switch_ramp}}, V_a = V_i - V_{\text{dc}} \\
&\text{For } (32^\circ + \text{delay angle}) > \theta_r \text{ or } \theta_r > (47^\circ + \text{advance angle}), \text{ if } i_a > 0, V_a = V_i - V_{\text{dc}} \\
&\text{For } (32^\circ + \text{delay angle}) > \theta_r \text{ or } \theta_r > (47^\circ + \text{advance angle}), \text{ if } i_a = 0, V_a = 0
\end{aligned} \tag{4.50}$$

The logic can also be deduced for phases b, c and d, as follows:

$$\begin{aligned}
&\text{For } (47^\circ + \text{delay angle}) \leq \theta_r \leq (2^\circ + \text{advance angle}), \text{ if } v_b \geq V_{\text{switch_ramp}}, V_b = V_i \\
&\text{For } (47^\circ + \text{delay angle}) \leq \theta_r \leq (2^\circ + \text{advance angle}), \text{ if } v_b < V_{\text{switch_ramp}}, V_b = V_i - V_{\text{dc}} \\
&\text{For } (47^\circ + \text{delay angle}) > \theta_r \text{ or } \theta_r > (2^\circ + \text{advance angle}), \text{ if } i_b > 0, V_b = V_i - V_{\text{dc}} \\
&\text{For } (47^\circ + \text{delay angle}) > \theta_r \text{ or } \theta_r > (2^\circ + \text{advance angle}), \text{ if } i_b = 0, V_b = 0
\end{aligned} \tag{4.51}$$

$$\begin{aligned}
&\text{For } (2^\circ + \text{delay angle}) \leq \theta_r \leq (17^\circ + \text{advance angle}), \text{ if } v_c \geq V_{\text{switch_ramp}}, V_c = V_i \\
&\text{For } (2^\circ + \text{delay angle}) \leq \theta_r \leq (17^\circ + \text{advance angle}), \text{ if } v_c < V_{\text{switch_ramp}}, V_c = V_i - V_{\text{dc}} \\
&\text{For } (2^\circ + \text{delay angle}) > \theta_r \text{ or } \theta_r > (17^\circ + \text{advance angle}), \text{ if } i_c > 0, V_c = V_i - V_{\text{dc}} \\
&\text{For } (2^\circ + \text{delay angle}) > \theta_r \text{ or } \theta_r > (17^\circ + \text{advance angle}), \text{ if } i_c = 0, V_c = 0
\end{aligned} \tag{4.52}$$

$$\begin{aligned}
&\text{For } (17^\circ + \text{delay angle}) \leq \theta_r \leq (32^\circ + \text{advance angle}), \text{ if } v_d \geq V_{\text{switch_ramp}}, V_d = V_i \\
&\text{For } (17^\circ + \text{delay angle}) \leq \theta_r \leq (32^\circ + \text{advance angle}), \text{ if } v_d < V_{\text{switch_ramp}}, V_d = V_i - V_{\text{dc}} \\
&\text{For } (17^\circ + \text{delay angle}) > \theta_r \text{ or } \theta_r > (32^\circ + \text{advance angle}), \text{ if } i_d > 0, V_d = V_i - V_{\text{dc}} \\
&\text{For } (17^\circ + \text{delay angle}) > \theta_r \text{ or } \theta_r > (32^\circ + \text{advance angle}), \text{ if } i_d = 0, V_d = 0
\end{aligned} \tag{4.53}$$

Now that the phase voltages are obtained, the flux linkage for each phase is calculated as,

$$\frac{d\lambda_k}{dt} = v_k - R_s i_k, \text{ for } k = a, b, c, d \tag{4.54}$$

The knowledge of the phase flux linkages and rotor position allows the calculation of each phase current from the two dimensional table relating the flux linkage and rotor position for different current values. This table is obtained by finite element analysis as shown in Chapter 2 and is plotted for phase a in Figure 4.8. The other phase linkages are offset by the requisite amount.

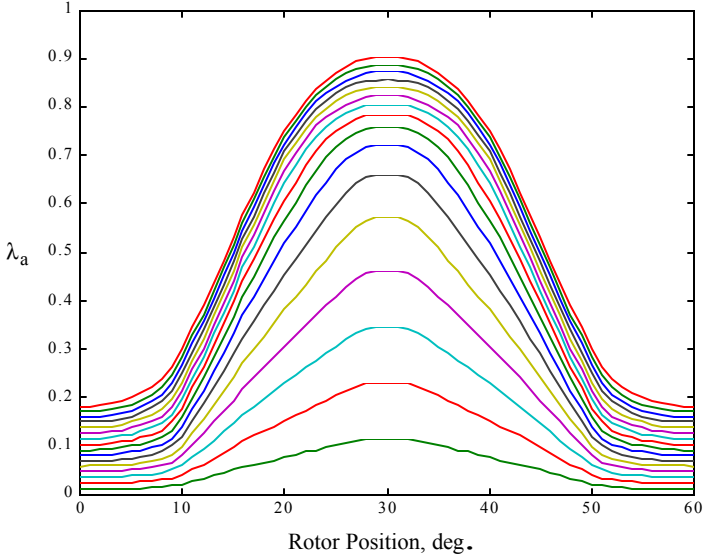


Figure 4.8 Plot of phase a flux linkages vs. rotor position for different currents

The torque due to each phase current, T_{ek} , is obtained by straight-forward two-dimensional interpolation of the values in the table of torque vs. rotor position for different currents that is plotted in Figure 4.9.

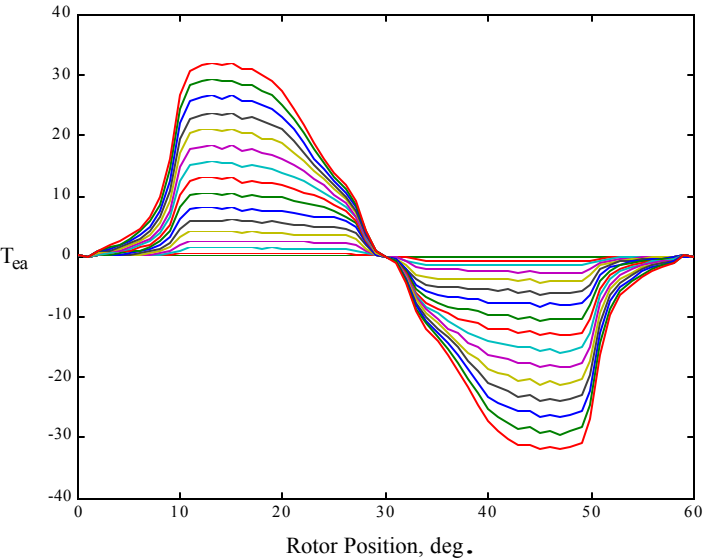


Figure 4.9 Plot of torque vs. rotor position for different phase currents

The total torque developed in the machine is calculated as,

$$T_e = T_{ea} + T_{eb} + T_{ec} + T_{ed} \quad (4.55)$$

The machine speed ω_m can be obtained from,

$$\frac{d\omega_m}{dt} = \frac{T_e - T_l - B\omega_m}{J} \quad (4.56)$$

where, T_l is the load torque, J is the moment of inertia and B is the friction coefficient.

Finally, the rotor position can be obtained from the machine speed since,

$$\frac{d\theta_r}{dt} = \omega_m \quad (4.57)$$

It has to be noted that if θ_r exceeds 60° , it is reset to 0° and if it goes below 0° (reverse rotation), the value is reset to 60° .

In equation (4.45), it is assumed that the voltage V_i is available. This voltage is generated as follows. The reference voltage V_i^* is obtained from

$$V_i^* = R_s i_L^* + K_b \omega_m^* + C_L \quad (4.58)$$

The constant value C_L is used to compensate for the $L_a \frac{di_a}{dt}$ factor instead of actually calculating the value.

The back emf of the machine can be defined as,

$$E = K_b \omega_m \quad (4.59)$$

During the falling inductance region of phase a when the current is being forced to zero, the equation of the machine is given by,

$$R i_a + L_a \frac{di_a}{dt} - E = V_i - V_{dc} \quad (4.60)$$

Unless the condition $V_{dc} > V_i + E$ is enforced, positive voltage is applied to the phase. Hence, the above condition is the limiting factor in deciding the maximum speed at which the machine can be run.

The reference voltage is compared with the actual input voltage and the error is passed through a proportional controller with a limiter. The upper value of the limiter is restricted to the current reference value obtained in (4.48). The output of the limiter is the inductor reference current. This is compared with the actual inductor current and the error is passed through a proportional controller with a limiter that limits the value to the maximum and minimum value of the PWM ramp. The control voltage v_{cb} is calculated as,

$$v_{cb} = \frac{1}{V_{ramp,max} - V_{ramp,min}} \quad (4.61)$$

This control voltage is compared to the PWM ramp to obtain the on and off period of the main switch.

The control voltage is limited as follows,

$$\begin{aligned} v_{cb} &= V_{ramp,max}, \text{ if } v_{cb} > V_{ramp,max} \\ v_{cb} &= V_{ramp,min}, \text{ if } v_{cb} < V_{ramp,min} \end{aligned} \quad (4.62)$$

The main switch is controlled by the following logic,

$$\begin{aligned} \text{If } v_{cb} &\geq V_{ramp}, T \text{ is turned on} \\ \text{If } v_{cb} &< V_{ramp}, T \text{ is turned off} \end{aligned} \quad (4.63)$$

When the buck converter switch T is on, the input voltage to the machine phases can be written as,

$$V_i = \frac{1}{C} \int i_C dt \quad (4.64)$$

where i_C is the capacitor current.

The above equation can be rewritten as,

$$\frac{dV_i}{dt} = \frac{i_C}{C} \Rightarrow dV_i = \frac{i_C}{C} dt = \frac{i_L - \sum i_k}{C} dt, k = a, b, c, d \quad (4.65)$$

where i_L is the inductor current.

The equation for the inductor current can be written as,

$$V_{dc} = L \frac{di_L}{dt} + V_i \quad (4.66)$$

The above equation can be rewritten as,

$$\frac{di_L}{dt} = \frac{V_{dc} - V_i}{L} \Rightarrow di_L = \frac{V_{dc} - V_i}{L} dt \quad (4.67)$$

Equations (4.65) and (4.67) are the equations used in the simulation when the switch T is on.

When the switch T is off, equation (4.67) is replaced by the following equation,

$$di_L = \frac{-V_i}{L} dt \quad (4.68)$$

Using the Euler's method of integration, the new input voltage is obtained as,

$$V_i = V_i + dV_i, \quad (4.69)$$

and the new inductor current is obtained as,

$$i_L = i_L + di_L. \quad (4.70)$$

The voltage V_i that is obtained in (4.69) is used in the simulation of the phases.

4.3 Design of the prototype SRM Buck Converter Drive

The test machine has the following parameters:

Power Output $P_o = 0.8$ h.p., Speed $N = 1500$ r.p.m., Maximum DC link voltage = 200 V, Number of stator poles = 8, Number of rotor poles = 6, Stator resistance $R_s = 0.8 \Omega$, $J = 0.03$ kg-m/s², $B = 0.018$ N.m/rad/sec, PWM switching frequency of the main switch = 20 kHz.

If the peak ripple current is limited to 1.25 A, the inductor L can be calculated as,

$$L = \frac{V_{dc}}{2f_c i_{a,rip}} = \frac{200}{2 * 20000 * 1.25} = 4\text{mH}.$$

Assuming that the stored energy can be depleted in $n = 45$ cycles, the capacitor C is designed as,

$$C = 2n \frac{2i_{a,\max}}{f_c V_{dc}} = 2n \frac{2i_{a,\max}}{f_c V_{dc}} = 2 \cdot 45 \frac{2 \cdot 10}{20000 \cdot 200} = 450 \mu\text{F}.$$

The rated torque is given as,

$$T_{e,\text{rated}} = \frac{P_o}{\omega_m} = \frac{0.8 \cdot 746}{\left(\frac{2\pi \cdot 1500}{60}\right) 157.08} = 3.8 \text{ N-m}.$$

Assuming that the load is proportional to the speed, at rated speed and rated load torque,

$$B_\ell = \frac{T_e}{\omega_m} = \frac{3.8}{\left(\frac{2\pi \cdot 1500}{60}\right)} = 0.024$$

The total inertia of the machine can be calculated as,

$$B_t = B + B_\ell = 0.018 + 0.024 = 0.042 \text{ N-m/rad/sec}$$

$$T_m = \frac{J}{B_t} = \frac{0.03}{0.042} = 0.714 \text{ s}.$$

$$\tau = \frac{L_{a,\max}}{R_s} = \frac{100 \times 10^{-3}}{0.8} = 0.125 \text{ s}.,$$

From the prototype design in Chapter 2, the rate of change of inductance with respect to position can be approximated to the maximum value as $g_L = 0.34 \text{ H/rad}$.

Setting,

$$b = \frac{1}{T_m} + \frac{1}{\tau} + \frac{\omega_{mo} g_L}{L_a} = \frac{1}{0.714} + \frac{1}{0.125} + \frac{157.08 \cdot 0.34}{100 \cdot 10^{-3}} = 543.47$$

and

$$c = \frac{1}{T_m \tau} + \frac{\omega_{mo} g_L}{T_m L_a} + \frac{g_L^2 i_{a0}^2}{L_a J} = \frac{1}{0.714 \cdot 0.125} + \frac{157.08 \cdot 0.34}{0.714 \cdot 100 \cdot 10^{-3}} + \frac{0.34^2 \cdot 7^2}{100 \cdot 10^{-3} \cdot 0.03} = 2647.34$$

T_1 and T_2 are calculated as,

$$-T_1 = \frac{-b - \sqrt{b^2 - 4c}}{2} = \frac{-543.47 - \sqrt{543.47^2 - 4 \cdot 2647.34}}{2} = -538.55$$

$$-T_2 = \frac{-b + \sqrt{b^2 - 4c}}{2} = \frac{-543.47 + \sqrt{543.47^2 - 4 * 2647.34}}{2} = -4.92$$

Assuming operation at rated speed and load, the input voltage is calculated as,

$$V_i = R_s i_{\text{rated}} + K_b \omega_m + C_L = 0.8 * 7 + 0.34 * 7 * \frac{2\pi * 1500}{60} + 10 = 389.45V.$$

It can be seen that the back emf is calculated as,

$$E = K_b \omega_m = 0.34 * 7 * \frac{2\pi * 1500}{60} = 373.85V.$$

It has been shown before that the condition $V_{dc} > V_i + E$ has to be satisfied. Therefore,

$$V_{dc} > 2E + R_s i_{\text{rated}} + C_L \text{ or, } \omega_{\text{max}} = \frac{V_{dc} - R_s i_{\text{rated}} - C_L}{2K_b}. \text{ Therefore,}$$

$$\omega_{\text{max}} = \frac{200 - 0.8 * 7 - 10}{2 * 0.34 * 7} = 38.74 \text{ rads / sec} = 369.93 \text{ r.p.m.}$$

To obtain a speed of 1500 r.p.m., the dc link voltage has to be increased.

The maximum input voltage is given by,

$$V_i = R_s i_{\text{rated}} + K_b \omega_m + C_L = 0.8 * 7 + 0.34 * 7 * 38.74 + 10 = 107.8V.$$

The gain of the converter can be calculated from

$$K_r = \frac{V_i}{V_{\text{ramp, max}} - V_{\text{ramp, min}}} = \frac{107.8}{2 - 0} = 53.9$$

The current control loop transfer function is written as,

$$G_{ic}(s) = \frac{\frac{sK_i K_r}{L_a}}{s^2 + s \left((T_1 + T_2) + \frac{K_i K_r}{L_a} \right) + T_1 T_2}$$

Selecting the current controller proportional gain $K_i = 100$, the frequency response of the current controlled system is shown in Figure 4.10. The bandwidth of the system is approximately 55000 rads/sec. This is far greater than the required bandwidth of 6283 rads/sec (1/20 times the switching frequency).

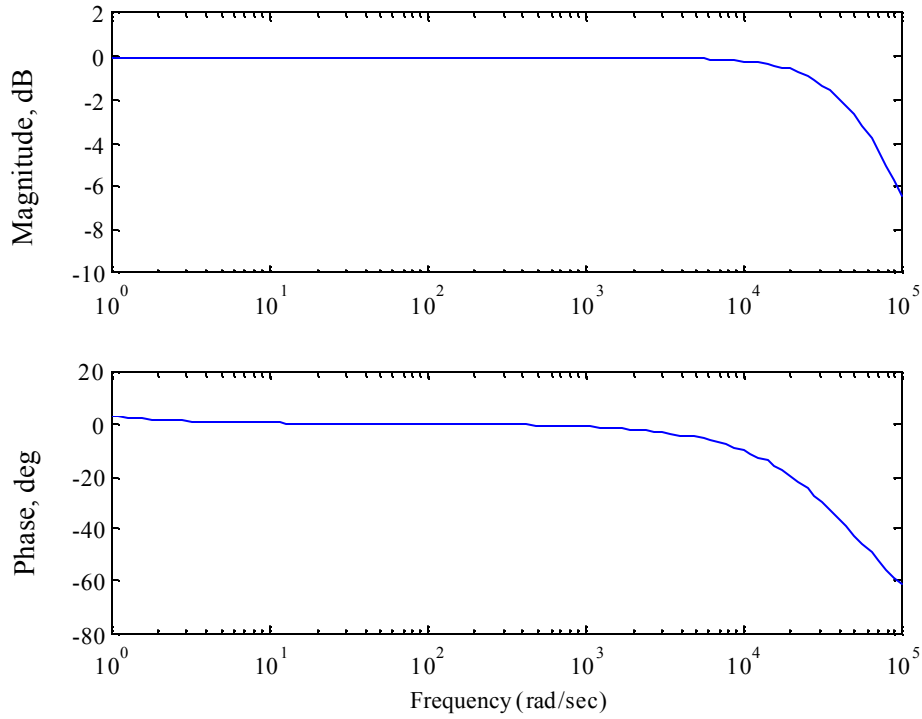


Figure 4.10 Frequency response of the current controlled system

The speed controlled system has a transfer function of,

$$\frac{\omega_m}{\omega_m^*} = \frac{\frac{sK_i K_r}{L_a} \frac{K_b}{B_t} K_s}{\left(s^2 + s \left((T_1 + T_2) + \frac{K_i K_r}{L_a} \right) + T_1 T_2 \right) s T_m + \frac{sK_i K_r}{L_a} K_s \frac{K_b}{B_t}}$$

Selecting the speed controller proportional gain $K_s = 10$, the frequency response of the speed controlled system is shown in Figure 4.11. The bandwidth of the system is approximately 811 rads/sec. This is greater than the required bandwidth of 628.3 rads/sec (10% of current loop bandwidth). Figure 4.12 shows the step response of the system. The step response shows no overshoot and a fairly quick settling time.

The equivalent load impedance of the buck converter can be calculated as,

$$Z = \frac{R_s i_{a,\max} + K_b \omega_m^* + C_L}{i_{a,\max}} = \frac{0.8 * 7 + 0.34 * 7 * 38.74 + 10}{7} = 15.4 \Omega$$

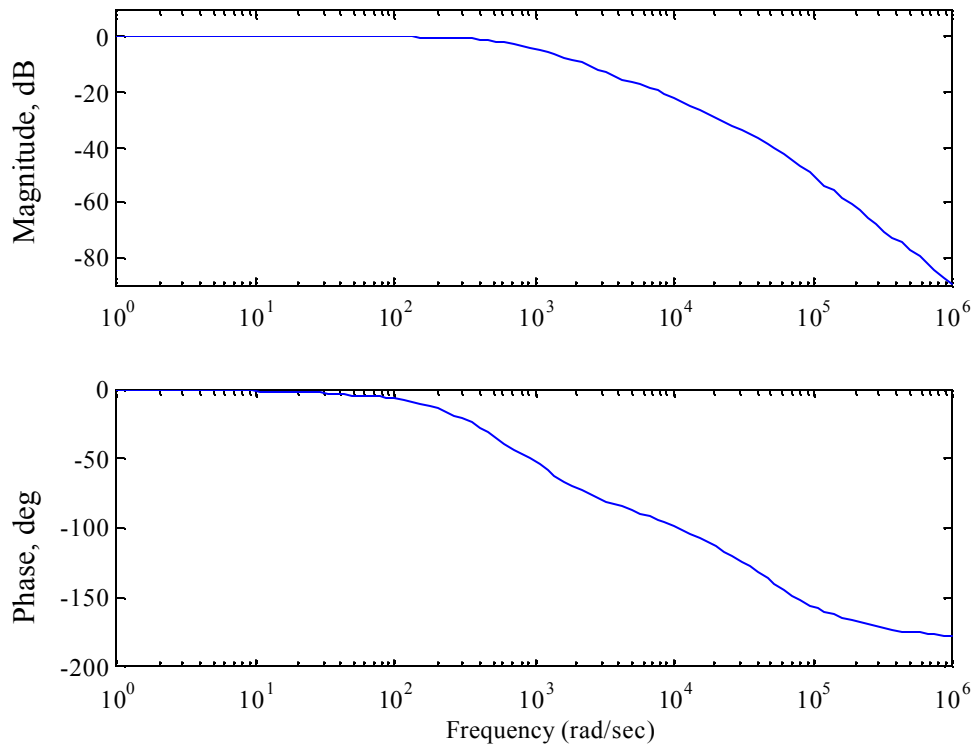


Figure 4.11 Frequency response of the speed controlled system

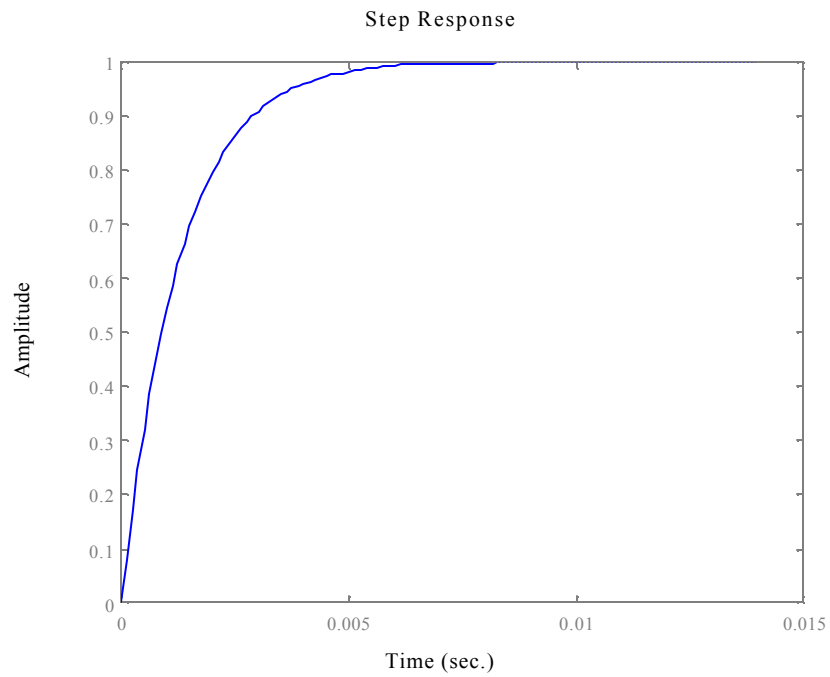


Figure 4.12 Step response of the speed controlled system

The transfer function from the inductor current to the duty cycle is given by,

$$G_{bi}(s) = \frac{i_L(s)}{d(s)} = \frac{(sZC + 1)}{s^2LZC + sL + Z} V_{dc} = \frac{(15.4 * 450 * 10^{-6} s + 1)}{s^2 4 * 10^{-3} * 15.4 * 450 * 10^{-6} + 4 * 10^{-3} s + 15.4} 200$$

$$= \frac{(1.386s + 200)}{2.772 * 10^{-5} s^2 + 4 * 10^{-3} s + 15.4}$$

The closed loop current control loop with a proportional gain of the controller as 1 is calculated as,

$$\frac{i_L}{i_L^*} = \frac{(1.386s + 200)}{6.93 * 10^{-10} s^3 + 2.782 * 10^{-5} s^2 + 1.39s + 215.4}$$

The step response of the closed loop system is shown in Figure 4.13. The response shows an overshoot which is acceptable since the peak value is lesser than the absolute maximum value of 10A.

The closed loop voltage control system with a proportional gain of 2 is given by,

$$\frac{V_i}{V_i^*} = \frac{(42.69s + 6160)}{4.802 * 10^{-12} s^4 + 1.935 * 10^{-7} s^3 + 0.009663s^2 + 45.57s + 6375}$$

The closed loop step response is shown in Figure 4.14. The system shows no overshoot and a fairly small settling time. The response is acceptable for the system.

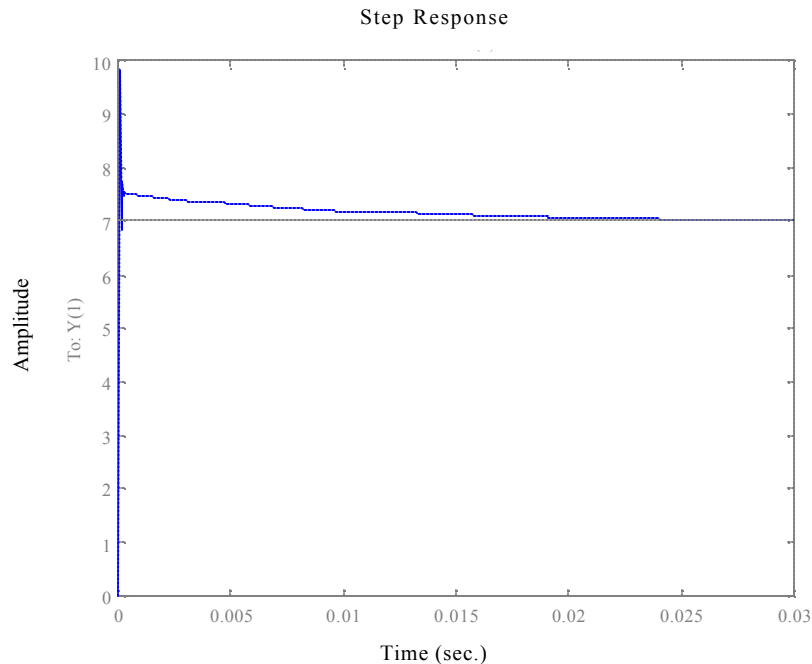


Figure 4.13 Closed loop response of the current controlled buck converter system

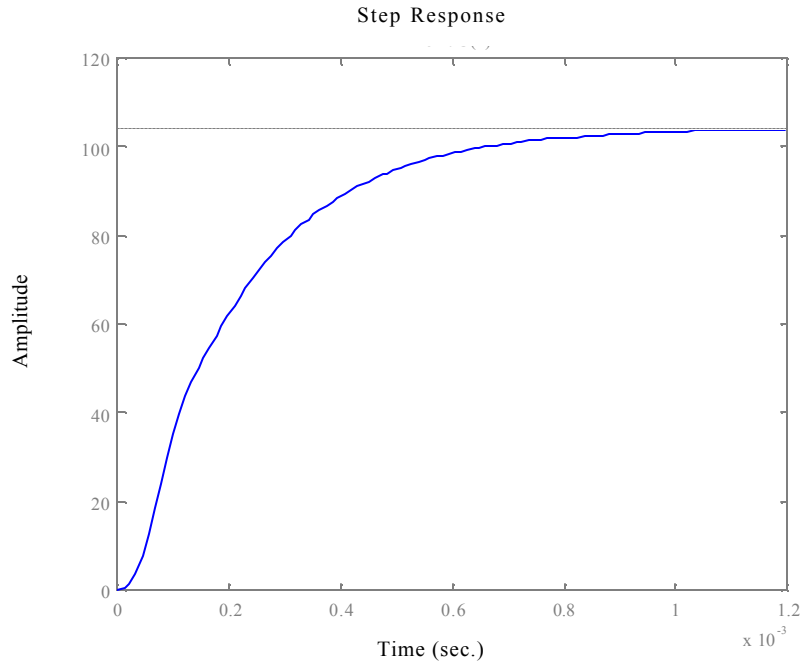


Figure 4.14 Closed loop response of the voltage controlled buck converter system

4.4 Drive System Simulation

Figure 4.15 shows the simulation of the switched reluctance motor with a buck converter front end. The speed is initially commanded to 1 p.u. or 38.74 rads/sec. The input voltage is seen to rise with the reference speed. The sequence of currents in the positive direction is seen to be abcd from Figure 4.16. The torque, which is not regulated, is seen to have ripples. After the speed settles to the commanded value, the torque is seen to supply primarily the load torque. After 0.08s, a negative speed of 1 p.u. is commanded. The sequence of currents when the machine is running in the negative direction is seen to be dcba. While the machine is changing directions, the currents in the phases are still active, signifying that the machine is operating in the fourth quadrant. During the reversal of direction, there are some portions when the developed torque is almost zero. This is due to the fact that the phases are firing on the negative slope and since two phases are not energized at the same time, there could be portions when the developed torque is extremely low even for high currents. The operation in the negative direction is seen to be very similar to that in the positive direction as expected.

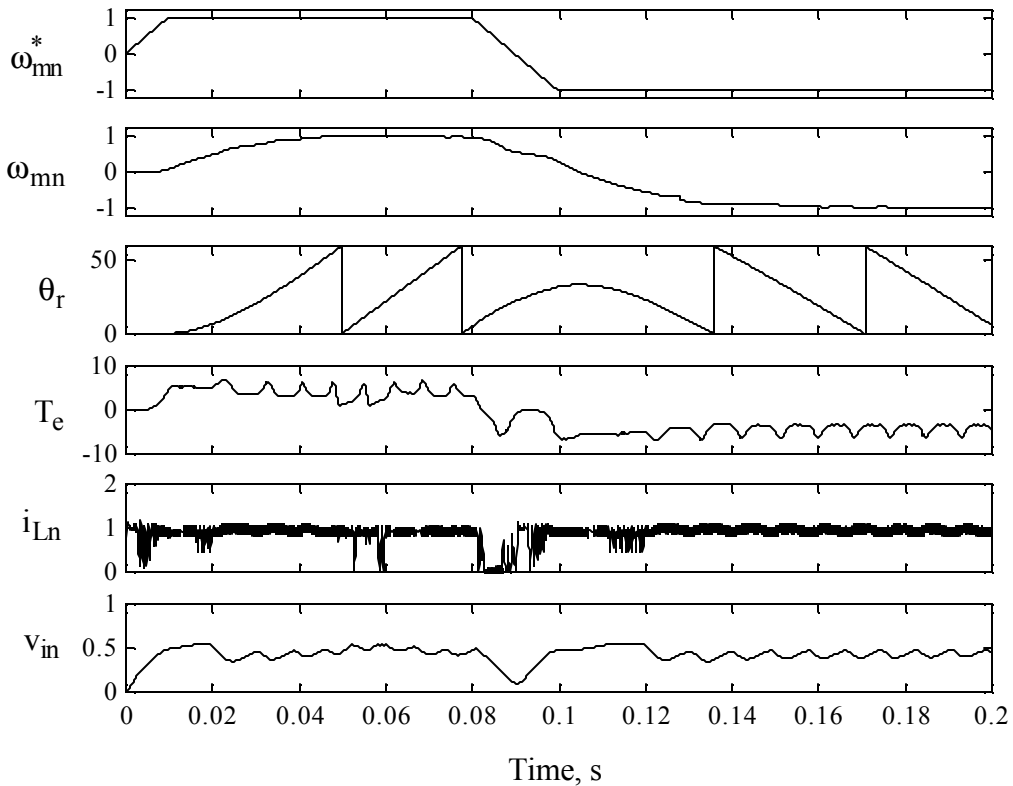


Figure 4.15 Simulation of a speed drive system with a buck converter front end

The simulations of the drive show excessive torque ripples. This is a definite indication of the phase current not reaching zero before the negative inductance slope region begins. Although there is a positive torque output from the machine that will sustain the rotation of the machine, the acoustic noise of the drive will be high. The only way to avoid this would be to advance the firing of the phase and also the point of commutation of the current. In the experimental prototype, the point where commutation begins is fixed. In the prototype, commutation has to be done within a period of δ° of rotation. This leads to the calculation of maximum speed practically obtainable from the drive if the maximum phase current is restricted as well as the maximum voltage is known. During commutation, assuming that the speed is N rpm and θ_c is the angle available for commutation in degrees, the following equations can be used to calculate maximum speed.

$$V_i - V_{dc} = L \frac{di}{dt}$$

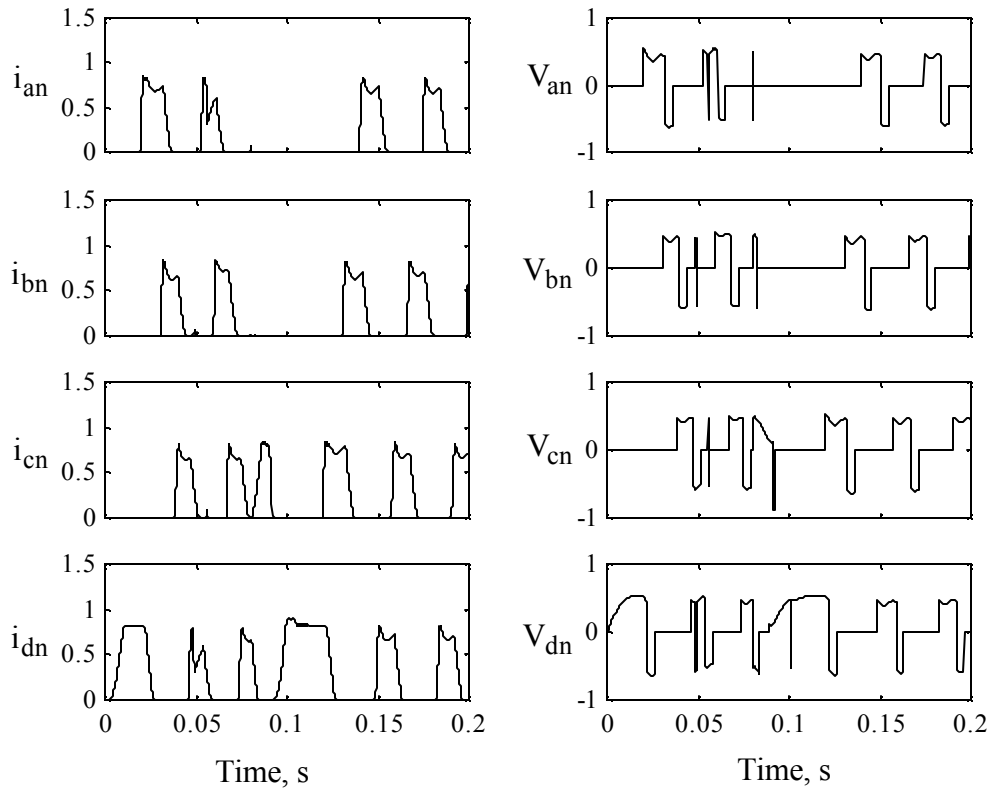


Figure 4.16 Plots of phase currents and phase voltages

$$K_b i \frac{2\pi N}{60} + R_s i + C_L - V_{dc} = L \frac{-i}{\frac{N}{60} 360}$$

For the prototype, with $K_b = 0.34$, $R_s = 0.8 \Omega$, $i = 7 \text{ A}$, $C_L = 10 \text{ V}$, $V_{dc} = 200 \text{ V}$, $L = 110 \text{ mH}$ and $\theta_c = 8^\circ$, the maximum speed can be calculated as $N = 223 \text{ r.p.m.}$ It should be clearly noted here that if the commutation angle were larger, the maximum speed would also increase significantly.

Figure 4.17 shows the plot of the drive with the maximum speed set to 223 r.p.m. It can be seen that the torque response has much lesser ripples. This indicates that the currents are completely commutated before the negative slope of the inductance starts. The small ripples that are seen in the torque is the effect of firing a phase current before the command to commutate the previous phase current is given. This will not cause large acoustic noises.

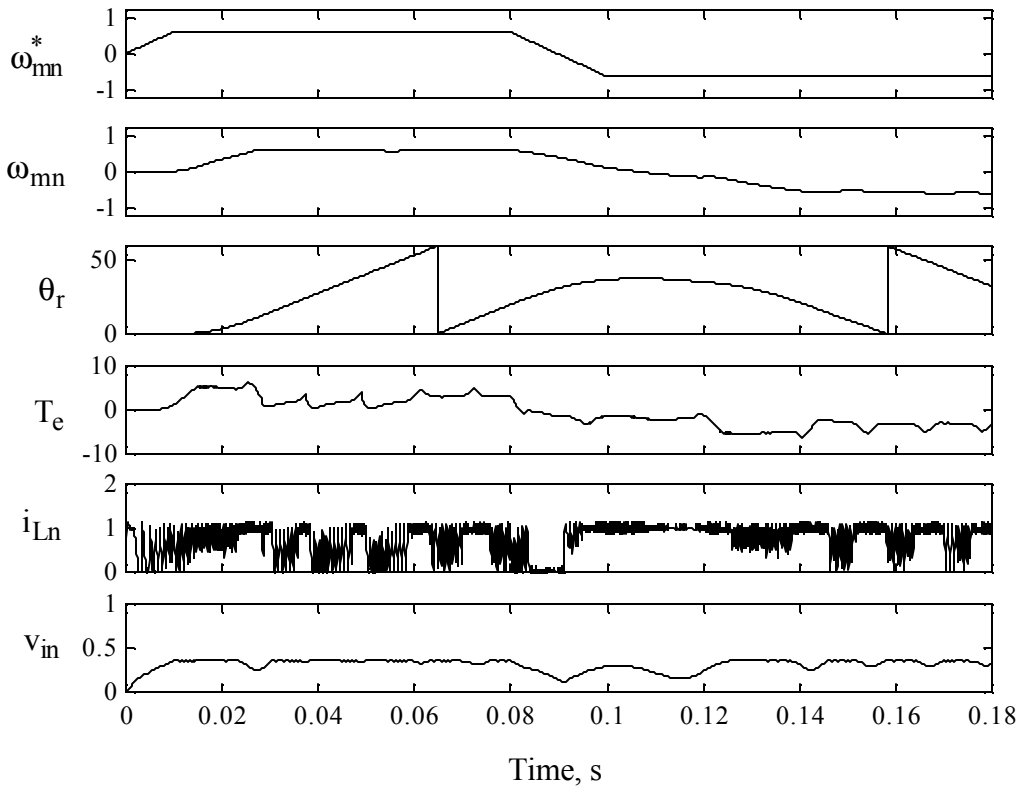


Figure 4.17 Simulation of the speed drive system with a maximum reference of 223 r.p.m.

4.5 Experimental Correlation

The switched reluctance with the buck converter front-end was experimentally implemented. The first plot in Figure 4.19 is the experimental plot of the commanded speed. The machine is commanded to a speed of 223 r.p.m. with a dc link voltage of 200V. After a suitable time, the command is changed to a negative value. As the controller is implemented in a DSP, it appears as though it the commanded values goes to zero and then goes back to a positive value when in fact it goes to the negative commanded value. This will be evident in the plot of currents. The second plot in Figure 4.19 is the plot of actual speed of the machine. After initial small delay, the machine is seen to rise to the commanded value. When the speed command is changed to the negative reference, the speed is seen to come down to zero and then rise back in the negative direction. The output voltage of the buck converter V_i is dependent on reference speed and follows the reference speed. The reference inductor current i_L^* is also plotted. Figure 4.18 shows

the simulation plots for the buck converter system. The plots are seen to be very similar to the experimental plots shown in Figure 4.19.

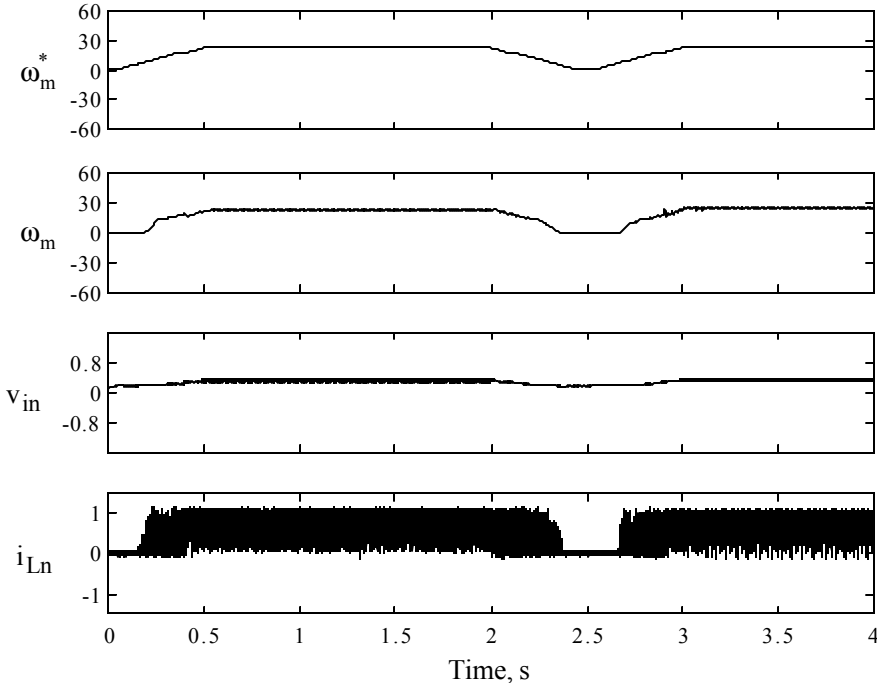


Figure 4.18 Simulation plots of the switched reluctance motor

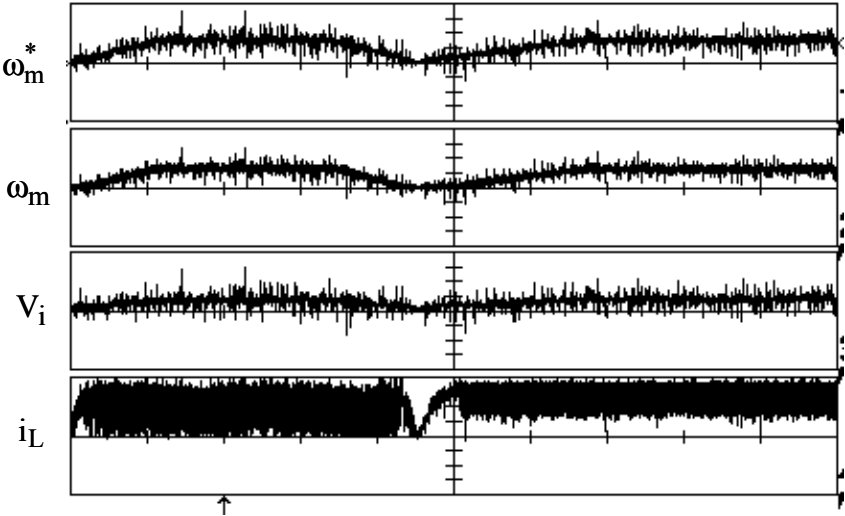


Figure 4.19 Experimental plots of the switched reluctance motor with the buck-converter front end. (ω_m^* and ω_m are 15 rads/sec per division, V_i is 80 V/division, i_L is 2.1A/division, the time is 0.4 s/division)

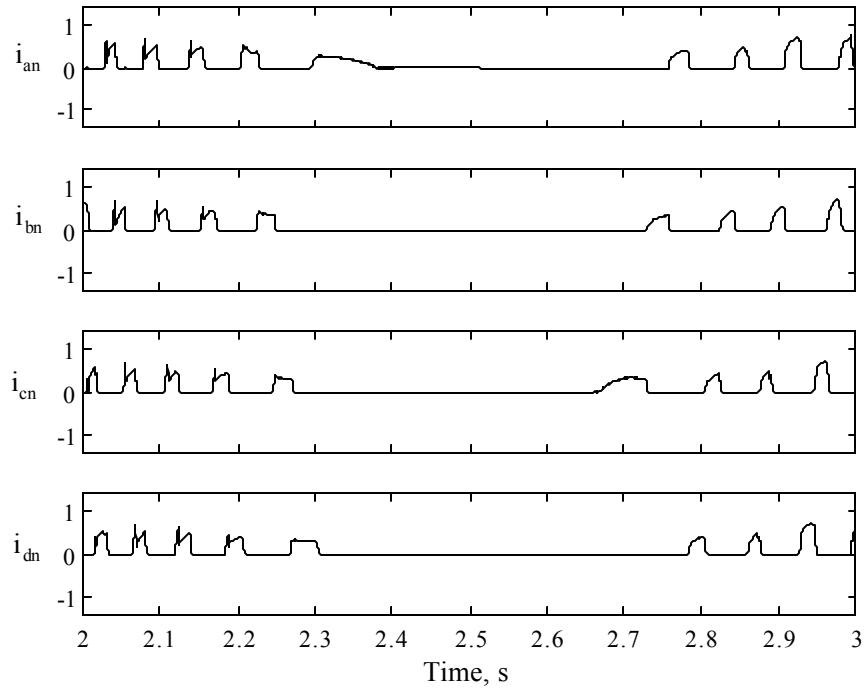


Figure 4.20 Simulation plots of the currents of the switched reluctance motor during reversal of direction

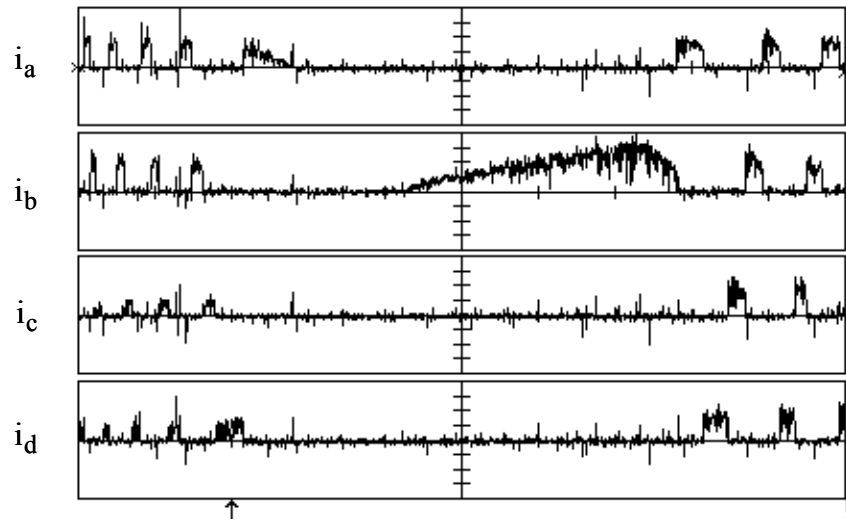


Figure 4.21 Phase current plots of the switched reluctance motor drive (1 vertical division = 2.5A, 1 horizontal division = 0.1 s)

the negative direction. The simulation plots of the phase currents during speed reversal is shown in Figure 4.20. The simulation plots are seen to be similar to the experimental plots.

4.6 Summary

This chapter shows the development of buck-converter front-end based switched reluctance motor drives. The design of the drive and the controllers are explained in detail in the chapter. A linear model based controller is developed and is verified to work for the nonlinear model by simulations. The design of the drive for a prototype machine is described and simulation results are presented. Experimental results for the prototype system are shown. The results from the experimental setup are seen to closely match the simulation results. The development of the drive is a unique contribution of this dissertation. In prior research, only the description of the converter was given in [KRI96]. This dissertation follows through with the simulations and experimental verification of the prior research.

Chapter 5. Permanent Magnet Brushless DC Motor Drive: Converter and Control

Permanent Magnet Brushless DC (PMBDC) motors share a few characteristics with the Switched Reluctance Motors that bring up the possibilities of the two machines sharing the same converter configuration. A 3 phase PMBDC motor that has 3 windings with an access to the neutral point (trapezoidal PMBDC) has a constant back emf for 120 electrical degrees both in the positive and negative half cycles that is analogous to the rising and falling inductance profiles of the SRM. The main difference is that the magnitude does not change like a SRM, whose inductance changes with rotor position and varying currents, making the control easier. Different converter strategies for control of trapezoidal PMBDC machines are described in [KRI01]. A particular configuration of operation of the PMBDC called half-wave operation [KRI98] uses only unipolar currents in the windings very similar to the SRM that leads to the possibility of using the same converter for both the SRM and PMBDC. The control strategies would vary but if it is implemented with a DSP, the implication is that only the right program has to be downloaded to the chip.

The chapter is organized as follows. Section 5.1 outlines the principle of operation of the PMBDC in the half-wave mode. Section 5.2 describes the proposed converter and the operation in different modes. Section 5.3 goes over the design of the passive components of the proposed converter. The design of the speed and current controllers of the drive as well as the controllers for the front-end buck converter and described in detail in Section 5.4. Section 5.5 describes the drive schematic as well as the simulation equations of the motor and controller. Section 5.6 develops the parameters of a prototype drive with the proposed converter while Section 5.7 covers the dynamic simulation of the drive. Section 5.8 shows the plots obtained from the prototype drive in operation. Section 5.9 focuses on the merits and demerits of the proposed converter in detail. Conclusions are summarized in Section 5.10.

5.1 Principle of Half-wave Operation of the PMBDC

Assume the direction of the motor is clockwise, which may be considered as positive with a phase sequence of a-b-c of motor phase windings. The motoring operation is initiated when the phase voltage is constant positive for a fixed speed and with the duration of 120 electrical degrees as shown in Figure 5.1. The average air-gap power is positive indicating quadrant I

operation. The motoring operation is similar in the reverse direction, except that the phase energization sequence will be a-c-b in the motor phase windings. This corresponds to quadrant III operation. This can be visualized by imagining the rotor position from the higher to the lower values. It can be noticed that the air gap power is still positive. That is not hard to imagine as the consumption of power is assumed to be equal to a positive value. The operation during the other quadrants are explained later although it can be mentioned here that the quadrants IV and II operation have the waveforms as shown in Figure 5.2 with the motor running in the forward direction and the reverse direction. The air gap power is negative signifying regeneration.

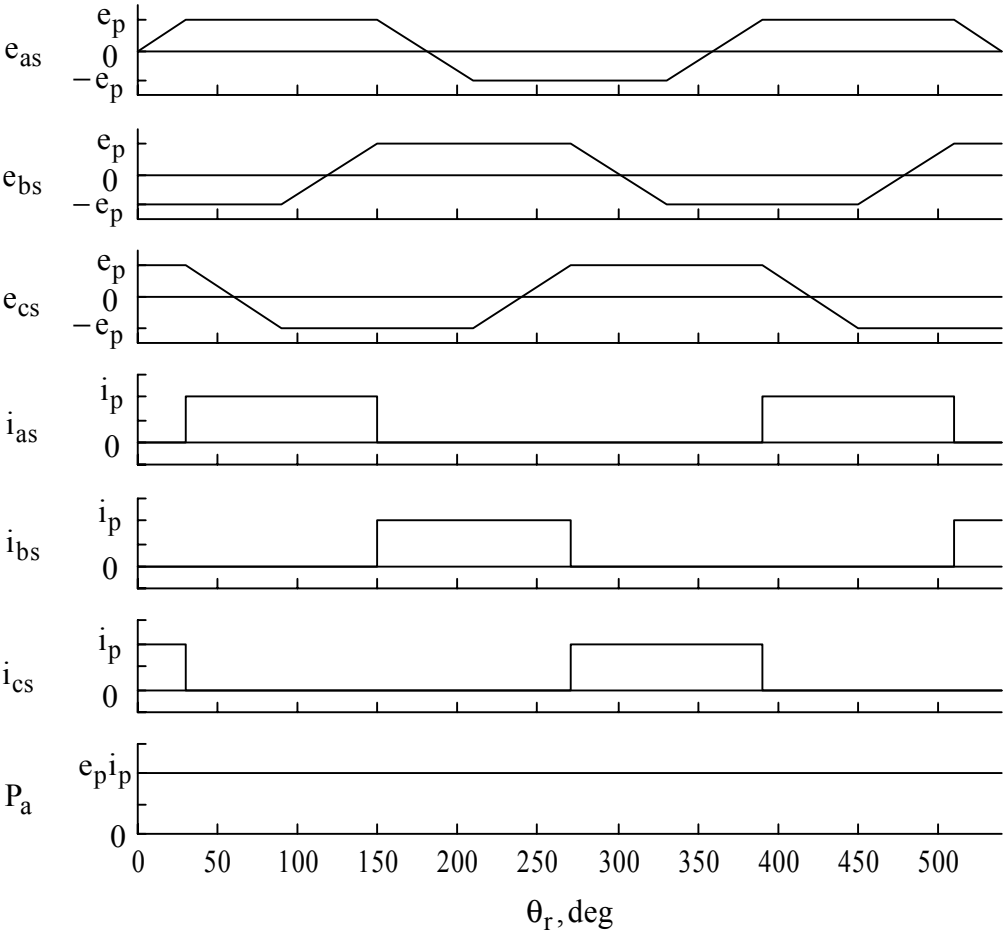


Figure 5.1 Voltage, current and air-gap power waveforms of the half-wave converter based PMBDC in the first and third quadrants

5.2 Converter Topology

A half-wave converter can be designed to be similar to the asymmetric converter described in the chapter on converters for switched reluctance motors. In the case of a 3 phase PMBDC, the converter would have 6 switches and diodes. This configuration has no significant advantages over the full-wave converter while having an output equal to only half that of the full-wave converter. Therefore, a pre-requisite for the converter is that it should have less than 6 switches per phase. A converter with single switch per phase can be implemented but has the disadvantage of not being able to operate in all 4 quadrants. Hence, configurations with more than one and less than two switches per phase have to be designed and implemented. A few different topologies have been discussed in [KRI99]. One of the topologies is discussed here.

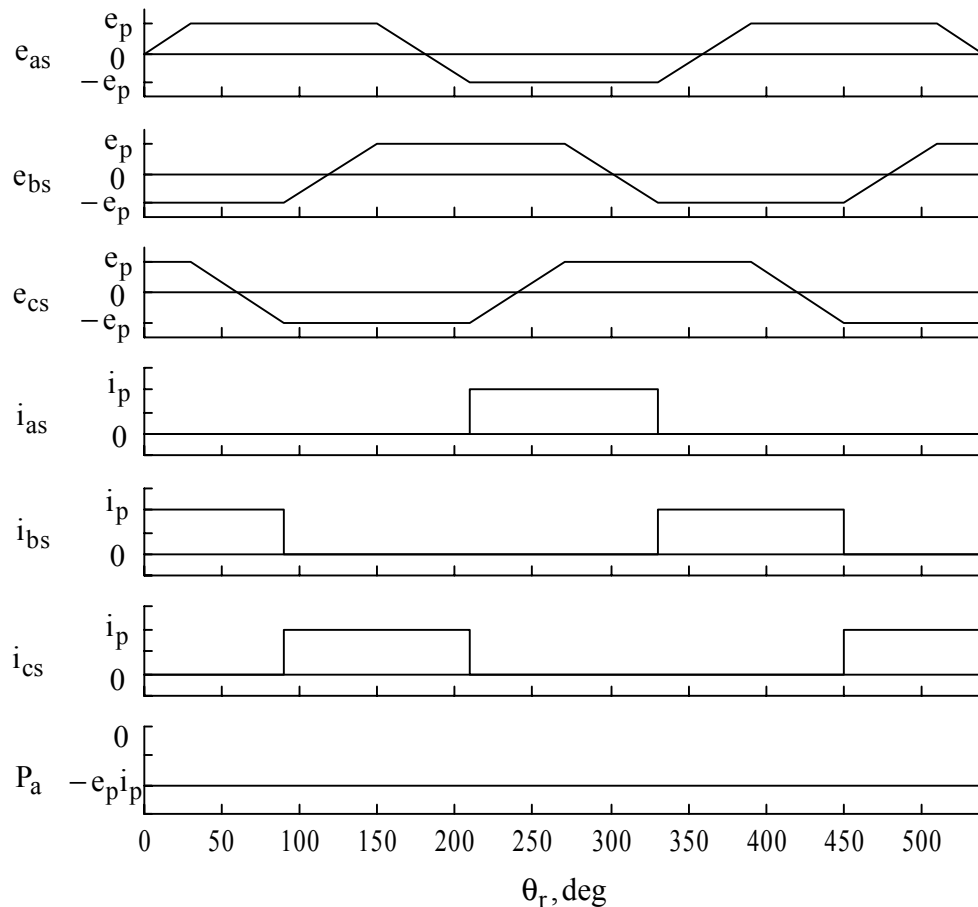


Figure 5.2 Voltage, current and air-gap power waveforms of the half-wave converter based PMBDC in the second and fourth quadrants

The proposed converter circuit with four switches and diodes is shown in Figure 5.3. Switch T, diode D, inductor L and capacitor C form a step-down chopper power stage. The chopper power stage varies the input dc source voltage to the machine windings. Since there is only one switch per phase, the current in it is unidirectional and similar to a half-wave converter driven PMBDC. The motoring (I quadrant) and regenerative (IV quadrant) control of the PMBDC are briefly described.

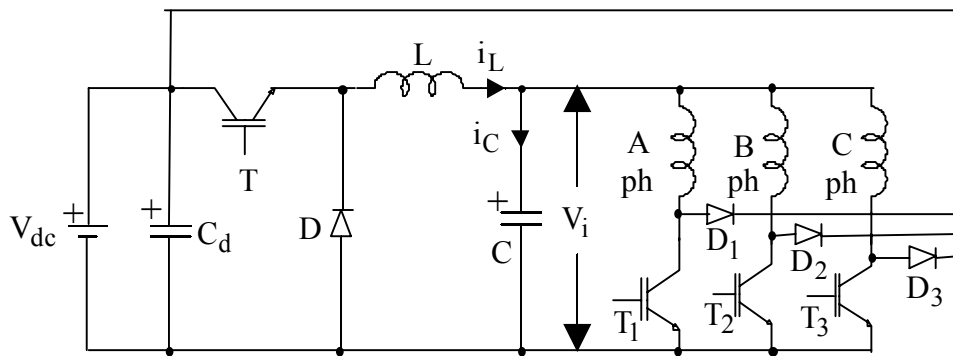


Figure 5.3 Converter topology with a buck converter on the front end

Motoring:

Assume the direction of the motor is clockwise, which may be considered as positive with a phase sequence of a-b-c of motor phase windings. The motoring operation is initiated when the phase voltage is constant positive for a fixed speed and with the duration of 120 electrical degrees as in shown in Figure 5.5. Phase a is energized when the switch T_1 is turned on and the equivalent circuit is shown in Figure 5.4(a). To regulate current, T_1 is turned off, which initiates routing of the current through the freewheeling diode D_1 , source voltage V_{dc} and capacitor C, applying a voltage of $(V_i - V_{dc})$ across the machine phases as shown in Figure 5.4 (b).

Waveforms of essential variables are shown in Figure 5.5. The average air-gap power P_a and input power P_i are positive indicating quadrant I operation. The motoring operation is similar in the reverse direction, except that the phase energization sequence will be a-c-b in the motor phase windings. This corresponds to quadrant III operation.

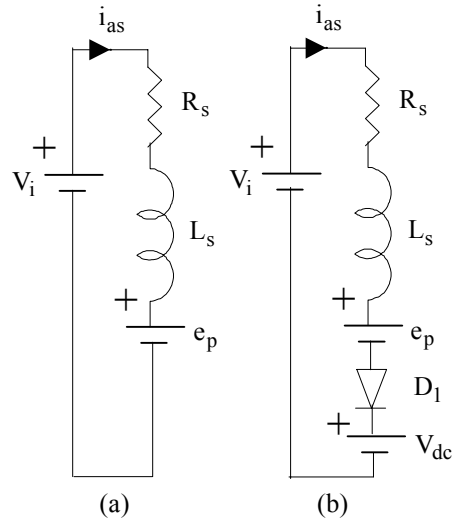


Figure 5.4 (a) : I Quadrant motoring operation with phase a of the PMBDC drive, switch T_1 on

Figure 5.4 (b) : I Quadrant motoring operation with phase a of the PMBDC drive, switch T_1 off with continuous current in phase a

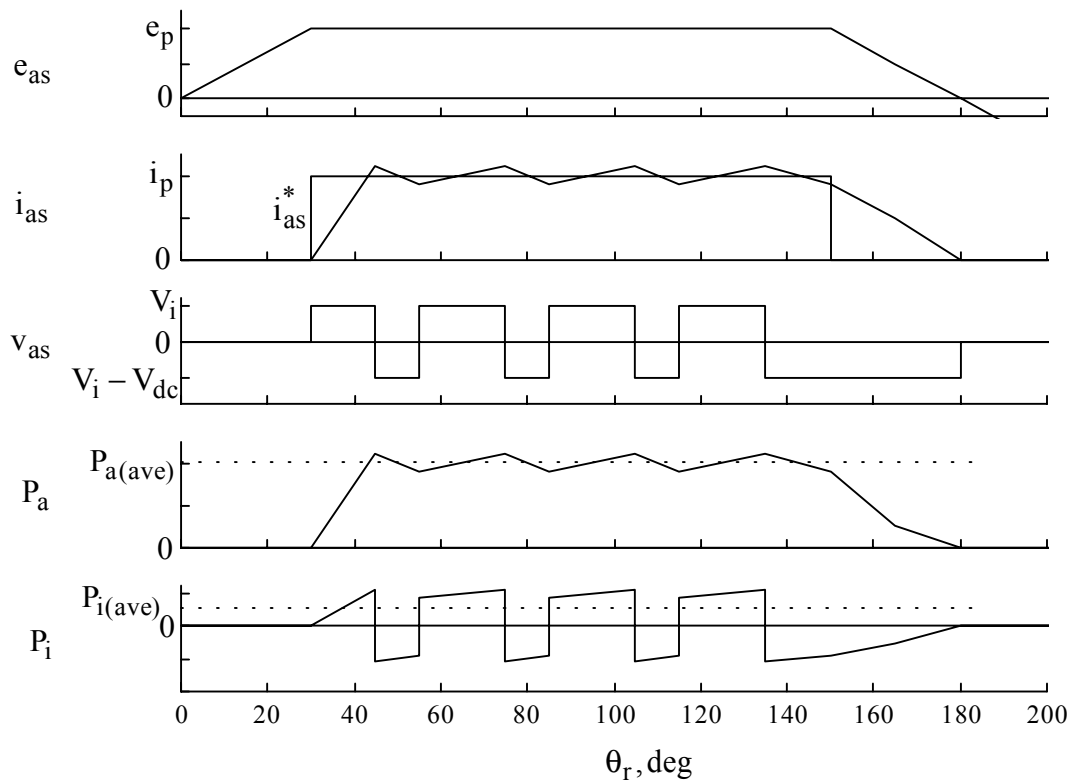


Figure 5.5 I Quadrant Motoring Operation: waveforms of the variables

Regenerating:

To transfer energy from the load to the supply, the PMBDC has to be operated as a generator, i.e., by providing negative torque to the machine. Negative torque is achieved by turning on T_1 during the negative constant emf period. The essential waveforms are shown in Figure 5.7 and the equivalent circuits during on time and off time of switch T_1 are shown in Figure 5.6(a) and Figure 5.6(b), respectively.

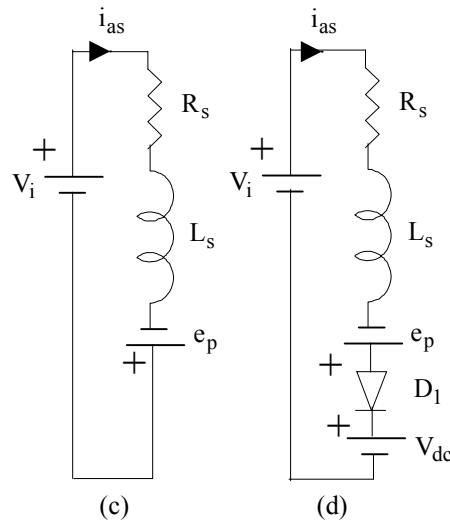


Figure 5.6 (a) : IV Quadrant regenerative operation with phase a of the PMBDC drive, switch T_1 on

Figure 5.6(b) : IV Quadrant regenerative operation with phase a of the PMBDC drive, switch T_1 off with continuous current in phase a

5.3 Design of Buck Converter Passive Components

The design of L and C in the buck converter is done by the procedure outlined in [KRI96]. The inductor rating is based on the ripple current rating that allows minimum energy storage to enable faster charging of the capacitor C. The maximum capacitor ripple is,

$$\Delta i_{C,max} = \frac{V_{dc}}{Lf_c} = I_p \tag{5.1}$$

If the peak current is limited to twice the rated current, the inductor L can be calculated as,

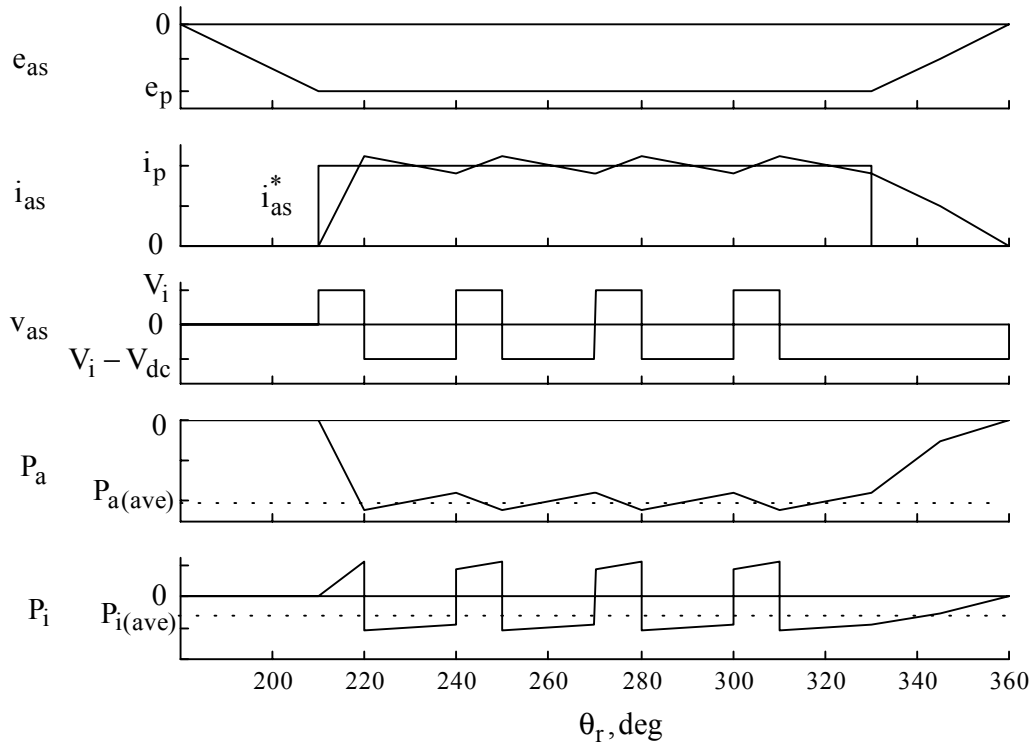


Figure 5.7 IV Quadrant Motoring Operation: waveforms of the variables

$$L = \frac{V_{dc}}{2f_c i_{a,rated}}, \text{H} \quad (5.2)$$

The capacitor C is designed so that the energy stored can be depleted in n cycles of PWM and transferred to the machine windings. Therefore,

$$\frac{1}{2} C V_i^2 = n \frac{V_i I_p}{f_c} \Rightarrow C = 2n \frac{2i_{a,rated}}{f_c V_i} \quad (5.3)$$

The minimum value of capacitance is obtained when $V_i = V_{dc}$. Therefore,

$$C = 2n \frac{2i_{a,rated}}{f_c V_{dc}} \quad (5.4)$$

5.4 Design of Current and Speed Controllers

The current and speed controllers are designed by the procedure outlined in [KRI99]. The design of the controllers can be primarily considered when a single phase is conducting at a time although there will be some portions when two phases are conducting at a time. It may not be necessary to design for the short periods of multi-phase conduction unlike the full-wave converters where two phases are always conducting at any given instant.

Assuming that phase a is under consideration, the voltage equation with this particular half-wave converter is written as,

$$V_i = R_s i_a + L_a \frac{di_a}{dt} + e_a = R_s i_a + L_a \frac{di_a}{dt} + K_b \omega_m \quad (5.5)$$

The electromagnetic torque can be calculated as,

$$T_e = K_t i_a \quad (5.6)$$

Assuming that the load is proportional to the speed, at rated speed and rated load torque,

$$B_\ell = \frac{T_e}{\omega_m} \quad (5.7)$$

The total inertia of the machine can be calculated as,

$$B_t = B + B_\ell \quad (5.8)$$

The last two blocks in the forward loop of the block diagram can be replaced by a single block as shown in Figure 5.9.

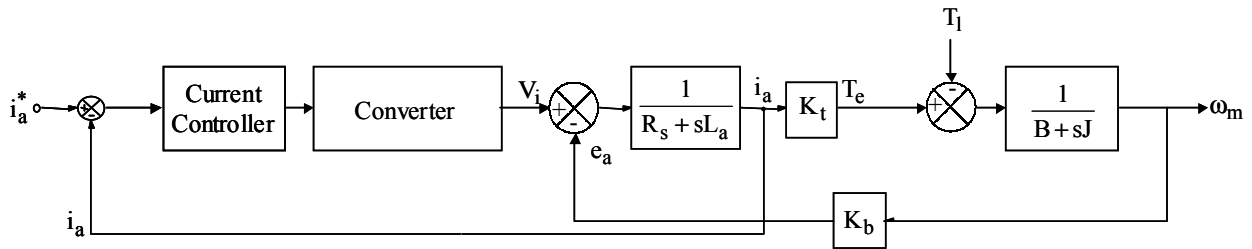


Figure 5.8 PMBDC and current control loop.

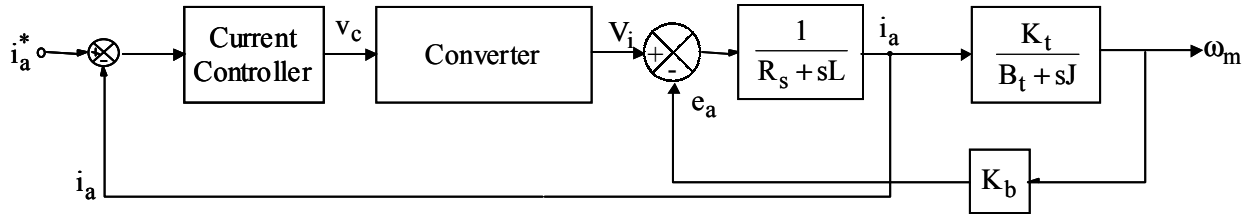


Figure 5.9 PMBDC and current control loop – Simplification 1

The machine transfer function is given by,

$$\begin{aligned} \frac{\omega_m(s)}{V_i(s)} &= \frac{K_t}{B_t + sJ} \frac{1}{1 + \frac{1}{\frac{R_s + sL_a}{K_b K_t}} \frac{1}{B_t + sJ}} = \frac{K_t}{B_t + sJ} \frac{1}{\frac{(R_s + sL_a)(B_t + sJ) + K_b K_t}{(R_s + sL_a)(B_t + sJ)}} \\ &= \frac{K_t}{(R_s + sL_a)(B_t + sJ) + K_b K_t} \end{aligned} \quad (5.9)$$

Defining the mechanical time constant of the machine and the electrical time constant of the machine respectively as,

$$T_m = \frac{J}{B_t}, \quad (5.10)$$

$$\tau = \frac{L_a}{R_s}, \quad (5.11)$$

equation (5.9) can be rewritten as,

$$\frac{\omega_m(s)}{V_i(s)} = \frac{K_t}{R_s B_t (1 + s\tau)(1 + sT_m) + K_b K_t} = \frac{\frac{K_t}{R_s B_t}}{(1 + s\tau)(1 + sT_m) + \frac{K_b K_t}{R_s B_t}} \quad (5.12)$$

To calculate the current loop transfer function and its response, it is necessary to calculate the transfer function,

$$\begin{aligned} \frac{i_a(s)}{V_i(s)} &= \frac{\frac{1}{R_s + sL_a}}{1 + \frac{1}{R_s + sL_a} \frac{K_b K_t}{B_t + sJ}} = \frac{\frac{1}{R_s + sL_a}}{\frac{(R_s + sL_a)(B_t + sJ) + K_b K_t}{(R_s + sL_a)(B_t + sJ)}} = \frac{(B_t + sJ)}{(R_s + sL_a)(B_t + sJ) + K_b K_t} \\ &= \frac{B_t \left(1 + s \frac{J}{B_t}\right)}{L_a J \left(s^2 + s \left(\frac{B_t}{J} + \frac{R_s}{L_a}\right) + \frac{R_s B_t}{L_a J} + \frac{K_b K_t}{L_a J}\right)} = \frac{(1 + sT_m)}{L_a T_m \left(s^2 + s \left(\frac{1}{T_m} + \frac{1}{\tau}\right) + \frac{1}{T_m \tau} + \frac{K_b K_t}{L_a J}\right)} \end{aligned} \quad (5.13)$$

Setting $b = \frac{1}{T_m} + \frac{1}{\tau}$ and $c = \frac{1}{T_m \tau} + \frac{K_b K_t}{L_a J}$, T_1 and T_2 are calculated as,

$$-T_1 = \frac{-b - \sqrt{b^2 - 4c}}{2} \quad (5.14)$$

$$-T_2 = \frac{-b + \sqrt{b^2 - 4c}}{2} \quad (5.15)$$

Therefore, (5.13) is rewritten as,

$$\frac{i_a(s)}{V_i(s)} = \frac{(1 + sT_m)}{L_a T_m (s + T_1)(s + T_2)} \quad (5.16)$$

The current control loop is shown in Figure 5.10.

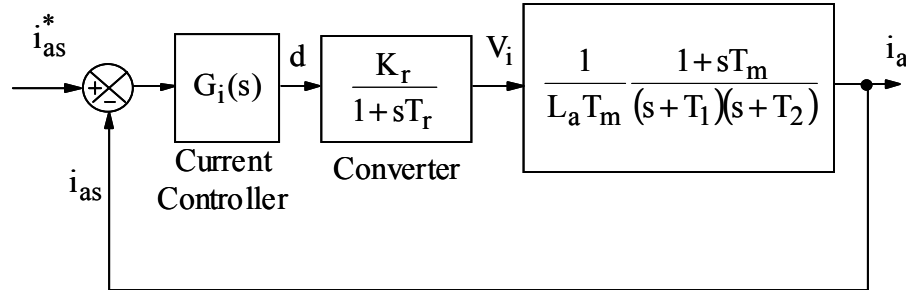


Figure 5.10 Current control loop.

The transfer function of the pulse width modulator is obtained as,

$$G_r(s) = \frac{d(s)}{V_i(s)} = \frac{K_r}{1 + sT_r} \quad (5.17)$$

where the gain K_r is given by $K_r = \frac{V_i}{V_{\text{ramp,max}} - V_{\text{ramp,min}}}$ and the delay T_r is given by

$$T_r = \frac{1}{2f_c}.$$

The current controller is of the proportional type. It is represented as,

$$G_i(s) = K_i \quad (5.18)$$

The closed loop transfer function of the current loop system is given by,

$$G_{ic}(s) = \frac{K_i \frac{K_r}{1+sT_r} \frac{(1+sT_m)}{L_a T_m (s+T_1)(s+T_2)}}{1 + K_i \frac{K_r}{1+sT_r} \frac{(1+sT_m)}{L_a T_m (s+T_1)(s+T_2)}} \quad (5.19)$$

The following approximations are made in the vicinity of the crossover frequency as,

$$1+sT_r \cong 1 \quad (5.20)$$

$$1+sT_m \cong sT_m \quad (5.21)$$

The current loop system is simplified as,

$$\begin{aligned} G_{ic}(s) &= \frac{K_i K_r \frac{s}{L_a (s+T_1)(s+T_2)}}{1 + K_i K_r \frac{s}{L_a (s+T_1)(s+T_2)}} = \frac{\frac{sK_i K_r}{L_a (s+T_1)(s+T_2)}}{\frac{L_a (s+T_1)(s+T_2) + sK_i K_r}{L_a (s+T_1)(s+T_2)}} \\ &= \frac{sK_i K_r}{L_a (s+T_1)(s+T_2) + sK_i K_r} = \frac{\frac{sK_i K_r}{L_a}}{s^2 + s\left((T_1+T_2) + \frac{K_i K_r}{L_a}\right) + T_1 T_2} \end{aligned} \quad (5.22)$$

If the value of K_i can be designed to have a bandwidth of about 1/20 times the switching frequency.

The speed control system is shown in Figure 5.11.

The speed controller is of the proportional type. It is represented as,

$$G_s(s) = K_s \quad (5.23)$$

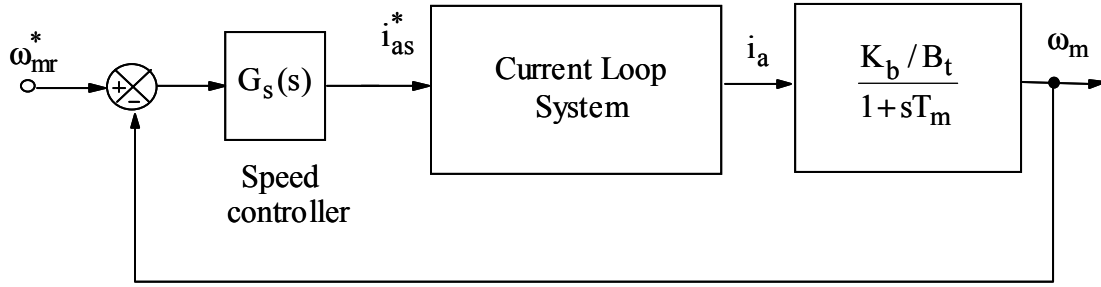


Figure 5.11 Speed control loop

The transfer function of the overall system is given by,

$$\frac{\omega_m}{\omega_m^*} = \frac{K_s \frac{sK_i K_r}{L_a} \frac{K_b}{B_t}}{s^2 + s \left((T_1 + T_2) + \frac{K_i K_r}{L_a} \right) + T_1 T_2} \frac{1}{1 + sT_m} \quad (5.24)$$

$$1 + K_s \frac{sK_i K_r}{L_a} \frac{K_b}{B_t} \frac{1}{s^2 + s \left((T_1 + T_2) + \frac{K_i K_r}{L_a} \right) + T_1 T_2} \frac{1}{1 + sT_m}$$

Using the assumption in (5.21),

$$\frac{\omega_m}{\omega_m^*} = \frac{\frac{sK_i K_r}{L_a} \frac{K_b}{B_t} K_s \frac{1}{sT_m}}{s^2 + s \left((T_1 + T_2) + \frac{K_i K_r}{L_a} \right) + T_1 T_2} \frac{1}{sT_m + \frac{sK_i K_r}{L_a} K_s \frac{K_b}{B_t}} \quad (5.25)$$

$$\frac{\omega_m}{\omega_m^*} = \frac{\frac{sK_i K_r}{L_a} \frac{K_b}{B_t} K_s}{\left(s^2 + s \left((T_1 + T_2) + \frac{K_i K_r}{L_a} \right) + T_1 T_2 \right) sT_m + \frac{sK_i K_r}{L_a} K_s \frac{K_b}{B_t}}$$

The value for K_s can be designed such that the speed loop bandwidth is about 10% of the current loop bandwidth. It should be remembered that the output of the speed controller is normally the

torque and the torque constant should be accounted for in the process of obtaining the current command.

Unlike the traditional inverter used in PMBDC motor drives, a buck converter is used in this configuration. From equation (5.5) the required input voltage to the machine V_i can be calculated from the actual speed of the machine. The buck converter circuit can be assumed to be a system that delivers the required input voltage to the machine windings and can be considered as an independent system. The converter can be modeled as follows. The equivalent circuit of the buck converter is shown in Figure 5.12.

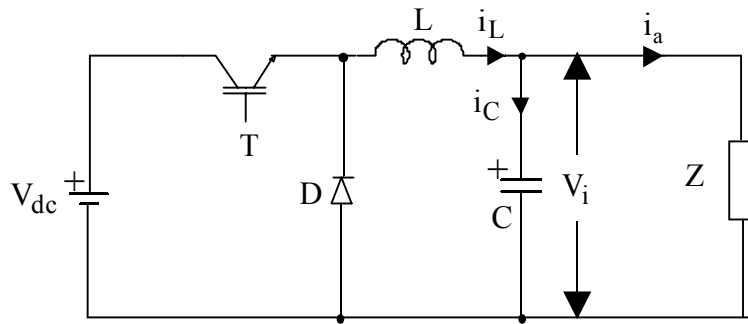


Figure 5.12 Equivalent Buck Converter Circuit

If the maximum allowed current in the machine is restricted to $i_{a,max}$, the equivalent load Z can be calculated in steady state as,

$$Z = \frac{R_s i_{a,max} + K_b \omega_m^* + C_L}{i_{a,max}} \quad (5.26)$$

The value C_L represents the product of rate of change of current and self inductance and is assumed to be a constant. Although the machine normally operates at the rated current, it may be wise to design for a maximum current since the current controllers are designed with the maximum value in mind.

When the main switch T is on, the state equations can be written as,

$$\begin{bmatrix} \frac{di_L}{dt} \\ \frac{dV_i}{dt} \end{bmatrix} = \begin{bmatrix} 0 & -\frac{1}{L} \\ \frac{1}{C} & -\frac{1}{ZC} \end{bmatrix} \begin{bmatrix} i_L \\ V_i \end{bmatrix} + \begin{bmatrix} \frac{1}{L} \\ 0 \end{bmatrix} V_{dc} = A_1 x + B_1 u \quad (5.27)$$

$$V_i = \begin{bmatrix} 0 & 1 \end{bmatrix} \begin{bmatrix} i_L \\ V_i \end{bmatrix} = C_1 x$$

When the main switch T is off, the state equations can be written as,

$$\begin{bmatrix} \frac{di_L}{dt} \\ \frac{dV_i}{dt} \end{bmatrix} = \begin{bmatrix} 0 & -\frac{1}{L} \\ \frac{1}{C} & -\frac{1}{ZC} \end{bmatrix} \begin{bmatrix} i_L \\ V_i \end{bmatrix} + \begin{bmatrix} 0 \\ 0 \end{bmatrix} V_{dc} = A_2 x + B_2 u \quad (5.28)$$

$$V_i = \begin{bmatrix} 0 & 1 \end{bmatrix} \begin{bmatrix} i_L \\ V_i \end{bmatrix} = C_2 x$$

If $d(s)$ is the transfer function of the input duty cycle, the converter transfer function can be obtained as [MOH89],

$$\frac{V_i(s)}{d(s)} = C[s\mathbf{I} - \mathbf{A}]^{-1} \cdot [(A_1 - A_2)x(s) + (B_1 - B_2)V_{dc}(s)] + (C_1 - C_2)x(s) \quad (5.29)$$

where $\mathbf{C} = d C_1 + (1 - d) C_2 = C_2$ and $\mathbf{A} = d A_1 + (1 - d) A_2 = A_2$.

Therefore the transfer function is calculated as,

$$\begin{aligned} G_b(s) = \frac{V_i(s)}{d(s)} &= \begin{bmatrix} 0 & 1 \end{bmatrix} \left[\begin{bmatrix} s & 0 \\ 0 & s \end{bmatrix} - \begin{bmatrix} 0 & -\frac{1}{L} \\ \frac{1}{C} & -\frac{1}{ZC} \end{bmatrix} \right]^{-1} \cdot \begin{bmatrix} V_{dc} \\ L \\ 0 \end{bmatrix} \\ &= \begin{bmatrix} 0 & 1 \end{bmatrix} \begin{bmatrix} \frac{(sZC+1)L}{s^2LZC+sL+Z} & -\frac{ZC}{s^2LZC+sL+Z} \\ \frac{ZL}{s^2LZC+sL+Z} & \frac{sZCL}{s^2LZC+sL+Z} \end{bmatrix} \cdot \begin{bmatrix} V_{dc} \\ L \\ 0 \end{bmatrix} \\ &= \begin{bmatrix} \frac{ZL}{s^2LZC+sL+Z} & \frac{sZCL}{s^2LZC+sL+Z} \end{bmatrix} \begin{bmatrix} V_{dc} \\ L \\ 0 \end{bmatrix} \\ &= \frac{Z}{(s^2LZC+sL+Z)} V_{dc} = \frac{1}{\left(s^2LC + s\frac{L}{Z} + 1\right)} V_{dc} \end{aligned} \quad (5.30)$$

The transfer function of the inductor current to the duty cycle can be obtained as,

$$\begin{aligned}
 G_{bi}(s) &= \frac{i_L(s)}{d(s)} = [1 \quad 0] \left[\begin{array}{c|c} \begin{bmatrix} s & 0 \\ 0 & s \end{bmatrix} & \begin{bmatrix} 0 & -\frac{1}{L} \\ \frac{1}{C} & -\frac{1}{ZC} \end{bmatrix} \\ \hline \begin{bmatrix} 0 & 0 \end{bmatrix} & \begin{bmatrix} 0 & -\frac{1}{L} \\ \frac{1}{C} & -\frac{1}{ZC} \end{bmatrix} \end{array} \right]^{-1} \cdot \begin{bmatrix} V_{dc} \\ L \\ 0 \end{bmatrix} \\
 &= [1 \quad 0] \begin{bmatrix} \frac{(sZC+1)L}{s^2LZC+sL+Z} & -\frac{ZC}{s^2LZC+sL+Z} \\ \frac{ZL}{s^2LZC+sL+Z} & \frac{sZCL}{s^2LZC+sL+Z} \end{bmatrix} \cdot \begin{bmatrix} V_{dc} \\ L \\ 0 \end{bmatrix} \\
 &= \begin{bmatrix} \frac{(sZC+1)L}{s^2LZC+sL+Z} & -\frac{ZC}{s^2LZC+sL+Z} \end{bmatrix} \begin{bmatrix} V_{dc} \\ L \\ 0 \end{bmatrix} = \frac{(sZC+1)}{s^2LZC+sL+Z} V_{dc}
 \end{aligned} \tag{5.31}$$

The transfer function of the pulse width modulator is obtained as,

$$G_{rb}(s) = \frac{d(s)}{V_i^*(s)} = \frac{K_{rb}}{1+sT_{rb}} \tag{5.32}$$

where the gain K_{rb} is given by $K_{rb} = \frac{1}{V_{ramp,max} - V_{ramp,min}}$ and the delay T_{rb} is given by

$$T_{rb} = \frac{1}{2f_{cb}}.$$

The current control system of the buck converter uses a proportional control and the current control loop is shown in Figure 5.13. The proportional gain of the current controller is designed such that the response is extremely fast.

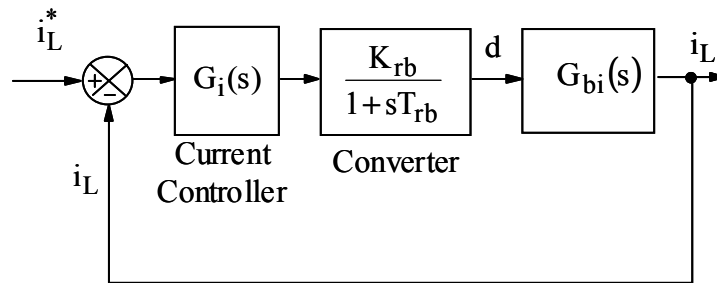


Figure 5.13 Current Loop of the buck converter system

The transfer function of the output voltage to the inductor current can be derived from (5.30) and (5.31) as,

$$\frac{V_i(s)}{i_L(s)} = \frac{V_i(s)}{d(s)} \frac{d(s)}{i_L(s)} = \frac{Z}{sZC+1} \quad (5.33)$$

The closed loop buck converter system is shown in Figure 5.14. The voltage controller is designed to be of a proportional type. The gain of the controller is set such that the output response has a minimal overshoot as well as fast response.

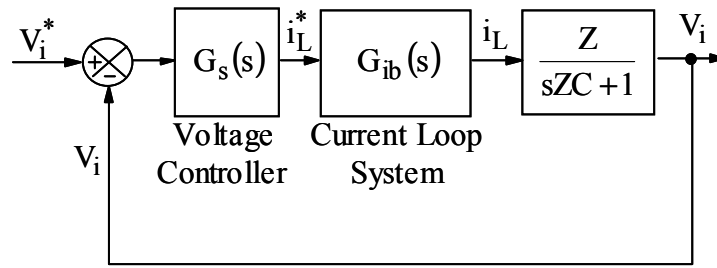


Figure 5.14 Closed Loop Buck Converter System

5.5 PMBDC Drive System Schematic

The PMBDC speed drive schematic is shown in Figure 5.15. For convenience, the torque drive without the outer speed loop is first discussed and the conversion from the torque drive to the speed drive is left to end of the section.

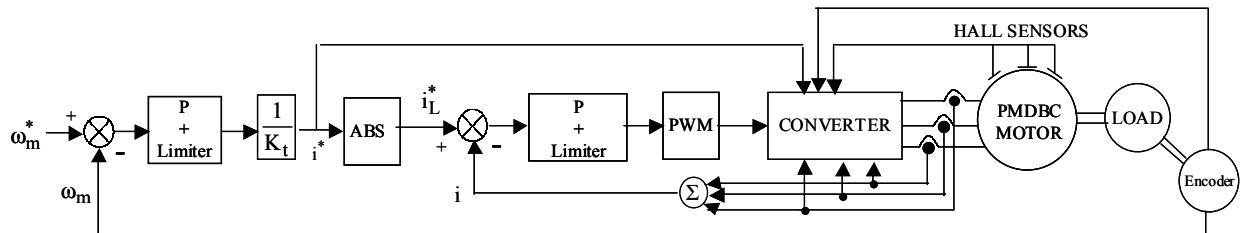


Figure 5.15 Schematic of the PMBDC Drive System

Let us assume a reference torque T_e^* is to be generated in the machine. In the torque drive, it is generally assumed that the speed is constant. The reference current can be calculated from the reference torque as,

$$i^* = \frac{T_e^*}{K_t} \quad (5.34)$$

Since the reference torque can be positive or negative, consequently, the reference current can also be positive or negative. Since the converter itself uses only unipolar current and the current polarity is normally used only to decide which phase has to be excited, the main reference current i_L^* can be written as,

$$i_L^* = |i^*| \quad (5.35)$$

The reference current is compared with the active phase currents to obtain the current error as,

$$i_{L,err} = i_L^* - i_x, x = a, b, c \text{ based on active phase} \quad (5.36)$$

The three phase functions are written as,

$$f_a = \begin{cases} \theta_r \frac{6}{\pi}, & 0 \leq \theta_r < \frac{\pi}{6} \\ 1, & \frac{\pi}{6} \leq \theta_r < \frac{5\pi}{6} \\ (\pi - \theta_r) \frac{6}{\pi}, & \frac{5\pi}{6} \leq \theta_r < \frac{7\pi}{6} \\ -1, & \frac{7\pi}{6} \leq \theta_r < \frac{11\pi}{6} \\ (-2\pi + \theta_r) \frac{6}{\pi}, & \frac{11\pi}{6} \leq \theta_r < 2\pi \end{cases} \quad (5.37)$$

$$f_b = \begin{cases} -1, & 0 \leq \theta_r < \frac{\pi}{2} \\ \left(-\frac{2\pi}{3} + \theta_r\right) \frac{6}{\pi}, & \frac{\pi}{2} \leq \theta_r < \frac{5\pi}{6} \\ 1, & \frac{5\pi}{6} \leq \theta_r < \frac{3\pi}{2} \\ \left(\frac{5\pi}{3} - \theta_r\right) \frac{6}{\pi}, & \frac{3\pi}{2} \leq \theta_r < \frac{11\pi}{6} \\ -1, & \frac{11\pi}{6} \leq \theta_r < 2\pi \end{cases} \quad (5.38)$$

$$f_c = \begin{cases} 1, & 0 \leq \theta_r < \frac{\pi}{6} \\ \left(\frac{\pi}{3} - \theta_r\right) \frac{6}{\pi}, & \frac{\pi}{6} \leq \theta_r < \frac{\pi}{2} \\ -1, & \frac{\pi}{2} \leq \theta_r < \frac{7\pi}{6} \\ \left(-\frac{4\pi}{3} + \theta_r\right) \frac{6}{\pi}, & \frac{7\pi}{6} \leq \theta_r < \frac{3\pi}{2} \\ 1, & \frac{3\pi}{2} \leq \theta_r < 2\pi \end{cases} \quad (5.39)$$

In the above three equations θ_r is the rotor position and it repeats every 2π radians. The three functions are plotted as shown in Figure 5.16.

The three phase back emfs are calculated as,

$$e_k = K_b \omega_m f_k, \quad k = a, b, c \quad (5.40)$$

where, K_b is the back emf constant and ω_m is the machine speed in rads/sec.

Based on the rotor position and the quadrant of operation, the equations to obtain phase a current is described below. The logic can be extended to the other phases. It should be noted that during the operation of each phase, the current in the phase has to be regulated. Although, the reduced input voltage will have the effect of limiting the current in the phase, nevertheless the presence of the capacitor C may lead to extremely high phase currents if not regulated properly.

The current error is passed through a PI controller with a gain of K_i to obtain the control voltage v_c that is limited to the maximum carrier ramp voltage used for comparison. The PWM carrier voltage is operating at a frequency of f_c with a minimum value of 0V and a maximum value of 2V. The control voltage is given as,

$$v_k = K_i \left(i_L^* - i_k \right) \quad k = a, b, c \quad (5.41)$$

Obviously the control voltages are limited to maximum and minimum values of the ramp voltage $V_{\text{switch_ramp}}$. For phase a, if the operation is in the I quadrant, i.e., $i^* \geq 0$ and $\omega_m \geq 0$, and

$$\frac{\pi}{6} \leq \theta_r \leq \frac{5\pi}{6},$$

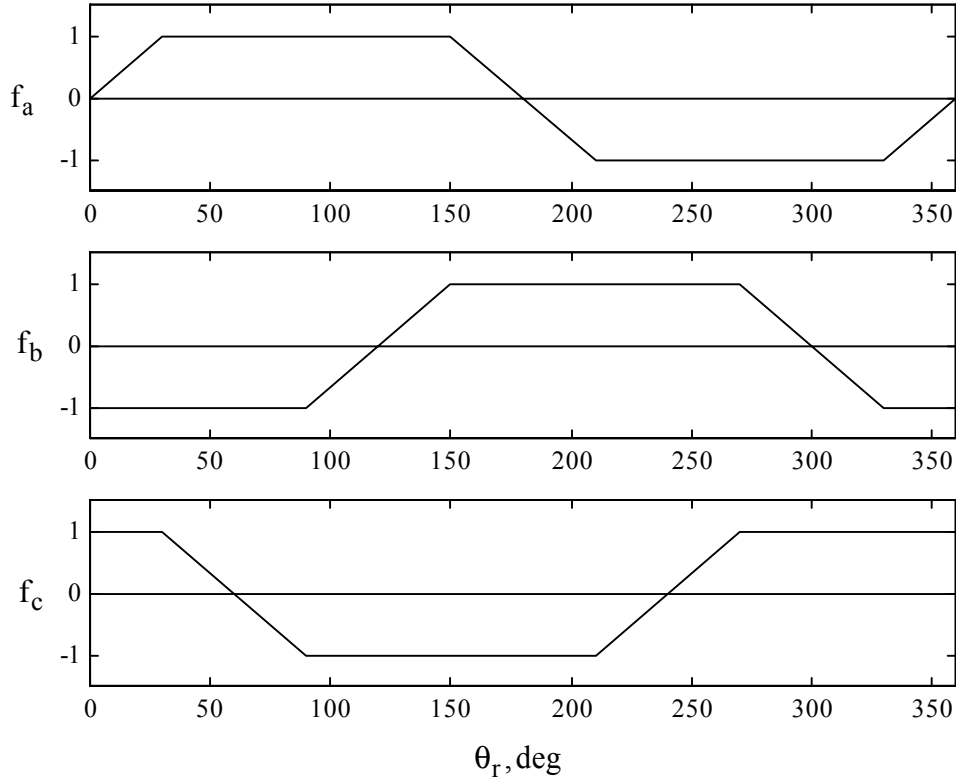


Figure 5.16 Plot of the back emf functions

$$\text{If } v_k \geq V_{\text{switch_ramp}}, V_a = V_i \quad (5.42)$$

$$\text{If } v_k < V_{\text{switch_ramp}}, V_a = V_i - V_{\text{dc}}$$

If the rotor position is $\frac{5\pi}{6} \leq \theta_r \leq \frac{7\pi}{6}$, and $i_a > 0$, the phase switch is completely turned off and the applied voltage is $V_a = V_i - V_{\text{dc}}$ as long as the current is flowing in the windings and when the phase current reaches zero, the applied voltage is assumed to be $V_a = 0$.

The equation of the phase current a is given by,

$$L_a \frac{di_a}{dt} + M \left(\frac{di_b}{dt} + \frac{di_c}{dt} \right) = V_a - e_a - R_s i_a \quad (5.43)$$

The above equation can be rewritten as,

$$di_a = \frac{(V_a - e_a - R_s i_a) dt - M(di_b + di_c)}{L_a} \quad (5.44)$$

Using the Euler's method of integration, the new phase current is calculated as,

$$i_a = i_a + di_a \quad (5.45)$$

The other phase currents can be calculated similarly in the appropriate regions. A scrutiny of the phase functions will indicate the operational requirements in the other quadrants.

The torque developed in the machine is given by,

$$T_e = K_t (f_a i_a + f_b i_b + f_c i_c) \quad (5.46)$$

where K_t is the torque constant.

In a speed controlled PMBDC, the speed equation can be written as,

$$J \frac{d\omega_m}{dt} = T_e - T_l - B\omega_m \Rightarrow d\omega_m = \frac{(T_e - T_l - B\omega_m) dt}{J} \quad (5.47)$$

where T_l is the load torque, J is the inertia and B is the friction coefficient. The rotor speed can be calculated using Euler's integration method as,

$$\omega_m = \omega_m + d\omega_m \quad (5.48)$$

Closing the outer speed loop regulates the speed. The reference speed ω_m^* is compared to the actual speed ω_m and the speed error is obtained as,

$$\omega_{m, \text{err}} = \omega_m^* - \omega_m \quad (5.49)$$

The speed error is passed through a P controller with gains of K_s to obtain the reference torque T_e^* . The reference torque is limited to a maximum positive and negative value.

$$T_e^* = K_s \omega_{m, \text{err}} \quad (5.50)$$

From the reference torque the reference current is calculated as described in equation (5.34) and hence the loop is closed.

In equation (5.42), it is assumed that the voltage V_i is available. This voltage is generated as follows. The reference voltage V_i^* is obtained from

$$V_i^* = R_s i_L^* + K_b \omega_m^* + C_L \quad (5.51)$$

The constant value C_L is used to compensate for the $L \frac{di}{dt}$ factor instead of actually calculating the value. The reference voltage is compared with the actual input voltage and the error is passed through a proportional controller with a limiter. The upper value of the limiter is restricted to the current reference value obtained in (5.35). The output of the limiter is the inductor reference current. This is compared with the actual inductor current and the error is passed through a proportional controller with a limiter that limits the value to the maximum and minimum value of the PWM ramp. The control voltage v_{cb} is calculated as,

$$v_{cb} = \frac{1}{V_{ramp,max} - V_{ramp,min}} \quad (5.52)$$

This control voltage is compared to the PWM ramp to obtain the on and off period of the main switch.

The control voltage is limited as follows,

$$\begin{aligned} v_{cb} &= V_{ramp,max}, \text{ if } v_{cb} > V_{ramp,max} \\ v_{cb} &= V_{ramp,min}, \text{ if } v_{cb} < V_{ramp,min} \end{aligned} \quad (5.53)$$

The main switch is controlled by the following logic,

$$\begin{aligned} \text{If } v_{cb} \geq V_{ramp}, & \text{ T is turned on} \\ \text{If } v_{cb} < V_{ramp}, & \text{ T is turned off} \end{aligned} \quad (5.54)$$

When the buck converter switch T is on, the input voltage to the machine phases can be written as,

$$V_i = \frac{1}{C} \int i_C dt \quad (5.55)$$

where i_C is the capacitor current.

The above equation can be rewritten as,

$$\frac{dV_i}{dt} = \frac{i_C}{C} \Rightarrow dV_i = \frac{i_C}{C} dt = \frac{i_L - (i_a + i_b + i_c)}{C} dt \quad (5.56)$$

where i_L is the inductor current.

The equation for the inductor current can be written as,

$$V_{dc} = L \frac{di_L}{dt} + V_i \quad (5.57)$$

The above equation can be rewritten as,

$$\frac{di_L}{dt} = \frac{V_{dc} - V_i}{L} \Rightarrow di_L = \frac{V_{dc} - V_i}{L} dt \quad (5.58)$$

Equations (5.56) and (5.58) are the equations used in the simulation when the switch T is on.

When the switch T is off, equation (5.58) is replaced by the following equation,

$$di_L = \frac{-V_i}{L} dt \quad (5.59)$$

Using the Euler's method of integration, the new input voltage is obtained as,

$$V_i = V_i + dV_i, \quad (5.60)$$

and the new inductor current is obtained as,

$$i_L = i_L + di_L. \quad (5.61)$$

The voltage V_i that is obtained in (5.60) is used in the simulation of the phases in equation (5.42).

5.6 Design of a prototype PMBDC Machine Drive

The test machine has the following parameters:

Power Output $P_o = 1$ h.p., Speed $N = 1500$ r.p.m., Maximum DC link voltage = 130 V, Rated Current = 7.61 A, Number of poles $P = 4$, Stator resistance $R_s = 0.41 \Omega$, Self inductance $L = 5.5$ mH, Mutual inductance = 1.5 mH, Back emf constant = 0.275 volt/rad/sec, Torque constant = 0.624 N.m/A, $J = 0.03$ kg-m/s², $B = 0.07$ N.m/rad/sec, PWM switching frequency of the main switch = 20 kHz.

If the peak ripple current is limited to 10% of the rated current, the inductor L can be calculated as,

$$L = \frac{V_{dc}}{2f_c i_{a,rip}} = \frac{130}{2 * 20000 * 0.1 * 7.61} = 4.27 \text{mH} \approx 4 \text{mH}.$$

Assuming that the stored energy can be depleted in $n = 30$ cycles, the capacitor C is designed as,

$$C = 2n \frac{2i_{a,max}}{f_c V_{dc}} = 2 \cdot 30 \frac{2 \cdot 10}{20000 \cdot 130} = 461.5 \mu\text{F} \approx 450 \mu\text{F}.$$

The rated torque is calculated as,

$$T_e = i_a K_t = 7.61 \cdot 0.624 = 4.749 \text{ N-m}.$$

Assuming that the load is proportional to the speed, at rated speed and rated load torque,

$$B_\ell = \frac{T_e}{\omega_m} = \frac{4.749}{\frac{2\pi \cdot 1500}{60}} = 0.03$$

The total inertia of the machine can be calculated as,

$$B_t = B + B_\ell = 0.07 + 0.03 = 0.1 \text{ N-m/rad/sec}$$

$$T_m = \frac{J}{B_t} = \frac{0.03}{0.1} = 0.3 \text{ s}.$$

$$\tau = \frac{L_a}{R_s} = \frac{5.5 \times 10^{-3}}{0.41} = 0.0134 \text{ s}.,$$

Setting

$$b = \frac{1}{T_m} + \frac{1}{\tau} = \frac{1}{0.3} + \frac{1}{0.0134} = 77.96$$

and

$$c = \frac{1}{T_m \tau} + \frac{K_b K_t}{L_a J} = \frac{1}{0.3 * 0.0134} + \frac{0.275 * 0.624}{5.5 * 10^{-3} * 0.03} = 1288.76$$

T_1 and T_2 are calculated as,

$$-T_1 = \frac{-b - \sqrt{b^2 - 4c}}{2} = \frac{-77.96 - \sqrt{77.96^2 - 4 * 1288.76}}{2} = -54.168$$

$$-T_2 = \frac{-b + \sqrt{b^2 - 4c}}{2} = \frac{-77.96 + \sqrt{77.96^2 - 4 * 1288.76}}{2} = -23.79$$

Assuming operation at rated speed and load, the input voltage is calculated as,

$$V_i = R_s i_{\text{rated}} + K_b \omega_m + C_L = 0.41 * 7.61 + 0.275 * \frac{2\pi * 1500}{60} + 5 = 51.32V.$$

The gain of the converter can be calculated from

$$K_r = \frac{V_i}{V_{\text{ramp,max}} - V_{\text{ramp,min}}} = \frac{51.32}{2 - 0} = 25.65$$

The current control loop transfer function is written as,

$$G_{ic}(s) = \frac{\frac{sK_i K_r}{L_a}}{s^2 + s \left((T_1 + T_2) + \frac{K_i K_r}{L_a} \right) + T_1 T_2}$$

Selecting the current controller proportional gain $K_i = 2$, the frequency response of the current controlled system is shown in Figure 5.17. The bandwidth of the simplified system is approximately 9320 rads/sec and the bandwidth of the full system without simplifications is about 11000 rads/sec. This is far greater than the required bandwidth of 6283 rads/sec (1/20 times the switching frequency).

The speed controlled system has a transfer function of,

$$\frac{\omega_m}{\omega_m^*} = \frac{\frac{sK_i K_r}{L_a} \frac{K_b}{B_t} K_s}{\left(s^2 + s \left((T_1 + T_2) + \frac{K_i K_r}{L_a} \right) + T_1 T_2 \right) s T_m + \frac{sK_i K_r}{L_a} K_s \frac{K_b}{B_t}}$$

Selecting the speed controller proportional gain $K_s = 100$, the frequency response of the speed controlled system is shown in Figure 5.18. The bandwidth of the system is approximately 740 rads/sec. This is greater than the required bandwidth of 628.3 rads/sec (10% of current loop bandwidth). It can also be seen that the frequency response of the simplified system described above and the frequency response of the overall system with no simplifications show minor differences thereby making the assumptions made in the design valid. Figure 5.19 shows the step

response of the system with no simplifications. The step response shows no overshoot and a fairly quick settling time.

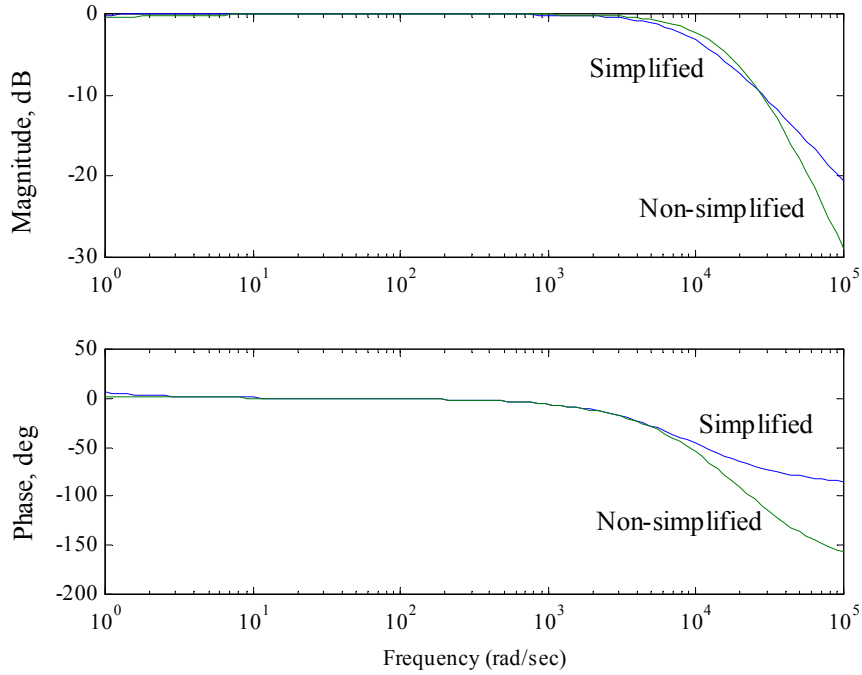


Figure 5.17 Frequency response of the current controlled system

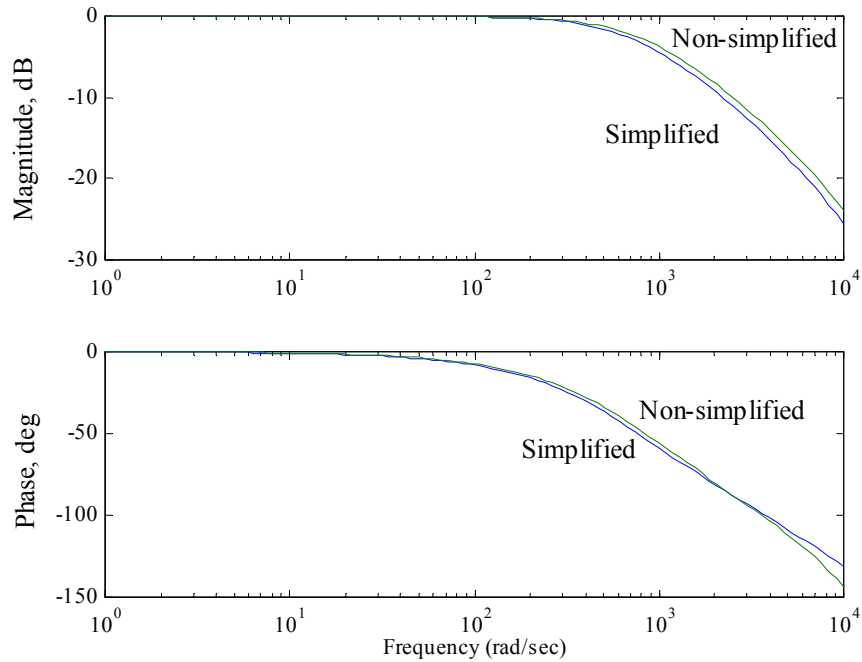


Figure 5.18 Frequency response of the speed controlled system

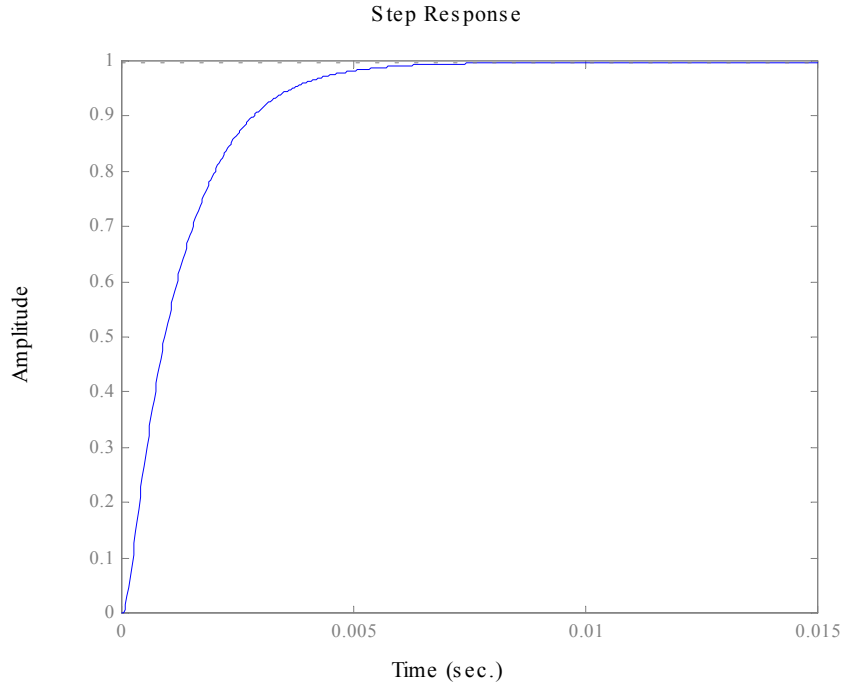


Figure 5.19 Step response of the speed controlled system with no simplifications

The equivalent load impedance of the buck converter can be calculated as,

$$Z = \frac{R_s i_{a,\max} + K_b \omega_m^* + C_L}{i_{a,\max}} = \frac{0.41 * 7.61 + 0.275 * \frac{2\pi * 1500}{60} + 10}{7.61} = 7.4\Omega.$$

The transfer function from the inductor current to the duty cycle is given by,

$$G_{bi}(s) = \frac{i_L(s)}{d(s)} = \frac{(sZC+1)}{s^2LZC+sL+Z} V_{dc} = \frac{(7.4 * 450 * 10^{-6} s + 1)}{s^2 4 * 10^{-3} * 7.4 * 450 * 10^{-6} + 4 * 10^{-3} s + 7.4} 130$$

$$= \frac{(0.4329s + 130)}{1.3221 * 10^{-5} s^2 + 4 * 10^{-3} s + 7.4}$$

The closed loop current control loop with a proportional gain of the controller as 1 is calculated as,

$$\frac{i_L}{i_L^*} = \frac{(0.4329s + 130)}{3.33 * 10^{-10} s^3 + 1.342 * 10^{-5} s^2 + 0.4371s + 137.4}$$

The step response of the closed loop system is shown in Figure 5.20. The response shows an overshoot which is acceptable since the peak value is lesser than the absolute maximum value of 10A.

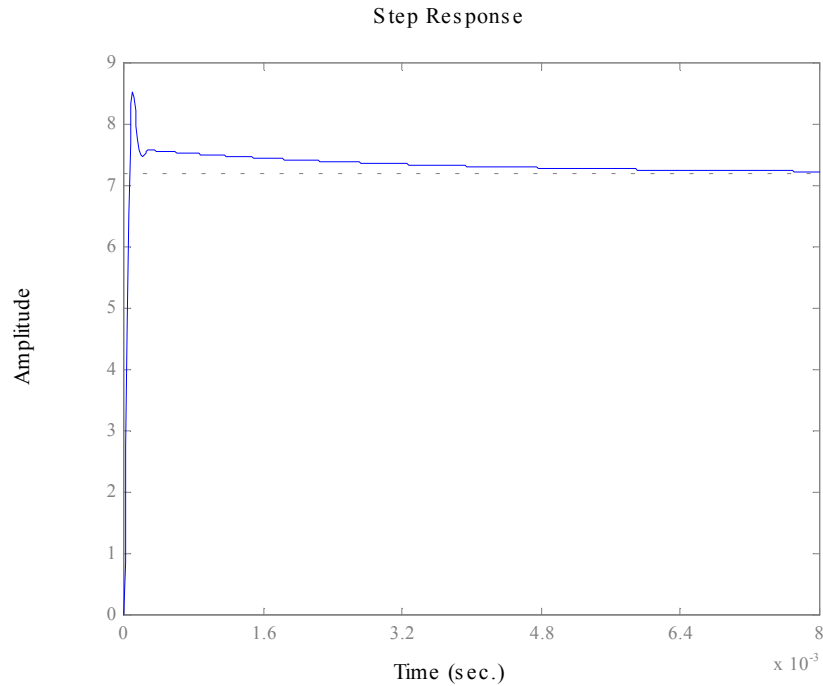


Figure 5.20 Closed loop response of the current controlled buck converter system

The closed loop voltage control system with a proportional gain of 5 is given by,

$$\frac{V_i}{V_i^*} = \frac{(16.02s + 4810)}{1.109 * 10^{-12} s^4 + 4.503 * 10^{-8} s^3 + 0.001469s^2 + 16.91s + 4948}$$

The closed loop step response is shown in Figure 5.21. The system shows very small overshoot and a fairly small settling time. The response is acceptable for the system.

5.7 Drive System Simulation

Figure 5.22 shows the simulation of a speed drive. The machine is commanded to 1 p.u. speed as a ramp. The maximum torque is limited to 1.314 p.u.. The input voltage is seen to have minor oscillations. The sequence of operation is seen to be as abc signifying positive direction. The torque and the current drop to lower values once the machine speed is close to the reference speed to supply the load torque.

Figure 5.23 shows the simulation of a speed drive. The machine is initially commanded to 1 p.u. speed and at 0.3 s is commanded to -1 p.u. speed. The maximum torque is limited to 1.314 p.u..

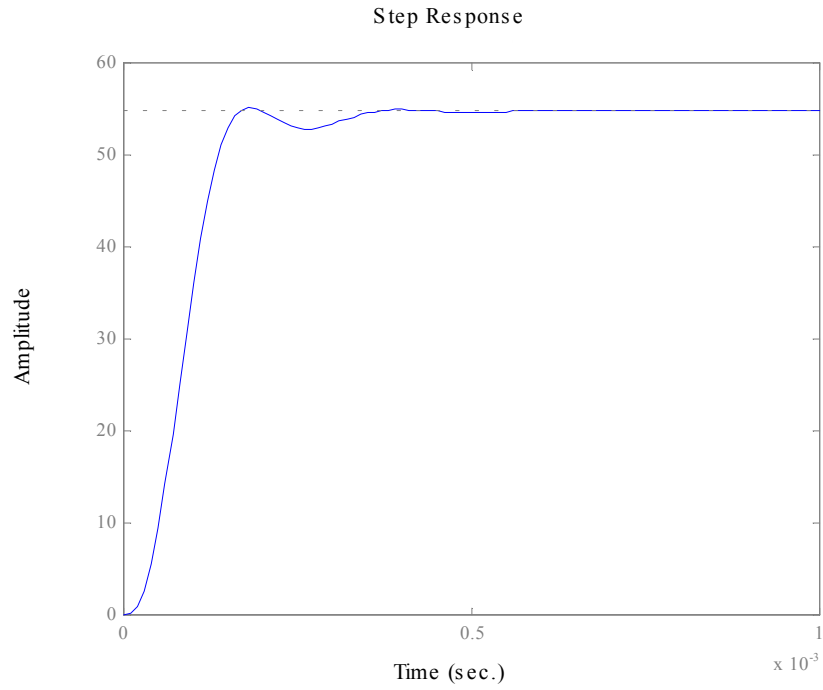


Figure 5.21 Closed loop response of the voltage controlled buck converter system

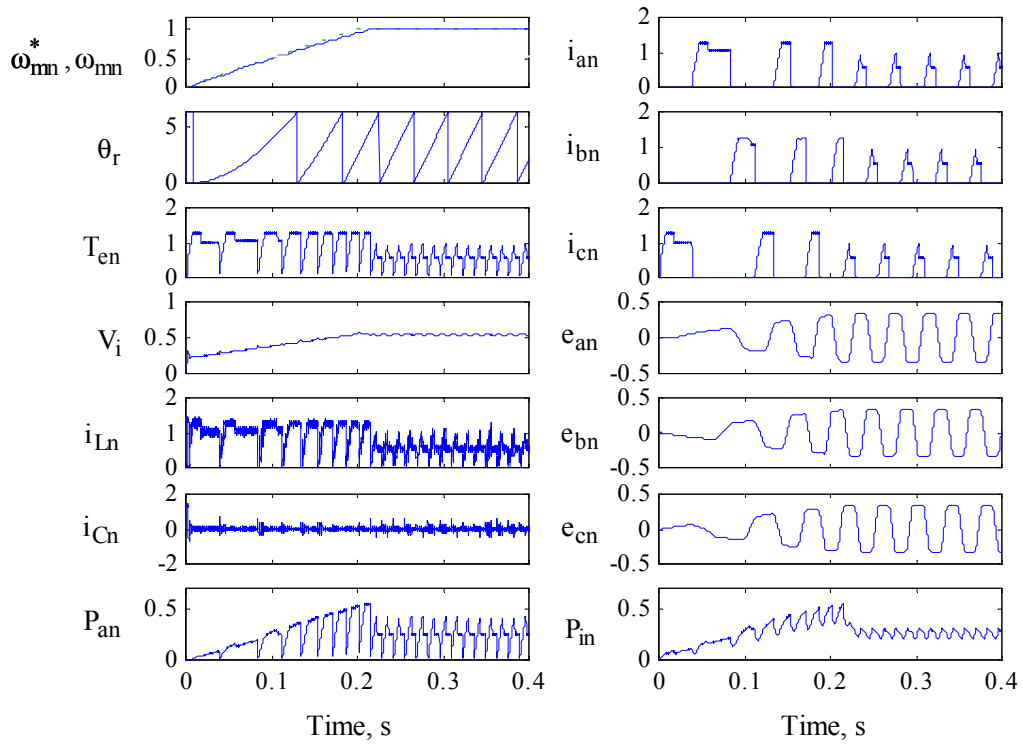


Figure 5.22 Simulation of a speed drive

During the reversal of direction it can be clearly seen that the sequence of excitation changes from abc to acb. The current as described before is unidirectional but positive and negative rotation as well as positive and negative torques are obtained. During quadrants I and III, the air gap power and input power are positive signifying that the machine is operating in the motoring mode but during the quadrant IV operation, the power is negative signifying regeneration. The simulations show the speed command as a ramp similar to the real system. Step changes was attempted but showed high inductor currents as well as phase currents which activated the over current protection circuits of the real system thereby shutting down the system.

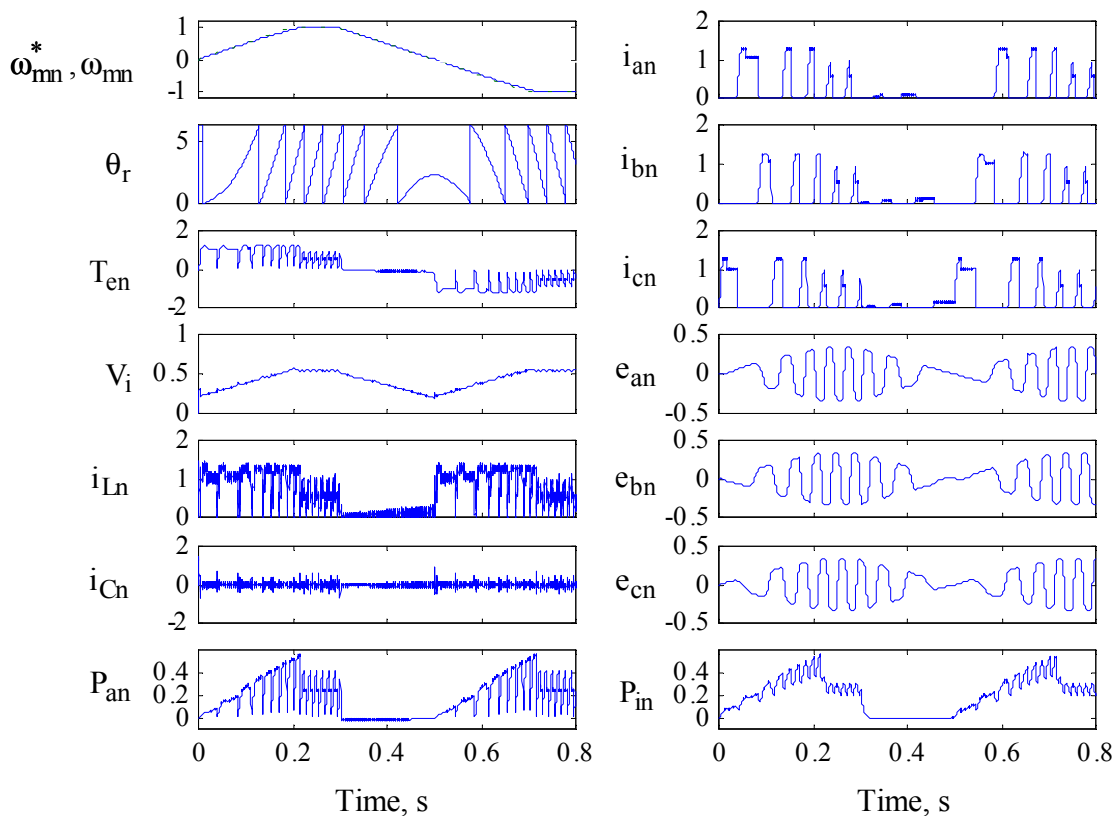


Figure 5.23 Simulation of a four quadrant speed drive

Figure 5.24 shows the simulation of the speed drive with higher values of moment of inertia and friction similar to the experimental prototype system. The simulation shows a delay in the rise of the actual speed when compared with the rise of the reference speed. The previous simulations assume lower values of moment of inertia and friction to show the operation in various quadrants.

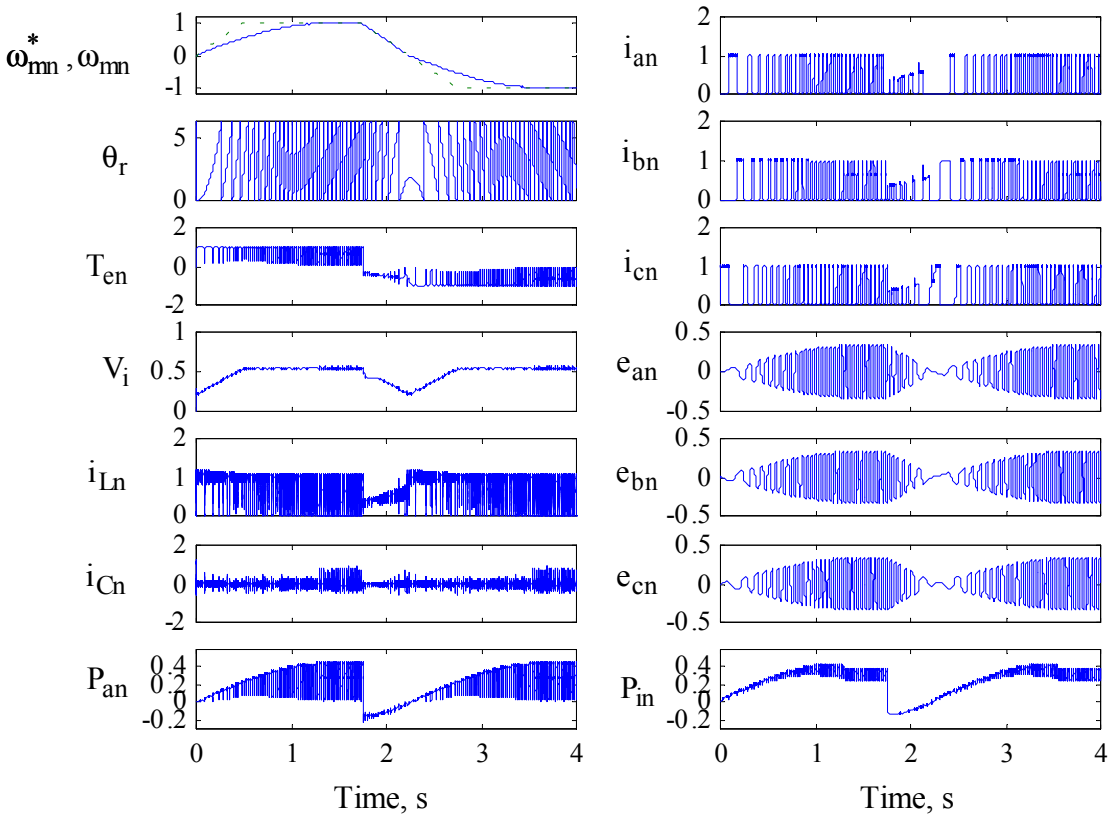


Figure 5.24 Simulation of a prototype speed drive

5.8 Experimental Results

The buck converter described above was built and verified. The waveforms of the various variables are shown below. Figure 5.26 shows the plot of reference speed and actual speed. The reference speed rises to 1500 r.p.m. After it reaches that commanded speed, it is commanded to a speed of -1500 r.p.m. The initial reference speed takes about 2 seconds to reach the rated value. The actual speed is seen to reach the commanded value in about 3.8 seconds. This discrepancy is present due to the larger than anticipated friction and moment of inertia of the machine. Also the limits placed on the reference input voltage slow down the response of the actual system. It must be noted that since these values are captured from the DACs of the DSP, 0 r.p.m. is represented by 2.5V. Also the code in the DSP was written to accept only absolute value of the command and the reverse direction was obtained by changing the firing sequence of the switches. Hence it appears as if the speed reaches zero and goes back to positive maximum speed when in fact, there is a reversal in rotation. The speed reference and actual speed variables from Figure 5.24

are plotted again in Figure 5.25 with absolute values to provide a comparison with experimental values.

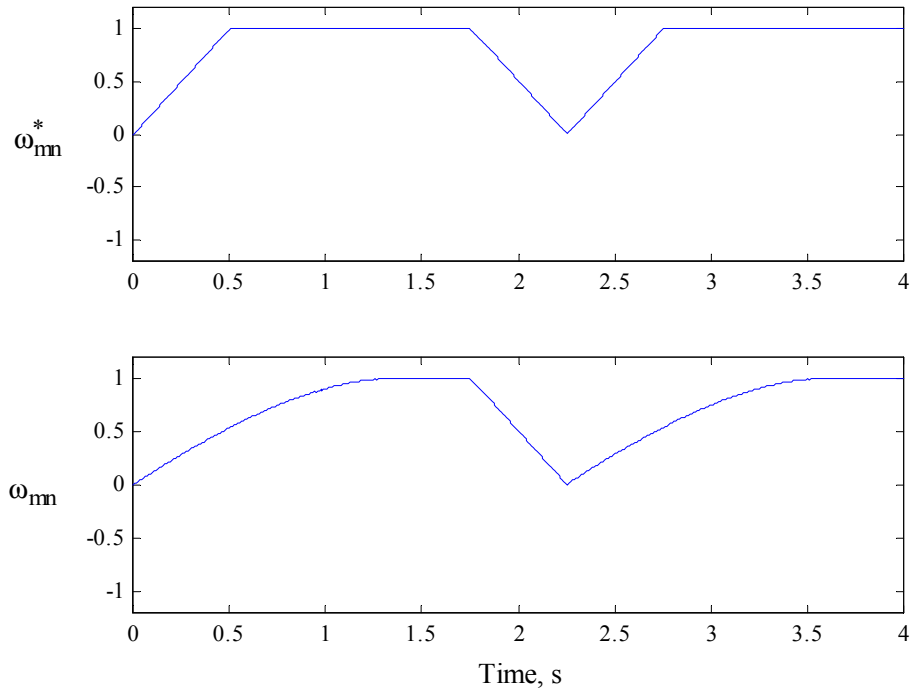


Figure 5.25 Simulation plot of speed reference and actual speed with absolute values to compare with experimental results

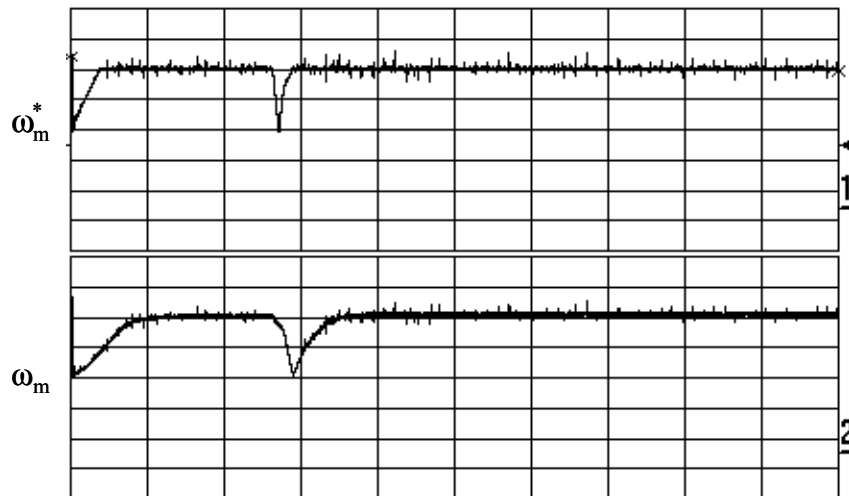


Figure 5.26 Plot of reference speed and actual speed
(1 vertical division = 721.15 r.p.m. , 1 horizontal division = 2 secs.)

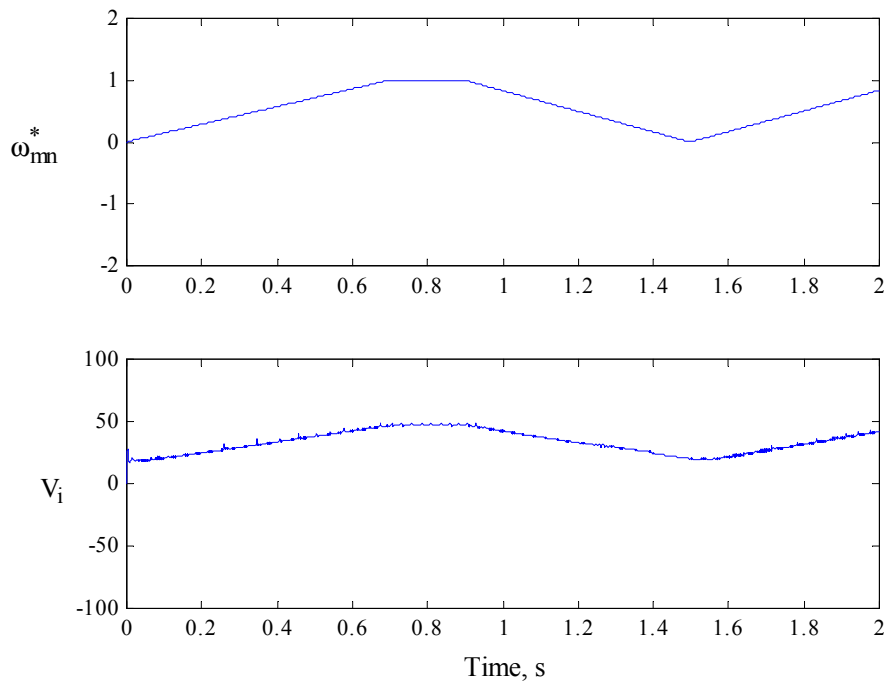


Figure 5.27 Simulation plots of speed reference and buck converter output voltage

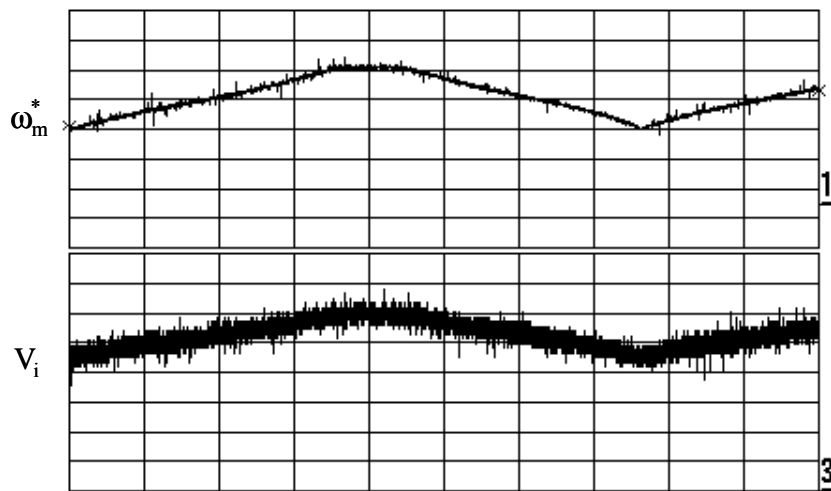


Figure 5.28 Plot of reference speed and output voltage of the buck converter

(Speed: 1 division = 721.15 r.p.m, Voltage: 1 division is 25V, one horizontal division is 0.2 secs)

Figure 5.28 shows the plot of reference speed and output voltage of the converter V_i . The

converter has a fixed minimum voltage of 10V to account for the $L \frac{di}{dt}$ factor described

previously. The input voltage rises with speed and stabilizes at a fixed level and when the speed

drops, it also falls and then rises again as the speed increases as the voltage is dependent on speed. This can be cross verified with the simulations shown in Figure 5.27.

Figure 5.30 shows the three gate drive signals to the various phases. The sequence can be clearly seen to be abc indicating positive direction rotation. It must be noted that due to the restrictions of the DSP, phases a and b are active low signals while phase c is seen to be an active high signal. Figure 5.32 shows the plot of the gate drive signals in the negative direction clearly showing an acb sequence. The signals can be compared to the gate drive signals obtained from the simulation in Figure 5.24 as shown in Figure 5.29 and Figure 5.31. The only difference is that in the simulation, all the signals are active high whereas in the experimental setup, phases A and B are active low and phase C is active high.

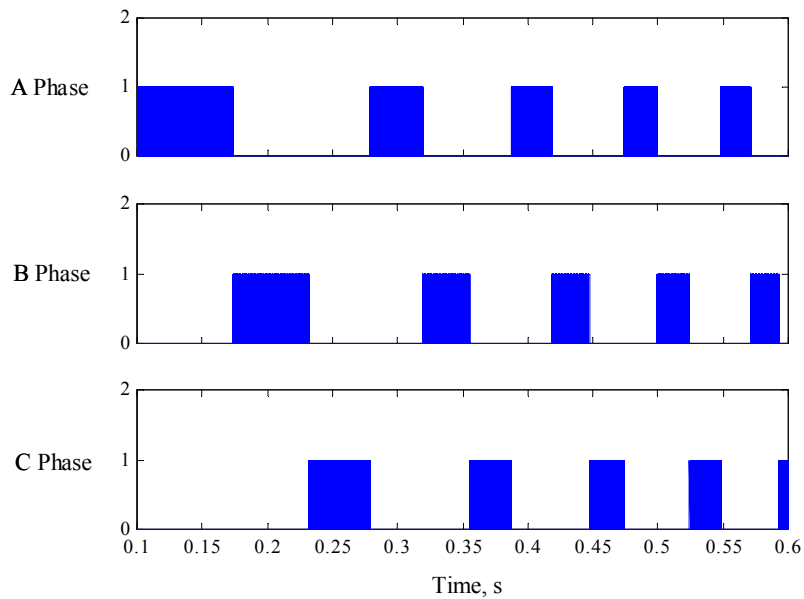


Figure 5.29 Gate drive signals from the simulation in Figure 5.24 in the positive direction

Figure 5.33 shows the expanded scale of the currents from the simulation plots shown in Figure 5.24. Figure 5.34 shows the currents in the various phases when the machine is loaded to the rated value experimentally. The limits on the DSP were set to restrict the maximum reference inductor current to 8 A. The phase currents are seen to closely follow the reference current. The experimental results are seen to closely follow the simulation results.

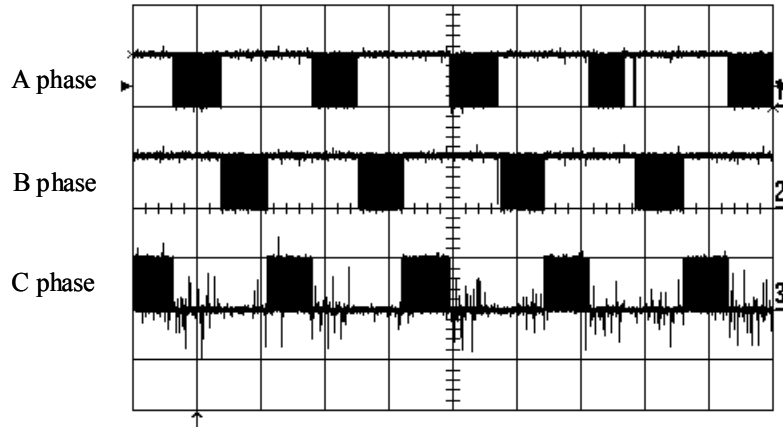


Figure 5.30 Plot of the three phase gate drive signals in the positive direction (A and B phases are active low signals and C phase is active high)

(1 horizontal division is 10 ms, 1 vertical division is 5V)

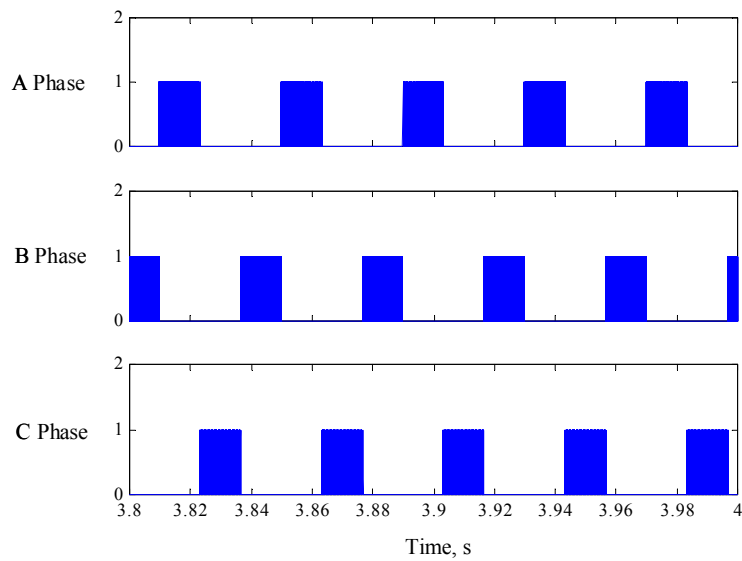


Figure 5.31 Gate drive signals from the simulation in Figure 5.24 in the negative direction

5.9 Merits and Demerits of the Proposed Converter

The merits of the proposed topology are listed below:

1. Only four switches and diodes are required for four-quadrant operation.
2. Reduced gating driver circuits and logic power supplies.

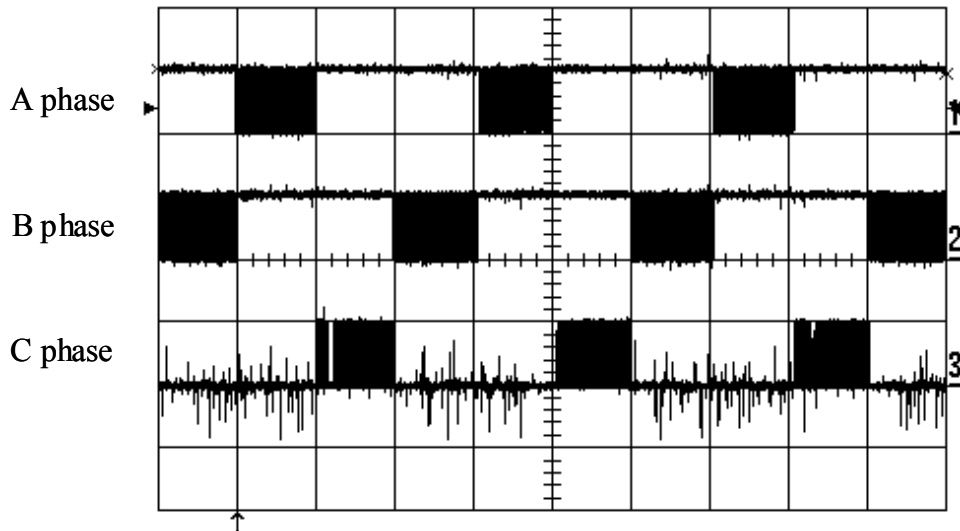


Figure 5.32 Plot of the three phase gate drive signals in the negative direction
(1 horizontal division is 10 ms, 1 vertical division is 5V)

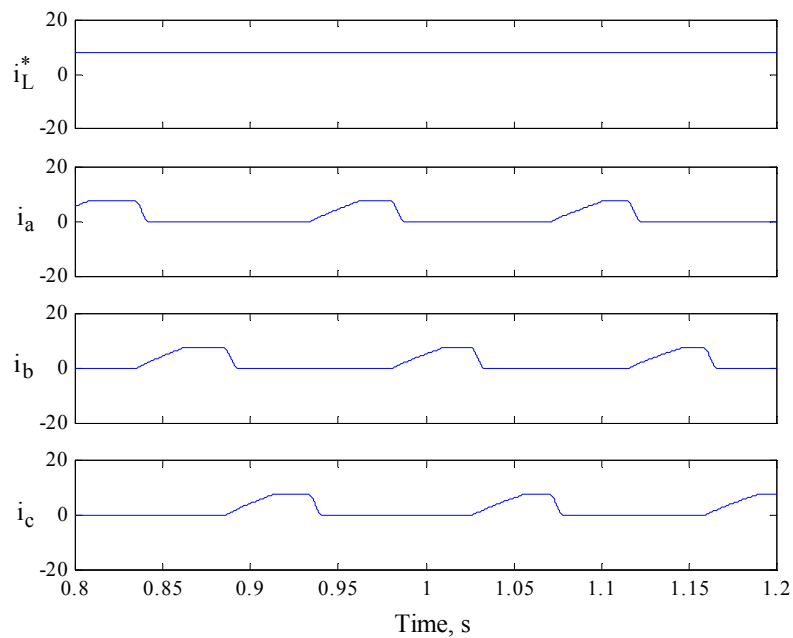


Figure 5.33 Expanded phase current simulation results expanded from Figure 5.24

3. Full 4-quadrant operational capability
4. Reduced possibility of shoot-through fault, as switch is in series with the machine phase winding
5. Possible to operate with one switch failure or one phase winding failure.

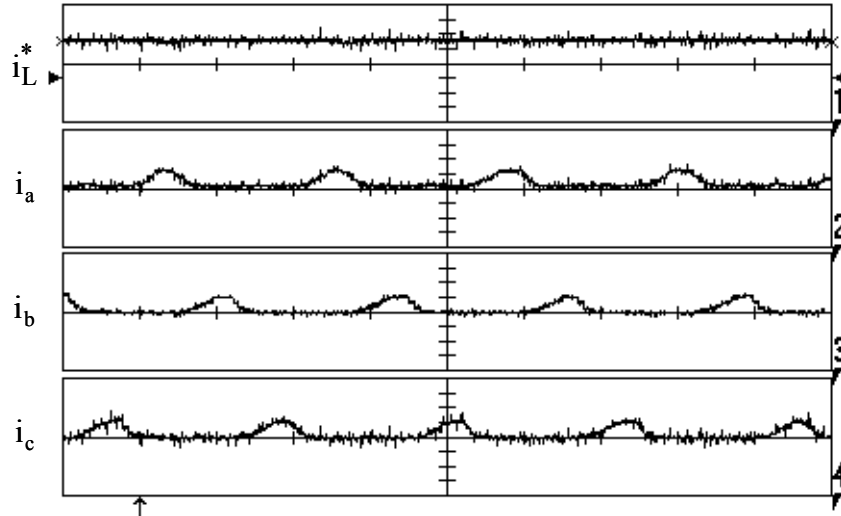


Figure 5.34 Plot of the reference and actual phase currents (1 vertical division = 5A, 1 horizontal division is 10ms)

6. Lower switch losses

7. Machine does not see high frequency ripple in steady state operation, thereby reducing losses and noise associated with continuous switching.

8. Since the configuration is similar to that of the SRM drive, the same converter can be used for both drives with changes in the control scheme which can be easily implemented in a DSP based system.

The topology has a few demerits that are listed below:

1. Poorer utilization of the machine due to half-wave operation.

2. Larger self-inductance in machine results in large electrical time constant leading to a slow response in current and hence in torque when compared to full-wave converter fed drive.

3. The control of the system requires the use of a voltage sensor in the buck converter circuit to control the output voltage of the buck converter. Although, voltage sensors are now available easily in the market and are about the same size as the current sensors, the extra sensor does add to the cost of the system.

4. An inductor in series with the main current restricts the use of this converter to smaller rating drives. For larger drives, the current flowing in the buck converter will be high and the size of the inductor will increase.

Table 5.1 Comparison of the proposed converter and full-wave based converter PMBDC drives

Aspects	Proposed converter-based PMBDC	Full-wave converter-based PMBDC
Number of power switches	4	6
Number of diodes	4	6
Phase and Chopper switch voltage (min.)	V_{dc}	V_{dc}
Phase and Chopper switch current (peak)	I_p	I_p
Motor phase current (rms)	$\frac{I_p}{\sqrt{3}}$	$\sqrt{\frac{2}{3}}I_p$
Number of capacitors	2	1
Capacitor voltage	V_{dc}	V_{dc}
Number of isolated logic supplies for isolated operation	2	4
Number of gate drivers	4	6
Switch Conduction losses	$\cong v_{sw}I_p(1+h)$	$2hv_{sw}I_p$
Diode Conduction losses	$\cong v_dI_p(1-h)$	$2v_dI_p(1-h)$
VA rating (peak)	$4V_{dc}I_p$	$6V_{dc}I_p$
VA rating (rms)	$(1+\sqrt{3})V_{dc}I_p$	$2\sqrt{3}V_{dc}I_p$

5.10 Conclusions

The PMBDC drive with a front-end buck converter is successfully implemented. The results obtained experimentally were seen to coincide with the simulations of the drive. It is successfully shown that a single converter can be used for both SRM and PMBDC drives with only changes in the code in the DSP and few minor changes in the hardware necessitated by the fact that the load machines used were different as were the tachogenerator feedbacks.

Chapter 6. Contributions and Future Work

The major contributions of this dissertation are summarized as follows.

1. This dissertation covers the design procedure of a 8/6 switched reluctance motor from the first principles. No major assumptions were made in the design procedure although a few assumptions are made in the analysis section of the design procedure. This differs from some of the sources cited in the procedure of designing the machine, which is simplified for a person with basic knowledge of electromagnetics to achieve an intuitive procedure. Extensive background knowledge of switched reluctance motors is not required to use the design procedure outlined. Certain references such as [KRI01] do have a design procedure outlined but this does require a lot of background knowledge to implement. The methodical approach to designing the machine is one of the major contributions of this dissertation.
2. The calculation of the unaligned inductance follows the basic principles of electromagnetics and does not rely on any previous sources whose documentation is hard to verify. The procedure outlined is easy to follow and while it has approximately the same error as in other methods when compared to the finite element analysis, the value tends to be higher than the finite element analysis value which is fortuitous as far as machine design is concerned since the analytical output torque would be calculated to be lower than the finite element value or the actual measured value in the machine. This would lead to a slight over-design of the machine that would be perfectly acceptable rather than designing a machine that would not produce the required output torque.
3. The procedure for calculating inductances for various rotor positions has been developed. The selection of the various flux tubes and their areas are intuitive with many approximations. The results do show some variation when compared with the finite element analysis. Better accuracy can probably be achieved by defining more regions of variations but is not required. The values at the aligned and unaligned positions show a very small margin of error and these values are used in the calculation of analytical torque developed in the machine. The outlining of the procedure is in a manner to allow users to develop their own procedure with minor modifications. This procedure has now been described in [KRI01].
4. A detailed procedure to calculate the eddy-current losses was described. This procedure does not rely on the approximations of the flux variations in a cycle but instead accounts for the

rise time of the current and the variation of inductance with the current. The procedure also helps to accurately predict the actual maximum torque developed in the machine and this is an invaluable result, as other methods tend to approximate the possible output torque.

5. The process of finding the hysteresis losses although adapted from [HAY95] does not rely on approximate flux profiles. Instead accurate flux plots are used to find the hysteresis losses. The calculation and documentation of the iron losses is one of the significant contributions of this dissertation.
6. The dissertation covers the description of a new converter configuration for switched reluctance motors. The converter was first described in literature in [KRI96] and subsequently in [KRI01]. The different modes of operation are described in detail along with the various advantages and disadvantages.
7. This dissertation describes the design procedure for a SRM drive using the new buck converter configuration. This material has not been published before. The design procedure was verified with computer simulations. Experimental verifications of the drive have been done in this dissertation.
8. The unique nature of the buck converter allows it to be used to drive a permanent magnet brushless dc motor in a half-wave configuration. This was first recognized in [KRI98]. This allowed for the development of a universal drive, i.e., the same hardware could be used to drive two different machines with only small changes in code.
9. The design procedure for the buck converter drive for permanent magnet brushless dc machines was done in the dissertation. The design was verified with experimental simulations that have now been published in [KRI99]. The experimental results were obtained for the first time for such a drive.
10. The dissertation shows the implementation of two different drives using a DSP based controller and a single converter configuration. This is a major contribution of the dissertation.

The future work following this dissertation could be outlined as follows:

1. There is a need to correlate the iron losses that have been calculated analytically with experimental verifications. Towards that end, an efficient measurement method has to be developed.

2. Thermal models have to be developed for the switched reluctance motor and the temperature rise in the machine has to be calculated so as to understand the requirements of cooling. The definition of the losses in every portion of the machine in this dissertation will help to refine the model for future researchers interested in thermal modeling.
3. The field of mechanical design of switched reluctance machines focused towards acoustic noise reduction is a vast topic that has started emerging. There is a strong need to relate the acoustic noise to the dimensions of the machine thereby refining the design procedure towards building quieter machines.

Bibliography

- KRA53 Kraus, J.D., “*Electromagnetics*”, McGraw-Hill Book Company, New York, 1953.
- NAS69 Nasar, S.A., “DC Switched Reluctance Motor”, *Proc. IEE* Vol. 116, No. 6, pp. 1048-1049, June 1969.
- IEC71 International Electrotechnical Commission, “Dimensions and output ratings for rotating electrical machines – Frame numbers 56 to 400 and flange numbers F55 to F1080”, Publication 72, Geneva, Switzerland, 1971.
- BYR76 Byrne, J. and Lacy, J.C., “Electrodynamic system comprising a variable reluctance machine”, *U.S. Patent 3956678*, May 1976.
- COR79 Corda, J. and Stephenson, J.M., “An Analytical Estimation of the Minimum and Maximum Inductances of a Double-Salient Motor”, *Proc. of the International Conf. On Stepping Motors and Systems*, pp. 50-59, Leeds, UK, 1979.
- LAW80 Lawrenson, P.J., Stephenson, J.M., Blenkinsop, P.T., Corda, J. and Fulton, N.N., “Variable-speed Switched Reluctance Motors”, *Proc. IEE* Vol. 127, Pt B, No. 4, pp. 253-265, July 1980.
- DAV81 Davis, R.M., Ray, W.F. and Blake, R.J., “Inverter drive for switched reluctance motor: circuits and component ratings”, *Proc. IEE* Vol. 128, Pt B, No. 2, pp. 126-136, Mar. 1981.
- SAW84 Sawhney, A.K., “*A Course in Electrical Machine Design*”, Dhanpat Rai and Sons, New Delhi, India, 1984.
- ARU85 Arumugam, R., Lowther, D.A., Krishnan, R. and Lindsay, J.F., “Magnetic field analysis of switched reluctance motor using 2-dimensional finite element model”, *IEEE Transactions on Magnetics*, Vol. MAG-21, No. 5, pp. 1883-1885, 1985.
- BAS85 Bass, J.T., Ehsani, M., Miller, T.J.E and Steigerwald, R.L., “Development of a unipolar converter for variable reluctance motor drives” *Conference Record. 1985 IEEE Industry Applications Society Annual Meeting*, pp.1062-1068, Toronto, CA, Sept. 1985.
- MIL85 Miller, T.J.E., “Converter volt-ampere requirements of the switched reluctance motor drive”, *IEEE Transactions on Industry Applications*, vol. 21, No. 5, pp. 1136-1144,

Sept./Oct. 1985.

- JAH86 Jahns, T.M., Kliman, G.B. and Neumann, T.W., "Interior permanent-magnet synchronous motors for adjustable-speed drives", *IEEE Transactions on Industry Applications*, vol.IA-22, no.4, pp.738-47, July-Aug. 1986.
- LIN86 Lindsay, J.F., Arumugam, R. and Krishnan, R., "Finite-element analysis characterization of a switched reluctance motor with multitooth per stator pole", *Proc. IEE* Vol. 133, Pt B, No. 6, pp. 347-353, Nov. 1986.
- SOU87 Sourirajan, A., "Computer Aided Design of a Switched Reluctance Motor", MS thesis, Virginia Tech, 1987.
- KRI88 Krishnan, R., Arumugam, R. and Lindsay, J.F., "Design Procedure for Switched-Reluctance Motors", *IEEE Transactions on Industry Applications*, vol. 24, No. 3, pp. 456-461, May/June 1988.
- ARU88 Arumugam, R., Lindsay, J.F. and Krishnan, R., "Sensitivity of Pole Arc/Pole pitch ratio on Switched Reluctance Motor Performance", *Proc. IEEE IAS Ann. Mtg.*, pp. , Pittsburgh, Oct. 1988.
- MAT89 Materu, P.N., "Design and Steady-state Analysis of the Switched Reluctance Motor Drive", Ph.D. Dissertation, Virginia Tech, 1989.
- MOH89 Mohan, N., Undeland, T.M. and Robbins, W.P., "*Power Electronics: Converters, Applications, and Design*", John Wiley and Sons, New York, 1989.
- KRI90 Krishnan, R. and Materu, P.N., "Design of a Single-Switch-per-Phase Converter for Switched Reluctance Motor Drives", *IEEE Transactions on Industrial Electronics*, vol. 37, No. 6, pp. 469-476, December 1990.
- MAT92 Materu, P.N. and Krishnan, R., "Estimation of Switched-Reluctance Motor Losses", *IEEE Transactions on Industry Applications*, vol. 28, No. 3, pp. 668-679, May/June 1992.
- KRI93 Krishnan, R. and Materu, P.N., "Analysis and Design of a Low-Cost Converter for Switched Reluctance Motor Drives", *IEEE Transactions on Industry Applications*, vol. 29, No. 2, pp. 320-327, March/April 1993.
- MIL93 Miller, TJE, "*Switched Reluctance Motors and their Control*", Magna Physics Publishing and Clarendon Press, Oxford, 1993.
- RAD94 Radun, A.V., "Design Considerations for the Switched Reluctance Motor", *IEEE*

- Transactions on Industry Applications*, vol. 31, No. 5, pp. 1079-1087, Sept./Oct. 1994.
- HAY95 Hayashi, Y. and Miller, T.J.E., "A New Approach to Calculating Core Losses in the SRM", *IEEE Transactions on Industry Applications*, vol. 31, No. 5, pp. 1039-1046, Sept./Oct. 1995.
- KRI95 Krishnan, R. and Vijayraghavan, P., "Parameter compensation of permanent magnet synchronous machines through airgap power feedback", Proceedings of the 1995 IEEE IECON, pp. 411-16, Orlando, FL, Nov. 1995.
- JAC96 Jackson, T.W., "Analysis and Design of a Novel Controller Architecture and Design Methodology for Speed Control of Switched Reluctance Motors", MS thesis, Virginia Tech, 1996.
- KRI96 Krishnan, R., "A novel converter topology for switched reluctance motor drives", *PESC 96 Record. 27th Annual IEEE Power Electronics Specialists Conference*, pp. 1811-16 vol.2, Baveno, Italy, 23-27 June 1996
- TAN97 Tang, Y., "Characterization, Numerical Analysis, and Design of Switched Reluctance Motors", *IEEE Transactions on Industry Applications*, vol. 33, No. 6, pp. 1544-1552, Nov./Dec. 1997.
- BAR98 Barnes M, and Pollock C., "Power electronic converters for switched reluctance drives", *IEEE Transactions on Power Electronics*, vol.13, no.6, pp.1100-11, Nov. 1998.
- KRI98 Krishnan, R. and Vijayraghavan, P., "A New Power Converter Topology for PM Brushless DC Motor Drives", *Proceedings of the 1998 IEEE IECON. 24th Annual Conference of the IEEE Industrial Electronics Society*, pp. 709-714 vol.2, Aachen, Germany; 31 Aug.-4 Sep. 1998.
- KRI99 Krishnan, R., "Permanent Magnet Synchronous and Brushless DC Motor Drives: Theory, operation, performance, modeling, simulation, analysis and design", Lecture Notes, Virginia Tech, 1999.
- KRI991 Krishnan, R. and Praveen Vijayraghavan, "Fast Estimation and Compensation of Rotor Flux Linkage in Permanent Magnet Synchronous Machines", Proceedings of the 1999 IEEE International Symposium on Industrial Electronics (ISIE'99), 661-666, Bled, Slovenia, July 11-16, 1999.

- RAD99 Radun, A., "Analytical calculation of the switched reluctance motor's unaligned inductance", *IEEE Transactions on Magnetics*, Vol. MAG-35, No. 6, pp. 4473-4481, Nov. 1999.
- RAD00 Radun, A., "Analytically computing the flux linked by a switched reluctance motor phase when the stator and rotor poles overlap", *IEEE Transactions on Magnetics*, Vol. MAG-36, No. 4, pt. 2, pp. 1996-2003, July 2000.
- KRI01 Krishnan, R., "Switched Reluctance Motor Drives: Modeling, Simulation, Analysis, Design, and Applications", CRC Press, 2001.
- KRI011 Krishnan, R., "Electric motor drives: modeling, analysis, and control", Prentice Hall, 2001.

Vita

Praveen Vijayraghavan was born on December 1, 1969 in Bombay, India. He graduated from high school from Poorna Prajna Education Center in Bangalore, India in 1985. He then completed his Pre-University degree from Seshadripuram Pre-University College in Bangalore, India in 1987. He got his B.E. degree from R.V. College of Engineering in the Bangalore University in Bangalore, India. He graduated from the Electrical Engineering Department in 1991 with a 5th rank in the entire Bangalore University. He started working in Integrated Electric Co. (P) Ltd. in Bangalore, India as a design engineer. He then joined the Systems and Controls Engineering program at Case Western Reserve University in Cleveland, OH. He graduated with his M.S. degree in 1993. He then started working on his Doctoral degree in the Bradley Department of Electrical and Computer Engineering Department at Virginia Tech. During his stay at Virginia Tech, he worked as an instructor teaching Signals and Systems to junior class students for a semester. He was also the Chief Operating Officer of the Personal Electric Rapid Transit Systems (PERTS) group of Virtual Corporation for 4 years. During his tenure as the COO of PERTS, he oversaw the construction of a 16' linear switched reluctance propulsion prototype as well as a 20' magnetic levitation prototype. He completed his dissertation in the field of Switched Reluctance Machines. His research interests include linear and rotary switched reluctance machines and their control, control of permanent magnet brushless dc machines, vector control of induction machines and noise reduction methods for electric machines. He intends to take up the position of Senior Design Engineer in Integrated Electric Co. (P) Ltd. in Bangalore, India from January 2002.